This is to certify that the

dissertation entitled

Evaluating the Rheological Properties
of Power-Law Fluids Using
Mixer Viscometry

presented by

Maria Elena Castell Perez

has been accepted towards fulfillment
of the requirements for

PhD. degree in Agricultural Engineering

James F. Steffe
Major professor

Date 2/8/90

EVALUATING THE RHEOLOGICAL PROPERTIES OF POWER-LAW FLUIDS USING MIXER VISCOMETRY

By

Maria Elena Castell-Perez

A DISSERTATION

Submitted to
Michigan State University
in partial fulfillment of the requirements
for the degree of

DOCTOR OF PHILOSOPHY

IN

Agricultural Engineering

Department of Agricultural Engineering

1990

A

standard

simple,

cylinder

tions to

xiting s

T

linear st

with the

Model 2,

accounts

ective m

diameter

R

concentri

ate ra

ABSTRACT

EVALUATING THE RHEOLOGICAL PROPERTIES OF POWER-LAW FLUIDS USING MIXER VISCOMETRY

By

Maria Elena Castell Perez

A new procedure was developed to determine the flow properties of standard power-law fluids using mixer viscometry data. The procedure is simple, accurate, and needs little data collection. A concentric cylinder analogy was used as an approximation of mixer viscometry equations to describe an average shear rate and average shear stress in the mixing system.

Two system models were evaluated for approximation of the average shear stress in the mixing system: (1) Model 1, representing the analogy with the concentric cylinders systems with negligible end effects; (2) Model 2, representing the same analogy with the addition of a term which accounts for the end effects. In the case of a flag impeller, an alternative model was evaluated, i.e., Model 3 representing a cylinder of diameter d_e with two blades attached.

Results were compared to those obtained with a conventional concentric cylinder viscometer (Haake Rotovisko) over the same shear rate range (1-40 1/s) with standard power-law fluids (aqueous CMC

solutions). The best approximation of the average shear stress of standard power-law fluids was obtained with the Model 2 (concentric cylinders analogy with end effects) for the paddle impellers. Model 3 ($d = d_e$) gave the best results for the flag impeller.

The procedure was evaluated with an actual power-law food product, creamy salad dressing. In this case Model 2 also gave the best results for the paddle impellers. For the flag impeller, Model 3 yielded higher values of the average shear stress, with Model 1 (concentric cylinders analogy with negligible end effects) being the best model for approximation of the average shear stress of the tested food material.

Established mixer viscometry methods, the viscosity matching and the slope method, were evaluated for determination of average shear rates when agitating time-independent non-Newtonian fluids. Results indicate that the use of a constant value of the mixer proportionality constant, k', is not valid for all ranges of fluid rheological properties, system geometry and operating conditions. The relationship between the average shear rate and the impeller rotational speed was found to be different for different rheological properties and system geometries. The effect of the fluid properties on the value of k' is not clearly understood and needs further investigation.

Approved _____ _____

Major Professor Date

Approved _____ _____

Department Chairperson Date

To Rosana

Thanks for your unvaluable help,

Elena

the

guide

each

Dr. D

Door

Manj

Many

these

hone

Suppo

at Ma

stude

Drive

ACKNOWLEDGMENTS

I am deeply indebted to Dr. James F. Steffe for suggestion of the research topic and his continuous support, interest, and patient guidance throughout the course of this study.

Sincere appreciation is extended to the guidance committee members: Dr. Ajit K. Srivastava, Agricultural Engineering Department, Dr. Daina M. Briedis, Chemical Engineering Department, Dr. Alden M. Booren, Food Science and Human Nutrition Department and Dr. Juan Menjivar, Nabisco Brands, who served as an outside examiner.

I want to thank my wonderful family, Bernardo, Rosario, Caty, Many, Jose and Lili, for their love and words of encouragement during these special years and for understanding my necessary long absence from home; to Dolores Peres, who always believed in me.

Special thanks goes to Dr. Fred Bakker-Arkema for his moral support.

I would also like to thank the Romance Languages Department at Michigan State University for providing the financial assistance.

Special thanks is extended to the entire faculty, staff and students of the Agricultural Engineering Department, Michigan State University, for their moral support.

LIST OF TABL

LIST OF FIGU

LIST OF SYMB

1. INTRODUCT

2. OBJECTIVE

3. LITERATUR

3.1 USING
3.1.1

3.2 CALCU
METHO
3.2.1

3.2.2

3.2.3

3.2.4

3.3 MIXIN
3.3.1

3.3.2

3.3.3

TABLE OF CONTENTS

	Page
LIST OF TABLES	x
LIST OF FIGURES	xiii
LIST OF SYMBOLS	xix
1. **INTRODUCTION**	1
2. **OBJECTIVES**	3
3. **LITERATURE REVIEW**	4
3.1 USING MIXING TO EVALUATE RHEOLOGICAL PROPERTIES	4
3.1.1 Applications of Mixer Viscometry	5
3.2 CALCULATION TECHNIQUES IN MIXER VISCOMETRY - TRADITIONAL METHODS	9
3.2.1 Analysis of Time-Independent Behavior	11
3.2.1.1 Viscosity Matching Method	11
3.2.1.2 Linear Shear Stress Method	17
3.2.1.3 Slope Method	24
3.2.1.4 Combined Slope and Linear Shear Stress Method	26
3.2.1.5 Methods Using a Helical Screw	27
3.2.1.5.1 Pressure Difference Method	27
3.2.1.5.2 Direct Determination of the Flow Curve Method	28
3.2.2 Yield Stress Determination	30
3.2.3 Analysis of Time-Dependent Behavior	34
3.2.3.1 Rheological Model Plus Linear Shear Rate Method	35
3.2.3.2 Combined Rheological and Kinetic Model Plus Linear Shear Rate Method	36
3.2.3.3 Subjective Assessment of Thixotropy Using a Vane Impeller	41
3.2.4 Elastic Fluids	42
3.2.4.1 Power Requirements	43
3.2.4.2 The Weissenberg Effect	50
3.3 MIXING THEORY	53
3.3.1 Power Consumption in Mixing Vessels	53
3.3.1.1 Relation Between Flow Pattern and Power Consumption in a Cylindrical Vessel	53
3.3.2 Dimensional Analysis for Mixing	57
3.3.3 Laminar Mixing Region	60

3.3.3.1 Laminar Fluid Motion in Agitated Vessels..... 60
3.3.3.2 Laminar Flow Criterion..... 63
3.3.3.2.1 Critical Reynolds Number..... 63

3.3.4 Shear Rate Distribution in a Cylindrical Mixing Vessel..... 67
3.3.4.1 Theoretical Expressions for the Rate of Shear in a Mixing Vessel..... 69
3.3.4.1.1 Concentric Cylinders..... 69
3.3.4.1.2 Empirical and Theoretical Expressions for the Impeller Proportionality Constant, k'..... 73

4. THEORY: ALTERNATIVE METHOD TO EVALUATE MIXER VISCOMETRY DATA... 78

4.1 DETERMINATION OF FLOW CURVES..... 78
4.1.1 Shear Stress and Shear Rate Approximations..... 79
4.1.1.1 Model Systems..... 79
4.1.1.2 Shear Rate Approximations..... 80
4.1.1.3 Shear Stress Approximations..... 86
4.1.1.3.1 Model 1 (Concentric cylinders with negligible end effects)..... 86
4.1.1.3.2 Model 2 (Concentric cylinders with end effects)..... 88
4.1.1.3.3 Model 3 (Flag Impeller)..... 91

5. MATERIALS AND METHODS..... 93

5.1 EQUIPMENT AND MATERIALS..... 93
5.1.1 The Brookfield Mixer..... 93
5.1.2 Data Acquisition System..... 94
5.1.3 Impellers and Cups..... 94
5.1.4 Fluids..... 96

5.2 EXPERIMENTAL DESIGN AND PROCEDURE..... 96
5.2.1 Design of Experiment..... 96
5.2.2 Procedure..... 98
5.2.2.1 Preparation of Non-Newtonian Fluids..... 98
5.2.2.2 Determination of Rheological Properties of Non-Newtonian Fluids..... 101
5.2.2.3 Calibration of Brookfield Viscometers..... 101
5.2.2.4 Data Collection..... 102

5.3 CALCULATIONS USING TRADITIONAL MIXER VISCOMETRY METHODS.... 105
5.3.1 Viscosity Matching Methods..... 105
5.3.2 Slope Method..... 105

5.4 CALCULATIONS USING NEW MIXER VISCOMETRY METHOD..... 105
5.4.1 Determination of Average Shear Rate..... 105
5.4.2 Determination of Average Shear Stress..... 106
5.4.3 Procedure for the use of a mixer viscometer to directly determine the rheological properties of power-law fluids..... 107

6. RESULTS AND DISCUSSION..... 109

6.1 ESTIMA
METHOD
6.1.1
6.1.2 S
6.1.3 S
6.2 DETERM
USING
6.2.1
6.2.2
6.3 GENERAL
VISCOME
6.3.1 M
6.3.2 N
SUMMARY AND
SUGGESTIONS
APPENDICES
APPENDIX A

6.1 ESTIMATION OF AVERAGE SHEAR RATE USING MIXERS: TRADITIONAL METHODS 109
6.1.1 Matching Viscosities 109
6.1.1.1 Power Curves Method (Metzner and Otto, 1957) 109
6.1.1.1.1 Estimation of Average Shear Rates .. 119
6.1.1.1.2 Factors Affecting Average Shear Rates (and k') 129
6.1.1.1.2.1 Impeller Rotational Speed 129
6.1.1.1.2.2 Fluid Properties 129
6.1.1.1.2.3 Cup Diameter 130
6.1.1.1.2.4 Impeller Size (Blade Height) 131
6.1.1.2 Mixer Torque Curves Method (Mackey et al., 1987) 132
6.1.1.2.1 Factors Affecting k' 142
6.1.1.2.1.1 Impeller Rotational Speed 142
6.1.1.2.1.2 Fluid Properties 142
6.1.1.2.1.3 Cup Diameter 148
6.1.1.2.1.4 Impeller Size (Blade Height) 151
6.1.1.2.2 Estimation of Average Shear Rates .. 154
6.1.2 Slope Method 160
6.1.2.1 Factors Affecting k' 164
6.1.2.1.1 System Geometry 164
6.1.2.2 Estimation of Average Shear rates and Apparent Viscosity 171
6.1.3 Summary of Discussion 176
6.2 DETERMINATION OF RHEOLOGICAL PROPERTIES OF POWER-LAW FLUIDS USING THE ALTERNATIVE MIXER VISCOMETRY METHOD 177
6.2.1 Determination of the Flow Behavior Index, n 177
6.2.2 Determination of Shear Stress-Shear Rate Relationships 180
6.2.2.1 Average Shear Rate In the Mixing System 180
6.2.2.2 Average Shear Stress In the Mixing System 190
6.2.2.2.1 Torque Approximations 190
6.2.2.3 Flow Curves 200
6.2.2.3.1 Ideal Fluids 200
6.2.2.3.2 Food Product 208
6.3 GENERAL RECOMMENDATIONS FOR APPLICATION OF MIXER VISCOMETRY 227
6.3.1 Mixer System Used in This Study 227
6.3.2 New Mixer Viscometer System 230
7. SUMMARY AND CONCLUSIONS 233
8. SUGGESTIONS FOR FURTHER STUDY 238
9. APPENDICES
APPENDIX A - DIMENSIONLESS ANALYSIS FOR MIXING VESSELS

APPENDIX
APPENDIX

10. REFERENCE

(NEWTONIAN FLUIDS)..... 239
A.1 - Development of Dimensionless Functions for Power-Law Fluids (Used in Slope Method)..... 243
APPENDIX B - EXPERIMENTAL RESULTS..... 245
APPENDIX C - PROCEDURE FOR THE USE OF THE MIXER BROOKFIELD VISCOMETER FOR NEWTONIAN FLUIDS..... 263
10. REFERENCES..... 271

TABLE

3.1 Pr
Th

3.2 Sy

3.3 Mo
Ne

3.4 En
ox

5.1 Ex

6.1 Re

6.2 Re

6.3 Va
Pa

6.4 Va
Fl

6.5 Re

6.6 Va
In

6.7 Va
In

6.8 Va

6.9 Va
fu

6.10 Re

6.11 Va
la
Co

6.12 Va
la
Co

6.13 Va

LIST OF TABLES

TABLE		Page
3.1	Products and Rheological Characteristics Considered In The Mixing Systems (Castell-Perez and Steffe, 1989)....	7
3.2	Studies on Mixing of Elastic Fluids.....	44
3.3	Modified Impeller Reynolds Numbers for Mixing of Non-Newtonian Fluids.....	65
3.4	Empirical and Theoretical Expressions for Determination of the Impeller Proportionality Constant, k'.....	74
5.1	Experimental Design.....	99
6.1	Regression Results of Eqn. (6.2) (Paddle Impellers)....	114
6.2	Regression Results of Eqn. (6.3) (Flag Impeller).....	115
6.3	Values of k', defined by Eqn. (3.8) ($k' = \dot{\gamma}_{av}/N$), for Paddle Impellers.....	127
6.4	Values of k', defined by Eqn. (3.8) ($k' = \dot{\gamma}_{av}/N$), for Flag Impeller.....	128
6.5	Regression Results for the fit of Eqn. (6.10).....	1
6.6	Values of k', defined by Eqn. (6.12), for Paddle Impellers.....	140
6.7	Values of k', defined by Eqn. (6.12), for Flag Impeller.....	141
6.8	Values of k' (evaluated using the Slope Method).....	165
6.9	Values of k' (evaluated using the Slope Method) as a function of impeller rotational speed.....	169
6.10	Regression Results of Eqn. (6.13) (Paddle Impellers)...	170
6.11	Values of the Flow Behavior Index of Standard Power-law Fluids Using the Mixer System (Paddles) and a Concentric Cylinders Viscometer (Haake Rotovisko).....	181
6.12	Values of the Flow Behavior Index of Standard Power-law Fluids Using the Mixer System (Flag) and a Concentric Cylinders Viscometer (Haake Rotovisko).....	182
6.13	Values of the Fluid Consistency Coefficient of Standard	

Power-law Fluids Using the Mixer System (Paddles) [Model 1: Negligible end effects; Eqn. (4.14)] and a Concentric Cylinders Viscometer (Haake Rotovisko)..... 202

6.14 Values of the Fluid Consistency Coefficient of Standard Power-law Fluids Using the Mixer System (Flag) [Model 1: Negligible end effects; Eqn. (4.14)] and a Concentric Cylinders Viscometer (Haake Rotovisko)..... 203

6.15 Values of the Fluid Consistency Coefficient of Standard Power-law Fluids Using the Mixer System (Paddles) [Model 2: Concentric cylinders with end effects; Eqn. (4.21)] and a Concentric Cylinders Viscometer (Haake Rotovisko). 204

6.16 Values of the Fluid Consistency Coefficient of Standard Power-law Fluids Using the Mixer System (Flag) [Model 2: Concentric cylinders viscometer; Eqn. (4.21)] and a Concentric Cylinders Viscometer (Haake Rotovisko)..... 205

6.17 Values of the Fluid Consistency Coefficient of Standard Power-law Fluids Using the Mixer System (Flag) [Model 3: $d - d_e$; Eqn. (6.23.1)] and a Concentric Cylinders Viscometer (Haake Rotovisko)..... 206

6.18 Values of the Flow Behavior Index (n) and the Fluid Consistency Coefficient of Salad Dressing Using the Mixer System (Paddles) [Model 1, Eqn. (4.14)]) and a Concentric Cylinders Viscometer (Haake Rotovisko)..... 219

6.19 Values of the Flow Behavior Index (n) and the Fluid Consistency Coefficient of Salad Dressing Using the Mixer System (Paddles) [Model 2, Eqn. (4.21)]) and a Concentric Cylinders Viscometer (Haake Rotovisko)..... 220

6.20 Values of the Flow Behavior Index (n) and the Fluid Consistency Coefficient of Salad Dressing Using the Mixer System (Flag) and a Concentric Cylinders Viscometer (Haake Rotovisko)..... 221

A.1 Pertinent Quantities Involved In Fluid Agitation Processes (Newtonian Fluids)..... 242

B.1 Regression Results of $P_o = \alpha_0 (R_e)^{\alpha_1} (Fr)^{\alpha_2}$ (Paddle Impellers)..... 245

B.2 Regression Results of $P_o = \beta_0 (R_e)^{\beta_1} (Fr)^{\beta_2}$ (Flag Impeller)..... 246

B.3 Values of β_1 , β_2 and β_3 from $k' = \beta_1 (d/b)^{\beta_2} + \beta_3$ (Matching Method of Power Curves) for Power-law Fluids. 247

C.1 Factors for Use of the Mixer Impellers with the Brookfield Viscometer..... 264

C.2 Table for the fit of Eqn. (C.2)..... 267

C.3 Values of Viscosity of a Newtonian Fluid (η = 4.84 Pa s) Obtained with The Impeller Factors..... 269

LIST OF FIGURES

FIGURE		Page
3.1	Typical Impellers Used In The Determination Of Rheological Properties With A Mixer (Castell-Perez and Steffe, 1989).....	6
3.2	Mixer Viscometry Techniques.....	10
3.3	Flow patterns in Agitated Vessels. A) Newtonian Fluid. B) Elastic Fluid (Rod-climbing).....	51
3.4	a) Simplified Flow Model for Power Correlation; b) Relative Velocity Distribution Between Paddle and Liquid (Nagata, 1975).....	54
3.5	Fluid Motion in Agitated Vessels (Nagata, 1975).....	61
3.6	Schematic Diagram Showing The Relation Between Power Number and Reynolds Number for a Paddle Impeller (Nagata, 1975).....	62
4.1	Model Systems. A) Paddle Impeller; B) Flag Impeller; C) Flag Impeller (Model 3).....	81
5.1	Paddle and Flag Impellers (all dimensions are in cm.)...	95
5.2	Sample containers and cup base (all dimensions are in cm.).....	97
5.3	Mixing System.....	100
5.4	Schematic Diagram of Experimental System.....	104
6.1	Power Number/Reynolds Number Relationship for Newtonian Fluids Using the Paddle Impellers (Cup diameter = 5.5 cm).....	110
6.2	Power Number/Reynolds Number Relationship for Newtonian Fluids Using the Paddle Impellers (Cup diameter = 3.5 cm).....	111
6.3	Power Number/Reynolds Number Relationship for Newtonian Fluids Using the Paddle Impellers (Cup diameter = 2.54 cm).....	112
6.4	a) Predicted P_o Versus Observed P_o ; b) Power Correlation For The Paddle Impellers.....	117
6.5	a) Predicted P_o Versus Observed P_o ; b) Power Correlation	

For The Flag Impeller..... 118

6.6 a) Shear Stress Versus Shear Rate; b) Apparent Viscosity Versus Shear Rate (Hydroxypropyl Methylcellulose 1%).... 120

6.7 Average Mixing Shear Rate as a Function of Rotational Speed of the Paddle Impellers. a) System 3; b) System 4. 121

6.8 Average Mixing Shear Rate as a Function of Rotational Speed of the Paddle Impellers. a) System 5; b) System 6. 123

6.9 Average Mixing Shear Rate as a Function of Rotational Speed of the Paddle Impellers. a) System 7; b) System 8. 124

6.10 Average Mixing Shear Rate as a Function of Rotational Speed of the Flag Impeller. a) CMC 1.5%; b) CMC 1%..... 125

6.11 Average Mixing Shear Rate as a Function of Rotational Speed of the Flag Impeller. a) CMC 2%; b) System 3..... 126

6.12 Average Mixing Shear Rate as a Function of Rotational Speed of the Paddle Impellers (d/D=0.327). a) CMC 2%; b) CMC 1%..... 133

6.13 Plot of Mixer Proportionality Constant as a Function of Impeller Size for the Non-Newtonian Fluids (d/D=0.327).. 134

6.14 Mixer Torque Versus Viscosity Times Speed for Calculating Mixer Coefficient, k_2 (Paddle Impellers)..... 137

6.15 Predicted Mixer Coefficient Versus Observed Mixer Coefficient (Paddle Impellers)..... 138

6.16 Mixer Torque Versus Viscosity Times Speed for Calculating Mixer Coefficient, k_2 (Flag Impeller)..... 139

6.17 Mixer Proportionality Constant, k', Versus Rotational Speed, N, for Paddle Impellers When Mixing a Non-Newtonian Fluid (CMC 1%)..... 143

6.18 Mixer Proportionality Constant, k', Versus Rotational Speed, N, for Flag Impeller When Mixing Non-Newtonian Fluids. a) CMC 1%; b) CMC 2%..... 144

6.19 Plot of Mixer Proportionality Constant, k', Versus Rotational Speed, N, for Non-Newtonian Fluids (Paddle Impellers)..... 145

6.20 Plot of Mixer Proportionality Constant, k', as a Function of Flow Behavior Index, n (Flag Impeller)..... 146

6.21 Plot of Mixer Proportionality Constant, k', as a Function of Fluid Consistency Coefficient, m (Flag Impeller)..... 147

6.22 Plot of Mixer Proportionality Constant, k', as a Function

of Flow Behavior Index, n (Paddle Impeller)..... 149

6.23 Plot of Mixer Proportionality Constant, k', as a Function of Fluid Consistency Coefficient, m (Paddle Impeller)... 150

6.24 Plot of Mixer Proportionality Constant, k', as a Function of System Geometry. a) Impeller Size (d/b); b) Cup Size (d/D)..... 152

6.25 Plot of Mixer Proportionality Constant, k', as a Function of Fluid Consistency Coefficient, m (Pa s^n) for Different Paddle Impellers. a) 100 rpm; b) 20 rpm..... 153

6.26 Average Shear Rate as a Function of Impeller Rotational Speed for a Paddle Impeller (CMC 1%)..... 155

6.27 Average Shear Rate as a Function of Impeller Rotational Speed for a Paddle Impeller (CMC 2%)..... 156

6.28 Average Shear Rate as a Function of Impeller Rotational Speed for a Flag Impeller (CMC 1%)..... 157

6.29 Average Shear Rate as a Function of Impeller Rotational Speed for a Flag Impeller (CMC 2%)..... 158

6.30 Apparent Viscosity as a Function of Average Shear Rate for a Paddle Impeller (CMC 2%)..... 159

6.31 Apparent Viscosity as a Function of Average Shear Rate for a Flag Impeller (CMC 2%)..... 161

6.32 Plots of Dimensionless Functions $[P/(md^3N^{n+1})]$ Versus (1-n) for the Paddle Impellers..... 162

6.33 Plots of Dimensionless Functions $[P/(md^3N^{n+1})]$ Versus (1-n) for the Flag Impeller..... 163

6.34 Plots of Dimensionless Functions $[P/(md^3N^{n+1})]$ Versus (1-n) for the Paddle Impellers at Different Values of N.. 166

6.35 Plots of Dimensionless Functions $[P/(md^3N^{n+1})]$ Versus (1-n) for the Flag Impeller at Different Values of N..... 168

6.36 Average Mixing Shear Rate as a Function of Rotational Speed. a) Different Cups; b) Different Paddles..... 172

6.37 Average Mixing Shear Rate as a Function of Rotational Speed for the Flag Impeller..... 173

6.38 Apparent Viscosity as a Function of Average Shear Rate Using the Paddle Impellers. a) CMC 2%; b) CMC 1%..... 174

6.39 Apparent Viscosity as a Function of Average Shear Rate Using the Flag Impeller..... 175

6.40 Plot of the torque on the impeller shaft M versus rotational speed of the impeller N for 2% wt% aqueous solution of CMC (Paddle impellers)..... 178

6.41 Plot of the torque on the impeller shaft M versus rotational speed of the impeller N for 2% wt% aqueous solution of CMC (Flag impeller)..... 179

6.42 Experimental Versus Calculated Values of k'; a) k' Defined by Eqn. (4.5); b) k' Defined by Eqns. (4.5) and (6.13) for small gap (Paddle Impellers)..... 184

6.43 Experimental Versus Calculated Values of k'; a) k' Defined by Eqn. (4.7) (Paddle Impellers)..... 186

6.44 Experimental Versus Calculated Values of k'; a) k' Defined by Eqn. (4.7); b) k' Defined by Eqn. (4.7) ($d=d_e$)..... 189

6.45 Measured Versus Predicted Values of Torque on the Impeller Shaft Using Eqn. (4.14) (o) and Eqn. (4.21) (x); a) CMC 1.5%; b) CMC 1% (Paddle Impeller # 1, (d/b) = 1.8) [EE = Model 2 (end effects); NEE = Model 1 (no end effects)].. 192

6.46 Measured Versus Predicted Values of Torque on the Impeller Shaft Using Eqn. (4.14) (o) and Eqn. (4.21) (x); a) CMC 2% [EE = Model 2 (end effects); NEE = Model 1 (no end effects)]..... 194

6.47 Measured Versus Predicted Values of Torque on the Impeller Shaft Using Eqn. (4.14) (o) and Eqn. (4.21) (x); a) CMC 1.5%; b) CMC 1% (Paddle Impeller # 5, (d/b) = 0.36) [EE = Model 2 (end effects); NEE = Model 1 (no end effects)].. 195

6.48 Measured Versus Predicted Values of Torque on the Impeller Shaft for All Systems and Fluids (Paddle Impellers); a) Eqn. (4.14) (Model 1 = NEE); b) Eqn. (4.21) (Model 2 = EE)..... 196

6.49 Measured Versus Predicted Values of Torque on the Impeller Shaft for All Systems and Fluids (Flag Impeller) Using Eqn. (4.14) (Model 1) (Negligible end effects)..... 198

6.50 Measured Versus Predicted Values of Torque on the Impeller Shaft for All Systems and Fluids (Flag Impeller); a) Eqn. (4.21) (Model 2); b) Eqn. (6.23.1) (Model 3)..... 199

6.51 Flow Curve for 2% wt% Aqueous Solution of CMC Determined Using the Mixer Viscometer with a Paddle Impeller..... 201

6.52 Comparison of the Flow Curve for a Standard Fluid Determined Using the Concentric Cylinders Viscometer with the Data Obtained Using the Mixer Viscometer with the Paddle Impellers in a Large Cup [Model 2, Eqn. (4.21)]); a) CMC 1%; b) CMC 2%..... 209

6.53 Comparison of the Flow Curve for a Standard Fluid Determined Using the Concentric Cylinders Viscometer with the Data Obtained Using the Mixer Viscometer with the Paddle Impellers in a Small Cup [Model 2, Eqn. (4.21)]); a) CMC 1%; b) CMC 2%..... 210

6.54 Comparison of the Flow Curve for a Standard Fluid Determined Using the Concentric Cylinders Viscometer with the Data Obtained Using the Mixer Viscometer with a Flag Impeller [Model 3, Eqn. (6.23.1)] a) CMC 1%; b) CMC 2%..... 211

6.55 Comparison of the Flow Curve for a Standard Fluid Determined Using the Concentric Cylinders Viscometer with the Data Obtained Using the Mixer Viscometer with a Flag Impeller [Model 1, Eqn. (4.14)]; a) CMC 1%; b) CMC 2%..... 212

6.56 Comparison of the Flow Curve for a Standard Fluid Determined Using the Concentric Cylinders Viscometer with the Data Obtained Using the Mixer Viscometer with a Flag Impeller [Model 2, Eqn. (4.21)]; a) CMC 1%; b) CMC 2%..... 213

6.57 Comparison of the Flow Curve for Salad Dressing Determined Using the Concentric Cylinders Viscometer with the Data Obtained Using the Mixer Viscometer with the Paddle Impellers [Model 2, Eqn. (4.21)]; a) Large Cup; b) Small Cup..... 250

6.58 Comparison of the Flow Curve for Salad Dressing Determined Using the Concentric Cylinders Viscometer with the Data Obtained Using the Mixer Viscometer with a Flag Impeller [Model 3, Eqn. (6.23.1)]..... 216

6.59 Comparison of the Flow Curve for Salad Dressing Determined Using the Concentric Cylinders Viscometer with the Data Obtained Using the Mixer Viscometer with a Flag Impeller [Model 1, Eqn. (4.14)..... 217

6.60 Comparison of the Flow Curve for Salad Dressing Determined Using the Concentric Cylinders Viscometer with the Data Obtained Using the Mixer Viscometer with a Flag Impeller [Model 2, Eqn. (4.21)..... 218

6.61 Apparent Viscosity as a Function of Average Shear Rate for Salad Dressing. Flag Impeller (Model 1: Concentric cylinders with negligible end effects [NEE])..... 223

6.62 Apparent Viscosity as a Function of Average Shear Rate for Salad Dressing. Flag Impeller (Model 2: Concentric cylinders with end effects [EE])..... 224

6.63 Apparent Viscosity as a Function of Average Shear Rate for Salad Dressing. Flag Impeller (Model 3: Concentric Cylinders

with end effects; $d = d_e$)..... 225

6.64 Apparent Viscosity as a Function of Average Shear Rate for Salad Dressing. Flag Impeller. a) Small Gap; b) Wide Gap. 226

6.65 Flow Diagram of General Procedure for Mixer Viscometry... 231

B.1 a) Shear Stress Versus Shear Rate; b) Apparent Viscosity Versus Shear Rate (Hydroxypropyl Methylcellulose 1.5%)... 248

B.2 a) Shear Stress Versus Shear Rate; b) Apparent Viscosity Versus Shear Rate (Hydroxypropyl Methylcellulose 2%)..... 249

B.3 Average Mixing Shear Rate as a Function of Rotational Speed of the Paddle Impellers. a) System 1; b) System 2 (Torque Curves- Matching Method)..... 250

B.4 Average Mixing Shear Rate as a Function of Rotational Speed of the Paddle Impellers. a) System 9; b) System 10 (Torque Curves- Matching Method)..... 251

B.5 Average Mixing Shear Rate as a Function of Rotational Speed of the Flag Impeller. a) System 2; b) System 1 (Torque Curves- Matching Method)..... 252

B.6 Average Mixing Shear Rate as a Function of Impeller Rotational Speed for Two Paddle Impellers. (Torque Curves- Matching Method)..... 253

B.7 Apparent Viscosity as a Function of Average Shear Rate for a Paddle Impeller (CMC 1%) (Torque Curves- Matching method) 254

B.8 Apparent Viscosity as a Function of Average Shear Rate for a Flag Impeller (CMC 1%) (Torque Curves- Matching method) 255

B.9 Plots of Dimensionless Functions $[P/(md^3N^{n+1})]$ Versus (1-n) for the Flag Impeller (Slope Method)..... 256

B.10 Plots of Dimensionless Functions $[P/(md^3N^{n+1})]$ Versus (1-n) for the Paddle Impellers (Slope Method). a) System 3; b) System 2..... 257

B.11 Plots of Dimensionless Functions $[P/(md^3N^{n+1})]$ Versus (1-n) for the Paddle Impellers (Slope Method). a) System 6; b) System 4..... 258

B.12 Plots of Dimensionless Functions $[P/(md^3N^{n+1})]$ Versus (1-n) for the Paddle Impellers (Slope Method). a) System 8; b) System 7..... 259

B.13 Plots of Dimensionless Functions $[P/(md^3N^{n+1})]$ Versus (1-n) for the Paddle Impellers (Slope Method). a) System 10; b) System 9..... 260

B.14 Flow Curves for 1% wt% Aqueous Solution of CMC Determined Using the Mixer Viscometer With the Paddle Impellers..... 261

B.15 Flow Curves for 2% wt% Aqueous Solution of CMC Determined Using the Mixer Viscometer With the Paddle Impellers..... 262

C.1 a) Plot of C_1 Versus Impeller Rotational Speed; b) Plot of η versus Torque Reading (Paddle Impeller, d/b=0.45)... 266

LIST OF SYMBOLS

a	instrument constant, N m/reading	[Eqn. (3.33)]
a	model parameter, l/s	[Eqn. (3.57)]
a_1	parameter, Pa/s	[Eqn. (3.61)]
A	constant dependent on geometry	[Eqn. (3.1)]
A'	constant, $N\ s^b/m^2$	[Eqn. (3.66)]
A_1	surface of screw channel, m^2	
A_2	surface of the edge of the screw flight, m^2	
b	model parameter, dimensionless	[Eqn. (3.57)]
b	parameter, Pa/s	[Eqn. (3.63)]
b	impeller blade height, m	
b'	constant, dimensionless	[Eqn. (3.66)]
B	empirical coefficient	[Eqn. (3.86)]
B	constant, $kg\ m^2\ s^{n-2}$	[Eqn. (3.39)]
B_1	constant, l/m^3	[Eqn. (C.2)]
B_2	constant, -n	[Eqn. (C.2)]
C	constant, dimensionless	[Eqn. (3.78)]
C	constant, dimensionless	[Eqn. (3.41)]
C_i	constant, m^3	[Eqn. (3.29)]
Cr_1	correction factor	[Eqn. (3.50)]
C_1	integration constant	[Eqn. (3.114)]
C_1	constant, s/m^3	[Eqn. (C.1)]
d	impeller diameter, m	

d_c	diameter of cylindrical section, m	
	(Model System 3)	[Eqn. (4.32)]
d_e	equivalent diameter of helical screw impeller, m	
d_e	equivalent diameter of flag impeller, m	
	(Model System 3)	[Eqn. (4.32)]
d_o	outside cylinder diameter, m	
D	tank (container) diameter, m	
$\mathbf{D}$	defromation rate tensor, 1/s	[Eqn. (3.103)]
D_v	vane diameter, m	
f	empirical coefficient	[Eqn. (3.86)]
F	internal resisting force of fluid, N	[Eqn. (3.78)]
g	gravitational acceleration, m/s^2	
h	distance from free surface of liquid and bottom of cylinder, m	
H	height of inner cylinder, m	
H_v	vane height, m	
k'	impeller proportionality constant, 1/rev	
k''	constant, dimensionless	[Eqn. (3.16)]
k_1	rate constant, 1/s	[Eqn. (3.59)]
k_2	constant, $1/m^3$	[Eqn. (3.13)]
K	constant, m^3	[Eqn. (4.23)]
K_3	constant, m^3	[Eqn. (4.35)]
K_m	constant, Pa s^n	[Eqn. (3.53)]
K_o	consistency coefficient at time zero, Pa s^{n_o}	
ℓ	length of impeller blade, m	[Eqn. (4.32)]
l	length of impeller blade, m	
l_1	inner cylinder length, m	[Eqn. (3.32)]

L	Tank length, m
m	consistency coefficient, Pa s^n or kg s^{n-2}/m
m_x	consistency coefficient of investigated fluid, Pa s^n
m_y	consistency coefficient of known fluid, Pa s^n
M	torque, N m or kg m^2/s^2
M_e	equilibrium torque, N m
M_e	torque resulting from the shearing in the two end surfaces of a cylinder, N m [Eqn. (4.10)]
M_o	initial torque, N m
M_s	torque to agitate standard solution, N m
M_x	torque required to agitate investigated fluid, N m
M_w	torque resulting from the shearing in the cylindrical wall, N m [Eqn. (4.10)]
M_y	torque required to agitate known fluid, N m
M_1	torque in screw channel, N m [Eqn. (3.49)]
M_2	torque in gap, N m [Eqn. (3.49)]
n	flow behavior index, dimensionless
n_b	number of impeller blades
n_m	flow behavior index, dimensionless [Eqn. (3.53)]
n_o	flow behavior index at time zero, dimensionless
n_x	flow behavior index of investigated fluid, dimensionless
n_y	flow behavior index of known fluid, dimensionless
N	impeller rotational speed, rev/s
N_1	first normal stress function, Pa
p	empirical coefficient [Eqn. (3.86)]
p	parameter (≥ 0) [Eqn. (4.31)]
P	power, N m/s or kg m^2/s^3

r	impeller radius, m	
r	radial distance from the axis to any section of the impeller, m	[Eqn. (3.80)]
r_c	radius of the cylindrically rotating zone, m	
r_m	arithmetic mean radius, m	[Eqn. (3.32)]
r_1	inner cylinder radius, m	[Eqn. (3.32)]
r_2	outer cylinder radius, m	[Eqn. (3.32)]
R	impeller (cylinder) radius, m	[Eqn. (4.17)]
R_b	inner cylinder (bob) radius, m	
R_c	outer cylinder (cup) radius, m	
R_i	radius of inner cylinder, m	
s	fluid rheological parameter, dimensionless	
t	time, min	
t_1	fluid characteristic time, s	
T_o	vane yield stress, Pa or N /m^2	
T_m	maximum measured torque (vane method), N m	
u	impeller velocity, m/s	
u_{rel}	impeller relative velocity, m/s	
z	instrument constant, Pa/reading	[Eqn. (3.31)]
Z	instrument constant, Pa/reading	[Eqn. (3.36)]
Z_1	clearance from surface to top of impeller, m	
Z_2	clearance from bottom of impeller, m	

Greek Symbols

α	instrument reading	[Eqn. (3.31)]
α_o	empirical coefficient	

α_1	empirical coefficient
α_2	empirical coefficient
α_3	empirical cofficient
β_0	empirical coefficient
β_1	empirical coefficient
β_2	empirical coefficient
β_3	empirical coefficient
$\dot{\gamma}$	shear rate, 1/s
$\dot{\gamma}_{av}$	average shear rate, 1/s
$\dot{\gamma}_o$	standard shear rate, 1/s
ψ	geometric ratio, d_o/d_e [Eqn. (3.50)]
ψ_1	first normal stress coefficient, Pa s^2
λ	time dependent parameter, dimensionless [Eqns. (3.57-58)]
λ_o	initial value of λ, dimensionless
λ_e	equilibrium structural parameter, dimensionless
η	Newtonian viscosity, Pa s
η_a	non-Newtonian (apparent) viscosity, Pa s
η_{ao}	apparent viscosity at time zero, Pa s
η_{ax}	apparent viscosity of investigated fluid, Pa s
η_{ay}	apparent viscosity of known fluid, Pa s
η_c	Casson viscosity, Pa s
η_e	apparent viscosity at equilibrium, Pa s
η_o	limiting viscosity at zero shear rate, Pa s
Ω	angular velocity, rad/s
ρ	fluid density, kg/m^3
σ	shear stress, Pa
σ_{ao}	approximate initial shear stress, Pa

σ_{av}	average shear stress, Pa or N/m^2
σ_{ax}	approximate shear stress, Pa [Eqn. (3.63)]
σ_e	approximate equilibrium shear stress, Pa
σ_e	shear stress at the end surface of the cylinder, Pa
σ_o	yield stress, Pa
σ_{om}	Mizrahi-Berk yield stress, Pa
σ_s	shear stress of standard solution, Pa
σ_w	shear stress at the wall, Pa
σ_x	shear stress of investigated fluid, Pa
σ_y	shear stress of known fluid, Pa
σ_{yo}	yield stress, Pa
σ_{yl}	shear stress, Pa
T	stress tensor, Pa
ω	angular velocity of rotation, rad/s

Dimensionless Numbers

E_l	Elasticity Number
Γ	Torque [Eqn. (3.68)]
ma	Aberystwyth Number
P_o	Power Number
R_e	Mixing Reynolds Number
R_{ge}	Generalized Reynolds Number
R_{en}	Power-law Reynolds Number [Eqn. (6.8)]
T	Torque [Eqn. (3.72)]
W_i	Weissenberg Number

CHAPTER 1

INTRODUCTION

Many food materials, especially the suspension-type, present non-Newtonian flow characteristics. To evaluate, design, and control processing systems for the product, the engineer needs to understand the flow properties of these materials. This work is motivated by the need for new instrumentation and methodologies to evaluate the rheological behavior of suspension-type food products.

When dealing with food materials that are suspensions (tomato sauce, baby foods, salad dressings, etc.), conventional narrow gap viscometers (such as tube, cone-and-plate and concentric cylinders viscometers) become unsuitable for complete characterization because of effects such as phase separation (and consequent slip at the walls), and blocking of the measuring gap by particle aggregates. Significant errors in measurements can also occur due to the destruction of the particles.

An alternative instrument to use in evaluating the flow properties of suspension-type fluids is the "impeller" or "mixer" viscometer, based upon the theory of mixing non-Newtonian fluids developed by Metzner and Otto (1957). The method has proven to be useful for determination of rheological properties of viscous fermentation broths (Bongenaar et al., 1973; Kemblowski et al., 1988) and suspension-type food products (Rao, 1975; Steffe and Ford, 1984).

The Metzner and Otto approach is based on the assumption of a direct proportionality between average shear rate in the fluid and rotational speed of the impeller, and the proportionality constant, k',

depending only on the geometry of the impeller. This assumption implies that the investigated fluid has no effect on the proportionality constant. The application of an average shear rate given by the above assumption has successfully been applied in the development of power correlations in mixing vessels. For rheological applications, however, it could lead to significant errors in the evaluation of the rheological behavior of shear-dependent fluids. Hence it is necessary to explore the implications of using the linear shear rate in mixers, to quantify the interaction of the mixer proportionality constant, k', and system geometry as well as fluid properties, and to develop a procedure for evaluating fluid properties (especifically, power-law) using a mixer viscometer.

The movement of solid surfaces (e.g., an impeller) in contact with a fluid causes the fluid to move in some characteristic pattern which results in the development of internal stresses and the application, on the solid surfaces, of characteristic forces which must be contonuously counterbalanced (e.g. by a drive motor) ir order to sustain the fluid motion (Charles, 1978). The nature of the flow pattern and the magnitudes of internal stresses and applied forces depend primarily on the geometry of the system, the rate of fluid motion and the rheological properties of the fluid.

Approximate expressions for the determination of the shear stress and shear rate in a vessel with an impeller can be obtained using approximate geometries (such as the concentric cylinders analogy) for the system, since the complicated geometry of the system makes the solution of the proper set of differential equations of motion a difficult task.

CHAPTER 2

OBJECTIVES

The objectives of this dissertation are:

1. To review and evaluate established mixer viscometry methods.
2. To analyze the influence of system geometry, operating conditions and fluid properties on mixing shear rates when agitating power-law fluids.
3. To obtain expressions for estimation of the shear stress and the shear rate in the mixing systems.
4. To develop a new procedure for rheological characterization of power-law fluids, using mixer viscometry data.

CHAPTER 3

LITERATURE REVIEW

In the food and chemical industry many operations are dependent on effective agitation and mixing of fluids; therefore, an understanding of the phenomena involved in mixing fluids with complex rheology (time-dependency, shear-thinning, elasticity) is increasingly important.

The chapter leads of with a review of certain aspects of the use of mixers and mixing principles to evaluate the rheological behavior of fluid or semi-solid materials and a summary of the developments in the area. The theory of mixing is reviewed in the second part of the chapter.

3.1) USING MIXING TO EVALUATE RHEOLOGICAL PROPERTIES

Use of mixers for rheological evaluation was initially suggested by Metzner and Otto (1957) with the development of a method of approximating power-law parameters for non-Newtonian pseudoplastic (shear-thinning) fluids using an apparent viscosity, η_a calculated from data obtained with a mixing vessel. Their results were verified by Calderbank (1958) and Metzner and Taylor (1960), who observed that local fluid shear rates were found to be directly proportional to impeller speed, for both Newtonian and non-Newtonian fluids, and high shear rates occurred close to the impeller. Saravacos and Moyer (1967) observed similar behavior when studying the rheological parameters of fruit purees in agitated kettles. They found that the apparent viscosity

decreased considerably at high agitation speeds for pseudoplastic fluids and the shear rate at a particular speed of agitation varied with the distance from the center of rotation.

The general principle of measurement used in mixer viscometry is based on the determination of the torque on the shaft of the impeller as a function of its rotational speed. Thus, a suitable value of the apparent viscosity for a non-Newtonian fluid can be obtained from viscometric measurements if a representative value of shear rate $\dot{\gamma}$ in the given vessel can be predicted. It must be noted that due to the relatively complex flow (complex velocity profiles, hence shear rates) established in the mixing vessel, mixer viscometry only results in approximate data and only average values can be determined. The mixing vessel is generally a cylindrical container with numerous possible impeller configurations (Figure 3.1).

3.1.1) Applications of Mixer Viscometry

Mixers for rheological studies have been used by investigators in the food and fermentation areas (Table 3.1). In a review of the equipment used in fermentation studies, Solomons (1971) expressed the need for an "in-situ" measurement system and suggested the possibility of using a rotating impeller instead of the usual "cup and bob" type of viscometer to determine the rheological properties of fermentation cultures. An initial application of a mixer as a viscometer was considered by Bongenaar et al. (1973), who developed a reproducible method of characterizing the rheological properties of mold suspensions using a turbine impeller instead of a rotating cylinder in a rotational

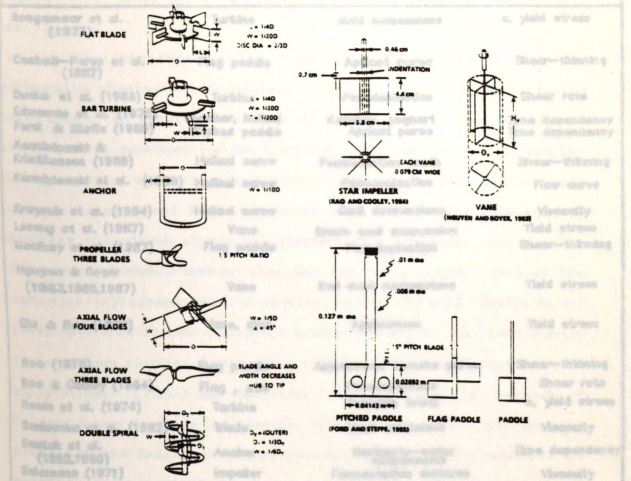

Figure 3.1: Typical Impellers Used In The Determination Of Rheological Properties With A Mixer (Castell-Perez and Steffe, 1989).

Table 3.1: Products And Rheological Characteristics Considered In The Mixing Systems (Castell-Perez and Steffe, 1989).

Reference	Mixing System(s)	Product(s)	Characteristic
Bongenaar et al. (1973)	Turbine	Mold suspensions	σ_0 yield stress
Castell-Perez et al. (1987)	Flag paddle	Apricot puree	Shear-thinning
Ducla et al. (1983)	Turbine	Pseudoplastics	Shear rate
Edwards et al. (1978)	Anchor, helical	Ketchup, yoghurt	Time dependency
Ford & Steffe (1986)	Pitched paddle	Apricot puree	Time dependency
Kemblowski & Kristiansen (1986)	Helical screw	Fermentation broth	Shear-thinning
Kemblowski et al. (1988)	Helical screw	Pseudoplastics	Flow curve
Krayniik et al. (1984)	Helical screw	Coal suspensions	Viscosity
Leong et al. (1987)	Vane	Brown coal suspension	Yield stress
Mackey et al. (1987)	Flag paddle	Pseudoplastics	Shear-thinning
Nguyen & Boger (1983,1985,1987)	Vane	Red mud suspensions	Yield stress
Qiu & Rao (1988)	Vane, star	Applesauce	Yield stress
Rao (1975)	Flag paddle	Applesauce, tomato puree	Shear-thinning
Rao & Cooley (1984)	Flag , star	Pseudoplastics	Shear rate
Roels et al. (1974)	Turbine	Penicillin broth	σ_0 yield stress
Sadowska et al. (1982)	Blade	Meat emulsions	Viscosity
Sestak et al. (1982,1986)	Anchor	Bentonite-water suspensions	Time dependency
Solomons (1971)	Impeller	Fermentation cultures	Viscosity
Steffe & Ford (1985)	Pitched paddle	Apricot puree	Shear-thinning
Steffe et al. (1988)	Flag paddle	Starch slurries	Peak viscosity
Tamura et al. (1988)	Helical screw	Tomato sauce	Viscosity
Vocadlo & Charles (1971)	Grooved cyl.	Kaolin suspensions	Yield stress
Volsey et al. (1977)	Flat paddle	Starch slurries	Peak viscosity
Walker et al. (1988)	Helical	Wheat flour	Peak viscosity
Whalen et al. (1987)	Turbine	Whey-corn mashes	Viscosity
Yoshimura et al. (1987)	Vane	oil-water emulsions	Yield stress

viscometer. This method solved the problem of particle settling and phase separation because the impeller achieved mixing and no water layer was developed adjacent to the impeller blades (Charles,1978). In recent years, many types of rheological behavior have been studied using mixers (Table 3.1): shear-thinning, yield stress, time-dependency, elasticity, etc.

Some investigators have used the mixer concept to determine subjective rheological parameters that are a function of measuring instrument. An example of this is the Ottawa Starch Viscometer (Voisey et al., 1977) developed for measuring the properties of starch slurries during cooking, where the starch slurry is mixed by a flat paddle rotating at constant speed in a stationary bowl. The torque generated by shearing the starch slurry was recorder by a transducer, and the test time was considerably shorter than for other instruments such as the Brabender Amylograph. With a similar concept in mind, Steffe et al. (1989) developed a mixer viscometer system to evaluate the flow behavior of corn starch slurries during gelatinization. The method requires small sample volumes (13 ml.) and short test times. A commercial version of the instrument is being implemented. Walker et al. (1988) described the latest efforts dedicated to the evaluation of pasting behavior of starches. An instrument developed for the wheat industry, the Rapid Visco-Analizer (RVA), uses a disposable cup and plastic paddle, and gives a pasting curve resembling the Brabender curve. The method also requires small sample sizes (25 ml.) and short test times. The instrument has been tested and is comercially available.

Adoption of mixer viscometry techniques has been limited by the relatively high cost of the necessary instrumentation. The performance

of a low cost concentric cylinder viscometer was analyzed by Griffith and Rao (1978). Castell-Perez et al. (1987) developed a low cost mixer viscometer system, based on the Brookfield Viscometer, for determination of the rheological properties of power-law fluids.

Due to the growing interest in on-line instruments for the measurement of rheological properties of fluids during processing, Kemblowski et al. (1988) developed a measuring system consisting of a helical screw impeller rotating in a draught tube, based on torque measurements, for on-line viscometry. Tamura et al. (1988) investigated the applicability of the helical screw rheometer developed by Kraynik et al. (1984) for on-line rheological measurements.

From the point of view of improved process efficiency and quality of the final product, applications of mixer viscometry techniques rather than conventional techniques have been and can be used to successfully investigate the flow properties of food products, with a major potential for semi-solid, suspension-type food materials.

3.2) CALCULATION TECHNIQUES IN MIXER VISCOMETRY - TRADITIONAL METHODS

Various techniques using a mixer viscometer for the determination of the rheological behavior of food materials have been developed and tested. Procedures may vary from the geometry of the mixing system to the type of fluid and rheological behavior considered. Because many food materials, especially the suspension-type, present non-Newtonian flow characteristics, mixer viscometry efforts have dealt primarily with the rheological characterization of non-Newtonian fluids. Specific calculation techniques, summarized in Figure 3.2, are discussed in

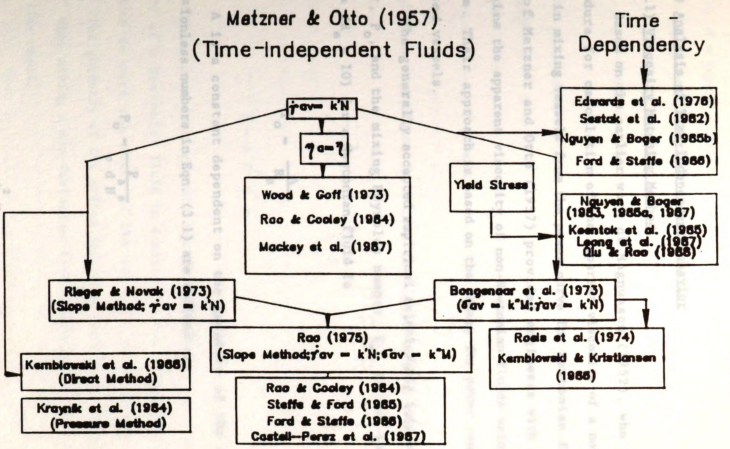

Figure 3.2: Mixer Viscometry Techniques

the following sections.

3.2.1) Analysis of Time-Independent Behavior

3.2.1.1) Viscosity Matching Method

Based on the earlier work of Magnusson (1952), who proposed a procedure for calculation of the apparent viscosity of a non-Newtonian fluid in mixing vessels from the power curve for Newtonian fluids, the work of Metzner and Otto (1957) provided engineers with a method to determine the apparent viscosity of non-Newtonian fluids using a mixing system. Their approach is based on the theory for power consumption in agitated vessels.

The generally accepted empirical relationship between the Power number, P_o, and the mixing Reynolds number, R_e, in the laminar flow region ($R_e < 10$) for a Newtonian fluid is

$$P_o = \frac{A}{R_e} \tag{3.1}$$

where A is a constant dependent on the geometry of the system. The dimensionless numbers in Eqn. (3.1) are defined as

$$P_o = \frac{P}{\rho d^5 N^3} \tag{3.2}$$

and

$$R_e = \frac{\rho d^2 N}{\eta} \tag{3.3}$$

where:

d = impeller diameter, m

N = impeller rotational speed, rev/s

ρ = fluid density, kg/m^3

η = Newtonian viscosity, Pa s

and the power input, P, is related to the torque M exerted on the impeller by

$$P = 2\pi NM \tag{3.4}$$

Combining the equations, the following relationship is obtained,

$$\frac{P}{\rho d^5 N^3} = \frac{A \eta}{\rho d^2 N} \tag{3.5}$$

and

$$P = A d^3 N^2 \eta \tag{3.6}$$

Thus, power measurements can be used to characterize the viscosity of a Newtonian fluid in a mixing system by measuring the torque required to turn the shaft of the impeller at a certain rotational speed. The geometry of the system and fluid density must also be known.

When mixing a non-Newtonian fluid, especially one obeying the power-law model,

$$\sigma = m \dot{\gamma}^n \tag{3.7}$$

where:

σ = shear stress, Pa

$\dot{\gamma}$ = shear rate, 1/s

m = consistency coefficient, Pa s^n

n = flow behavior index, dimensionless

the viscosity increases from a minimum value closer to the impeller to a maximum value in regions far away from the impeller (Ulbrecht and Carreau, 1985). Metzner and Otto suggested that Eqn. (3.1) could be valid for a non-Newtonian fluid if an apparent viscosity, η_a, evaluated at an average shear rate given by

$$\dot{\gamma} = k'N \tag{3.8}$$

were used. Equation (3.8) assumes that the average shear rate around the impeller is proportional to the rotational speed of the impeller, N, being k' the impeller proportionality constant.

Once the average shear rate, $\dot{\gamma}_{av}$, has been calculated, an average apparent viscosity can then be obtained (Nagata, 1975). In their experimental procedure, Metzner and Otto utilized two identical sets of mixing equipment, one containing a Newtonian fluid and the other a non-Newtonian fluid. Using the same impeller speed and varying the viscosity of the Newtonian fluid so that the power measured at each impeller is the same, the apparent viscosities should be the same in both instruments. Thus, they were able to determine the apparent viscosity, η_a, of the non-Newtonian fluid by knowing the viscosity of the Newtonian under identical experimental conditions in the laminar region.

The procedure for data collection and analysis was:

1. Measurement of the torque required to rotate the impeller at a fixed rotational speed (Newtonian and non-Newtonian fluids).
2. Determination of Power Number- Reynolds Number curve for Newtonian fluids. The value of the constant A is determined from the slope of this curve.
3. Determination of power input and Power number, P_o, [Eqn. (3.2)] at each impeller speed N using non-Newtonian measurements in the mixing system.
4. From the curve obtained in (2), read the corresponding R_e and find the viscosity from the expression for the Reynolds number

$$\eta = \frac{\rho N d^2}{R_e} \qquad (3.9)$$

5. Let $\eta = \eta_a$. When the apparent viscosity of the non-Newtonian fluid is obtained, the corresponding average shear rate can be determined from the viscometric curve (σ versus $\dot{\gamma}$ data, obtained with a conventional viscometer), based on the assumption that $\eta = \sigma/\dot{\gamma}$.
6. Calculate the value of the mixer impeller proportionality constant k' at a specific value of the rotational speed N using Eqn. (3.8) , i.e., $k' = \dot{\gamma}/N$

Holland and Chapman (1966) outlined a more complete description of the technique developed by Metzner and Otto (1957):

1. With η_a obtained from Eqn. (3.9), plot η_a versus impeller speed N.
2. Experimentally determine the apparent viscosity of the non-Newtonian fluid in a conventional viscometer at various shear rates.
3. Plot log η_a versus log $\dot{\gamma}$.

4. From the plot of (1), determine the value of η_a at a specified N
5. From the plot of (3), read the value of $\dot{\gamma}$ which gives the same η_a of (4).
6. Plot these values of $\dot{\gamma}$ versus the values of impeller speed N.
7. Obtain the value of k' by measuring the slope of the plot made in step (6).

The "viscosity matching" method assumes the value of k' a constant which depends only on the geometry of the impeller. Even though this assumption has been used by numerous investigators, Metzner and Otto recommended further analysis to determine the effect of the power-law parameters (m and n) in the values of the proportionality constant k'. Wood and Goff (1973) applied the matching viscosities method to estimate the average shear rate in a Brabender Viscograph. The values of $\dot{\gamma}_{av}$ for the impeller were obtained from a plot of shear rate versus the viscosity (or apparent viscosity) of the Newtonian and non-Newtonian fluids. The magnitude of the shear rate where the two viscosities intersect is the average shear rate, $\dot{\gamma}_{av}$ (Wood and Goff, 1973).

An alternative procedure to obtain the average shear rate is by equating the two expressions for the viscosities. Hence,

$$\eta \dot{\gamma}_{av} = m \dot{\gamma}_{av}^{n} \tag{3.10}$$

$$\dot{\gamma}_{av}^{n-1} = \frac{\eta}{m} \tag{3.11}$$

and

$$\dot{\gamma}_{av} = [\eta/m]^{\frac{1}{n-1}} \tag{3.12}$$

This procedure was used by Rao and Cooley (1984) and Mackey et al. (1987) for determination of rheological properties of fluids

characterized by the power-law model.

Mackey et al. (1987) utilized the matching technique to investigate the effect of some parameters on the assumed constant value of k' using a Brookfield Viscometer. From power requirements:

$$\eta_a = \frac{2\pi M}{A d^3 N} = \frac{k_2 M}{N} \tag{3.13}$$

where $k_2 = \frac{2\pi}{A d^3}$, the mixer coefficient, is a constant dependent on the geometry of the system. To find k_2, the torque required to turn the impeller agitating a Newtonian fluid of known viscosity is measured as a function of the rotational speed. Torque M is plotted versus ηN and the slope is equal to $1/k_2$. Thus, the value of constant A from Eqn. (3.13) is determined. It is important to check that R_e <10 (laminar flow assumption).

The rheological properties of the investigated power-law fluids are determined with a rotational cylinder viscometer. Torque versus rotational speed data are also collected with the mixer viscometer. Using Metzner and Otto's approach of matching viscosities,

$$\eta = \eta_a = m(k'N)^{n-1} \tag{3.14}$$

Thus,

$$k' = \frac{1}{N}\left[\frac{k_2 M}{N m}\right]^{\frac{1}{n-1}} \tag{3.15}$$

where k' is a function of the geometry of the system, the rheological properties of the fluid and the operational conditions. The authors observed that the value of k' was significantly affected by the values of the flow behavior index and the rotational speed of the impeller. (At rotational speeds less than 1.05 rad/s (10 rpm), the value of k' was a strong function of n and N). Extensive work should be done to quantify the interaction of these parameters on the proportionality constant and the critical limits for the impeller-to-cup diameter ratio (d/D) must be identified.

3.2.1.2) Linear Shear Stress Method

Bongenaar et al. (1973) developed a technique for characterizing the rheological properties of mold suspensions using a mixer (turbine) viscometer. The instrument consisted of a standard 6-blade Rushton turbine impeller connected to a rotational viscometer and the torque on the impeller was measured as a function of the rotational speed. Data analysis considered that the shear rate was given by Metzner and Otto's (1957) assumption ($\dot{\gamma}_{av} = k'N$) and that the shear stress was directly proportional to the torque M,

$$\sigma_{av} = k''M \qquad (3.16)$$

where k" is a constant independent of the value of n. A constant value of k' (= 10) was selected based on the work done by Calderbank and Moo-Young (1959) for turbine impellers. The rheological parameters of the power-law fluid were determined as follows:

1. The value of the flow behavior index of the unknown suspension, n_x,

is obtained from the slope of the log-log plot of torque, M, versus rotational speed N.

2. To calculate the value of the consistency coefficient, m_x, the properties, n_y and m_y, of a calibration fluid are measured in a conventional rotational viscometer and the following expression is written

$$\frac{M_x}{M_y} = \frac{\sigma_x}{\sigma_y} = \frac{m_x N^{n_x} k'^{n_x}}{m_y N^{n_y} k'^{n_y}} \tag{3.17}$$

Thus,

$$m_x = \frac{M_x}{M_y} \left[\frac{(Nk')^{n_y}}{(Nk')^{n_x}} \right] m_y \tag{3.18}$$

In the case of $n_y = n_x$ (valid when $|n_x - n_y| < 0.1$), Eqn. (3.18) simplifies to

$$m_x = \frac{M_x}{M_y} m_y \tag{3.19}$$

with M_x and M_y as torque values for corresponding fluids measured in the mixer system.

The authors also worked with the η_a, defined as

$$\eta_a = \left(\frac{\sigma}{\dot{\gamma}}\right)_{\dot{\gamma} = \dot{\gamma}_o} \tag{3.20}$$

where $\dot{\gamma}_o$ is an arbitrary standard shear rate. Thus, for a power-law fluid

$$m = \frac{\eta_a}{\dot{\gamma}^{n-1}} \tag{3.21}$$

and

$$\frac{M_x}{M_y} = \frac{\eta_{ax}}{\eta_{ay}} \tag{3.22}$$

The procedure was also applied to fluids obeying the Casson model,

$$\sigma^{0.5} - \sigma_o^{0.5} = \eta_c^{0.5}\,\dot{\gamma}^{0.5} \tag{3.23}$$

with the Casson viscosity, η_c, obtained from the slope of a linear plot of $\sigma^{0.5}$ versus $\dot{\gamma}^{0.5}$. The yield stress, σ_o, is obtained from extrapolation of the M versus N plot, assuming that k' and k" are independent of the Casson rheological parameters. According to Charles (1978), it is not clear if the calculated viscosity is an intrinsic property of the fluid. However, analysis of data is based on well-proven and widely accepted empirical correlations and the method is useful for determining the rheological properties of viscous fermentation broths.

The mixer viscometry technique developed by Bongenaar et al. (1973) was applied by Roels et al. (1974) on their investigation of

fermentation broths. They observed that the use of a mixer prevented phase separation and settling of the particles. Their derivation for data analysis is as follows:

From power requirement theory in the laminar region,

$$P = A\,\eta_a N^2 d^3 \tag{3.24}$$

with A = 64 for a turbine impeller (using Newtonian fluids). Since the power P is related to the torque M,

$$M = \frac{64}{2\pi}\,\eta_a N d^3 \tag{3.25}$$

From measurement of torque M as a function of rotational speed N, the value of the apparent viscosity η_a can be obtained from Eqn. (3.25)

$$\eta_a = \frac{M 2\pi}{64\ N\ d^3} \tag{3.26}$$

Following Metzner and Otto's suggestion that $\dot{\gamma}_{av} = k'N$, with k' a constant and with $\sigma_{av} = \eta_a\,\dot{\gamma}_{av}$, or taking advantage of Eqn. (3.25),

$$\sigma_{av} = \frac{2\pi M k'}{64 d^3} \tag{3.27}$$

Equation (3.27) can also be written as

$$M = C_i\,\sigma \tag{3.28}$$

where:

$$C_i = \frac{64 d^3}{2\pi k'}\ , \tag{3.29}$$

is viewed as an instrument constant.

The measured torque as a function of N and the use of Eqns. (3.8) and (3.28) allows for determination of rheograms for the investigated fluid in the laminar flow region. Also, the apparent viscosity can be calculated from Eqn. (3.26). Different rheological models were analyzed and the authors concluded that the Casson model better described the rheology of a fermentation broth.

This technique requires further testing and results to be compared with those obtained with conventional viscometry methods. It must be emphasized that the impeller proportionality constant, k', was assumed a constant for the particular turbine impeller. When the torque is measured as a function of N, then the constant k' can be found from

$$\frac{\sigma}{\dot{\gamma}} = \eta_a = m\,\dot{\gamma}^{n-1} = m\,(k'N)^{n-1} \qquad (3.30)$$

Kemblowski and Kristiansen (1986) adapted the method developed by Roels et al. (1974) to design a suitable impeller-cylinder system for continuous on-line measurements in fermentation technology. The analysis assumed a two-cylinder system. Thus, in a rotational viscometer, the shear stress σ is given by

$$\sigma = z\,\alpha \qquad (3.31)$$

where:

z = a constant of the instrument, Pa/reading

α = instrument reading

The torque is then determined from the measured shear stress from the following expression: (concentric-cylinders with narrow gap)

$$\sigma = \frac{M}{2\pi l_1 r_m} \tag{3.32}$$

where:

l_1 = inner cylinder length, m

$r_m = (r_1 + r_2)/2$

and r_m = arithmetic mean of the radii of inner and outer cylinders, m

r_1 = inner cylinder radius, m

r_2 = outer cylinder radius, m

Combining Eqns. (3.31) and (3.32),

$$M = a\,\alpha \tag{3.33}$$

where a = instrument constant, N m/reading $= 2\pi l_1 r_m^2 z$ (3.34)

According to Eqn. (3.33), the value of the constant a, obtained from a concentric cylinder system, is used to evaluate the torque for the mixer system on the basis of the reading from the instrument, α. The average shear stress is then obtained from Eqn. (3.32) as

$$\sigma_{av} = \frac{2\pi k' a \alpha}{A\, d^3} \tag{3.35}$$

or

$$\sigma_{av} = Z\,\alpha \tag{3.36}$$

where Z = a constant for a given geometry of the impeller system, Pa/reading

with

$$Z = \frac{2\pi k' a}{A\, d^3} \tag{3.37}$$

The procedure to determine the value of k' for the particular impeller is as follows:

1. For power-law fluids, the shear dependent viscosity is given by Eqn. (3.30) and

$$\frac{2\pi M}{AN d^3} = m(k'N)^{n-1} \tag{3.38}$$

or

$$M = \frac{Amd^3 k'^{n-1}\, N^n}{2\pi} = BN^n \tag{3.39}$$

where B is found from experimental curves of torque versus rotational speed.

2. The value of the proportionality constant k' is now a function of the geometry of the impeller and rheological properties of the fluid, since

$$k' = \left[\frac{2\pi B}{Amd^3}\right]^{\frac{1}{n-1}} \tag{3.40}$$

with A determined from Newtonian P_o versus R_e curves according to Eqn. (3.1).

Eqns. (3.8) and (3.36) allow determination of the curve flow for the investigated fluid. The technique proved to be sensitive and able to detect the variation of rheological parameters, especially the consistency coefficient, m, resulting from the differences in processs parameters. Modifications of the instrument are being made for on-line application. It is important to recognize that this method assumes a narrow gap between the rotating unit and the cup. Hence, care must be taken not to violate this assumption when using a system with geometrical characteristics other than the ones used in this study (six-blade turbine impeller, H/d = 2.7 and 1.8, d/D = 0.93).

3.2.1.3) Slope Method

Based on the initial work of Metzner and Otto (1957), Rieger and Novak (1973) developed a method to determine the value of the impeller proportionality constant for the agitation of highly viscous fluids characterized by the power-law model, in the laminar region of flow. It is called the "slope method" in this study.

From dimensional analysis, the following relationship is obtained

$$\frac{P}{m\, d^{3}\, N^{n+1}} = C(n) \tag{3.41}$$

Using the power relationship given by Eqn. (3.1):

$$P_o = \frac{C(n)}{R_{en}} \tag{3.42}$$

with

$$R_{en} = \frac{d^{2}\, N^{2-n}\, \rho}{m} \tag{3.43}$$

and

$C(n)$ = constant, f(n, geometry)

For a Newtonian fluid,

$$P_o = \frac{A\ \eta}{N\ d^2\ \rho} \tag{3.44}$$

Replacing η with η_a for a power-law fluid,

$$P_o = \frac{A\ m\ (k'N)^{n-1}}{N\ d^2\ \rho} = \frac{A\ k'^{n-1}}{R_{en}} \tag{3.45}$$

Comparing Eqn. (3.45) with Eqn. (3.41),

$$C(n) = A\ k'^{n-1} \tag{3.46}$$

or

$$\log C = \log A - (1-n) \log k' \tag{3.47}$$

with C given by Eqn. (3.41)

The authors suggested that Eqn. (3.8) is valid for a particular impeller only if a plot of log $[P/(md^3N^{n+1})]$ versus (1-n) is a straight line [Eqn. (3.47)]. The slope of this line is equal to -log k'. If the plot were nonlinear, Eqn. (3.8) would be invalid since k' would not exist. Results suggested that the linear shear rate assumption was useful for engineering calculations of power consumption with certain mixer impellers. However, certain dependence of the value of the constant k' with the flow behavior index, n, was observed. This procedure has been tested to determine the average shear rates of food

materials by Rao (1975).

3.2.1.4) Combined Slope and Linear Shear Stress Method

Rao (1975) combined the procedure of Rieger and Novak (1973) for determination of the impeller proportionality constant with the procedure for determination of the rheological properties of power-law fluids developed by Bongenaar et al. (1973). This technique will be called the "Combined Slope and Linear Shear Stress Method" in this review, and it has been utilized with food products by several investigators (Rao and Cooley, 1984; Steffe and Ford, 1985; Ford and Steffe, 1986; Castell-Perez et al., 1987).

The procedure is as follows:

1. Collect torque versus rotational speed data of several non-Newtonian (power-law) fluids and the investigated fluid with the mixer system.
2. Determine the rheological properties of fluids with a concentric cylinder viscometer.
3. Plot log $[P/(md^3N^{n+1})]$ versus (1-n) (Rieger and Novak, 1973) using torque data obtained from mixer system. Find value of proportionality constant k' for that particular impeller at a specific value of rotational speed.
4. Find value of flow behavior index of investigated fluid n_x, from slope of log torque versus log rotational speed data from concentric cylinders.
5. Determine value of consistency coefficient of the investigated fluid m_x, from mixer torque data, fluid properties and k', Eqn. (3.18) (Bongenaar et al., 1973).

Rao and Cooley (1984) compared the mixer viscometry techniques

developed by Metzner and Otto (1957) (Viscosity Matching) and by Rieger and Novak (1973) (Slope) for complex geometry impellers and observed that results obtained from both techniques were in good agreement. They also observed that the "slope method" could lead to large errors when finding the value of k', since

$$k' = 10^{slope} \tag{3.48}$$

The advantage of this method is its relative simplicity as compared to the matching of viscosities required in Metzner and Otto's. However, the "viscosity matching" method seems to yield more consistent values of k' for a particular type of impeller.

3.2.1.5) Methods Using a Helical Screw

3.2.1.5.1) Pressure Difference Method

Using a helical screw, Kraynik et al. (1984) designed an instrument to measure the viscosity of concentrated suspensions of coal particles in organic solvents. This viscometry technique differs from all the others in the fact that it relates the pressure difference in the fluid to the viscosity of the fluid. The instrument is essentially a metering screw pump operating at zero discharge. The sample can be pressurized and the pressure difference is measured across two ports spaced at different heights along the outer wall by a series of pressure transducers (Kraynik et al., 1984).

The authors emphasize the advantages of pressure measurements over torque measurements in high-pressure rotational instruments where fitting seals are required around a rotating shaft that could affect

force measurements. This viscometer has potential in high-pressure viscometry and could be applied to determination of the pressure-dependence of viscosity. It is also suitable for chemically-reacting and heterogeneous fluids. Applications of this technique in on-line viscometry of food products has been investigated by Tamura et al. (1988).

3.2.1.5.2) Direct Determination of The Flow Curve Method

Kemblowski et al. (1988) suggested that the methods of correlation of Power number as a function of the Reynolds number using the Metzner and Otto assumption may be suitable for engineering purposes, but not precise enough for rheological applications. The authors developed a method which enables a direct determination of the flow curve without the need for power data obtained with Newtonian fluids.

The analysis assumes a system of two concentric cylinders to model the impeller system (helical screw impeller rotaing in a draught tube). The torque on the impeller shaft is the combination of the torque resulting from the shearing in the screw channel plus the torque resulting from the shearing in the gap between the edge of the screw flight and the innner surface of the draught tube (Kemblowski et al., 1988). Thus,

$$M = M_1 + M_2 \qquad (3.49)$$

where M_1 – torque resulting from shearing in screw channel, N m

M_2 – torque resulting from shearing in the gap, N m

The technique for determination of the flow curve of the investigated fluid is the following:

1. Using a helical screw impeller rotating in a draught tube as the measuring system, determine the torque M on the impeller shaft as a function of rotational speed N.
2. A log-log plot of M versus N should give a straight line for power law fluids and the slope is equal to n.
3. Calculate the parameters which characterize the geometry of the measuring system :

   A_1 - surface of the screw channel, m^2

   A_2 - surface of the edge of the screw flight, m^2

   d_e - equivalent diameter of the helical screw impeller according to Chavan et al. (1972), m

4. For a given value of rotational speed, the shear rate is determined from Metzner and Otto's assumption that

$$\dot{\gamma}_{av} = k'N \tag{3.8}$$

with $\dot{\gamma}_{av}$ - shear rate on the surface of the "equivalent" cylinder

and

$$k' = \frac{4\pi C r_1}{1 - \psi^2} \tag{3.50}$$

The shear stress is given by

$$\sigma_{av} = \frac{2M}{2Hd_e^2} \qquad (3.51)$$

where:

Cr_1 = correction factor = f(n, ψ) (See Calderbank and Moo-Young, 1959)

H = total height of the inner cylinder, m

M = experimentally determined torque on the impeller shaft during the shearing of the investigated fluid, N m

ψ = geometric ratio, d_o/d_e

d_o = outer cylinder diameter, m

Significant changes of k' with the value of n were observed. Comparison of experimental data with those obtained with a concentric cylinders system showed that the mixing instrument yielded reasonable results. Again, care must be taken when applying this method to different impeller geometries due to the importance of the d/D ratio in the development of the theoretical analysis.

3.2.2) Yield Stress Determination

Knowledge of the yield stress is important in handling, processing and transport of fluids. The presence of a yield stress can affect the settling of particles in concentrated suspensions (Nguyen and Boger, 1983). Also, agitation of such fluids often gives a well-mixed region close to the impeller and a stagnant or near-stagnant fluid in the remainder of the container if the yield stress is not exceeded (Solomon et al., 1981). This well-mixed region around the impeller has been called a cavern (Witcherle and Wein, 1981) and the boundary of the

cavern is defined by the surface where the local shear stress equals the fluid yield stress (Nienow and Elson, 1988).

Nguyen and Boger (1983) investigated the applicability of the use of a vane for yield stress measurements in concentrated non-food suspensions. Haimoni and Hannant (1988) used it on cement slurries.A vane (Figure 3.1) consists of 2-8 thin blades centered around a small cylindrical shaft. This technique has been called the "vane method".

In this technique, the fluid under investigation is placed in a container and the vane (which is attached to the torsional spring-driving motor system of a concentric cylinder viscometer) is fully immersed into the sample, then rotated very slowly at a constant speed, and the torque required to maintain this motion is recorded as a function of time.

The technique detects the yielding moment when the torque exerted on the vane shaft reaches a maximum. The presence of such a maximum in the torque response is a characteristic of yield stress materials which can be explained by the concept of structural deformation and breaking of bonds in flocculated suspensions (Nguyen and Boger, 1985a).

From a torque balance on the surface of the impeller, the yield stress can be calculated from the measured maximum torque, T_m , and the dimensions of the vane, by

$$T_o = \frac{2T_m}{\pi D_v^3} \left[\frac{H_v}{D_v} + \frac{1}{3} \right] \qquad (3.52)$$

where:

T_o = vane yield stress, Pa

T_m = maximum measured torque, N m

H_v = vane height, m

D_v = vane diameter, m

The method provided satisfactory yield stress measurements only if the vane was rotated at sufficiently low speeds. At high speeds, significant viscous resistance together with instrument inertia and insufficient damping may introduce errors to the measured T_m and hence to the calculated value of yield stress. Nguyen and Boger (1983) recommended some operational procedures:

1. Vane should be operated at rotational speeds below 10 rpm.
2. Depth of sample and diameter of the container should be at least twice as large as the length and diameter of the vane to minimize any effects caused by the walls of the container.
3. The vane should be placed at approximately the center of the container.
4. Geometric criteria (Nguyen and Boger, 1985a) for satisfactory measurements:

$$H_v/D_v < 3.5 \quad ; \quad D/D_v > 2.0$$

$$Z_1/D_v > 1.0 \quad ; \quad Z_2/D_v > 0.5$$

where:

D = container diameter, m

Z_1 = clearance from surface to top of impeller, m

Z_2 = clearance from bottom of impeller, m

Values of yield stress obtained with the vane were compared with

those obtained by other methods and the agreement confirmed that the vane method is useful for measuring accurately and directly the true yield stress of concentrated suspensions (Nguyen and Boger, 1985a). The advantageous features of this technique are:

1. Introduction of the vane into the sample does not significantly disturb the sample prior to measurement.
2. Wall slip effects are eliminated and particles remain unsettled.
3. It allows measurement of the yield stress under static conditions and within the material itself.
4. Technique requires short operation time and low cost apparatus.
5. Experiments are easy to perform and of high precision.

Keentok et al. (1985) observed that the vane diameter had negligible effect on the ratio of the diameter of the fracture zone to the diameter of the vane. Their data supports the use of the vane for yield stress measurements if a diameter correction is applied.

Leong et al. (1987) measured the yield stress of brown-coal water suspensions using this technique. Yoshimura et al. (1987) utilized this technique for the measurement of yield stress of oil-in-water emulsions, conducting stress-controlled rather than shear-controlled experiments.

Qiu and Rao (1988) investigated the determination of yield stresses of food materials using a mixer viscometer with the vane method. The authors observed that the magnitudes of σ_o for applesauce were higher than those obtained by extrapolation of the Herschel-Bulkey and the Mizrahi-Berk model,

$$\sigma = \sigma_{om}^2 + \left[K_m \dot{\gamma}^{n_m}\right]^2 \qquad (3.53)$$

where:

σ_{om}^2 = Mizrahi-Berk yield stress, Pa

K_m^2 = constant to be determined, Pa s^n

n_m = flow behavior index, dimensionless

and very similar to those magnitudes of the Bingham yield stress obtained by the common procedure of extrapolation of the linear portion of the shear stress-shear rate data. Two different impellers (a star impeller and a vane) were used and impeller geometry seemed to affect the values of σ_o. The technique proved suitable for the measurement of yield stresses of food suspensions for a specific impeller and rotational speed.

3.2.3) Analysis of Time-Dependent Behavior

A better understanding of the flow properties of time-dependent fluids is essential in handling and process design. For instance, reduction in the viscosity of the material by mechanical treatments prior to pumping may imply lower transport energy requirements and minimization of start-up problems usually associated with occasional pipeline shutdown (Nguyen and Boger, 1985b).

During the mixing process, an element of thixotropic fluid experiences short periods of time at high shear rates close to the impeller and longer periods in the lower shear rate regions remote from the impeller (Edwards et al., 1976). The rheological state of the material will depend upon this shear history and the instantaneous shear rate, which will affect the power requirements for the impeller.

3.2.3.1) Rheological Model Plus Linear Shear Rate Method

Edwards et al. (1976) developed a procedure for the calculation of power consumption with time when a thixotropic fluid is agitated from rest using an impeller which rotates at constant speed. Even though a simplifying assumption, the use of Metzner and Otto's linear relationship ($\dot{\gamma} = k'N$), provided a simple means of predicting the power input-time behavior for thixotropic fluids using the Newtonian data [value of constant A from Eqn. (3.1)] and that for time-independent non-Newtonian fluids (value of impeller proportionality constant, k').

If the thixotropic fluid is agitated for a time t in a mixing container using an impeller at rotational speed N, this is considered to be equivalent to shearing the fluid in a viscometer, from the same starting condition, at the average shear rate for time t. Thus, using the viscometer at constant shear rate, the average apparent viscosity η_a of the thixotropic fluid at time t can be measured. Experimental procedure consisted of:

1. Measurement of torque as a function of time as the impeller rotates at constant speed.
2. Obtaining equivalent η_a/time data in a concentric cylinder viscometer.
3. Calculating k' from a plot of η_a versus N .

Some evidence of the dependence of k' on fluid properties was present but the authors assumed an average value of the impeller constant. They concluded that it was possible to extend the average shear rate ($\dot{\gamma}_{av}$) concept for time-independent non-Newtonian fluids (Metzner and Otto, 1957) to the mixing of thixotropic fluids. The procedure

proved satisfactory for a variety of impellers and thixotropic fluids provided that the impeller was capable of maintaining the entire fluid in motion.

Nienow and Elson (1988) strongly suggested that this approach ($\dot{\gamma}_{av} \propto N$) should be carefully revised when using it for time-dependent fluids, especially shear-thickening fluids due to the still unknown flow behavior of dilatant fluids in mixed vessels. The authors conclude that the method for determination of k' developed by Metzner and Otto (1957) should be carefully revised and even repeated for different fluids and mixing systems.

3.2.3.2) Combined Rheological And Kinetic Model Plus Linear Shear Rate Method

Sestak et al. (1982) developed a procedure for calculating the time-dependent torque necessary for mixing inelastic thixotropic fluids by means of impellers. The relationships of the impeller (anchor agitator) torque versus time for constant rotational speeds when mixing a bentonite-water suspension, were measured. The deformation histories were expressed by means of initial values of the structural parameter, λ_0 , at the beginning of any mixing experiment. A stepwise change of rotational speed was engaged and time-dependent torque values were measured.

A time-dependent apparent viscosity given by

$$\eta_a = \frac{\sigma(t)}{\dot{\gamma}} \qquad (3.54)$$

was used, and an expression for the time-dependency of the impeller torque was obtained,

$$M = \frac{A}{2\pi k'} d^3 \sigma(t) \qquad (3.55)$$

The authors also compared several models of thixotropy and concluded that Cheng's model

$$\sigma = \sigma_{yo} + \sigma_{y1} + \dot{m}\dot{\gamma}^n \qquad (3.56)$$

$$\frac{d\lambda}{dt} = a(1-\lambda) - b\,\dot{\gamma}\,\lambda \qquad (3.57)$$

where:

σ_{yo} = yield stress, Pa

σ_{y1} = shear stress, Pa

λ = time-dependent structural parameter ($f(\dot{\gamma})$), which ranges from an initial value of 1.0 for zero shear time to an equilibrium value, λ_e, which is less than 1.0 (Tiu and Boger, 1974)

a = model parameter, 1/s

b = model parameter, dimensionless

was the best for calculations of the impeller torque-time variations for an arbitrary past deformation history of a thixotropic fluid in a mixing process. The ability of this model to include the influence of the past deformation history upon the instantaneous apparent viscosity of the fluid was also proven.

A more complete analysis was developed by Ford and Steffe (1986), who combined mixer viscometry techniques with a fundamental analysis of thixotropy to determine the basic parameters describing the time-dependent behavior of starch-thickened strained apricots. Tiu and Boger (1974) obtained a model to describe the structural breakdown of a product:

$$\sigma = \lambda \left[\sigma_{yo} + K_o \dot{\gamma}^{n_o} \right] \tag{3.58}$$

where:

K_o = consistency coefficient at time zero, Pa s^{n_o}

n_o = flow behavior index at time zero, dimensionless

λ = structural parameter, accounting for time-dependent effects, dimensionless

σ_{yo} = yield stress at time zero, Pa

with the decay of the structural equation assumed as a second order rate equation:

$$\frac{d\lambda}{dt} = -k_1(\lambda - \lambda_e)^2 \tag{3.59}$$

where:

k_1 = rate constant = $f(\dot{\gamma})$, 1/s

λ_e = equilibrium structural parameter, dimensionless

$\frac{d\lambda}{dt}$ = change in λ with respect to time, 1/s

The relationship between apparent viscosity and time is

$$\frac{1}{\eta_a - \eta_e} = \frac{1}{\eta_{ao} - \eta_e} + a_1 t \qquad (3.60)$$

where:

η_e - apparent viscosity at equilibrium, Pa s

η_{ao} - apparent viscosity at time zero, Pa s

t - time, s

$$a_1 = \frac{k_1 \dot{\gamma}}{\sigma_{yo} + K_o \dot{\gamma}^n} \qquad (3.61)$$

and the value of λ_e was calculated as:

$$\lambda_e = \frac{\eta_e \dot{\gamma}}{\sigma_{yo} + K_o \dot{\gamma}^n} \qquad (3.62)$$

The technique developed by Ford and Steffe (1986) is as follows:

1. Use Metzner and Otto's approximation: $\dot{\gamma}_{av} = k'N$ ($k' = 4.46$ for the paddle impeller used (Steffe and Ford, 1985)).
2. Use the linear shear stress assumption: $\sigma = k"M$ ($k" = 9835$ for the system used (Ford, 1984)).
3. Find an approximate shear stress for the sample, σ_{ax}, given by

$$\sigma_{ax} = \frac{\sigma_s}{M_s} M_x \qquad (3.63)$$

with σ_s - shear stress for standard solution, Pa

σ_x = shear stress for test sample, Pa

M_s = mixer torque when agitating standard solution, N m

M_x = mixer torque when agitating test sample, N m

4. Plot $1/(\eta_a - \eta_e)$ versus time for each sample.
5. From linear regression obtain values of a_1 (slope) and $1/(\eta_a - \eta_e)$ (intercept). [See Eqn. (3.60)]
6. Plot values of a_1 versus $\dot{\gamma}_{av}$.
7. The torque at time zero, M_o, is obtained as

$$M_o = \frac{4.46}{9835\ b} + M_e \qquad (3.64)$$

Equation (3.64) is obtained from $b = 1/(\eta_a - \eta_e)$. Since $\eta_a = \sigma/\dot{\gamma}_{av}$, the value of the slope b becomes, $b = \frac{\dot{\gamma}_{av}}{\sigma_{ao} - \sigma_e}$. Substituting the expressions for the shear rate and the shear stress and manipulating the data yields Eqn. (3.64).

8. Calculate the value of η_{ao} from Eqn. (3.63) using the calculated value of M_o.
9. Plot σ_{ao} versus $\dot{\gamma}_{av}$.
10. Find the values of K_o, n_o and σ_{yo} from linear regression using Herschel-Bulkley model: $\sigma - \sigma_o = \eta\ \dot{\gamma}^{\,n}$.
11. Determine λ_e using Eqn. (3.62).
12. Determine k_1 using Eqn. (3.61).
13. Obtain complete rheological characterization of sample [Eqns. (3.59) and (3.60)].

This technique mathematically describes irreversible breakdown and it proved useful for suspension-type products because the slip at the wall and breakdown problems involving product loading are minimized (Ford and Steffe, 1986).

3.2.3.3) Subjective Assessment of Thixotropy Using a Vane Impeller

When studying the time-dependent rheology of highly concentrated and flocculated suspensions of bauxite residue (red mud), Nguyen and Boger (1985b) found that the concentric cylinder viscometer was unsuitable since the transient data obtained were not reproducible due to the presence of slippage at the walls. A mixing system using a vane impeller was found to be particularly suited for following the time-dependent transformation of the structure of red mud suspensions without causing any significant disturbance to the material. The procedure was as follows:

1. Agitation of the suspension either in a capillary viscometer or in a separate container using an anchor impeller rotating at constant speed.
2. After a determined period of mixing, the impeller is stopped to allow for rheological measurements.
3. Using the vane method (Nguyen and Boger, 1983), the vane is slowly immersed into the sample, then rotated at a speed of 0.1 rpm, and torque measurements are recorded.
4. At the end of the test, the suspension is remixed and the procedure repeated until no further changes in the flow properties are observed.

The vane method was also employed to quantify the thixotropic recovery with resting time. In the recovery experiment, the suspension was allowed to rest undisturbed in closed containers and the yield stress was determined at intervals of resting time (Nguyen and Boger, 1985b).

Experimental results provided a complete description of the thixotropic behavior of highly concentrated red mud suspensions. The drastic reduction in the magnitude of the rheological properties with mixing, and the subsequent slow increase in the yield stress when at rest, may be a way to characterize irreversible thixotropic behavior. Simple thixotropic models were formulated for correlating the experimental results. The same technique was followed to characterize the time-dependent behavior of brown-coal suspensions (Leong et al., 1987).

3.2.4) Elastic Fluids

Many fluid and semi-solid foods exhibit **viscoelastic** behavior, i.e. they exhibit viscous and elastic properties simultaneously. Due to their complex rheology, a complete understanding of the phenomena involved in mixing these fluids is important in industrial operations to ensure proper selection of process and geometrical variables (Ulbrecht, 1974).

Even though the effects of fluid elasticity on agitators are not totally clear, elasticity is known to affect the power required for agitation and to produce differences in the flow fields around the mixing impeller. Generally, it is predicted that the viscoelastic nature of a fluid tends to reverse the direction of secondary flows induced by centrifugal force. White et al. (1977) observed that three different

flow regimes can exist in the mixing tank depending upon the level of viscoelasticity.

3.2.4.1) Power Requirements

In general, mixer viscometry techniques require the measurement of the power required to turn the impeller agitating the fluid. The calculation of torque (power) requirements for mixing viscoelastic fluids is also important in the design of fermentors or processing tanks (Prud'homme and Shaqfeh, 1984). The vast majority of studies on rheology of agitated fluids have focused only on shear viscosity. However, viscosity alone is not sufficient for calculating the torque required to mix a viscoelastic fluid. Thus, it is important to know under what conditions power correlations for viscoelastic fluids differ significantly from those of inelastic fluids.

The classical apparent viscosity approach introduced by Metzner and Otto (1957) for power consumption of non-Newtonian fluids in agitated tanks has been considered by researchers (Table 3.2) to investigate agitation requirements of viscoelastic fluids. Their findings indicate that mere use of the η_a of non-Newtonian fluids may not be applicable in the case of viscoelastic fluids as they exhibit different power consumptions due to their elastic nature. However, there seems to be a controversy as how viscoelasticity affects power requirements in agitated tanks. Other works (mainly theoretical) in mixing of viscoelastic fluids are also listed in Table 3.2.

Mashelkar et al. (1975b) observed that when agitating shear-thinning liquids even having moderate elastic properties, the power

Reference	Mixing System	Phenomenon
Beavers et al. (1980)	Concentric cylinders	Effects of geometry on rod-climbing (Numerical method)
Bohme et al. (1985)	Rotating disc	Weissenberg effect (Numerical)
Chavan et al. (1975)	Turbine	Power consumption
Choplin (1987)	Helical screw	Power consumption in fermentation broths
Collias & Prud'homme (1985)	Turbine	Power consumption
Crochet & Walters (1983)	Various impellers	Weissenberg effect (Numerical)
Dealy & Vu (1977-78)	Turbine	Power consumption
Ducla et al. (1983)	Turbine	Power consumption
Eitelberg (1983)	Concentric cylinders	Effects of geometry on rod-climbing (Numerical method)
Hoffman & Gottenberg (1973)	Cylindrical rod	Weissenberg effect
Joseph et al. (1984)	Cylindrical rod	Weissenberg effect
Kale et al. (1973)	Sphere	Power consumption
Magelli et al. (1986)	Turbine	Power consumption
Mashelkar et al. (1975b)	Turbine	Power consumption
Nienow et al. (1983)	Turbine	Power consumption
Oliver et al. (1984)	Turbine	Power consumption (Boger fluid)
Prud'homme & Shaqfeh (1984)	Turbine	Power consumption (Boger fluid)
Ranade & Ulbrecht (1977)	Turbine	Power consumption
Rieger & Novak (1974)	Turbine	Power consumption
Yagi & Yoshida (1975)	Turbine	Power consumption
Yap et al. (1979)	Helical ribbon	Power consumption

Table 3.2: Studies On Mixing Of Elastic Fluids

consumption is considerably less than that predicted by the classical apparent viscosity approach. The same behavior was observed by Ranade and Ulbrecht (1977) and Oliver et al. (1984). They also found that Metzner and Otto's approach is likely to fail in scaling-up on the basis of power consumption per unit volume due to the different power requirements. The need for extensive experimental work to evolve design procedures under these conditions using the dimensionless groups connected with the elasticity of the fluid was strongly emphasized.

Conversely, other investigators have observed an increase on power requirements when mixing viscoelastic fluids (Nienow et al., 1983; Prud'homme and Shaqfeh, 1984; Collias and Prud'homme, 1985). Nienow and Elson (1988), in a review of the mixing of rheologically complex non-Newtonian fluids in mixing tanks, concluded that viscoelastic properties of the fluid may either decrease or increase the power requirements. They state the impossibility of predicting which because of the complex flow patterns developed in the mixing tank which strongly depend on the geometry of the system and impeller, the type of fluid and the scale of operation.

Yap et al. (1979) assumed Metzner and Otto's method was adequate to describe the viscous properties of the fluid around the impeller blade only for fluids that exhibited low elasticity and for low values of rotational speed. This method assumes that the value of k' [from Eqn. (3.8)] is independent of the fluid and system characteristics. The authors developed an expression for generalized power consumption for fluids with a low degree of elasticity:

$$P_o = 24\, n_b [\, (R_{ge})^{0.93} (D/d)^{0.91} (d/l)^{1.23} \,]^{-1} \qquad (3.65)$$

where:

n_b = number of blades

D = diameter of vessel, m

d = diameter of impeller, m

l = length of impeller blade, m

$$R_{ge} = \text{Generalized Reynolds Number} = \frac{d^2 N \rho \, (t_1 \dot{\gamma}_{av})^{2s}}{\eta_o}$$

with t_1 = fluid characteristic time, s

s = fluid rheological parameter, dimensionless

η_o = limiting viscosity at zero shear rate, Pa s

This model was not successful with fluids showing a high degree of elastic behavior.

Nienow et al. (1983) assumed that the $\dot{\gamma}_{av}$ determined by the method of Metzner and Otto can be applied to parameters other than viscosity when studying the power requirements in aerated vessels. Thus,

$$W_i = \left[\frac{A'}{m} \right] (\dot{\gamma}_{av})^{b'-n} \qquad (3.66)$$

where A' is obtained from $N_1 = A' \dot{\gamma}^{b'}$ correlations. Also, the ratio of elastic to inertial forces can be similarly derived as

$$\frac{W_i}{R_e} = \left[\frac{A'}{\rho N d^2} \right] (\dot{\gamma}_{av})^{b'-1} \qquad (3.67)$$

where W_i = Weissenberg Number = $\frac{\psi_1 N}{\eta}$

ψ_1 = first normal stress coefficient, Pa s^2

The significance of this assumption was not clear from their findings and the authors suggested further work to test their results.

Since most viscoelastic fluids have strong shear-thinning viscosity, power changes may be due to changes in fluid viscosity or elasticity. Boger (1977/1978) observed that maltose syrup-separan solutions were highly viscoelastic fluids which exhibited a nearly constant viscosity with high elasticity (normal stress levels) over a broad shear rate range. This model fluid, called the Boger fluid, has been used to better assess the effects of elasticity on agitated tanks (Oliver et al., 1984; Prud'homme and Shaqfeh, 1984).

Prud'homme and Shaqfeh (1984) developed a correlation that explicitly includes fluid elasticity which provides a basis for assessing whether elastic effects are likely to cause significant increases in mixing torque (or power) requirements. Thus, the total torque is given by the torque that would prevail in mixing a Newtonian fluid times a contribution due to elasticity as follows:

$$\Gamma = (1+ma^{1/4})\ (12.7R_e + 2.41 \times 10^{-3}\ R_e^{\ 3}) \qquad (3.68)$$

[elastic] [Newtonian effects]

where:

Γ = dimensionless torque

and

$$ma = \frac{N_1}{2\ \rho\ r^2\ \omega^2} = \text{elastic parameter}, \qquad (3.69)$$

also called the Aberystwyth Number (Thomas and Walters, 1964)

where:

r = impeller radius, m

N_1 = first normal stress function, Pa

ω = angular velocity of rotation, rad/s

This correlation is based on data in the laminar flow regime and does not account for changes in the geometry of the system and fluid viscosity.

Collias and Prud'homme (1985) found that elasticity substantially increases power requirements of turbine impellers in the viscous (laminar) regime - the torque more than tripled for the most elastic fluid. However, the magnitude of the effect of elasticity depends on both the fluid properties and the size of the vessel. A procedure to determine the additional torque to mix an elastic fluid was developed. Secondary flow patterns are determined by the balance between inertial and elastic forces with

$$E_1 = \frac{\psi_1}{\rho\, d^2} \tag{3.70}$$

and

$$W_i = R_e \cdot E_1 \tag{3.71}$$

where:

E_1 = elasticity Number

A dimensionless torque, T, is determined as,

$$T = \frac{M \rho}{\eta d^2} = f(R_e, E_1) = g(R_e, W_i) \qquad (3.72)$$

for a given geometry. The Torque Number is related to the Power Number by,

$$2\pi T = P_o R_e^2 \qquad (3.73)$$

Viscosity and elasticity data were collected in a cone-and-plate viscometer. A correlation for torque as a function of R_e and E_1 was obtained by determining the $\dot{\gamma}_{av}$ in the vessel at each Reynolds Number using Metzner and Otto's relationship for turbine impellers:

$$\dot{\gamma}_{av} = 11 N \qquad (3.74)$$

Finally, the torque required, at a certain Reynolds Number, to mix a viscoelastic fluid (a mixture of corn syrup, water, glycerin and polyacrylamide polymer (Boger fluid)) using a turbine impeller, was determined by adding the torque required for a Newtonian fluid the additional torque due to elasticity, given by:

$$T = 13.12 R_e + 0.01167 R_e^3 + R_e^3 (71 E_1 - 3200 E_1^2) \qquad (3.75)$$

or, in terms of Weissenberg Number [Eqn. (3.71)]:

$$T = 13.12 R_e + 0.01167 R_e^3 + (71 W_i R_e^2 - 3200 W_i^2 R_e) \qquad (3.76)$$

Equations (3.75) and (3.76) provide quantitative results on the effects of elasticity on mixing torque in the laminar flow regime.

3.2.4.2) The Weissenberg Effect

Another manifestation of viscoelasticity is the climbing of the fluid up a rotating rod associated with nonlinear effects, the normal stress, which does not occur in Newtonian fluids (Joseph et al., 1984). This phenomenon is often called the **Weissenberg effect**. Figure 3.3 illustrates the rod-climbing phenomenon in a vessel agitated by an impeller. When the elastic force is sufficiently high, it overcomes the inertia and the fluid is pulled towards the impeller. Because of the role it may play in rheological testing and processing operations, the possibility of using the Weissenberg effect as a method of characterizing viscoelastic fluids has been investigated (Table 3.2).

Beavers et al. (1980) showed that the free surface deformations on a viscoelastic fluid sheared between two concentric cylinders when the Weissenberg effect occurrs, can be used to determine rheological data about the fluid. They also investigated the effect of the impeller diameter to vessel diameter ratio, using two concentric cylinders. When d/D approached unity, more complex shapes of the free surface occurred and it showed dependence on the rotational speed, N.

Eitelberg (1983) numerically analyzed the influence of the finite length of a rotating cylinder upon the Weissenberg effect. Results indicate that the secondary flow influences the shape of the free surface and that it is affected by the ratio of the distance from the free surface of the fluid to the end of the rotating cylinder, h, to the radius of the outer cylinder, r_2. The main result of this study is that

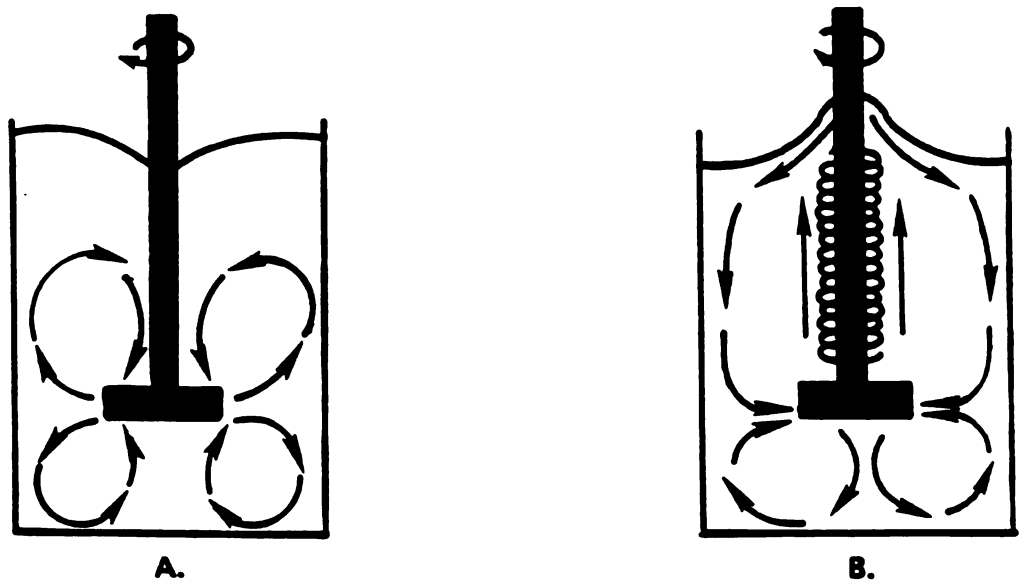

Figure 3.3: Flow Patterns In Agitated Vessels. A) Newtonian Fluid.
B) Elastic Fluid (Rod-climbing).

secondary flow does not reach the free surface if the distance h is considerably greater than r_2.

Even though rod (or shaft) climbing is a sure indication of viscoelasticity, the absence of the Weissenberg effect does not imply that the fluid is inelastic. Nienow and Elson (1988) indicated that certain geometric (shaft diameter) and operational (impeller rotational speed) variables as well as the presence of a yield stress, may reduce the climbing effect.

Available mixer viscometry techniques are considered unsuitable for viscoelastic foods due to the Weissenberg effect (Rao, 1977). However, the need to measure the rheological parameters (particularly elasticity) at the same time as the power data is obtained while agitating the fluids suggests the potential applicability of mixers for the evaluation of rheological properties of viscoelastic fluid foods. Reliable techniques could be developed which consider the effects of geometry on the Weissenberg effect as well as power requirement determination.

3.3) MIXING THEORY

3.3.1) Power Consumption In Mixing Vessels

3.3.1.1) Relation Between Flow Pattern and Power Consumption In A Cylindrical Vessel.

The state of flow in a cylindrical mixing vessel is complicated and there is some turbulence near the impeller blades. For simplicity, it is assumed that the tangential flow is predominant and the flow can be approximated as a type of Rankine's combined vortex (Nagata, 1975). When a low viscosity fluid is agitated in a cylindrical vessel, a cylindrically rotating zone around the central axis of the vessel is formed, where the fluid rotates with the same angular velocity as that of the impeller blade, while the flow in the outer part is similar to that of a free vortex as shown schematically in Figure 3.4a. The central area of the impeller [abcd] is assumed to have no relation to the power consumption and only the outer part (the tips of the impeller) [AadD] and [BbcC] have an important effect upon the power consumption (Nagata et al., 1957).

When a fluid of higher viscosity is agitated, the radius of the cylindrically rotating zone, r_c , decreases and it approaches zero at the transition from turbulent to laminar flow. Thus, the whole impeller area [ABCD] has a relative velocity, u_{rel} , to the fluid and contributes to the power consumption. Other vortices present in the low viscosity region such as V_1 , V_1' , V_2 and V_2' , are weak compared with the forced vortex in the central zone (Figure 3.4a).

In the range of turbulent flow, an impeller has a relative velocity $u_{rel} = AA' - AA''$. Figure 3.4b illustrates the relative velocity

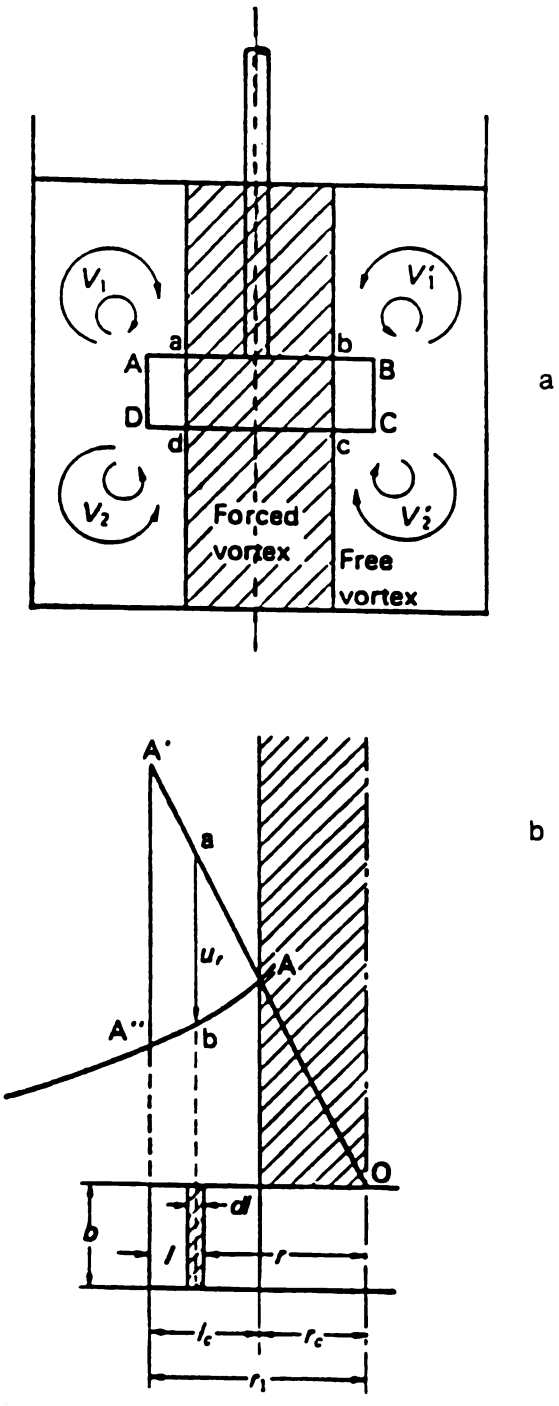

Figure 3.4: a) Simplified Flow Model for Power Correlation; b) Relative Velocity Distribution Between Paddle and Liquid (Nagata, 1975)

distribution in the case of a paddle impeller. The impeller power consumption to maintain the flow is considered as the energy per unit of time to overcome the resisting forces on the blades. The internal resisting force of fluid acting on an element of area bdl may be written as

$$dF = \rho C u_{rel}^2 b\, dl \tag{3.78}$$

where C is assumed to be a constant. When the impeller rotates opposite this resisting force at a relative velocity u_{rel}, the power consumption is expressed by

$$dP = \omega\ dM \tag{3.79}$$

or

$$dP = \omega\ 2r\ dF \tag{3.80}$$

where M = the moment of force acting on the impeller shaft, N m

ω = angular velocity = $2\pi N$, rad/s

r = radial distance from the axis to any section of the impeller

Thus,

$$dP = 4\pi N r\ dF \tag{3.81}$$

Substituting Eqn. (3.78) into Eqn. (3.81),

$$dP = 4\pi N b \rho C u_{rel}^2 r\, dl \tag{3.82}$$

By integration, the power consumption for the impeller is given by

$$P = \int_0^1 4\pi Nb\rho Cu_{rel}^2 r \, dl \qquad (3.83)$$

Integration of Eqn. (3.83) requires an evaluation of u_{rel}, which is a function of the hydrodynamics of the vessel. Thus, the fluid flow induced by a radial type impeller (paddle) rotating in an unbaffled vessel can be described by using the forced and free vortex theory:

$$u_{rel} = 0 \quad \text{when } r < r_c \qquad (3.84)$$

$$u_{rel} = 2\pi N \left(r - r_c^2/r \right) \text{ when } r > r_c \qquad (3.85)$$

where r_c is the radius of the forced vortex cylinder; it is a function of the Reynolds Number and goes to zero at small values of the R_e (laminar region).

An approximate equation for the power input in agitated vessels in the turbulent region is then obtained (Nagata et al., 1957):

$$P_o = \frac{P}{\rho N^3 d^5} = B \left[\frac{10^3 + 0.6fR_e^{\alpha}}{10^3 + 1.6fR_e^{\alpha}} \right]^p \qquad (3.86)$$

where α, p, f and B are the coefficient for the empirical Eqn.(3.86).

In the range of laminar flow, the power consumption increases with the viscosity of the fluid, and can be characterized by the following relationship

$$P_o = \frac{A}{R_e} \qquad (3.87)$$

Following this reasoning, Nagata (1975) developed an approximate equation for the power consumption of paddle impellers in agitated vessels with free surface for the complete range of flow regime. Combining Eqns.(3.86) and (3.87),

$$P_o = \frac{P}{\rho N^3 d^5} = B \left[\frac{10^3 + 0.6fR_e^{\alpha}}{10^3 + 1.6fR_e^{\alpha}}\right]^p + \frac{A}{R_e} \qquad (3.88)$$

[turbulent] [laminar]

with B, A, f, α and p determined experimentally. Equation (3.88) can be applied to wide ranges of Reynolds numbers and to various paddle geometries.

The above analysis is valid only under the following conditions:

1. The agitated fluid is Newtonian.
2. The system consists of a single impeller centered in the axis of a vertical cylindrical vessel with a flat bottom and no baffles.
3. The fluid in the cylindrically rotating zone rotates with the same angular velocity as the impeller.
4. The value of C in Eqn.(3.78) is constant.

3.3.2) Dimensional Analysis for Mixing

Power consumption data have often been correlated using dimensional analysis. The variables which affect fluid motion in mixing are of three types (Chavan and Mashelkar, 1980):

1. geometric (linear dimensions)

2. fluid properties [density (ρ), viscosity (η)]

3. kinematic and dynamic characteristics of flow [velocity (u), gravitational acceleration (g), power (P)]

In mixing with rotating mechanical impellers, the velocity is defined as the linear speed of the tip of the impeller (Rushton et al., 1950), so that

$$u = \pi dN \tag{3.89}$$

where, d = impeller diameter, m

N = impeller rotational speed, rev/s

Power input by the impeller, P, is used to produce the forces in the mass flow and also to overcome the force of gravity, g. The power required to rotate the shaft and blades of the impellers may be expected to be a function of many variables:

$$P = f(\, d,\ D,\ H,\ b,\ c,\ L,\ \rho,\ \eta,\ g,\ N) \tag{3.90}$$

Dimensional analysis (Appendix A) gives the general equation relating the physical variables most often encountered in mixing a Newtonian fluid,

$$\frac{P}{\rho N^3 d^5} = A \left[\frac{d^2 N \rho}{\eta}\right]^{\beta_1} \left[\frac{d N^2}{g}\right]^{\beta_2} \left[\frac{D}{d}\right]^{\beta_3} \left[\frac{b}{d}\right]^{\beta_4} \left[\frac{L}{d}\right]^{\beta_5} \left[\frac{b}{d}\right]^{\beta_6} \left[\frac{c}{d}\right]^{\beta_7} \tag{3.91}$$

The last five terms define the effects of system and impeller geometry. Thus, for geometrically similar systems,

$$\frac{P}{\rho N^3 d^5} = A \left[\frac{d^2 N \rho}{\eta}\right]^{\beta_1} \left[\frac{d N^2}{g}\right]^{\beta_2} \tag{3.92}$$

$$P_o = A (R_e)^{\beta_1} (F_r)^{\beta_2} \tag{3.93}$$

where:

$$P_o = \text{Power Number} = \frac{P}{\rho N^3 d^5} \tag{3.94}$$

$$R_e = \text{Impeller Reynolds Number} = \frac{d^2 N \rho}{\eta} \tag{3.95}$$

$$F_r = \text{Froude Number} = \frac{d N^2}{g} \tag{3.96}$$

White et al. (1934a) first defined the drag coefficient group now known as the Power Number, P_o, which characterizes the flow pattern and represents the ratio of the power dissipated per unit volume to the increase in kinetic energy.

The impeller Reynolds Number, R_e, has significance as a ratio of accelerate force to viscous force. The form [$d^2 N\rho/\eta$] has come into general use for characterizing mixer operations that employ rotating agitators (Hyman, 1962). When agitaing non-Newtonian fluids, the form of the Reynolds Number may vary, as is shown in section 3.2.1.

The Froude Number, F_r, is theoretically required to account for the vortex formation as a result of the influence of gravity in an agitated system. The influence of the F_r on power consumption seems to be important only in unbaffled vessels outside the laminar flow region (Green, 1953). The addition of baffles has little effect on power requirements in the laminar flow region (Treybal, 1956; Nagata et al.,

1957; Blasinski et al., 1970; Nagata, 1975). Also, high viscosity fluids (above 20 Pa s) have sufficient internal resistance to show little if any vortex motion, i.e., the surface of the fluid remains essentially horizontal (Nagata, 1975; Deak et al., 1985).

In general, the influence of the Froude Number on the mixing power requirement is considered negligible and practically non-existent in the laminar region of flow. Thus, the power consumption relationship can be expressed for each flow regions

Laminar flow or fully baffled vessel: $$P_o = A R_e^{\alpha_1} \quad (3.97)$$

Turbulent flow or unbaffled vessel: $$P_o = A R_e^{\alpha_1} F_r^{\alpha_2} \quad (3.98)$$

3.3.3) Laminar Mixing Region

3.3.3.1) Laminar Fluid Motion in Agitated Vessels

In the laminar flow region, the fluid around an impeller moves with the impeller rotation and the fluid distant from the impeller is almost stagnant (Figure 3.5). At very low R_e, there is no turbulent flow and the secondary circulation flow is very weak, so that the momentum transfer from the fluid near the impeller to the more remote parts of the fluid depends mainly upon the molecular viscosity of the fluid and therefore the amount transferred is small and the velocity of remote fluid is low. As the R_e increases, secondary circulation flow occurs and momentum transfer increases (Nagata et al., 1960).

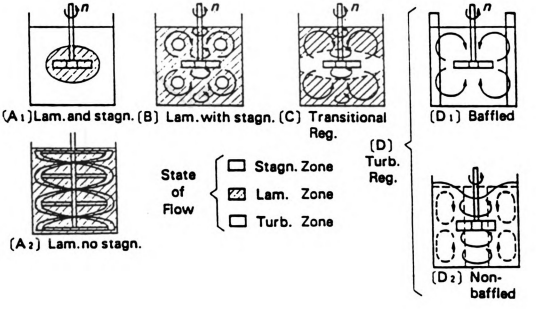

Figure 3.5: Fluid Motion in Agitated Vessels (Nagata, 1975)

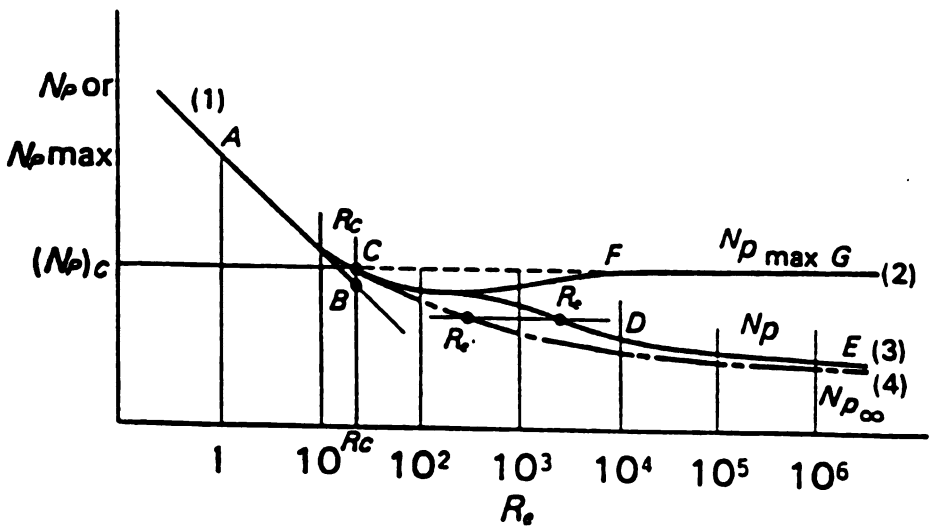

Figure 3.6: Schematic Diagram Showing The Relation Between Power Number and Reynolds Number For a Paddle Impeller (Nagata, 1975).

3.3.3.2) Laminar Flow Criterion

Because of the similarity of the power correlation curves [P_o versus R_e (Figure 3.6)] to the friction factor plot for pipeline flow, the region where the slope is equal to -1 is considered to represent a laminar (viscous) flow region. This has been experimentally verified by numerous researchers. Thus, for all impellers, the laminar flow regime is characterized by a linear decrease in the Power Number (P_o) with Reynolds Number (R_e),

$$P_o = \frac{A}{R_e} \tag{3.99}$$

Applicability of Eqn. (3.99) is limited by the critical value of the R_e which depends on the geometry of the mixed system alone for Newtonian fluids.

3.3.3.2.1) Critical Reynolds Number

In the mixing system, the transition from laminar to turbulent flow proceeds gradually and no distinct critical R_e exists for the flow in an agitated vessel as for other hydrodynamic processes such as pipeline flow (R_e = 2100) and sedimentation (R_e = 1). However, experimental values of the Reynolds Number defining the limit of laminar flow for mixing by mechanical agitators have been determined (Rushton et al., 1950; Green, 1953; Hirsekon and Miller, 1953; Nagata et al., 1957; Pollard and Kantyka, 1969; Nagata, 1975). Results show that the region of purely viscous (laminar) flow extends to R_e numbers from ten to one hundred (10-100) and it seems to be influenced by the geometry of the system (Chavan and Mashelkar, 1980). Thus, it may be incorrect to define

the laminar flow region unless impeller and vessel type is defined. Laminar flow can be achieved throughout the vessel by the correct design of the system, i.e., selecting the correct combination of impeller and vessel geometry, and diameter and rotational speed of the impeller.

The laminar flow region is also a function of the type of fluid being investigated. Metzner and Otto (1957) observed that the region extends to higher Reynolds Numbers in pseudoplastic fluids than in Newtonian fluids. For turbine impellers, a value of $R_e = 10$ was obtained for Newtonian fluids while laminar flow was observed until $R_e = 20$ for power law fluids with $0.25 < n < 0.45$.

The laminar flow region can be limited quite safely by defining $R_e < 10$. When this criterion is satisfied, baffles are not needed and it allows for maximum sensitivity when calculating the average shear rate in the agitated vessel.

When agitating non-Newtonian fluids, especially pseudoplastics, the use of a generalized (modified) Reynolds Number enables the approximate prediction of the power of the impeller at low R_e (Metzner, 1956). The values of the apparent viscosity, η_a, which are functions not only of the fluid properties but also of the conditions under which it is flowing (Begachev et al., 1980), are substituted into the expression for the Reynolds Number [Eqn.(3.95)]. A variety of <u>modified</u> Reynolds Numbers have been used by investigators in mixing studies (Table 3.3), where

$$R_e = \frac{d^2 N \rho}{\eta_a} \qquad (3.100)$$

By analogy with Newtonian fluids, an apparent viscosity is

Table 3.3 Modified Impeller Reynolds Numbers for Mixing of Non-Newtonian Fluids.

Reynolds Number (R_e)	Researchers	Impeller Type
$\frac{d^2 N \rho}{\eta_a}$	Magnusson (1952)	Paddle
	Hiraoka et al. (1979)	
	Rushton & Oldshue (1953)	
	Metzner & Otto (1957)	
	Metzner et al. (1961)	
	Godleski & Smith (1962)	Turbine
	Nienow et al. (1983)	
	Ducla et al. (1983)	
	Reher & Bohm (1970)	
	Hall & Godfrey (1970)	
	Nagata et al. (1971)	Helical
	Prokopec (1972)	
	Edwards et al. (1976)	
	Takahashi et al. (1984)	
	Shamlou & Edwards (1985)	
	Su & Holland (1967)	
	Rieger & Novak (1974)	Anchor
	Bourne et al. (1981)	
$\frac{d^2 N^{2-n} \rho}{m}$	Foresti & Liu (1959)	Turbine
	Metzner & Taylor (1960)	
	Wichterle & Wein (1981)	
	Bourne & Buttler (1969)	
	Chavan et al. (1972, 1975)	
	Chavan & Ulbrecht (1972, 1973)	Helical
	Rieger & Novak (1973)	
	Begachev et al. (1980)	
	Bertrand & Courdec (1985)	Anchor
	Sestak et al. (1986)	

Table 3.3 (cont'd.)

Reynolds Number (R_e)	Researchers	Impeller Type
$\frac{r^2 N^{2-n} \rho}{m}$	Mashelkar et al. (1975)	Disc
$\frac{d^2 N \rho}{\eta_p}$	Sawinsky et al. (1976) (Plastic fluid)	Anchor, Helical
$\frac{d^2 N^{2-n} \rho}{m} [H/h]^n [d/d+D]$	Foresti & Lui (1959)	Turbine Anchor
$\frac{d^2 N^{2-n} \rho}{(k')^{n-1} m}$	Hall & Godfrey (1970) Blasinski & Rzyski (1976)	Helical Turbine, Paddle, Screw
	Nienow et al. (1983)	Turbine
$\frac{N^{2-n} d^2 \rho}{m} \left[\frac{n}{6n+2}\right]$	Calderbank & Moo-Young (1959)	Paddle, Turbine, Anchor
$\frac{d^2 N \rho}{m} [k'N]^{1-n} \left[\frac{4n}{3n+1}\right]$	Calderbank & Moo-Young (1961)	Paddle, Turbine, Anchor
$\frac{d^2 N^{2-n} \rho}{m [a(n-1)]^{n-1}}$	Beckner & Smith (1966)	Anchor
$\frac{d^2 N^{2-n} \rho}{m} (4\pi)^{1-n}$	Pavlushenko & Gluz (1968)	concentric cylinders
$\frac{d^3 N \rho}{\eta D}$	Conti et al. (1981)	Disc Turbine

conveniently defined as follows:

$$\eta_a = \sigma/\dot{\gamma} = m\,(\dot{\gamma})^{n-1} \qquad (3.101)$$

for a power-law fluid. The equation shows that the apparent viscosity, η_a, can be obtained from the known deformation or shear rate, $\dot{\gamma}$.

3.3.4) SHEAR RATE DISTRIBUTION IN A CYLINDRICAL MIXING VESSEL

For non-Newtonian fluids, the apparent viscosity η_a varies throughout the mixing vessel due to variations in the shear rate ($\dot{\gamma}$). For pseudoplastic fluids (power-law fluids with $0<n<1$, also called shear-thinning fluids), the η_a of the fluid in the region near the impeller is rather low and increases progressively at regions away from the impeller. This results in high velocities and velocity gradients in the region near the impeller, which die away rapidly as distance from the impeller increases (Chavan and Mashelkar, 1980).

In rheological studies, a suitable value of the η_a for the non-Newtonian fluid is required. This can be obtained from viscometric measurements if the velocity gradient, i.e., shear rate (at least in the immediate vicinity of the impeller) in the given vessel can be predicted. However, it is precisely the determination of the shear rate in the agitated vessel which presents the main difficulty since it requires the knowledge of the velocity field. The flow of a non-Newtonian fluid in a mixing vessel has as yet not been described analytically because of the very complex flow structure in a vessel with a mixer (Witcherle et al., 1984). It is therefore convenient to use

other methods for determination of the shear rate distribution in a mixing vessel.

Following the idea of Magnusson (1952), Metzner and Otto (1957) proposed the use of an average shear rate ($\dot{\gamma}_{av}$) which is proportional to the impeller speed in pseudoplastic fluids in the laminar-flow region which is given by

$$\dot{\gamma}_{av} = k' N \tag{3.8}$$

The physical concept of the $\dot{\gamma}_{av}$ has been well-established as an important design parameter in the evaluation of the impeller performance and prediction of power consumption (Nguyen, 1983). The $\dot{\gamma}_{av}$ represents the rate of shear which has to exist around the impeller to produce an observed power consumption (Oldshue, 1983). It is important to recognize that it is a simplified approximation. Even though an experimental result, theoretical supporting evidence may be obtained from the expression for the shear rate at the bob of a concentric cylinder viscometer for a pseudoplastic fluid in an infinite cylinder (Ro >>> Ri), (Krieger and Maron, 1954):

$$\dot{\gamma} = \frac{4 \pi N}{n} \tag{3.102}$$

where k', from Eqn. (3.8), would be equal to $\frac{4 \pi}{n}$. Calderbank (1958) experimentally verified the linear relationship of the shear rate around an impeller in the laminar-flow region with the impeller speed, N.

The experimental and theoretical evaluation of the impeller proportionality constant, k', and consequently the rate of shear in the

mixing vessel, has been the subject of many studies. The most common approach is the analysis of a non-Newtonian fluid flowing between two concentric cylinders.

3.3.4.1) Theoretical Expressions For The Rate Of Shear In A Mixing Vessel

3.3.4.1.1) Concentric Cylinders

Expressions for the determination of the average shear rate in a vessel with an impeller have been determined by considering the mixing system as a two-cylinder system, with the impeller as a rotating cylinder.

It is known from theoretical hydrodynamics (Bird et al., 1960) that the generalized Newtonian law of internal friction for an incompressible fluid is

$$\mathbf{T} = 2\eta\,\mathbf{D} \tag{3.103}$$

where

$\mathbf{T}$ = stress tensor, Pa

η = fluid viscosity, Pa s

$\mathbf{D}$ = deformation rate tensor, 1/s

In cylindrical coordinates, equation (3.103) becomes (Bird et al., 1960),

$$\sigma_{rr} = 2\eta \frac{\omega_r}{\partial r}, \qquad \sigma_{r\theta} = \sigma_{\theta r} = \eta \left[r \frac{\partial}{\partial r} \frac{\omega_\theta}{r} + \frac{1}{r} \frac{\partial \omega_r}{\partial \theta} \right] \tag{3.104}$$

$$\sigma_{\theta\theta} = 2\eta \left[\frac{1}{r} \frac{\partial \omega_\theta}{\partial \theta} + \frac{\omega_r}{r} \right], \qquad \sigma_{\theta z} = \sigma_{z\theta} = \eta \left[r \frac{\partial \omega_\theta}{\partial z} + \frac{1}{r} \frac{\partial \omega_z}{\partial \theta} \right] \tag{3.105}$$

$$\sigma_{zz} = 2\eta \frac{\partial \omega_z}{\partial z}, \qquad \sigma_{zr} = \sigma_{rz} = \eta \left[r \frac{\partial \omega_z}{\partial r} + \frac{\partial \omega_r}{\partial z} \right] \tag{3.106}$$

For a rotary motion in steady-state laminar flow, the fluid moves in a circular pattern and only the tangential velocity prevails, i.e., $\omega_\theta = \omega_\theta (r)$ and $\omega_r = \omega_z = 0$. Then, the shear stress, σ, may be written as

$$\sigma_{r\theta} = \sigma_{\theta r} = \eta \, r \frac{\partial}{\partial r} \left[\frac{\omega_\theta}{r} \right] \tag{3.107}$$

For a Newtonian fluid, $\sigma = \eta \dot{\gamma}$, thus

$$\dot{\gamma} = \sigma/\eta = r \frac{\partial}{\partial r} \left[\frac{\omega_\theta}{r} \right] \tag{3.108}$$

Using Eqn. (3.108) an expression for the shear rate at the surface of a rotating cylinder in an infinite Newtonian fluid is obtained as

$$\dot{\gamma} = -4 \pi N \tag{3.109}$$

which relates the shear rate with the rotational speed of the impeller.

Pavlushenko and Gluz (1968) referred to the use of Eqn. (3.108) to determine the average shear rate in mixing <u>non-Newtonian</u> fluids by mechanical impellers. To develop the analysis, the motion of the fluid caused by the rotation of a cylinder is again assumed as an approximate model of the fluid flow produced by mixing with any of the usual impeller types and the problem of the steady motion of a non-newtonian fluid rotating between coaxial cylinders is considered. It is also

assumed that the internal cylinder with a radius Ri rotates at a constant angular velocity ($\omega = 2\pi N$) in a stationary cylinder with a radius of $R_o = (D/d)R_i$. End effects are considered negligible in this analysis.

At low velocities characterizing the flow of non-Newtonian fluids in vessels with impellers, the inertia forces and the pressure gradient have no marked effect on the phenomenon and may be neglected as a first approximation (Pavlushenko and Gluz, 1968). Another assumption is that the flow of the homogeneous, incompressible fluid is planar (because of the symmetry). Then, the following expression is obtained from the equations of motion in terms of stress components (cylindrical coordinates),

$$\frac{1}{r^2}\frac{\partial}{\partial r}(r^2\sigma_{r\theta}) = 0 \qquad (3.110)$$

This equation can be rewritten as

$$\frac{1}{r^2}\left[2r\sigma_{r\theta} + r^2\frac{\partial\sigma_{rr}}{\partial r}\right] = 0 \qquad (3.111)$$

Integrating Eqn.(3.111) once leads to,

$$r^2\sigma_{r\theta} = C_1 \qquad (3.112)$$

For a power-law fluid, $\sigma = m\dot{\gamma}^n$. Thus, the $\sigma_{r\theta}$ component of the stress tensor in cylindrical coordinates is,

$$\sigma_{r\theta} = -m \left[r \frac{\partial}{\partial r} \left[\frac{\omega_\theta}{r}\right] + \frac{1}{r} \frac{\partial \omega_r}{\partial \theta} \right]^{n-1} \left[r \frac{d}{dr} \left[\frac{\omega_\theta}{r}\right] \right] \qquad (3.113)$$

Using equation (3.112), this yields

$$C_1 = mr^{2+n} \left[\frac{d}{dr} \left(\frac{\omega_\theta}{r}\right)\right]^n \qquad (3.114)$$

After integration, $\omega_\theta = C_2 r^{(n-2)/n} + C_3 r$ (3.115)

Using the following boundary conditions:

(i) $\omega_\theta = 2\pi NRi$ at $r = R_i$ (3.116)

(ii) $\omega_\theta = 0$ at $r = R_o$

the expression for the angular velocity becomes

$$\omega_r = 2\pi Nr \left[\frac{1 - \left[\frac{R_o}{r}\right]^{2/n}}{1 - \left[\frac{R_o}{R_i}\right]^{2/n}} \right] \qquad (3.117)$$

and the expression for the shear rate is

$$\dot{\gamma} = r \frac{d}{dr} \left[\frac{\omega_\theta}{r}\right] = r \frac{d}{dr} \left[2\pi N \left[\frac{1 - \left[\frac{R_o}{r}\right]^{2/n}}{1 - \left[\frac{R_o}{R_i}\right]^{2/n}} \right] \right] =$$

$$-\frac{2}{n} 2\pi N \left[\frac{1}{1 - \left[\frac{R_o}{R_i}\right]^{2/n}} \right] \left[\frac{r}{R_o}\right]^{-2/n} \qquad (3.118)$$

At $r = R_i$, the expression simplifies to

$$\dot{\gamma} = - \frac{4\pi N}{n} \left[\frac{(D/d)^{2/n}}{1 - (D/d)^{2/n}} \right] \qquad (3.119)$$

Considering $\dot{\gamma} = k'N$, then

$$k' = - \frac{4\pi}{n} \left[\frac{(D/d)^{2/n}}{1 - (D/d)^{2/n}} \right] \qquad (3.120)$$

Equation (3.119) determines the average shear rate in a vessel with a mixer as a function of the rheological properties of the fluid, the mixing conditions, and the geometrical characteristics of the system and should give more accurate results for mixing of non-Newtonian (pseudoplastic) fluids than the use of the equation developed for Newtonian fluids [Eqn.(3.109)].

3.3.4.1.2) Empirical And Theoretical Expressions For The Impeller Proportionality Constant, k'

The suggestion of Metzner and Otto (1957) of a constant value of the impeller constant, k', which is a unique function of the geometry of the system has been questioned and other expressions for the constant have been determined (both theoretically and empirically) for the mixing of non-Newtonian (mostly pseudoplastic) fluids.

Expressions for the impeller proportionality constant, k', are summarized in Table 3.4. Looking carefully at the expressions, it seems that the value of k' can be a function of the geometry of the system (impeller shape and size, vessel size), the rheology of the fluid (values of shear-thinning index (n) and consistency coefficient (m) or

Table 3.4. Empirical and Theoretical Expressions for Determination of the Impeller Proportionality Constant, k'.

k'	Researcher	Impeller Type
	EMPIRICAL EXPRESSIONS	
$\dot{\gamma}/N$ = constant	Metzner and Otto (1957)	Turbine, paddle
	Used by: Roger & Bohm (1970), Bongenaar et al. (1973), Roels et al. (1974), Nagata (1975).	Helical, turbine, Turbine, paddle
ς (1-n)	Beckner & Smith (1966)	Anchor
$\varsigma = f(H_2/d)$		
slope of $\log [P/(mN^{n+1}d^3)]$ versus (1-n)	Rieger & Novak (1973)	Anchor, helical
	Used by: Rao (1975),	Flag
	Rao & Cooley (1984),	Flag, star
	Steffe & Ford (1986),	Pitched paddle
	Castell-Perez et al. (1987)	Flag
$35\, n^{\frac{n}{1-n}}$	Sestak et al. (1976)	Anchor
$\frac{2\pi}{\eta} \frac{1}{1-(d/D)^2}$	Hiraoka et al. (1979)	Paddle
$(4)^{\frac{1}{1-n}} (d/D)^2 (1/d)$	Yap et al. (1979)	Helical ribbon (viscoelasticity)
13.5 N + 4.43	Nguyen (1983)	Anchor
$\alpha (H_2/D)^{\beta}(s/D)^{\gamma}(w/D)^{\delta}$	Takahashi et al. (1984)	Helical ribbon

Table 3.4 (cont'd.)

k'	Researcher	Impeller Type
$\exp[4.2\ (d/D) - 0.5]$	Deak et al. (1985)	Ribbon
$34 - 144\ (c/D)$	Shamlou & Edwards (1985)	Helical ribbon
$\left[\frac{2\pi C}{Amd^3}\right]^{1/(n-1)}$	Kemblowski & Kristiansen (1986)	Six-blade turbine
$(1/N)\left[\frac{AM}{Nm}\right]^{1/(n-1)}$	Mackey et al. (1987)	Flag
THEORETICAL EXPRESSIONS		
$\left[\frac{4n}{3n+1}\right]^{n/(n-1)} B$	Calderbank & Moo-Young (1959, 1961)	Anchor (conc. cylinders)
$\frac{\frac{6\pi}{n}}{1 - (d/D)^{3/n}}$	Bourne (1965)	Sphere
$\frac{\beta\pi d}{0.5\ (D-d)}$	Mizushira et al. (1966)	Cylinders
$\frac{4\pi}{n}\left[\frac{(D/d)^{2/n}}{1 - (D/d)^{2/n}}\right]$	Pavlushenko & Gluz (1968)	Conc. cylinders
$4\pi\left[\frac{n\ (1 - (d/D))^{2/n}}{1 - (d/D)^2}\right]^{1/(1-n)}$	Bourne & Butler (1969)	Helical ribbon (Conc. cyl.)

k'	Researcher	Impeller Type
$\frac{\pi}{\sqrt{2}}\,[d/(d-D)]$	Mitsuishi & Hirai (1969)	Helical ribbon (parallel plates)
$\left[\frac{(4\pi)\,(D/d)^{n-1}\,-\,0.75}{n^n\,[\,(D/d)\,-\,0.75]^n}\right]^{\frac{1}{0.9(n-1)}}$	Schilo (1969)	Anchor
$\frac{\pi d}{H_2}$	Prokopec (1972)	Screw type
$\left[\frac{Ad}{\pi D^2 H}\right]^{1/(1-n)}\left[\frac{n\,[\,(D/de)^{2/n}\,-\,1]}{4\pi}\right]^{n/(1-n)}$	Chavan & Ulbrecht (1972)	Helical Screw (conc. cyl.)
$2\,\pi\left[\frac{\left[\eta_w\,\overline{(\omega_w\,+\,2)}\right]}{[\omega_w+\,2\,]_N}\,NN\right]^{1/(n-1)}$	Hiraoka et al. (1979)	Paddle (Numerical)
$4\pi\,[n\,(1-\eta^{2/n})]^{-1}$	Sinevic et al. (1986)	Coaxial cyl.
$2/n$	Nguyen & Boger (1987)	Vane
$\frac{4\pi\,C_{r1}}{[1\,-\,(1/\psi)^2]}$	Kemblowski et al. (1988)	Helical Screw (Conc. cyl.)

viscosity) and the operating conditions (impeller rotational speed). The geometry of the system also plays an important role, especially the ratio of diameters, d/D. This is particularly true for the theoretical expressions. In addition, the various expressions presented in Table 2.2 indicate the importance of the type of impeller to be used in the mixing process. This should be expected since the shape of the impeller affects the shear field in the agitated vessel.

Hall and Godfrey (1970) and Nagata (1975) confirmed that impeller pitch, and number of blades have no significant influence on the values of the impeller constant but it is greatly influenced by impeller size. The effect of the impeller height has been considered negligible by some investigators [White and Brenner (1934), Nagata (1975)].

The value of the shear-thinning index, n, also seems important in the determination of k'. This should be expected since the shear rate at a given distance from the impeller has been found to be slightly greater for a larger impeller (smaller D/d ratio) (Metzner and Taylor, 1960) and the more shear-thinning the fluid, the greater the difference.

CHAPTER 4

THEORY: ALTERNATIVE METHOD TO EVALUATE MIXER VISCOMETER DATA

This chapter consists of the presentation of the theoretical aspects for the development of a procedure for the rheological characterization of non-Newtonian (power-law) fluids with a mixer viscometer. The experimental verification of the developed procedure is presented in Chapter 6.

4.1) DETERMINATION OF FLOW CURVES

Traditional mixer viscometry techniques present two main disadvantages. First, the need for calibration with Newtonian fluids (P_o vs R_e curves) and secondly, the use of a simplifying assumption for the average shear rate ($\dot{\gamma}_{av} = k'N$), with k' a function of impeller geometry only. Taking into account these disadvantages, the application of these techniques in rheology has been questioned (Kemblowski et al., 1988; Nienow and Elson, 1988) and the need for new procedures to evaluate the rheological behavior of power-law fluids has been suggested.

The main purpose of this chapter is to develop a new procedure for direct determination of the flow curve (shear stress-shear rate relationships) of power-law fluids using a low-cost mixer viscometer.

The existing literature presents a similar attempt by Kemblowski et al. (1988) for a system of complex geometry (a helical screw impeller rotating in a draught tube) for application to fermentation broths using sophisticated instrumentation. Other attempts [Bongenaar et al., 1973; Rao, 1975; Metz et al. (1979); Kemblowski et al. (1986)] require

calibration with Newtonian fluids using power correlation methods. Expressions for the shear rate and shear stress of power law fluids have been developed for a disc spindle (Williams, 1979) but no attempts have been made for geometries such as the paddle or the flag impeller.

4.1.1) Shear Stress and Shear Rate Approximations

The movement of solid surfaces (e.g., an impeller) in contact with a fluid causes the fluid to move in some characteristic pattern which results in the development of internal stresses and the application, on the solid surfaces, of characteristic forces which must be continuously counterbalanced (e.g. by a drive motor) in order to sustain the fluid motion (Charles, 1978). The nature of the flow pattern and the magnitudes of internal stresses and applied forces depend primarily on the geometry of the system, the rate of fluid motion and the rheological properties of the fluid.

Approximate expressions for the determination of the shear stress and shear rate in a vessel with an impeller can be obtained using approximate geometries for the system, since the complicated geometry of the system makes the solution of the proper set of differential equations of motion a difficult task.

4.1.1.1) Model Systems

Consider the measuring system shown in Figures 4.1A and 4.1B. It consists of an impeller (paddle or flag) of height b and diameter d, rotating in a cylindrical cup, with the impeller replaced by a cylinder with the same dimensions of the impeller, b and d. The following assumptions were made for the model system:

i) the fluid is purely viscous and obeys the power-law model, $\sigma = m(\dot{\gamma})^n$.

ii) the fluid flow produced by stirring with any impeller type is approximated to the steady motion of fluid caused by the rotation of a cylinder [i.e., the impeller is replaced by a cylinder whose dimensions are equal to those of the impeller (d and b)].

iii) the shearing due to the immersed section of the impeller shaft is negligible.

iv) the resistance to flow caused by the top and bottom of the impeller is negligible.

The first of these assumptions can be readily checked. Assumptions (ii) and (iii) imply that the cylindrical model is sufficient to describe the viscometric flow induced by a rotating impeller and that the sheared surface of rotation is cylindrical. Even though this is not so, this approximation is reasonable for the purposes of this study. The adequacy of assumption (iv) will be tested in this investigation.

Also, since the complicated geometry of the impeller system does not allow for determination of the shear rate and shear stress at a fixed point of the system, average values should be used instead.

4.1.1.2) Shear Rate Approximations

The expression for the shear rate at the surface of a rotating cylinder in an infinite Newtonian fluid is

$$\dot{\gamma}_b = 4\pi N \qquad (4.1)$$

which relates the shear rate at the bob of the cylinder, $\dot{\gamma}_b$, with the

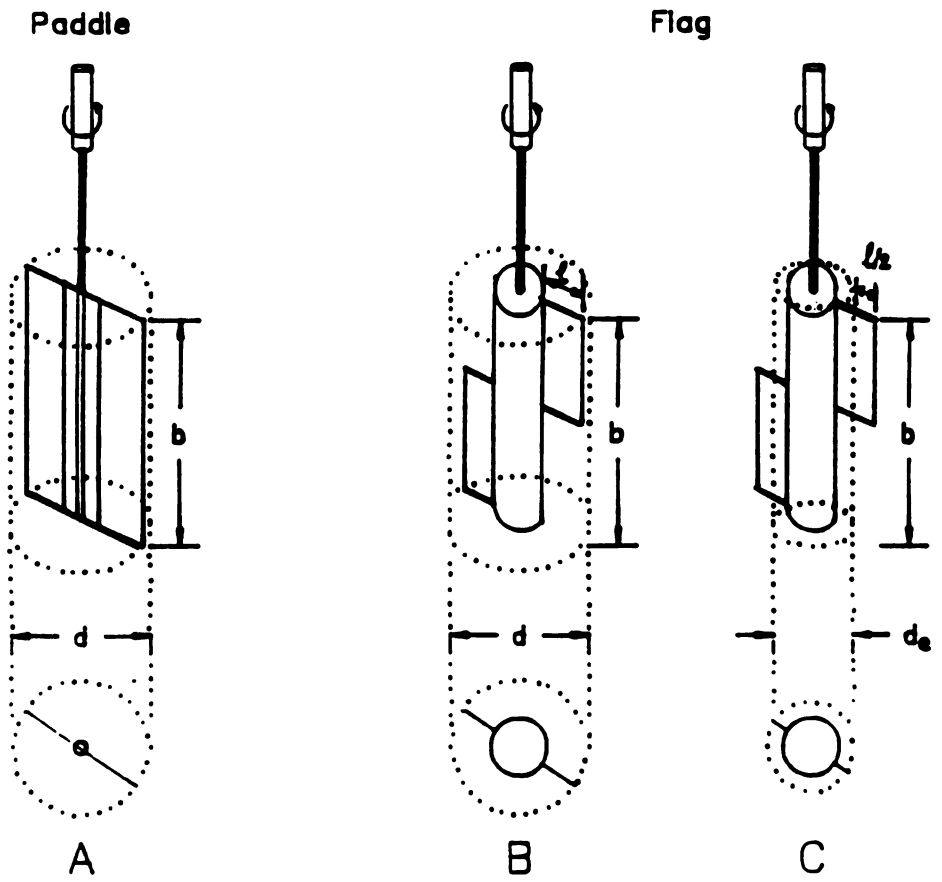

Figure 4.1: Model Systems. A) Paddle Impeller; B) Flag Impeller; C) Flag Impeller (Model 3)

rotational speed (rev/s) of the impeller, N.

Krieger and Maron (1954) worked on the shear rate problem for non-Newtonian fluids sheared within the (narrow) gap of a Couette viscometer by solving the corresponding equations of motion for a cylindrical system. The resultant shear rate equation for a fluid obeying the power-law is,

$$\dot{\gamma}_b = \frac{2\Omega}{n}\left[\frac{R_c^{2/n}}{R_c^{2/n} - R_b^{2/n}}\right] \qquad (4.2.1)$$

or

$$\dot{\gamma}_b = \frac{2\Omega}{n}\left[\frac{(R_c/R_b)^{2/n}}{(R_c/R_b)^{2/n} - 1}\right] \qquad (4.2.2)$$

with Ω = $2\pi N$ = angular velocity, rad/s

R_c = outer cylinder (cup) radius, m

R_b = innner cylinder (bob) radius, m

n = power-law index, dimensionless

N = cylinder rotational speed, rev/s

Equations (4.2.1) and (4.2.2) show the dependence of the shear rate at the surface of the rotating cylinder on the flow behavior index and the system geometry.

It is possible to approximate the complex situation of an impeller rotating in a tank by assuming that all fluid elements are exposed to an

"average shear rate" during the mixing process. Pavlushenko and Gluz (1968) considered approximating the shear rate in a mixing system with Eqn. (4.2.1) and (4.2.2) [See section (3.3.4.1.1) for the development] and the shear rate at the impeller (cylinder) surface is written as,

$$\dot{\gamma}_b = \frac{2\Omega}{n} \left[\frac{(D/d)^{2/n}}{(D/d)^{2/n} - 1} \right] \qquad (4.3.1)$$

or

$$\dot{\gamma}_b = \frac{4\pi N}{n} \left[\frac{(D/d)^{2/n}}{(D/d)^{2/n} - 1} \right] \qquad (4.3.2)$$

where

D = cup diameter, m

d = impeller diameter, m

The previous equations assume a dependence of the shear rate at the surface of the impeller on fluid properties, impeller speed (rpm) and system geometry, in a form identical to that of a cylindrical impeller. Thus, from Eqns. (4.3), an expression for the average shear rate in the real measuring system (a vessel with a mixer) is expected to present a similar form (but somewhat different due to the differences in geometry) to that of Eqn. (4.3.1) and (4.3.2) as follows:

$$\dot{\gamma}_{av} = \left\{ \beta_1 \left[\frac{(D/d)^{\alpha_1}}{(D/d)^{\alpha_2} - 1} \right] [b/d]^{\alpha_3} \right\} N \qquad (4.4)$$

where β_1 is a constant and, α_1, α_2 and α_3 are parameters dependent on the power-law index, n.

Equation (4.4) differs from Equations (4.2.1), (4.2.2), (4.3.1) and (4.3.2) in the addition of the term which takes into account the effect of impeller variation (i.e., impeller height, b). Equation (4.4) may also be written in the familiar form of the linear dependence of the average shear rate in a mixer on rotational speed, proposed by Metzner and Otto (1957),

$$\dot{\gamma}_{av} = k'N \tag{3.8}$$

with

$$k' = \beta_1 \left[\frac{(D/d)^{\alpha_1}}{(D/d)^{\alpha_2} - 1} \right] [b/d]^{\alpha_3} \tag{4.5}$$

where k' is the impeller proportionality constant, dependent on the system geometry (cup and impeller) and the rheological behavior of the fluid. The average shear rate of an impeller (paddle or flag) can be expected to be a function of these parameters.

Also, a direct relationship between the average shear rate and the geometric dimensionless numbers [(D/d) and (b/d)] can be expressed as follows:

$$\dot{\gamma}_{av} = \beta_1 \, [\, (D/d)^{\alpha_1} \, (b/d)^{\alpha_3} \,] N \tag{4.6}$$

where

$$k' = \beta_1 \left[(D/d)^{\alpha_1} (b/d)^{\alpha_3} \right] \qquad (4.7)$$

with β_1 a constant and, α_1 and α_3 parameters dependent on the power-law index, n. Eqn. (4.6) differs from Eqn. (4.4) in the simplification of the (D/d) term with the consequent elimination of α_2 . Thus, Eqn. (4.6) makes the (D/d) term a more significant parameter since the terms under brackets in Eqn. (4.4) is close to one.

In the case of a flag impeller (d/b= constant in this investigation), Eqn. (4.6) can be rewritten as follows:

$$\dot{\gamma}_{av} = \beta_1 [D/d]^{\alpha_1} \quad N \qquad (4.8)$$

and

$$k' = \beta_1 [D/d]^{\alpha_1} \qquad (4.9)$$

with β_1 and α_1 similar to Eqn. (4.6).

Equations (4.4) to (4.9) allow for determination of the average shear rate in the mixing system as a function of impeller and cup geometry and fluid properties for each value of the impeller rotational speed, N.

In summary, this section presents a series of equations which allow estimation of the average shear rate, $\dot{\gamma}_{av}$, when agitating a power-law fluid with an impeller (paddle or flag). The development of the equations for the average shear stress will be presented in the next section.

4.1.1.3) Shear Stress Approximations

4.1.1.3.1) Model 1 (Concentric cylinders analogy with negligible end effects)

Consider a stationary cylindrical cup of large radius, with laminar flow at the surface of the rotating inner cylinder of diameter d. The fluid exerts a tangential force on the outer cylinder while the inner cylinder exerts such a force on the fluid in contact with it. This force is transmitted through the fluid from one layer to the next. At any point in the fluid, the tangential force divided by the surface area on which it acts is defined as the shear stress, σ.

The torque (proportional to the drag offered by the fluid when the cylinder is rotated) on the shaft resulting from the rotation of the inner cylinder may be regarded as a sum of two parts: M_w , resulting from the shearing in the cylindrical wall, and M_e , resulting from the shearing in the two end surfaces. Thus,

$$M = M_w + 2M_e \tag{4.10}$$

or,

$$M = (2\pi rb)\sigma r + 2(2\pi r^2 \sigma) \tag{4.11}$$

with

σ = shear stress from fluid, Pa

b = inner cylinder height, m

r = any radius (in fluid) from axis, m

Taking into account assumption (iv), the second term of the right-hand side of Eqn. (4.11) is eliminated and Eqn. (4.11) becomes

$$M = 2\pi b r^2 \sigma \qquad (4.12)$$

At the innner cylinder wall (r=R),

$$M = 2\pi b R^2 \sigma_w \qquad (4.13)$$

with σ_w = shear stress on the wall of the inner cylinder, Pa

Let $\sigma_w = \sigma_{av}$ (since the shear stress cannot be determined at a fixed point). With R = d/2 , Eqn. (4.13) becomes

$$M = 2\pi b (d/2)^2 \sigma_{av} \qquad (4.14)$$

where M = torque on the shaft resulting from the rotation of the inner cylinder of diameter d and height b, (N m), i.e., the experimentally determined torque on the impeller shaft during the shearing of the fluid.

σ_{av} = average shear stress on the surface of the inner cylinder, Pa

The average shear stress, σ_{av} , can then be determined from Eqn. (4.14) as follows,

$$\sigma_{av} = \frac{2M}{\pi b d^2} \qquad (4.15)$$

Equation (4.15) represents the average shear stress in the real measuring system (impeller rotating in a cylindrical cup).

4.1.1.3.2) Model 2 (Concentric cylinders analogy with end effects)

The validity of assumption (iv) is questionable when the diameter of the outer cylinder is small and, therefore, the effect of the end surfaces of the system (top and bottom) become significant. The theoretical development for an approximate expression for the average shear stress takes advantage of the analysis used by Nguyen and Boger (1983) for the vane shear approach as a starting point and is as follows.

The total torque measured is composed of one component due to shearing on the cylindrical wall and another to shearing at the two end surfaces. The diameter of the cylindrical connecting rod is small in comparison with the paddle diameter and so the measured torque is due to the paddle surface only. The torque balance is given by

$$M = M_w + 2M_e \tag{4.16}$$

or

$$M = (2\pi Rb)\sigma_w R + 2\left[2\pi \int_0^R \sigma_e(r)\, r^2\, dr\right] \tag{4.17}$$

where

M = measured torque, N m

R = impeller (cylinder) radius, m

b = impeller (cylinder) height, m

$\sigma_e(r)$ = shear stress at the end surface (a function of radial

position r), Pa

σ_w = shear stress at the cylindrical wall, Pa

The main assumption of this approach is that σ_e is uniformly distributed over both end surfaces and that σ_e is equal to σ_w at the cylindrical wall. Thus, $\sigma_e = \sigma_w$, and integration of Eqn. (4.17) yields

$$M = [(2\pi)R^2 b]\sigma_w + 4\pi \int_0^R \sigma_w r^2 \, dr \tag{4.18}$$

$$M = [(2\pi)R^2 b]\sigma_w + 4\pi \, (r^3/3) \Big|_0^R \, \sigma_w \tag{4.19}$$

Equation (4.19) can be rewritten in terms of the impeller diameter, d. Thus,

$$M = [(\pi/2)d^2 b]\sigma_w + 4\pi \, \frac{d^3}{24} \, \sigma_w \tag{4.20}$$

Finally,

$$M = \frac{\pi d^3}{2} \left[\frac{b}{d} + \frac{1}{3}\right] \sigma_w \tag{4.21}$$

Assuming that the average shear stress is equal to the shear stress at the cylindrical wall ($\sigma_w = \sigma_{av}$), the dependence of the average shear stress in the real measuring system can be written as follows:

$$\sigma_{av} = \frac{M}{K} \tag{4.22}$$

with $$K = \frac{\pi d^3}{2}\left[\frac{b}{d} + \frac{1}{3}\right], \qquad (4.23)$$

an impeller parameter dependent on the impeller dimensions only. Equations (4.22) and (4.23) indicate that the σ_{av} can be calculated from the measured torque, M, and impeller dimensions (d and b).

Even though the assumption of uniformly distributed σ_e is valid only for a extremelly small cylinder ($d \to 0$), Nguyen and Boger (1985) demonstrated that the error involved in using Eqn. (4.22) is not significant when compared to an assumed relationship for the shear stress at the end surfaces, i.e.,

$$\sigma_e(r) = (r/R)^p \sigma_w, \text{ when } 0 \le r \le R \qquad (4.24)$$

where p = parameter (≥ 0). The two boundary conditions to be satisfied are:

$$\sigma_e = 0 \quad \text{at } r = 0 \qquad (4.25)$$

$$\sigma_e = \sigma_w \text{ at } r = R \qquad (4.26)$$

Integrating Eqn. (4.17), after the introduction of Eqn. (4.24) yields

$$M = (2\pi R^2 b)\,\sigma_w + 2\left[2\pi \int_0^R [r/R]^p r^2\, \sigma_w dr\right] \qquad (4.27)$$

$$M = (2\pi R^2 b)\,\sigma_w + 4\pi\sigma_w \int_0^R \frac{r^{p+2}}{R^p}\, \sigma_w dr\Bigg] \qquad (4.28)$$

$$M = (2\pi R^2 b)\,\sigma_w + \frac{4\pi\sigma_w}{(p+3)}\,\frac{R^{p+3}}{R^p}\Bigg|_0^R \qquad (4.29)$$

$$M = (2\pi R^2 b)\,\sigma_w + \frac{4\pi\sigma_w}{(p+3)}\,R^3 \qquad (4.30)$$

Rewriting Eqn. (4.30) in terms of the impeller diameter, d,

$$M = \frac{\pi d^3}{2}\left[\frac{b}{d} + \frac{1}{p+3}\right]\sigma_w \qquad (4.31)$$

The second term in the parentheses in Eqn. (4.31) accounts for the error involved when using impellers (cylinders) of finite diameter, d. If p = 0, Eqn. (4.31) yields Eqn. (4.21) (uniform shear stress distribution case).

4.1.1.3.3) Model 3 (Flag Impeller)

Because of the more complicated geometry of a flag impeller another model can be considered as shown in Figure 4.1C. The reasons for this alternative model are due to the particular geometry of the impeller, which consists of a central cylinder with two blades attached. Thus, the impeller is now replaced by an inner cylinder with an equivalent diameter d_e, where d_e is equal to half the length of each impeller blade plus the diameter of the cylindrical section, d_c. Thus,

$$d_e = 2\,(\tfrac{1}{2}\ell) + d_c \qquad (4.32)$$

with ℓ = blade length, m

Following the same analysis for the System Model 1 [concentric cylinders analogy with negligible end effects; Section (4.1.1.3.1)], the corresponding expression for the average shear stress in the cylindrical surface is given by

$$\sigma_{av} = \frac{2M}{\pi b d_e^2} \tag{4.33}$$

with d_e = equivalent diameter of ideal system model, m [Eqn. (4.32)]

b = cylinder height, m

In a similar manner, the expression for the average shear stress for the System Model 2 [Concentric cylinders analogy with end effects; Section (4.1.1.3.2)], is as follows:

$$\sigma_{av} = \frac{M}{K_s} \tag{4.34}$$

with

$$K_s = \frac{\pi d_e^3}{2}\left[\frac{b}{d_e} + \frac{1}{3}\right] \tag{4.35}$$

In summary, a series of equations for approximation of the average shear stress, σ_{av}, when agitating a power-law fluid with an impeller (paddle or flag) have been determined based on an analogy with the concentric cylinders case.

CHAPTER 5

MATERIALS AND METHODS

This chapter is divided into four main sections. The first section describes the equipment and the materials used for the data collection. In the second section, the procedure and the experimental design are presented. The third and fourth sections present the procedure for calculations using traditional and the new mixer viscometry methods, respectively.

5.1) EQUIPMENT AND MATERIALS

The Brookfield RVTD and HBTD mixer viscometers were monitored by a data acquisition system and torque responses were collected every two seconds. Six impellers (five paddles and one flag) and three sample cups were utilized in this investigation. Four Newtonian fluids and three Non-Newtonian fluids were selected as the main fluids.

5.1.1) The Brookfield Mixer

The Digital Brookfield Viscometer (Brookfield Engineering Laboratories, Inc., Stoughton, M.A.), is a rotational viscometer that measures the torque required to rotate an immersed element (the spindle) in a fluid. The spindle is driven by a synchronous motor through a calibrated spring and the deflection of the spring is indicated by a digital display. For a given viscosity, the viscous drag, or resistance to flow (indicated by the degree to which the spring winds up), is

proportional to the spindle's speed of rotation and is related to the spindle's size and shape (geometry).

Two digital viscometers, the Brookfield RVTDV-I and the Brookfield HBTDV-I were used in this investigation. The calibration spring torque were 7187 dyne cms and 57496 dyne cms (full scale), respectively. Eight rotational speeds (0.5 to 100 rpm) were selected. These viscometers are guaranteed to be accurate within 1% of the range in use (when utilizing the display reading) and have a sensitivity and reproducibility of 0.2%. Digital viscometers include a 0-10mV (or 0-1V) output signal for continuous data collection.

5.1.2) Data Acquisition System

The output signal from the Brookfield Viscometer was sent to a Data Acquisition System (Dianachart PC-Acquisitor Model PCA-14, Dianachart Inc., Rockaway, NJ). The acquisitor (A/D board with 48 channels) is connected to a IBM PC by using a parallel printer cable. The viscometer torque voltage was measured and stored onto a floppy disk. Software provides continuous on-screen display of measurements and a series of data handling alternatives. Published accuracy is ±0.02% of range (0.3μV-10V). Measurements were stored at two second intervals. When the experiment was completed, the disk data was read into a spreadsheet using LOTUS 1-2-3 and printed in tabular form.

5.1.3) Impellers and Cups

The impellers (Figure 5.1) were constructed from standard Brookfield spindle shafts (300 series stainless steel) shortened to the required length. The paddle impeller blades were ground from a solid

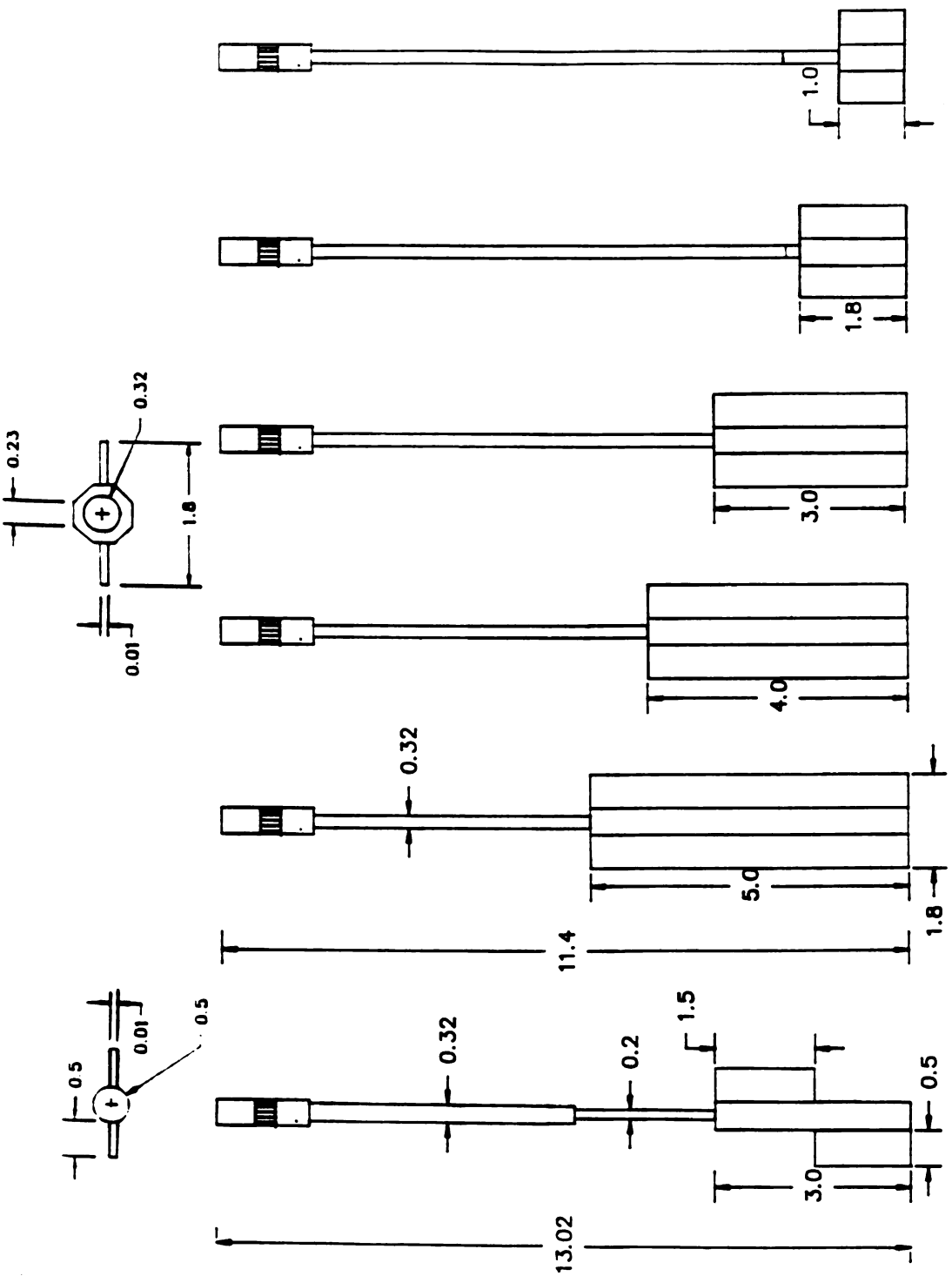

Figure 5.1: Paddle and Flag Impellers (all dimensions are in cm).

piece of stainless steel that had been drilled to allow a press fit on to the shaft. The flag impeller was supplied by Brookfield Engineering Laboratories as a component of a commercial version of the instrument described by Steffe et al. (1989).

The fluid containers (Figure 5.2) consisted of cylindrical cups, with flat bottoms, made with acrylic tubing (United States Plastic Corp., Lima, OH) cut to desired lenghts. The base of the cups and the standard base were constructed from a plastic sheet extruded from cellulose acetate butyrate plastic (United States Plastic Corp., Lima, OH). These materials guarantee high optical clarity, high impact resistance as well as light weight. Cups were constructed with fluid jackets for temperature control.

5.1.4) Fluids

Two types of fluids were used in this study, Newtonian and non-Newtonian fluids. The Newtonian fluids consisted of four Brookfield Viscosity Standards: non-toxic silicone fluids calibrated at 25°C (77°F) with viscosities of 100 cp, 993 cp, 4840 cp and 12200 cp (0.1-12.0 Pa s). The non-Newtonian fluids consisted of 1.0%, 1.5% and 2.0% (dry basis) concentrations of aqueous solutions of Hydroxypropyl Methylcellulose Premium (Methocel, Dow Chemical Co., Midland, MI).

5.2) EXPERIMENTAL DESIGN AND PROCEDURE

5.2.1) Design of Experiment

Data were collected to assess the variability in torque measurements (needed for further data analysis) introduced by the

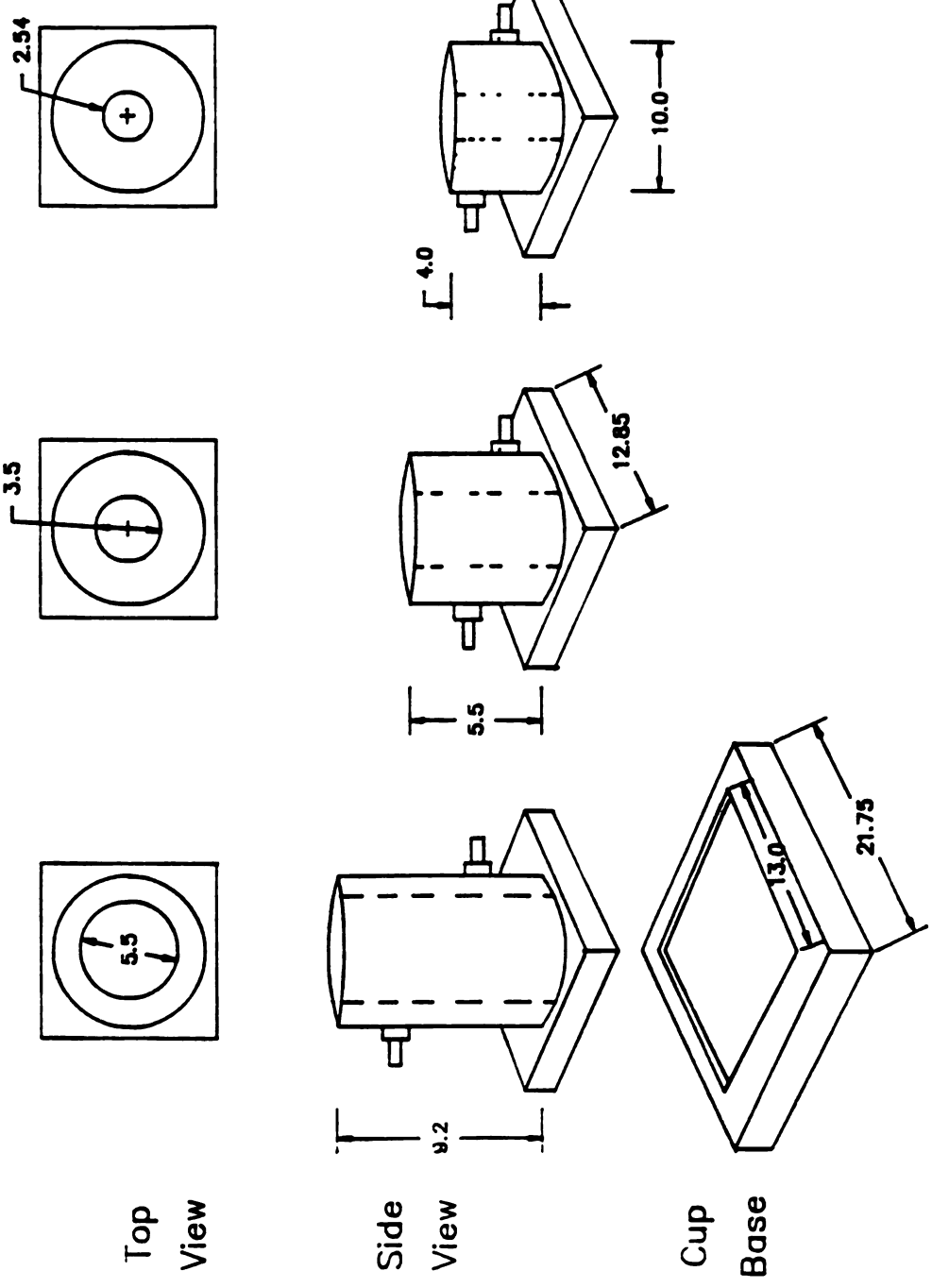

Figure 5.2: Sample Containers and Cup Base (all dimensions are in cm).

impeller and cup changes. Six impellers and three cups were used in a total of 13 treatment combinations. Tests were conducted in duplicate and the order was determined by randomization. Table 5.1 shows the different impeller/cup combinations investigated in this study. Impeller diameter, d,(Figure 5.3) was kept constant due to problems during manufacture of the paddles. The impeller blade height b, was varied to investigate the effect of impeller size. Three sample cups of different diameter, D, were used with a range of d/D ratio from 0.3 to 0.7.

To not vary a large number of geometric constants at once, the length of the sample cups was maintained at L = 1.5D. The fluid level, H, in the cups was kept at H = 1.2D. This distance was selected to keep all impellers sufficiently immersed in the fluid to avoid surface waves, especially for the bigger impellers. Preliminary tests showed that the position of the impeller, that is, the distance between the bottom of the impeller and the bottom of the cup, c, had no significant effect on torque readings when placed close to the top, in the middle, or close to the bottom. For practical considerations, impeller depth (c) was set at c = 0.5d since it made possible the immersion of the impellers under sufficient volume of fluid. The effect of the distance from the surface of the fluid to the top of the impeller's blade was assumed negligible as in Nagata (1975). The effect of different impeller shape was investigated by using a flag impeller (Figure 5.1).

5.2.2) Procedure

5.2.2.1) Preparation of Non-Newtonian Fluids

Aqueous solutions of Hydroxypropyl Methylcellulose were prepared by heating distilled water to 70°C (158°F) and slowly pouring the

Table

Table 5.1: Experimental Design.

SYSTEM	GEOMETRICAL DIMENSIONS [cm]			DIMENSIONLESS VARIABLES	
	D	d	b	d/D	d/b
		Paddle Impellers			
1	5.55	1.8	1.0	0.327	1.8
2	5.55	1.8	1.8	0.327	1.0
3	5.55	1.8	3.0	0.327	0.6
4	5.55	1.8	4.0	0.327	0.45
5	5.55	1.8	5.0	0.327	0.36
6	3.50	1.8	1.0	0.515	1.8
7	3.50	1.8	1.8	0.515	1.0
8	3.50	1.8	3.0	0.515	0.6
9	2.54	1.8	1.0	0.709	1.8
10	2.54	1.8	1.8	0.709	1.0
		Flag Impellers			
1	5.55	1.5	3.0	0.273	0.5
2	3.50	1.5	3.0	0.429	0.5
3	2.54	1.5	3.0	0.591	0.5

where: D = cup diameter
d = impeller diameter
b = impeller blade height

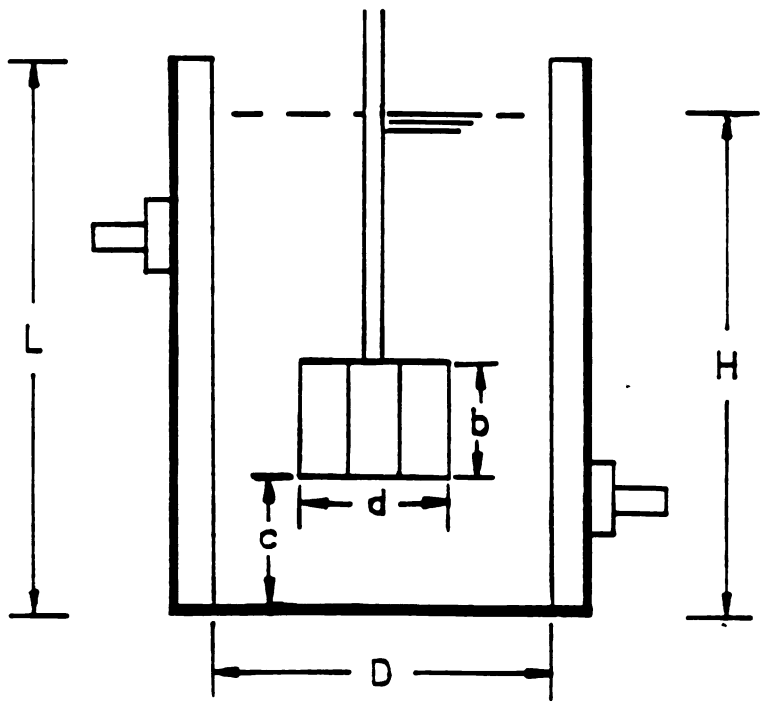

Figure 5.3: Mixing System

pe

Co

to

5.

Ha

se

co

ag

To

va

re

ev

be

ob

us

la

ex

(7

5.2

St

Wi

he

percent weight of sample into the water. Mixing was carried out with a Corning PC-351 Hot-Plate Stirrer. Solutions were cooled down and allowed to rest for a period of 24-48 hours to eliminate air bubbles.

5.2.2.2) Determination of Rheological Properties of Non-Newtonian Fluids

Rheological behavior of the materials was determined with a Haake RV-12 concentric cylinder viscometer with M-500 head and the MV-I sensor (d/D=0.90). The viscometer is interfaced to a Hewlett-Packard 85 computer and a 3457 data acquisition system. The samples were previously agitated for a period of 10 minutes to check for thixotropic behavior. Torque was monitored as a function of time and reached an equilibrium value after the completion of the test for all samples. Triplicate replications of torque versus rotational speed data were collected for every sample at 1-120 rpm (0.105-12.57 rad/s). The values of the flow behavior index, n, and the consistency coefficient, m (Table 5.2), were obtained from shear stress-shear rate data, with shear rate evaluated using the method developed by Krieger (1968). The fluids showed power-law behavior and no elastic characteristics, such as rod climbing. The experiments were carried out at a constant temperature of 25°C ± 1°C (77°C).

5.2.2.3) Calibration of Brookfield Viscometers

The viscosity of a Newtonian standard (Brookfield Viscosity Standards) was determined with the RVTDV-I and the HBTDV-I Brookfield Viscometers and cylindrical spindle # 7 (0.32 cm diameter, 5.37 cm height) to ensure proper instrument performance and high accuracy.

5.5.2.4) Data collection

Figure 5.4 illustrates the overall experimental system. Once loaded into the cup, the temperature of the fluid was controlled with a constant-temperature water bath connected to the cup jacket with standard tubing and fittings. Temperature of the sample was allowed to equilibrate up to 25°C (77°F). To ensure proper alignment of the impeller and cup system, a standard base enabled proper placement of the cups. A guard leg was initially utilized to determine the proper alignment of the impellers but removed before data collection. A selected impeller was immersed in the ution to a fixed mark with care to avoid excessive entrainment of air bubbles. The torque reading at a selected rotational speed was measured after steady state was reached (constant readings). Readings were collected during one minute at the specific value of rpm. For any given run, the rotational speed varied (a stepwise increase) and the range of rotational speed was the operating range of the viscometers (0.5, 1.0, 2.5, 5, 10, 20, 50, and 100 rpm). The tests were done in duplicate and the reproducibility of results was very high.

Neither surface waves nor vortex formation occurred in any of the impeller/cup/fluid combinations which satisfied the laminar flow condition ($Re<10$). After completion of the test (data collected with impeller rotating at 100 rpm), the impeller was removed and the next impeller was tested.

The above procedure was repeated for all systems and fluids. Results will be presented and discussed in the following chapter.

Table

S
S
S
S

(
(
(

[1] Means

Table 5.2: Rheological Properties of Sample Fluids

Newtonian Fluids (Brookfield Standards)		
Fluid	η (Pa s)	ρ (kg/m^3)
Standard 1	0.093 ± 0.001	928.570
Standard 2	0.923 ± 0.001	930.000
Standard 3	4.840 ± 0.001	966.829
Standard 4	12.200 ± 0.001	969.421

Non-Newtonian Fluids			
Fluid	m[1] (Pa s^n)	n[1]	ρ (kg/m^3)
CMC 1%	6.492 ± 0.03	0.504 ± 0.01	974.800
CMC 1.5%	28.417 ± 0.02	0.374 ± 0.007	1025.870
CMC 2%	59.275 ± 0.02	0.352 ± 0.003	1144.280

[1] Means of three replications for 0-2 rev/s for Haake Viscometer data.

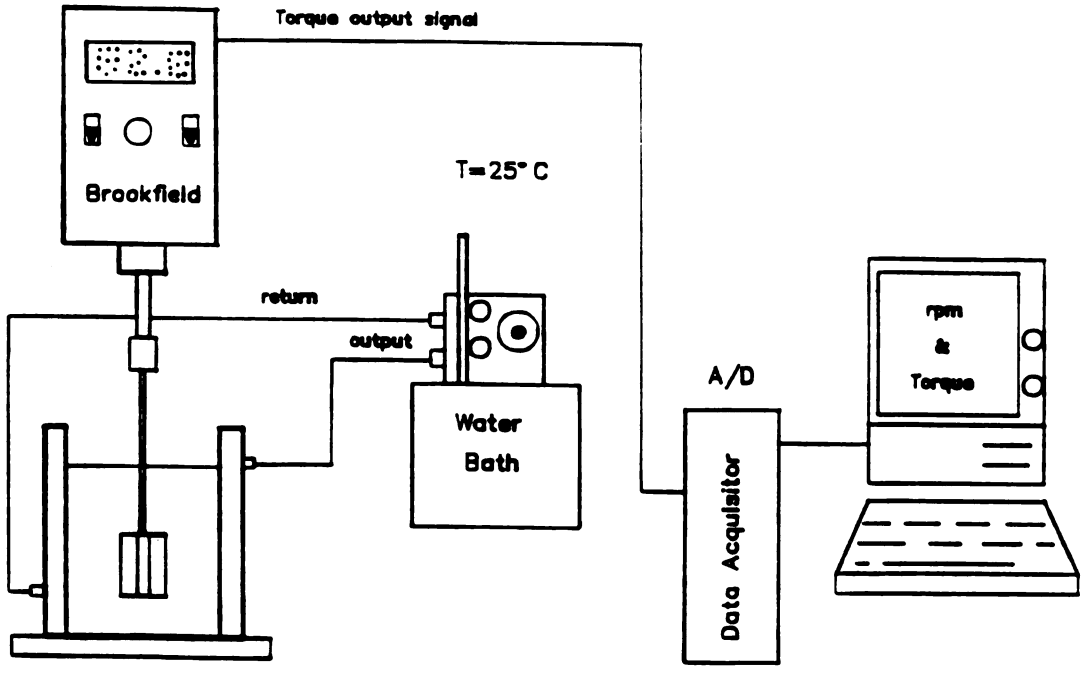

Figure 5.4: Schematic Diagram of Experimental System

5.3) CALCULATIONS USING TRADITIONAL MIXER VISCOMETRY METHODS

Three commonly used mixer viscometry methods were used for determination of the impeller proportionality constant, k', (thus, average shear rates) in the mixing system. The procedures are outlined in Chapter 3.

5.3.1) Viscosity Matching Methods

The procedure for the two matching methods: [Metzner and Otto, 1957; and Mackey et al., 1987] is outlined in Section (3.2.1.1). The main equations used in these methods are Eqns. (3.1), (3.8) and (3.15). Expressions for the P_o versus R_e relationships were developed for each impeller/cup combination for both the Newtonian and the non-Newtonian (power-law) fluids. Also, values of k' were determined as a function of fluid properties and system geometry.

5.3.2) Slope Method

The procedure is outlined in Section (3.2.1.3). The main equations are Eqns. (3.41), (3.45) and (3.47). Values of the impeller proportionality constant, k', were determined as a function of system geometry.

5.4) CALCULATIONS USING NEW MIXER VISCOMETRY METHODS

5.4.1) Determination of Average Shear Rate

The procedure for determination of the average shear rate in the mixing systems is as follows:

1) Using the values of k' obtained with traditional mixer viscometry methods, a model was found by fitting the data using stepwise regression. Thus, the values of β_1, α_1, α_2 and α_3 from Eqns. (4.31) through (4.35) were obtained for each impeller/cup combination and fluid under study and expressions for the average shear rate were obtained.
2) The values of k' obtained with traditional methods are plotted versus the values of k' calculated using the equations above. The equation which gives the better agreement is considered the best equation for approximation of the average shear rate in the mixing system.

5.4.2) Determination of Average Shear Stress

1) To check the applicability of the shear stress equations [Eqns. (4.6), (4.13) and (4.24)], the values of torque calculated from the corresponding equations are compared with the experimentally measured values of torque using the impeller (mixing) system. Hence, the torque equations for the paddle impellers are,

$$M = 2\pi b\,(d/2)^2\,\sigma_{av} \qquad (4.5)$$

for the concentric cylinders analogy with negligible end effects. When end effects are considered, the equation for torque is the following:

$$M = \frac{\pi d^3}{2}\left[\frac{b}{d} + \frac{1}{3}\right] \qquad (4.12)$$

F

M

w

n

ẏ

e

2) P

b

w

t

3) D

f

5.4.

foll

(shea

1) Me

ro

2) De

th

3) Se

For the flag impellers, the above equations apply in addition to Model System 3 ($d = d_e$),

$$M = 2\pi b \, (d_e/2)^2 \, \sigma_{av} \qquad (4.36)$$

where $\sigma_{av} = m \, (\dot{\gamma}_{av})^n$, for a fluid of known rheological properties, n and m. Thus, using the values of n and m and the expression for $\dot{\gamma}_{av}$, the values of an σ_{av} are obtained for use in the torque equations.

2) Plot calculated torque versus experimental torque. The equation that best represents the shear stress relationship in the mixing system will then be the one which gives better estimates of the experimental torque values.
3) Develop flow curves (average shear stress- average shear rate curves) for a set of geometric parameters (D, d and b).

5.4.3) Procedure for the use of a mixer viscometer to directly determine the rheological properties of power-law fluids

On the basis of the considerations presented in Chapter 4, the following procedure is proposed for the determination of the flow curve (shear stress-shear rate relationship) of a power-law fluid:

1) Measure the torque on the impeller shaft, M, as a function of rotational speed, N, using the mixer viscometer.
2) Determine the value of the flow behavior index, n, from the slope of the log-log plot of M vs. N.
3) Select the appropriate equations for the average shear rate and shear

stress in the mixing system by following the steps outlined in Sections (5.4.1) and (5.4.2).

4) For a given value of rotational speed, measured values of torque and known system dimensions, determine the average shear stress, σ_{av} , for the investigated fluid using the appropriate equation.

5) For a given value of rotational speed, known system dimensions and the value of the flow behavior index of the fluid, n, determine the average shear rate, $\dot{\gamma}_{av}$, using the appropriate equation.

6) Repeat steps 4) and 5) for the complete range of rotational speeds of the viscometer.

7) Evaluate the flow curves (rheograms) by plotting the σ_{av} versus the $\dot{\gamma}_{av}$, for the investigated fluid in log-log coordinates. The intercept of the log-log plot is the fluid consistency coefficient, m, in Pa s^n.

CHAPTER 6

RESULTS AND DISCUSSION

The results of the experimental investigation are presented and analyzed in this section. In the first part, results obtained with traditional mixer viscometry methods for estimating the average shear rate are presented and discussed. In the second part, results from the proposed method are described and its suitability determined for rheological characterization of power-law fluids. A procedure for using the Mixer Brookfield Viscometer with Newtonian fluids is presented in Appendix C.

6.1) ESTIMATION OF AVERAGE SHEAR RATE USING MIXERS: TRADITIONAL METHODS

6.1.1) Matching Viscosities

6.1.1.1) Power Curves Method (Metzner and Otto, 1957)

Newtonian mixing curves for the paddle impellers in terms of mixing power number (P_o) versus Reynolds number (R_e) are shown in Figures 6.1 to 6.3. Each figure represents power data for mixing the Newtonian fluids in the same selected sample cup. Data points are means of two replications. These plots indicate that in the viscous regime the power characteristics are in agreement with the relationship indicated by Metzner and Otto (1957) for the laminar region of flow,

$$P_o = \frac{A}{R_e} \qquad (6.1)$$

i.e, they follow a straight line with a slope of -1. Regression analysis

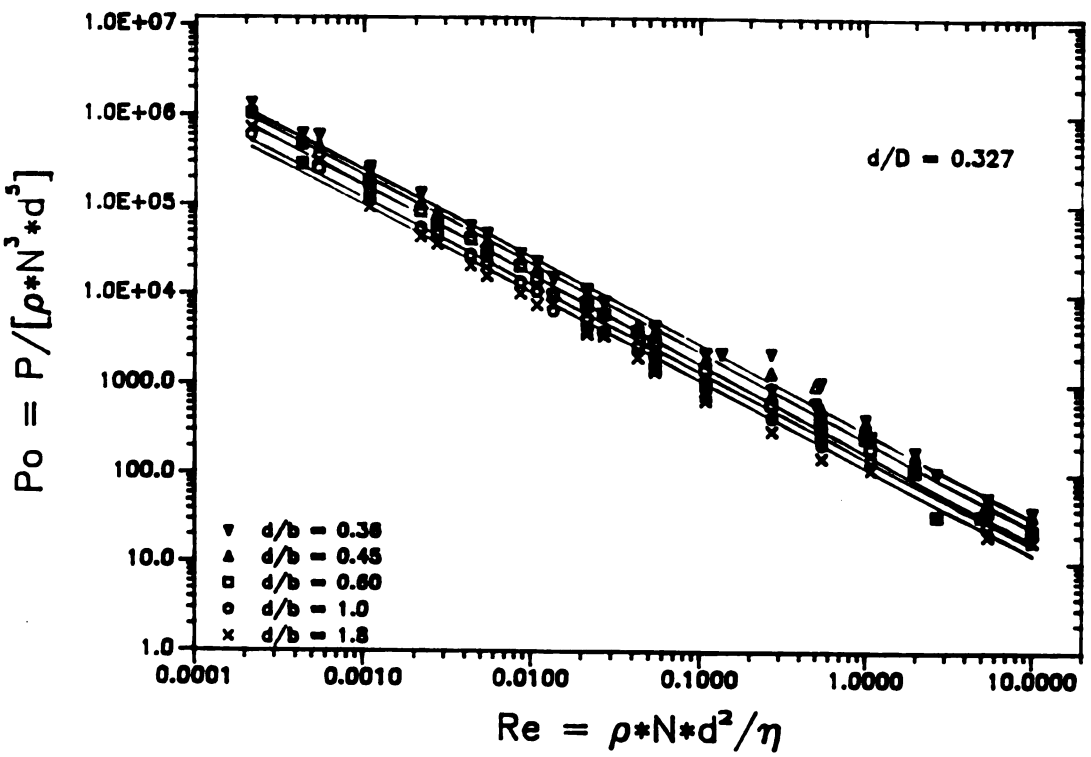

Figure 6.1: Power Number/Reynolds Number Relationship for Newtonian Fluids Using The Paddle Impellers (Cup diameter = 5.5 cm).

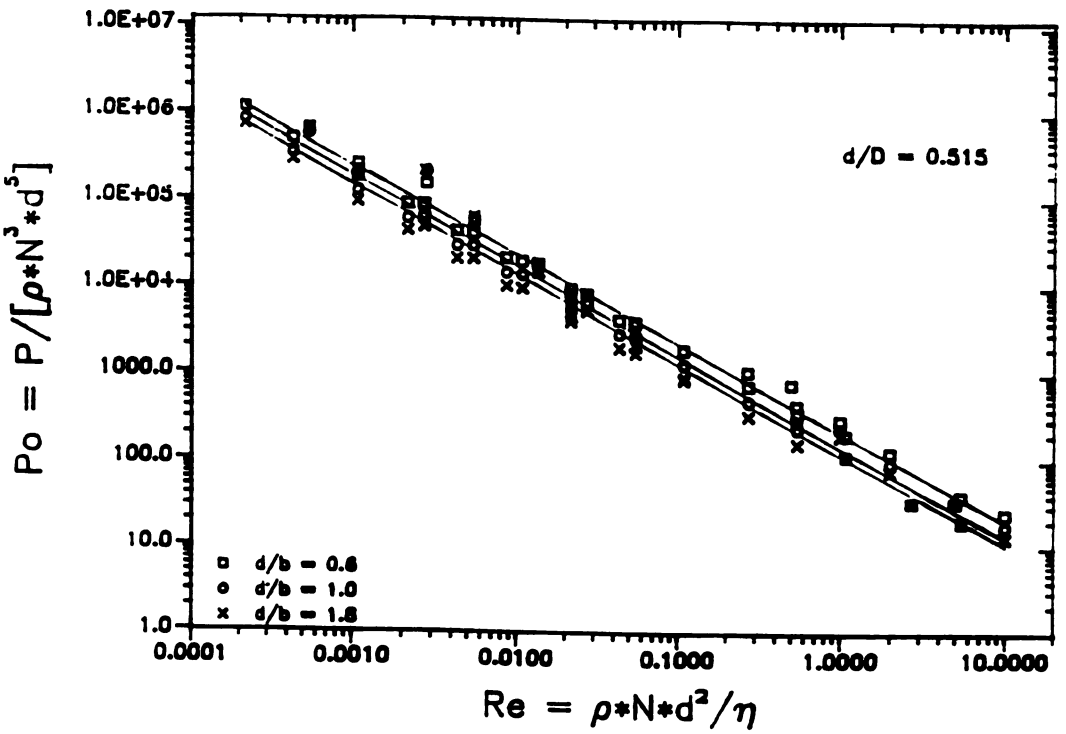

Figure 6.2: Power Number/Reynolds Number Relationship for Newtonian Fluids Using the Paddle Impellers (Cup diameter = 3.5 cm).

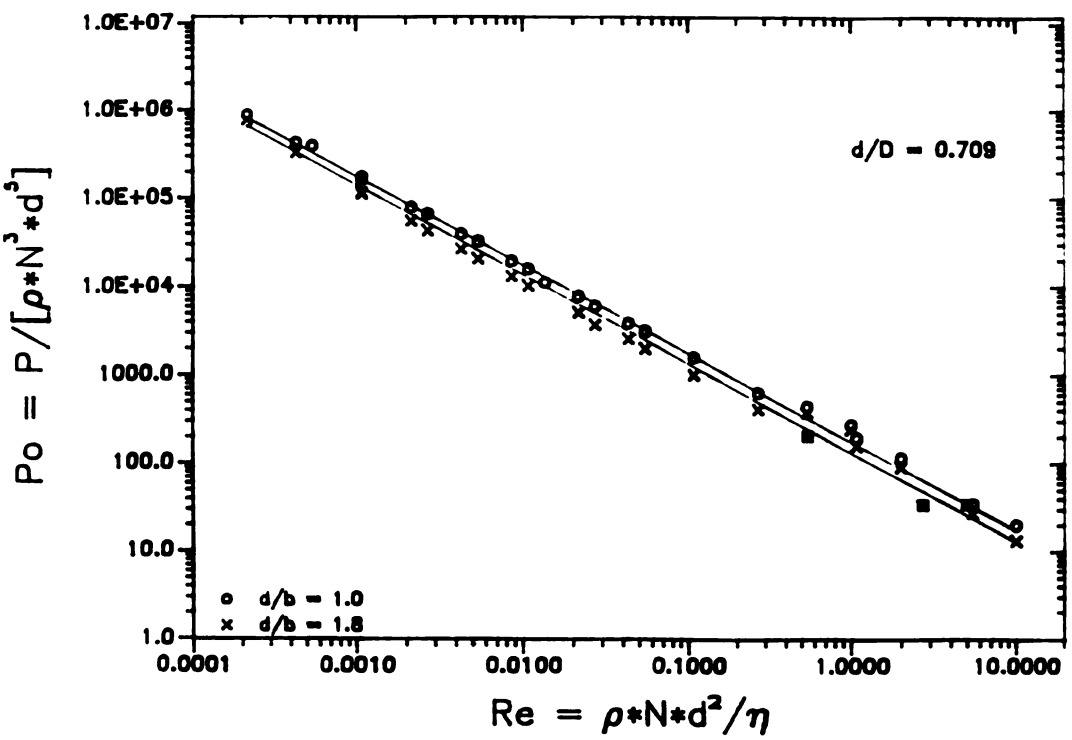

Figure 6.3: Power Number/Reynolds Number Relationship for Newtonian Fluids Using the Paddle impellers (Cup diameter = 2.54 cm).

on the data yielded slope values ranging from -0.98 to -1.03. Similar results were obtained with the flag impeller. The effect of the Froude Number, F_r , on power consumption was investigated and no significant effect was observed (Appendix B, Tables B1 and B2) for all systems.

To account for the effect of geometry, a generalized P_o versus R_e relationship was preferable and Eqn. (6.1) was transformed to

$$P_o = \alpha_0 R_e^{\alpha_1} (d/b)^{\alpha_2} (d/D)^{\alpha_3} \qquad (6.2)$$

for the paddle impellers, and

$$P_o = \beta_0 R_e^{\beta_1} (d/D)^{\beta_2} \qquad (6.3)$$

for the flag impeller. Equations (6.2) and (6.3) are nonlinear. To simplify the regression analysis, the following transformation was made,

$$\log P_o = \log \alpha_0 + \alpha_1 \log R_e + \alpha_2 \log (d/b) + \alpha_3 \log (d/D) \qquad (6.4)$$

$$\log P_o = \log \beta_0 + \beta_1 \log R_e + \beta_2 \log (d/D) \qquad (6.5)$$

The results of the regression are presented in Table 6.1 for the paddle impellers and Table 6.2 for the flag impeller. The resultant power prediction equations are,

Paddle impellers: (R^2=0.990)

$$P_o = 415.524 \left[R_e^{0.983} (d/b)^{0.223} (d/D)^{-1.058} \right]^{-1} \qquad (6.6)$$

Table 6.1: Regression Results of Eqn. (6.2) (Paddle Impellers)

Linear Multiple Regression Analysis

Regression Coefficient	Estimated Regression Coefficient	Estimated Standard Error	t^*
$\log \alpha_0$	415.524	--	--
α_1	-0.983	0.005	-174.50
α_2	-0.223	0.006	-6.52
α_3	1.058	0.006	17.40

Analysis of Variance

	Sum of Squares	Degrees of Freedom	Error Mean Squares	F^*
Regression	516.414	3	172.138	--
Residual	5.226	310	0.017	10211.5
Total	521.630	314		

$R^2 = 0.990$

* $\alpha = 0.05$

Table 6.2: Regression Results of Eqn. (6.3) (Flag Impeller)

Linear Multiple Regression Analysis

Regression Coefficient	Estimated Regression Coefficient	Estimated Standard Error	t^*
$\log \beta_0$	28.469	--	--
β_1	-0.972	0.015	-63.23
β_2	0.105	0.0156	0.72

Analysis of Variance

	Sum of Squares	Degrees of Freedom	Error Mean Squares	F^*
Regression	146.532	2	73.266	--
Residual	3.188	87	0.036	1999.2
Total	149.710	90		

$$R^2 = 0.980$$

Test of hypothesis for β_2 : C_1: $\beta_2 = 0$
C_2: $\beta_2 \neq 0$

For a level of significance of $\alpha = 0.05$, $t(0.975,87) = 2.00$

Since $t^* = 0.72 < t(0.975,87)$, we accept C_1 and conclude that $\beta_2 = 0$

Flag impeller: (R^2=0.980)

$$P_o = 25.912 \quad [R_e^{0.972}]^{-1} \qquad (6.7)$$

Figures 6.4 and 6.5 illustrate the validity of Eqns. (6.6) and (6.7) for the paddle and flag impellers, respectively. Figure 6.4a is the plot of predicted power numbers [Eqn. (6.6)] versus the "observed" power numbers (calculated with the measured values of torque) with the paddle. The correlation coefficient (0.990) shows the good agreement between observed and predicted values. The slope of Figure 6.4a (0.906) also indicates that Eqn. (6.6) predicts power numbers close to those observed. The closer the slope and the regression coefficient to the value of one, the better the model. Figure 6.4b presents the P_o [Eqn. (6.6)] versus R_e curves for Newtonian fluids using paddle impellers.

Figure 6.5a is the plot of predicted [Eqn. (6.7)] versus observed power numbers when using a flag impeller. The correlation coefficient (0.980) and the slope (0.900) indicate the ability of Eqn. (6.7) to predict power numbers. Figure 6.5b presents the P_o versus R_e curves for Newtonian fluids using the flag impeller. A t-student test was performed to verify whether the ratio of diameters (d/D) has any significance on the P_o for the flag impeller (Table 6.2). Results indicate that the effect of the geometric term is negligible. It is evident that Eqns. (6.6) and (6.7) are useful to indicate the effect of controllable mixing variables: cup diameter, impeller size and impeller shape.

Non-Newtonian mixing data (i.e. power numbers) were based on the correlation developed for Newtonian fluids. Power numbers for the non-Newtonian (power-law) fluids were calculated and, as Metzner and Otto

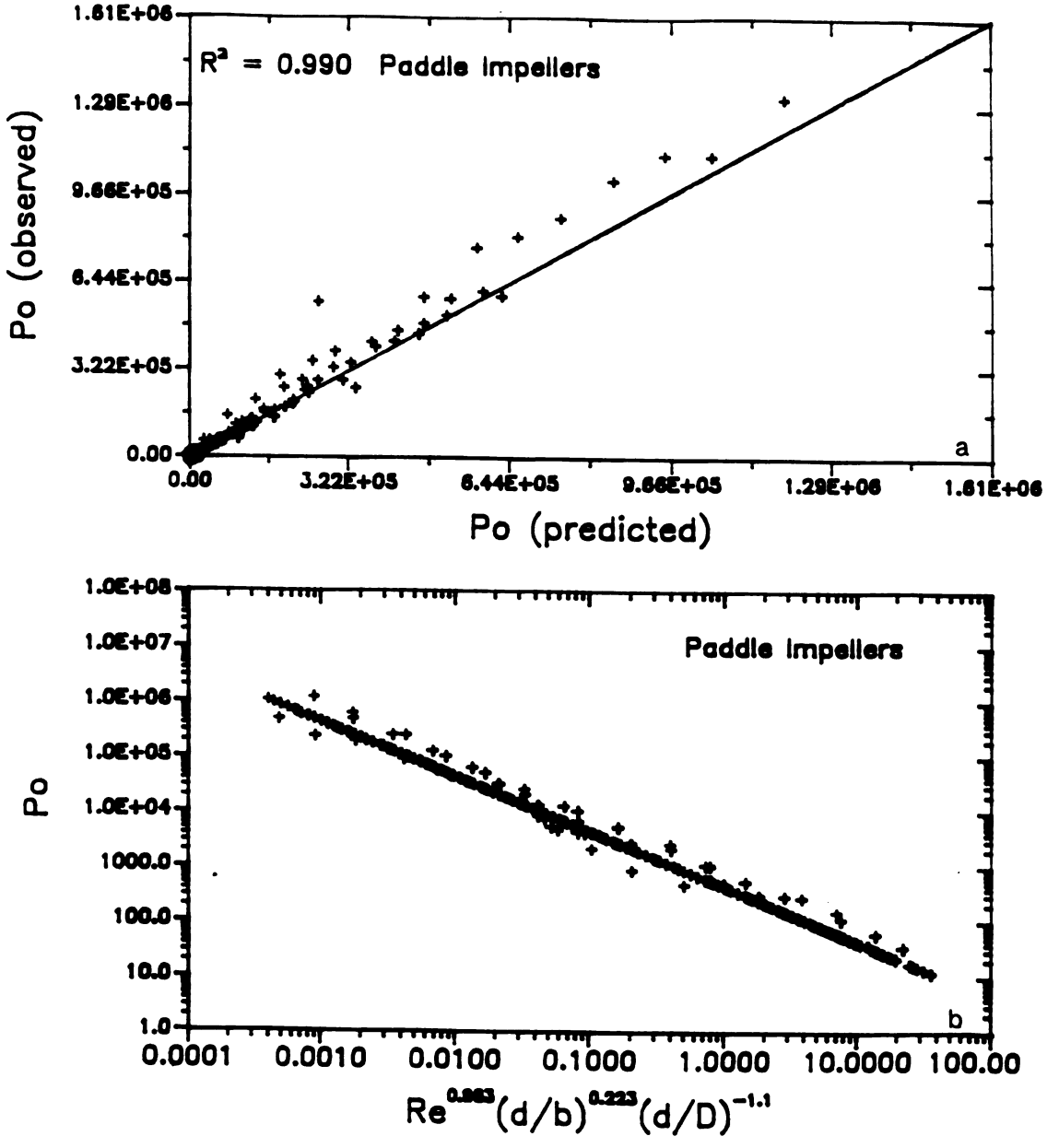

Figure 6.4: a) Predicted P_o Versus Observed P_o; b) Power Correlation For The Paddle Impellers.

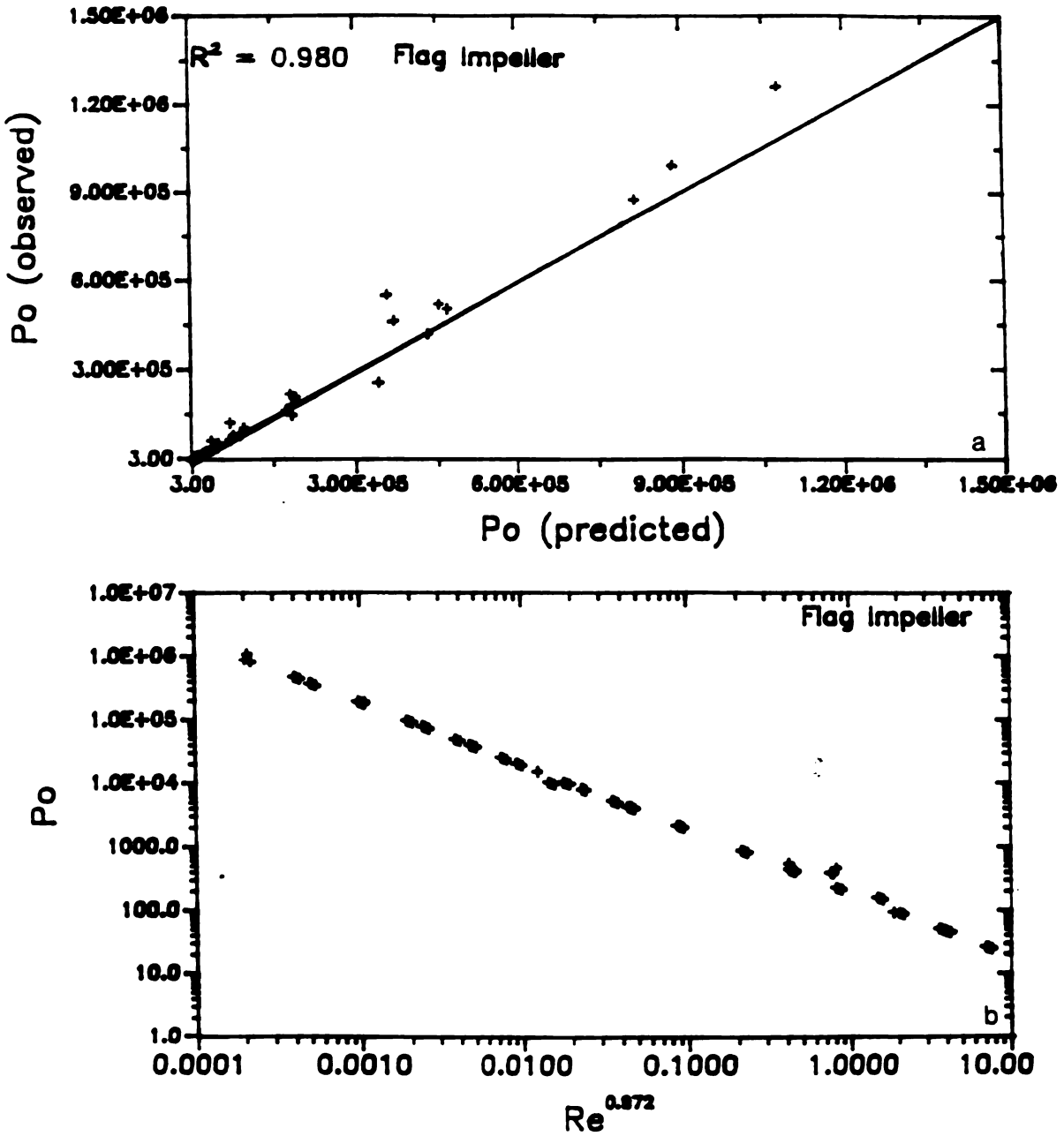

Figure 6.5: a) Predicted P_o Versus Observed P_o; b) Power Correlation For The Flag Impeller.

(1957) proposed, the corresponding Reynolds number was determined from the plots of Figures 6.4 and 6.5. Thus, The values of an "average" apparent viscosity, η_a, were obtained from

$$Re_n = \frac{\rho N d^2}{\eta_a} \qquad (6.8)$$

6.1.1.1.1) Estimation of Average Shear Rates

Figure 6.6 shows the plot of shear stress or apparent viscosity, η_a , calculated as σ/γ using Haake data, versus shear rate independently measured in a concentric cylinders viscometer (Haake Rotovisko) for a non-Newtonian fluid (CMC 1%, n=0.504, m=6.4195 Pa s^n). The plots for the other non-Newtonian fluids are presented in Appendix B (Figures B1 and B2). From the known shear stress (or η_a) versus shear rate relationship, a relationship between the average shear rate, $\dot{\gamma}_{av}$, and rotational speed, N, can be established. The values of η_a obtained from Eqn. (6.8) were used to determine the corresponding $\dot{\gamma}_{av}$ from plots such as Figure 6.6. The $\dot{\gamma}_{av}$ thus determined are shown as a function of impeller speed and geometry in Figures 6.7 through 6.9 for the paddle impellers (Figures B3 and B4 present the results for the other systems). These plots indicate that the shear rates vary with the geometry of the system as well with the properties of the fluid being agitated. Figure 6.7 shows the relationship between the average shear rate and the rotational speed of two impellers in the same container. The impeller in Figure 6.7a is 1 cm smaller (impeller blade height, b) than the impeller in Figure 6.7.b. Results indicate slighlty higher shear rates at specific values of rotational speed for the smaller impeller (Figure 6.7a).

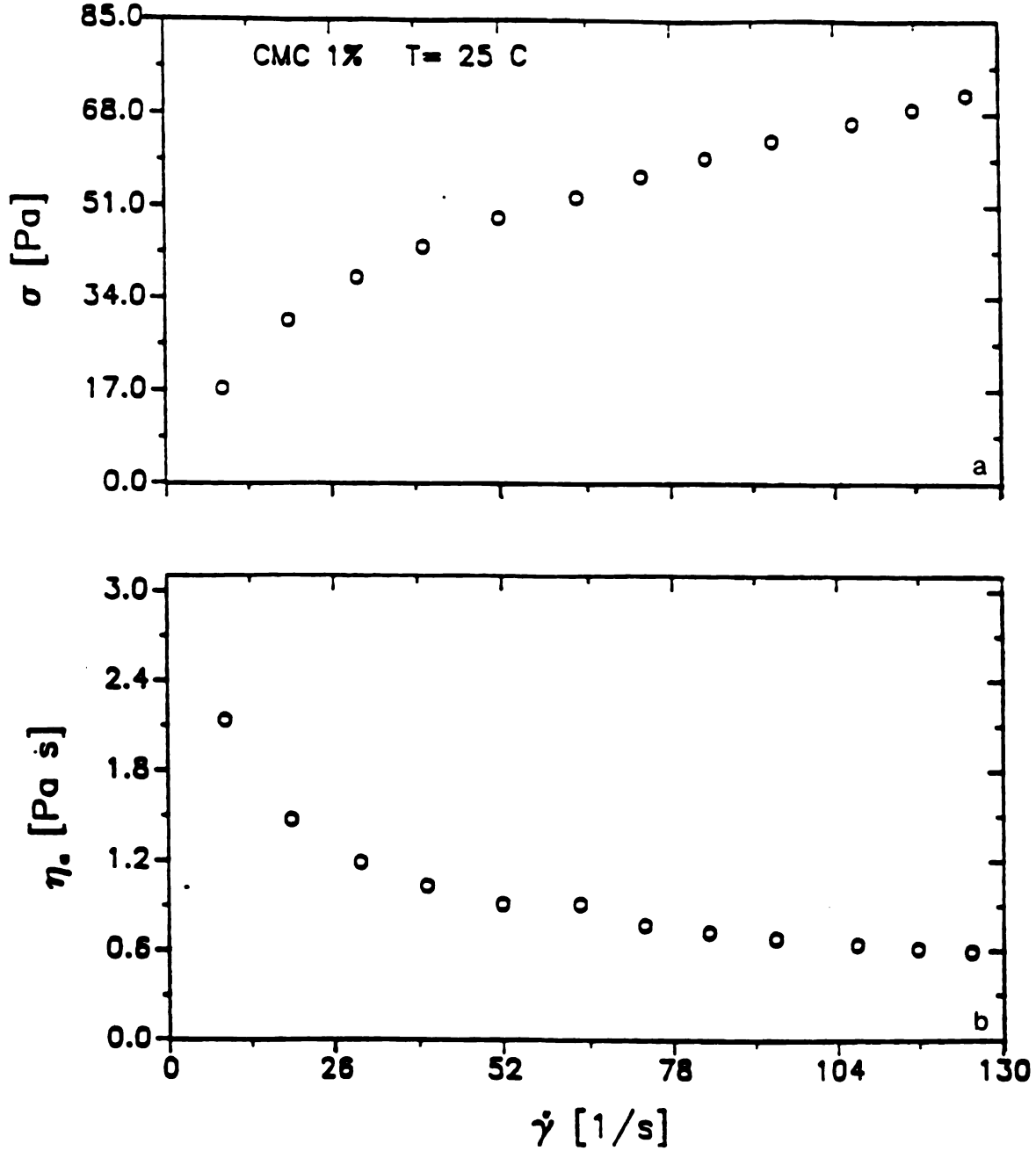

Figure 6.6: a) Shear Stress Versus Shear Rate; b) Apparent Viscosity Versus Shear Rate (Hydroxypropyl Methylcellulose 1%).

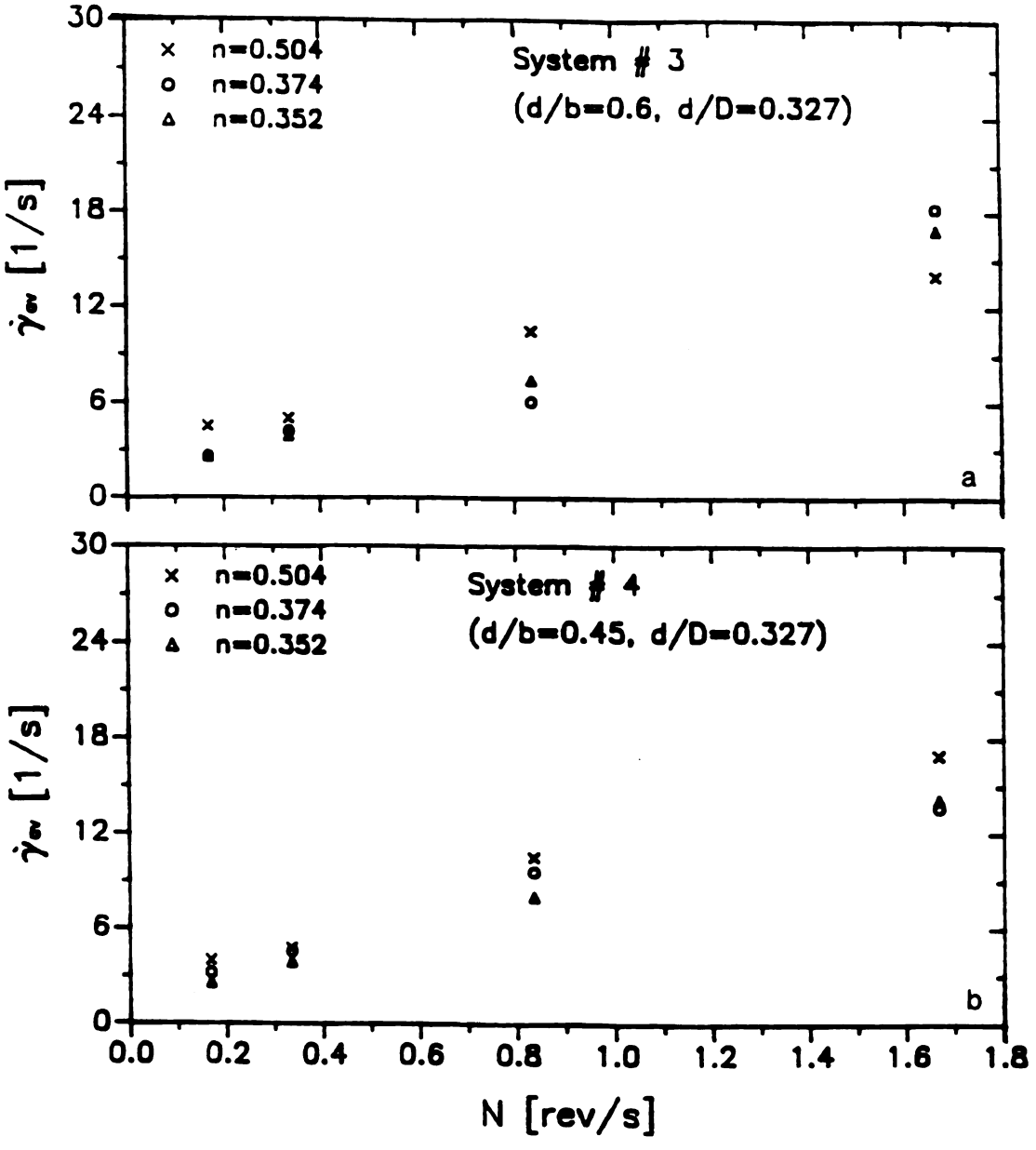

Figure 6.7: Average Mixing Shear Rate as a Function of Rotational Speed of the Paddle Impellers. a) System 3; b) System 4

Similar results are presented in Figures 6.8 and 6.9. Figure 6.8b shows the values of the average shear rate for a small impeller in a medium cup. Figure 6.9b shows the results for a bigger impeller (three times) in the same cup. Figure 6.10 presents the results for the flag impeller (Figures 6.11 and B5 show results for other conditions). The experimental data indicate that the results are dependent on the flow properties as well as on the geometry of the mixing system. In comparison with the paddle impellers, the flag impeller usually yields lower average shear rate values. This indicates that results are dependent on the shape of the impeller.

Regression analysis was used to determine the relationship between $\dot{\gamma}_{av}$ and N. Results are presented in Table 6.3 for the paddle impellers and Table 6.4 for the flag impeller. It may be seen that $\dot{\gamma}_{av}$ increases linearly with N for the paddle and flag impellers. Then, the average shear rate has the same form as the expression assumed by Metzner and Otto (1957),

$$\dot{\gamma}_{av} = k' N \qquad (3.8)$$

However, when agitating the less viscous fluid (n=0.504, m=6.4915 Pa s^n) with a paddle impeller (Table 6.3), a better fit of the data is given by the model $\dot{\gamma}_{av} = a + k'N$ (systems 3, 6, and 7) (It should be emphasized that this is only a mathematical expression with no necessary physical meaning). Table 6.4 shows that experimental data for the flag impeller always follow the relationship given by Eqn. (3.8). It seems that the values of k' are not as highly dependent on fluid properties and system geometry as for the paddle impellers (Table 6.3), where significant

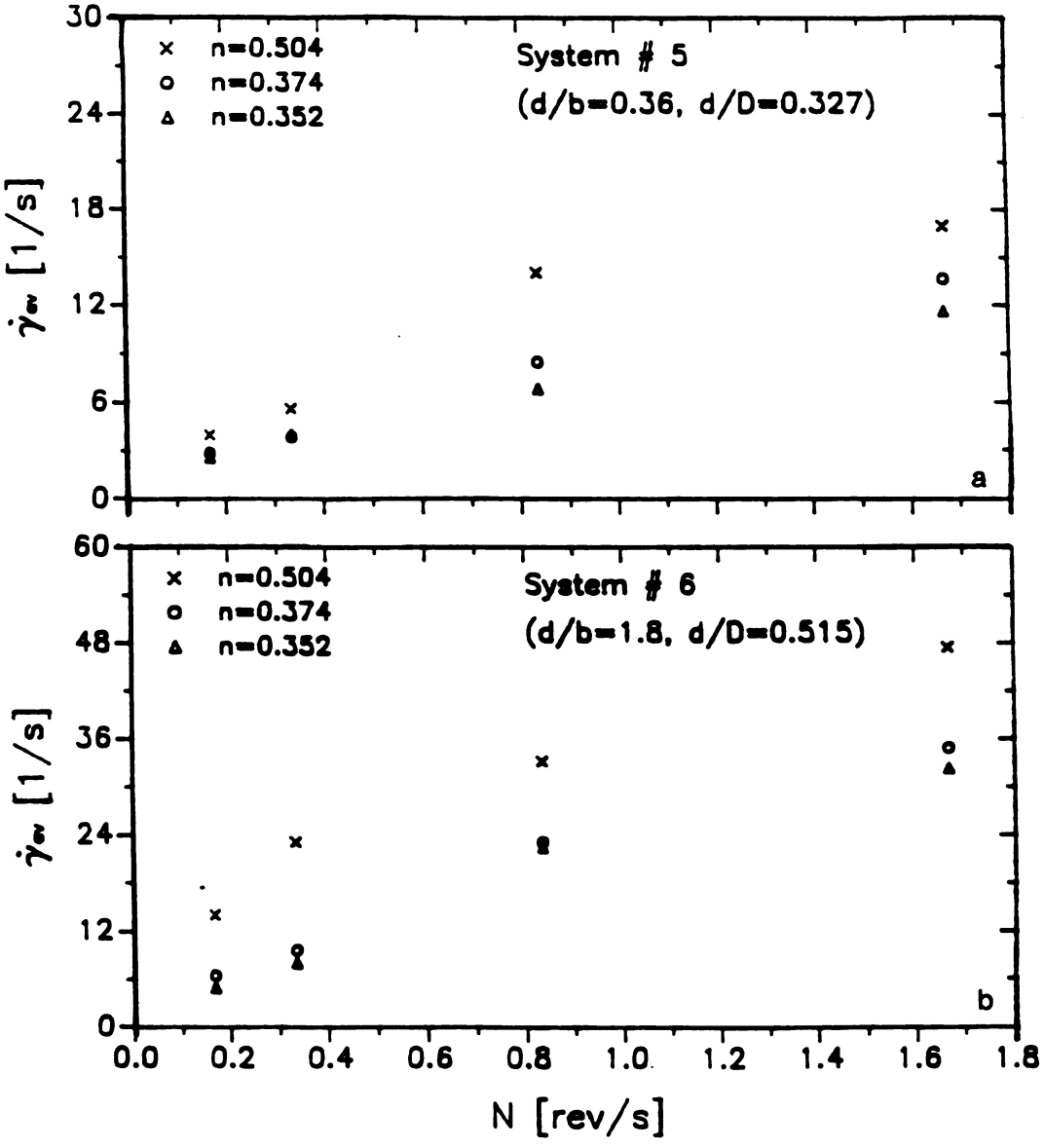

Figure 6.8: Average Mixing Shear Rate as a Function of Rotational Speed of the Paddle Impellers. a) System 5; b) System 6

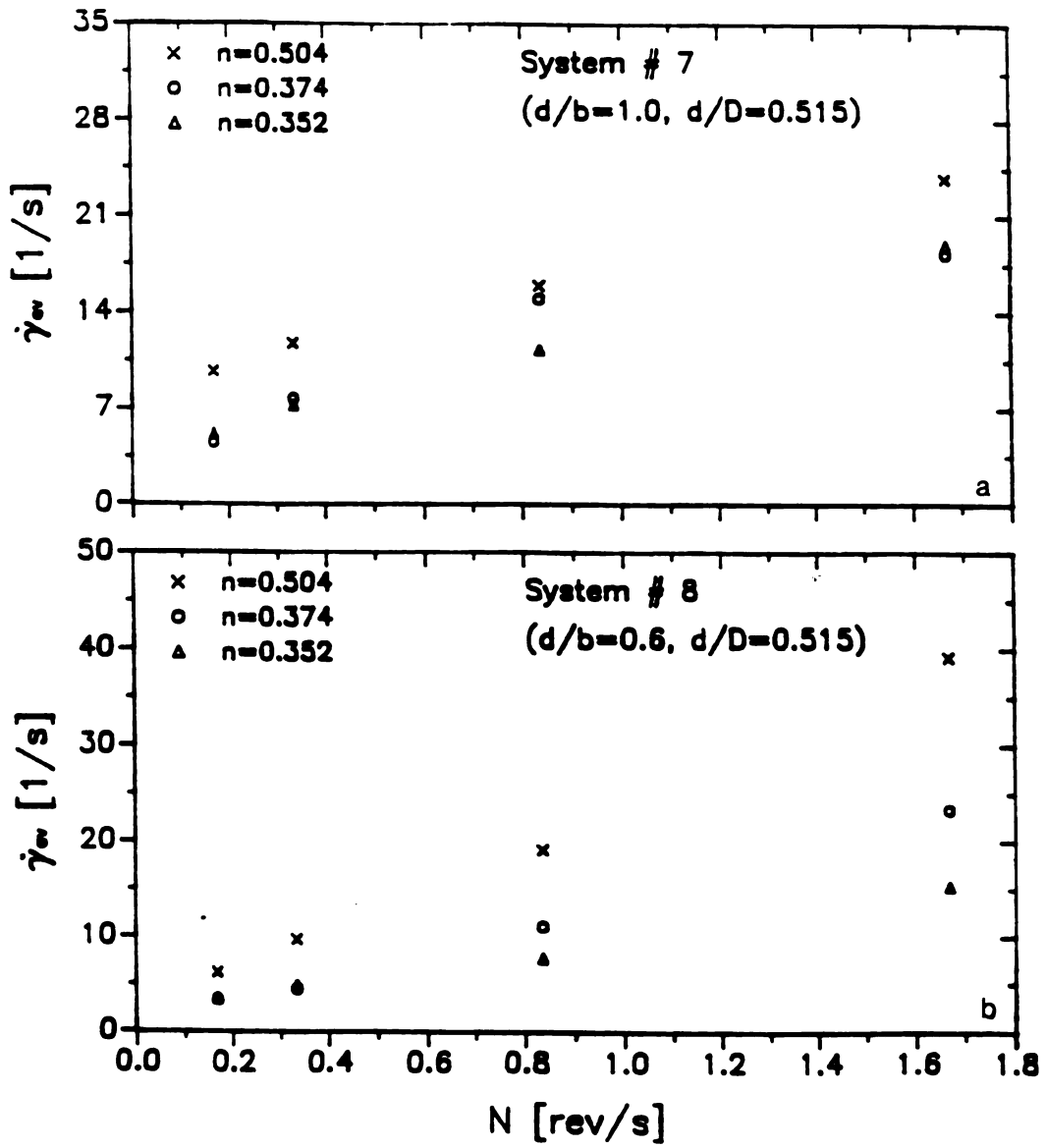

Figure 6.9: Average Mixing Shear Rate as a Function of Rotational Speed of the Paddle Impellers. a) System 7; b) System 8

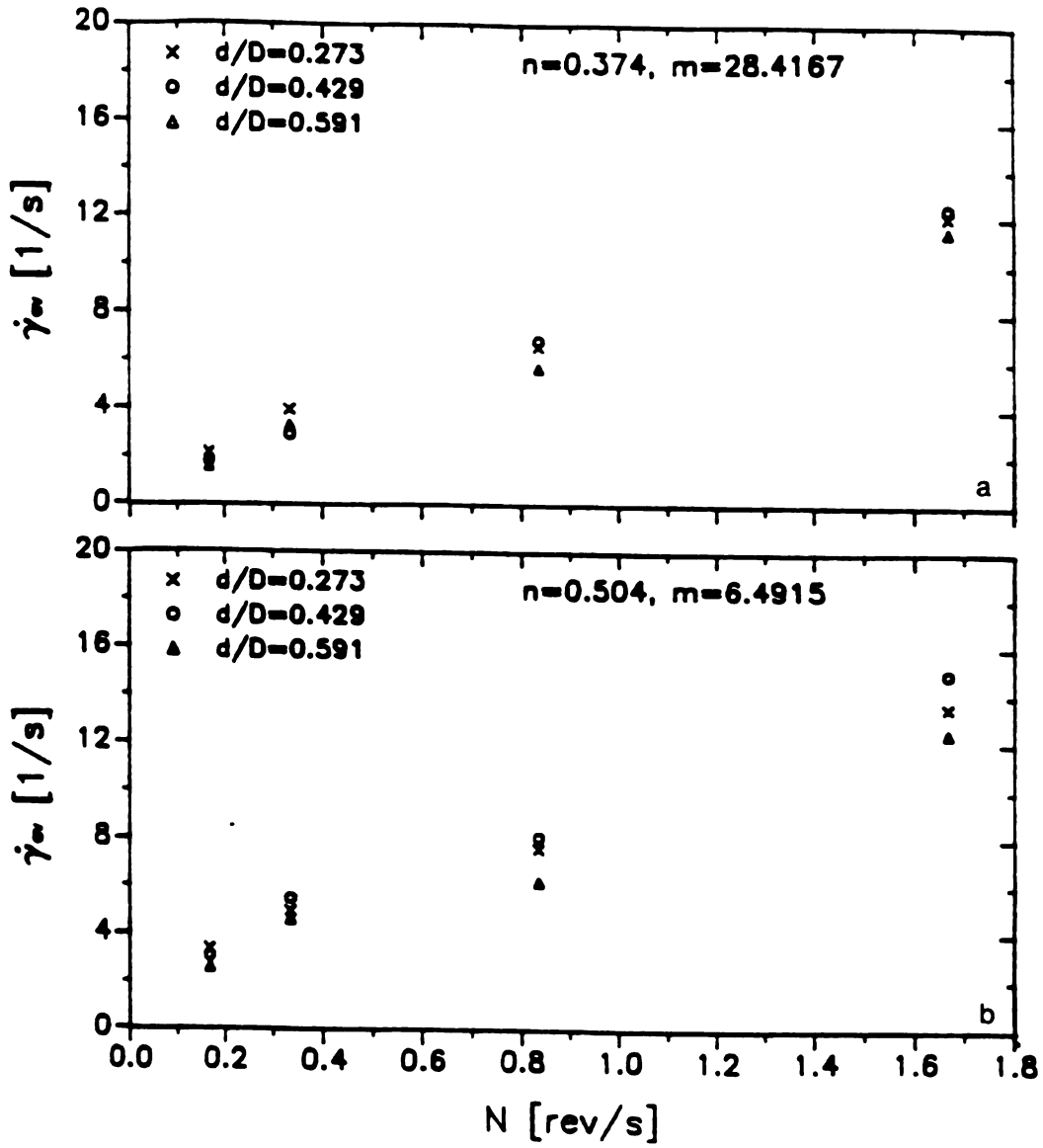

Figure 6.10: Average Mixing Shear Rate as a Function of Rotational Speed of the Flag Impeller. a) CMC 1.5%; b) CMC 1%

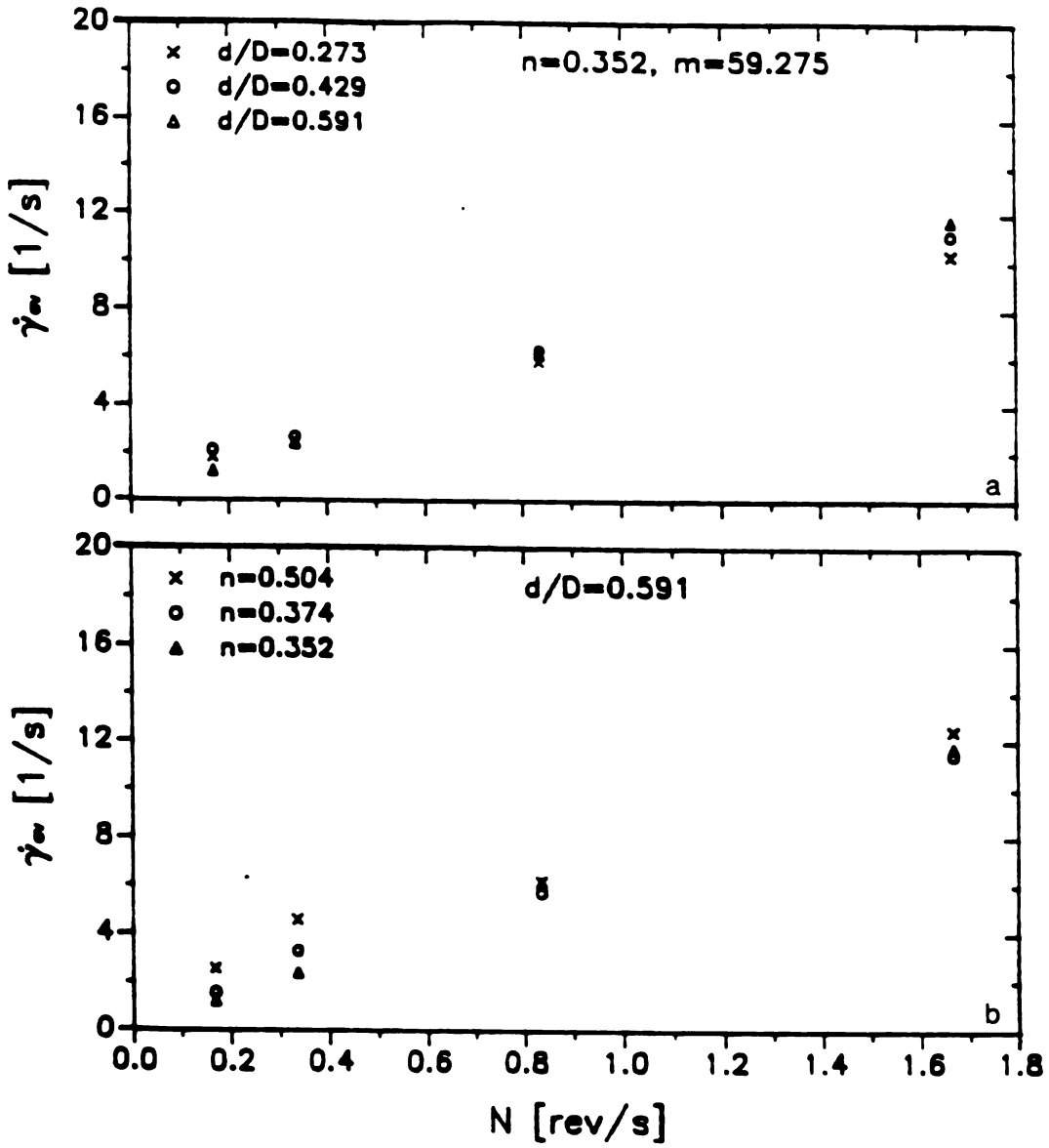

Figure 6.11: Average Mixing Shear Rate as a Function of Rotational Speed of the Flag Impeller. a) CMC 2%; b) System 3

Table 6.3: Values of k', defined by Eqn. (3.8) ($k' = \dot{\gamma}_{av}/N$), for Paddle Impellers.

FLUID	SYSTEM	k'	R^2
CMC 1%	1	33.527	0.994
	2	15.890	0.986
	3	9.535	0.938*
	4	10.855	0.979
	5	11.740	0.941
	6	32.309	0.925**
	7	16.154	0.899***
	8	23.647	0.996
	9	25.372	0.995
	10	20.424	0.993
CMC 1.5%	1	24.375	0.996
	2	13.568	0.988
	3	10.305	0.977
	4	9.051	0.964
	5	8.712	0.983
	6	22.564	0.981
	7	12.784	0.981
	8	13.859	0.998
	9	21.062	0.998
	10	19.511	0.989
CMC 2%	1	17.019	0.986
	2	10.776	0.976
	3	9.948	0.995
	4	8.834	0.991
	5	7.395	0.978
	6	20.999	0.979
	7	12.215	0.998
	8	9.417	0.981
	9	24.199	0.989
	10	13.937	0.998

* $\dot{\gamma}_{av} = 3.5072 + 6.6217N$, $R^2 = 0.973$

** $\dot{\gamma}_{av} = 13.695 + 20.9313N$, $R^2 = 0.966$

*** $\dot{\gamma}_{av} = 8.3535 + 9.2137N$, $R^2 = 0.999$

Table 6.4: Values of k', defined by Eqn. (3.8) ($k' = \dot{\gamma}_{av}/N$) for Flag Impeller.

FLUID	SYSTEM	k'	R^2
CMC 1%	1	8.602	0.969
	2	9.389	0.997
	3	7.704	0.974
CMC 1.5%	1	7.535	0.985
	2	7.639	0.997
	3	6.952	0.994
CMC 2%	1	6.411	0.993
	2	6.919	0.992
	3	7.087	1.000

differences are obtained for each fluid.

6.1.1.1.2) Factors Affecting Average Shear Rates (and k')

6.1.1.1.2.1) Impeller Rotational Speed

The relationship between the average shear rate and the impeller speed has been shown in Tables 6.3 and 6.4 for the paddles and flag impeller, respectively. The slope from the plots gives a value of k', independent of the value of N. However, if individual values of k' were obtained at specific values of N, a relationship between k' and N could be established.

6.1.1.1.2.2) Fluid Properties

Previous research has shown a possible dependence of k' (therefore, average shear rate) on the flow behavior index, n, with pseudoplastic fluids. However, this dependence has been found to be highly dependent on system geometry and impeller shape (Calderbank and Moo-Young, 1961; Beckner and Smith, 1966). Their results indicate a possible decrease in the value of k' with an increase in the value of n but results were not conclusive and this needs further study.

It is interesting to find that, in this investigation, the less shear-thinning fluid (i.e., larger value of n) generated higher values of k' (higher average shear rates) than that produced by the highly shear-thinning fluid (lower n value) when agitating the fluid with the paddle impellers (Figures 6.7 to 6.9). A similar behavior was observed by Sinevic et al. (1986) when agitating power-law fluids in a concentric cylinders system. It is reasonable to suggest that k' is not only a function of the flow behavior index, n, but it also varies with the

value of the fluid consistency coefficient, m. In this investigation, the less shear-thinning fluid (CMC 1%) was also the less viscous fluid. Also, a decrease in the gap between impeller and cup (d/D) reduces the effect of the properties of the fluid. With an impeller to cup diameter ratio of 0.709 or greater, k' was not significantly affected by n (Table 6.3, Systems #9 and #10).

Shear rates in a cylindrical container agitated by a flag impeller are not as significantly affected by the rheological properties of the fluid as in the case of the paddle impellers (Figures 6.10 and 6.11), with a slight variation at high rotational speeds for the less viscous fluid.

6.1.1.1.2.3) Cup Diameter

The diameter of the cylindrical cup where the fluid is being agitated does not have a significant effect on the value of k' when using paddle impellers. Figures 6.7a and 6.9b show results for the same impeller (b=3 cm; d/b=0.6) rotating in different cups. Impeller-to-cup ratios significantly less than 1.0 (d/D=0.327; Figure 6.7a), yielded lower shear rates values (at high rotational speeds) than those determined when using a larger impeller-to-cup diameter ratio, i.e. a smaller gap (d/D=0.515) (Figure 6.9b). The same behavior was observed with all the paddle impellers. However, Table 6.3 suggests that d/D may not have a significant effect on the values of k'. This was confirmed by results using multiple regression analysis.

As was expected, in the case of the flag impeller, the fluid container has no significant effect (Figures 6.10a to 6.11). However, it

is interesting to note that the more viscous fluid (also the more shear-thinning fluid), (Figure 6.11a) generated higher values of $\dot{\gamma}_{av}$ when increasing the d/D ratio (smaller gap), a trend not exactly followed by the less viscous fluids. It is suspected that the effect of the geometric term (d/D) is highly dependent on the type of fluid being agitated.

6.1.1.1.2.4) Impeller Size (Blade Height)

Values of the average shear rate determined for the five paddle impellers are shown in Figure 6.12 for two non-Newtonian fluids (CMC 1% and CMC 2%). The difference in values becomes important at high mixing speeds, with the smaller impeller (d/b=1.8) generating the higher average shear rates, especially when agitating a low viscosity fluid (Figure 6.12b). This is due to the fact that a small impeller produces low flow and thus, higher shear rates. The difference is smaller when agitating a high viscosity fluid (Figure 6.12a). In both cases, the difference in average shear rates generated by the different impellers is small at low mixing speeds. It is interesting to note that the k' values determined with the less viscous fluid (CMC 1%) show some inconsistency, i.e., they do not correlate with the height of the impeller blade. This phenomenon was not observed with the more viscous fluids. Again, the type of fluid being agitated seems to be an important factor in the determination of the proportionality constant, k' (Figure 6.13). Thus, the correlation between k' and the height of the impeller blade was determined for each fluid. The best fit was obtained with the following model,

$$k' = \beta_1 \, (d/b)^{\beta_2} + \beta_3 \qquad (6.9)$$

with β_1 , β_2 and β_3 as regression constants. Results from regression are shown in Table B3 (Appendix B).

In summary, results obtained with the method developed by Metzner and Otto (1957) indicate that the value of the mixer proportionality constant, k', is not only a function of the geometry of the system as the authors suggested but is is also highly dependent on the properties of the fluid under consideration.

6.1.1.2) Mixer Torque Curves Method (Mackey et al., 1987)

Following the procedure of matching Newtonian and non-Newtonian data employed by Mackey et al. (1987), the mixer torque, M, versus ηN plots for the Newtonian fluids are shown in Figure 6.14 for all treatments with the paddle impellers. As it was expected, linear results were obtained. The slope of the lines, $1/k_2$ (rev/m^3), with k_2 the mixer coefficient, seemed to be a function of the geometric variables d/b and d/D. Thus, the following model for the mixer coefficient, k_2, was proposed

$$k_2 = \alpha_o \, (d/b)^{\alpha_1} \, (d/D)^{\alpha_2} \qquad (6.10)$$

After linearization of Eqn. (6.10), multiple linear regression analysis (Table 6.5) indicates an excellent fit of the data. The prediction equation for the mixer coefficient, k_2, is given by

$$k_2 = 6121.262 \, (d/b)^{0.684} \, (d/D)^{-0.403} \qquad (6.11)$$

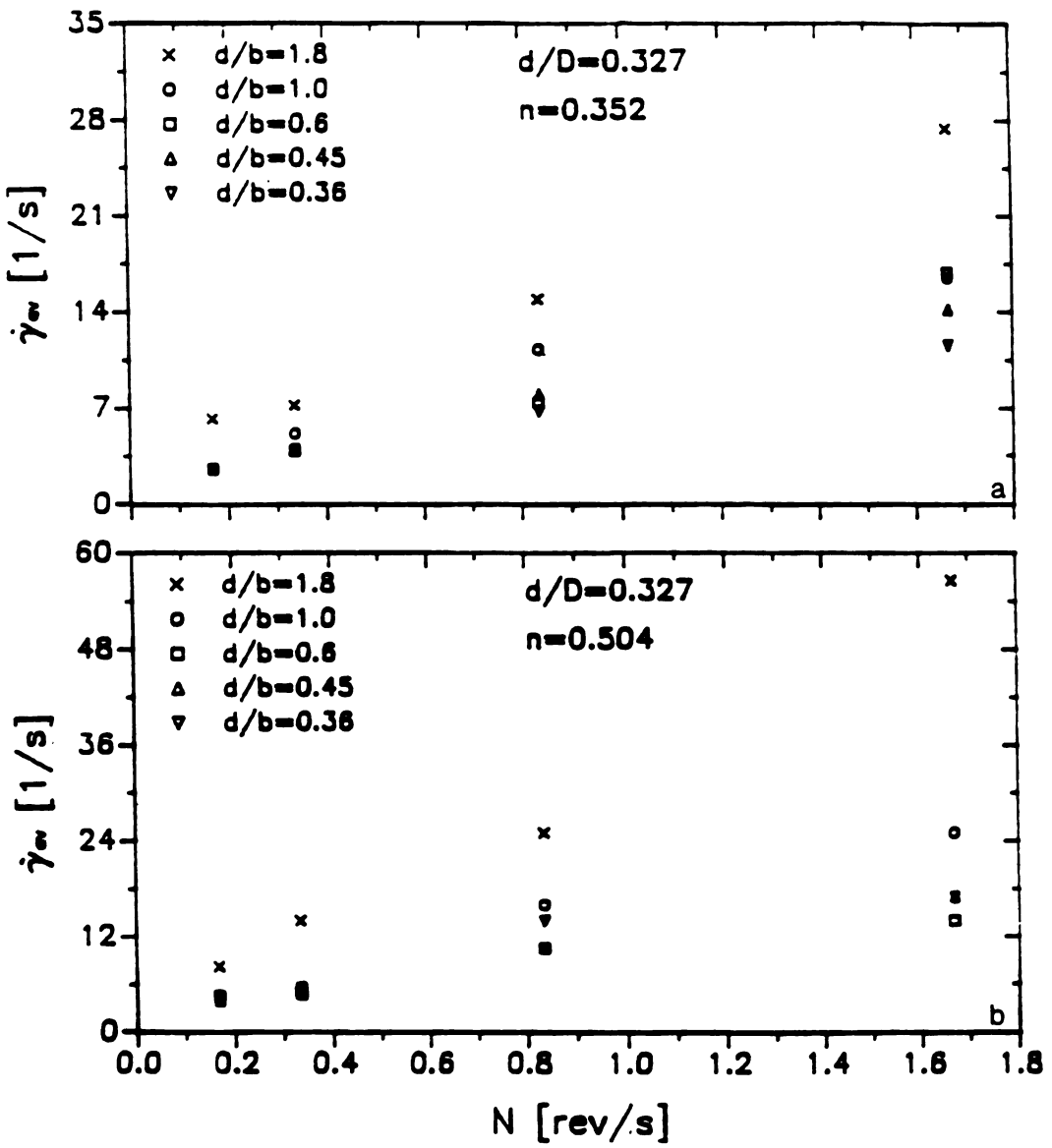

Figure 6.12: Average Mixing Shear Rate as a Function of Rotational Speed of the Paddle Impellers (d/D=0.327). a) CMC 2% b) CMC 1%

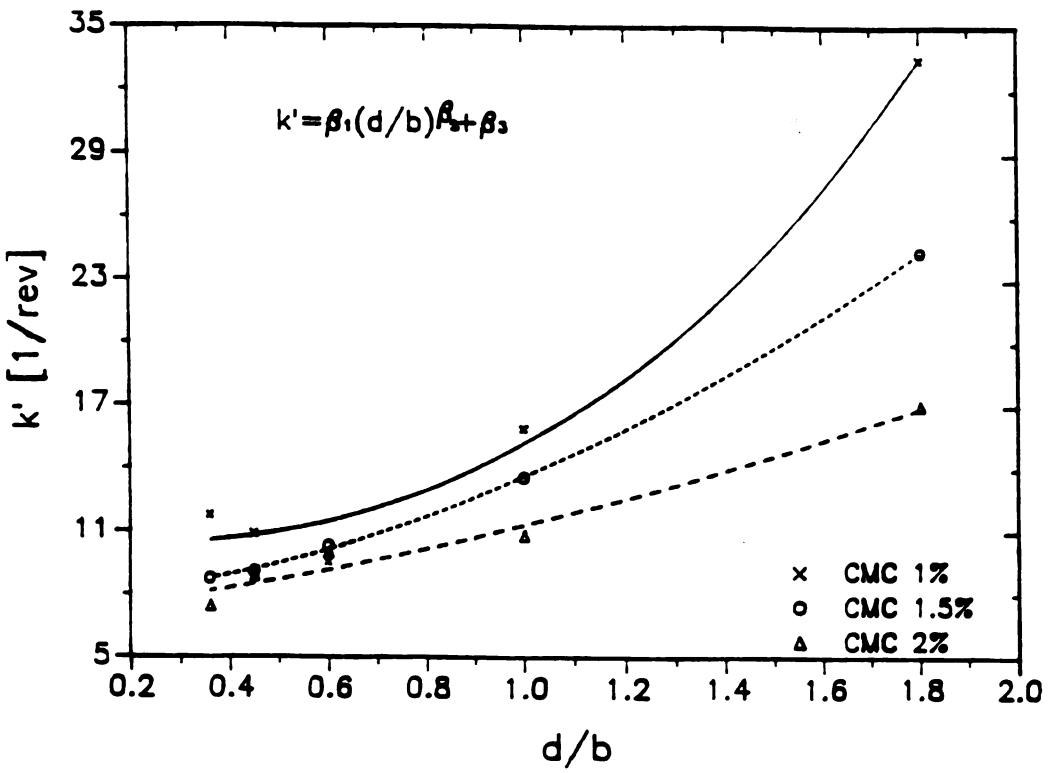

Figure 6.13: Plot of Mixer Proportionality Constant as a Function of Impeller Size for the Non-Newtonian Fluids (d/D=0.327)

Table 6.5

Regressi
Coeffici

log α_0
α_1
α_2

Regressio
Residual

Total

*
$\alpha = 0.0$

Table 6.5: Regression results for the fit of Eqn. (6.10)

Linear Multiple Regression Analysis

Regression Coefficient	Estimated Regression Coefficient	Estimated Standard Error	t^*
$\log \alpha_0$	6121.262	--	--
α_1	0.684	0.066	16.75
α_2	-0.403	0.066	-5.51

Analysis of Variance

	Sum of Squares	Degrees of Freedom	Error Mean Squares	F^*
Regression	0.222	2	0.111	--
Residual	0.005	7	0.028	143.51
Total	0.227	10		

$R^2 = 0.980$

*
$\alpha = 0.05$

$R^2 = 0.980$

Figure 6.15 presents the predicted values of k_2 using Eqn. (6.11) versus the values of k_2 determined from the slopes of the lines for the paddle impellers (Figure 6.14). The adequacy of the prediction equation is indicated by the regression coefficient and the slope of 0.990.

Figure 6.16 presents the plots of torque (M) versus viscosity times rotational speed (ηN) to determine the values of the mixer coefficient, k_2, for the flag impeller rotating in the different cups. It is clear that the value of k_2 is also a function of the geometry of the system for the flag impeller.

The value of the mixer proportionality constant, k', can then be calculated from the following equation [Section 3.2.1.1, Eqn. (3.15)],

$$k' = \frac{1}{N}\left[\frac{k_2\ M}{N\ m}\right]^{\frac{1}{n-1}} \qquad (6.12)$$

with k_2 a function of system geometry (Tables 6.6 and 6.7). Finally, the average shear rates are determined from

$$\dot{\gamma}_{av} = k'N \qquad (3.8)$$

The effect of the parameters in Eqn. (6.12) on the value of k' and, consequently, on the estimation of average mixing shear rates will be discussed in the following section.

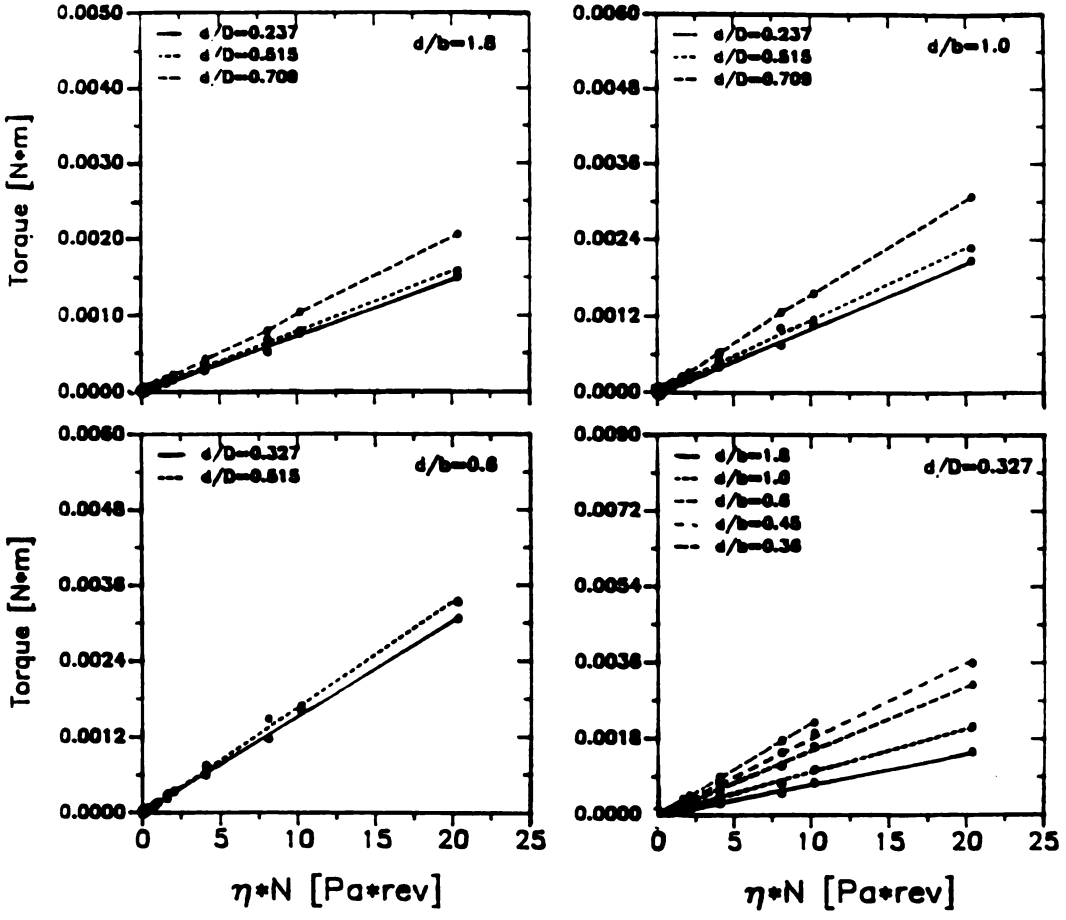

Figure 6.14: Mixer Torque Versus Viscosity Times Speed for Calculating Mixer Coefficient, k_2 (Paddle Impellers)

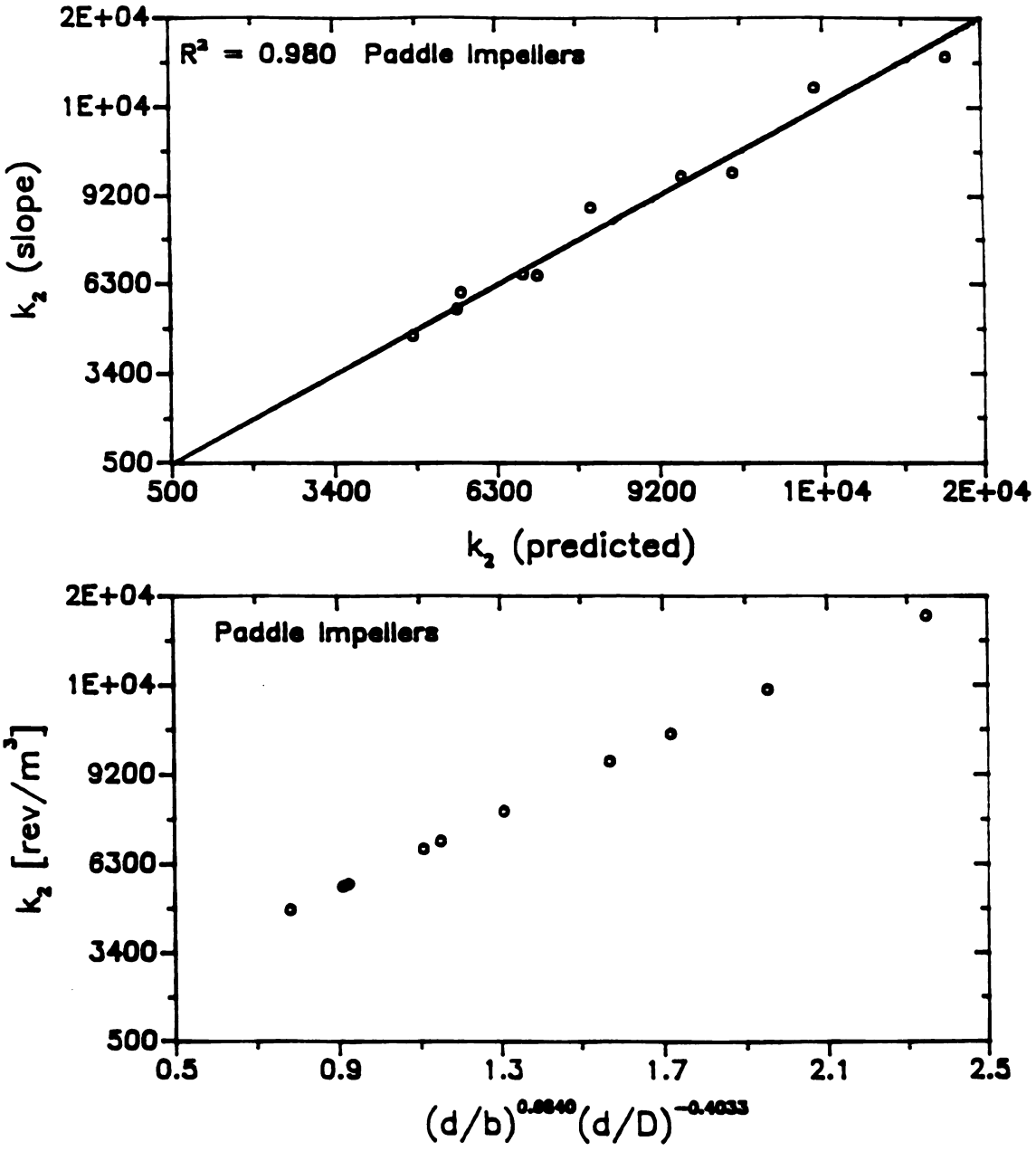

Figure 6.15: Predicted Mixer Coefficient Versus Observed Mixer Coefficient (Paddle Impellers)

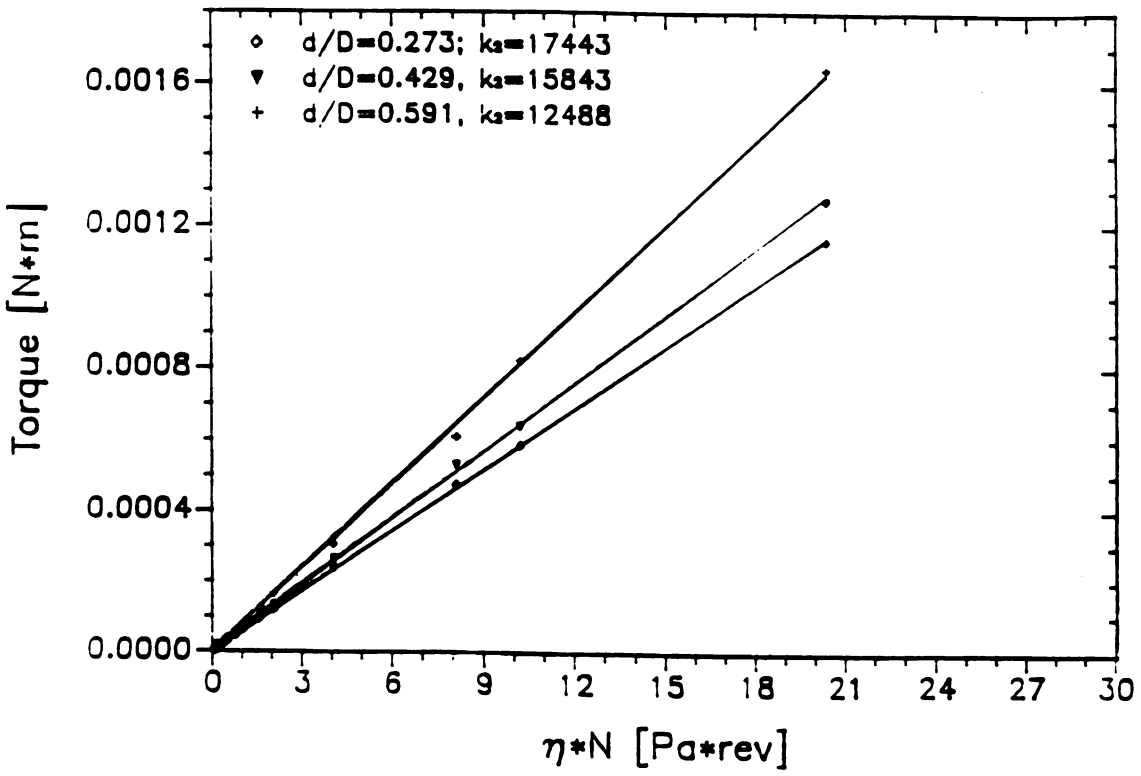

Figure 6.16: Mixer Torque Versus Viscosity Times Speed for Calculating Mixer Coefficient, k_2 (Flag Impeller)

Table 6.6: Values of k', defined by Eqn. (6.12), for Paddle Impellers

FLUID	SYSTEM	k' 5 rpm	k' 20 rpm	k' 100 rpm
CMC 1%	1	48.594	15.176	8.206
	2	36.983	14.329	8.685
	3	32.451	12.772	7.823
	4	26.583	11.296	6.808
	5	23.737	10.191	6.277
	6	61.948	23.409	14.274
	7	50.159	19.975	12.503
	8	37.851	16.298	10.130
	9	39.847	15.562	10.882
	10	38.515	16.101	10.8494
CMC 1.5%	1	26.094	12.872	8.325
	2	27.485	13.557	8.647
	3	23.803	11.939	7.636
	4	21.240	10.528	6.139
	5	19.219	9.525	5.742
	6	25.729	13.895	9.972
	7	26.456	13.807	9.354
	8	15.568	8.993	6.559
	9	21.019	11.468	8.692
	10	16.806	9.699	7.301
CMC 2%	1	21.400	11.537	8.024
	2	22.656	11.701	7.891
	3	20.392	10.602	7.099
	4	18.347	9.551	6.529
	5	16.347	8.683	5.665
	6	22.572	12.537	9.079
	7	34.282	16.127	9.605
	8	18.385	10.136	7.159
	9	10.903	8.914	6.099
	10	18.267	10.825	8.361

Table 6.7: Values of k', defined by Eqn. (6.12), for Flag Impeller

FLUID	SYSTEM	k'		
		5 rpm	20 rpm	100 rpm
CMC 1%	1	39.852	11.246	6.402
	2	38.589	14.038	8.458
	3	47.601	16.707	9.811
CMC 1.5%	1	22.475	10.756	7.111
	2	19.045	9.846	6.625
	3	21.788	11.445	7.833
CMC 2%	1	18.135	9.558	6.801
	2	18.184	9.727	6.866
	3	19.105	9.914	7.408

6.1.1.2.1) Factors Affecting k'

6.1.1.2.1.1) Impeller Rotational Speed

Equation (6.12) predicts a dependence of the proportionality constant, k', on the impeller rotational speed, N. Figure 6.17 shows that as N increases, the value for the proportionality constant of the paddle impellers decreases for any impeller and cup geometry. At values below 10 rpm (0.1667 rps), significant changes in the value of k' are observed. At higher rotational speeds, the proportionality constant might reach a constant value, independent of the system geometry.

Similar results were obtained with the flag impeller (Figure 6.18). Again, the proportionality constant, k', is significantly affected by impeller speeds less than 10 rpm (0.1667 rps). This behavior was also observed by Mackey et al. (1987) for a flag impeller.

6.1.1.2.1.2) Fluid Properties

The value of k' is also dependent on the rheological properties of the agitated fluid (Figure 6.19). When agitating a non-Newtonian fluid with a paddle impeller, as n increases the value of k' increases and the effect of n on k' diminishes significantly at high impellers speeds (from 10 to 100 rpm). Also, geometry effects become less important at that range of rotational speeds. Similar behavior was observed with the flag impeller.

Figures 6.20 and 6.21 illustrate the variations in the value of k' when agitating fluids with different rheological properties with a flag impeller at high rotational speeds (100 rpm) in different cups. Figure 6.20 presents the changes on the value of k' with the value of n,

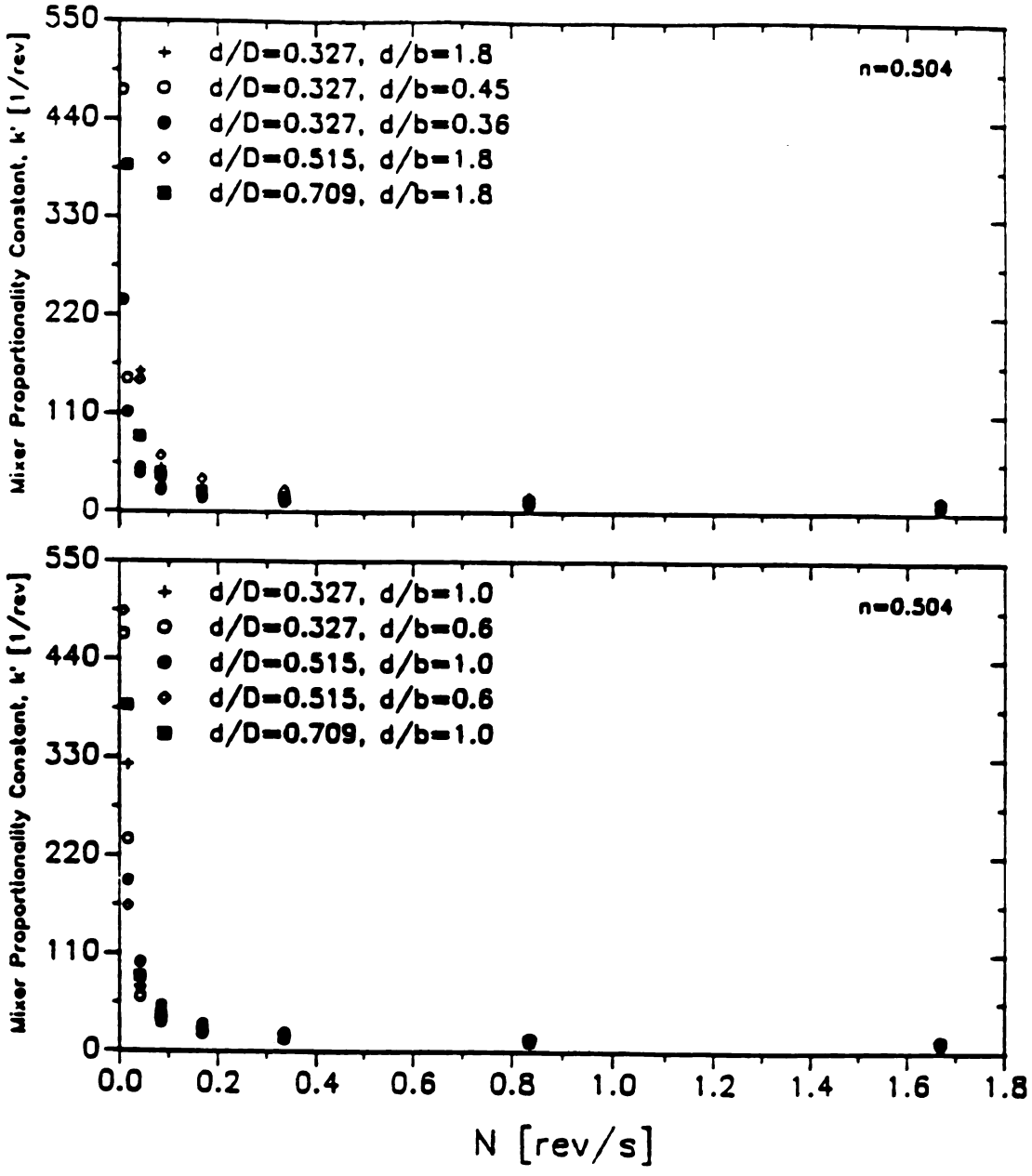

Figure 6.17: Mixer Proportionality Constant, k', Versus Rotational Speed, N, for Paddle Impellers When Mixing a Non-Newtonian Fluid (CMC 1%)

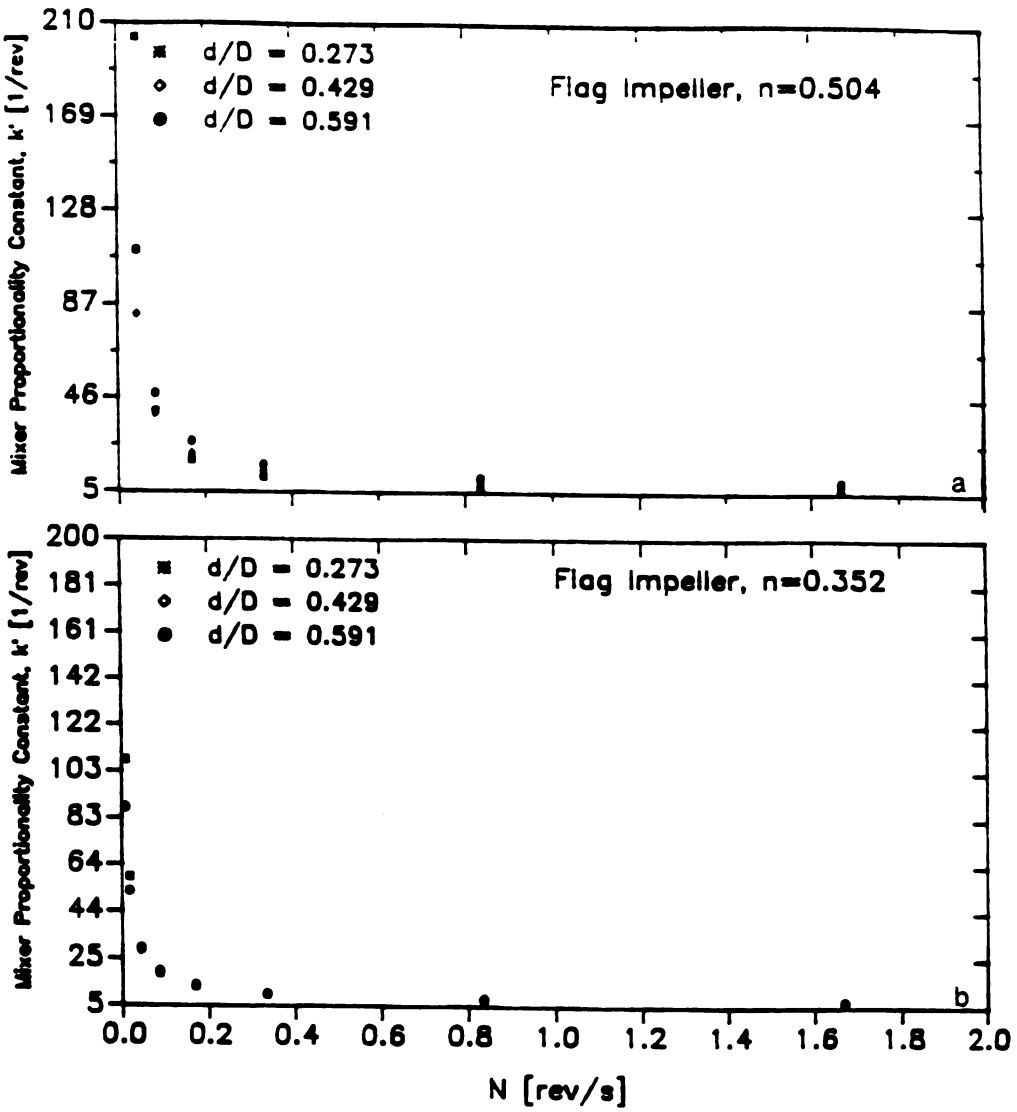

Figure 6.18: Mixer Proportionality Constant, k', Versus Rotational Speed, N, for Flag Impeller When Mixing Non-Newtonian Fluids. a) CMC 1%; b) CMC 2%

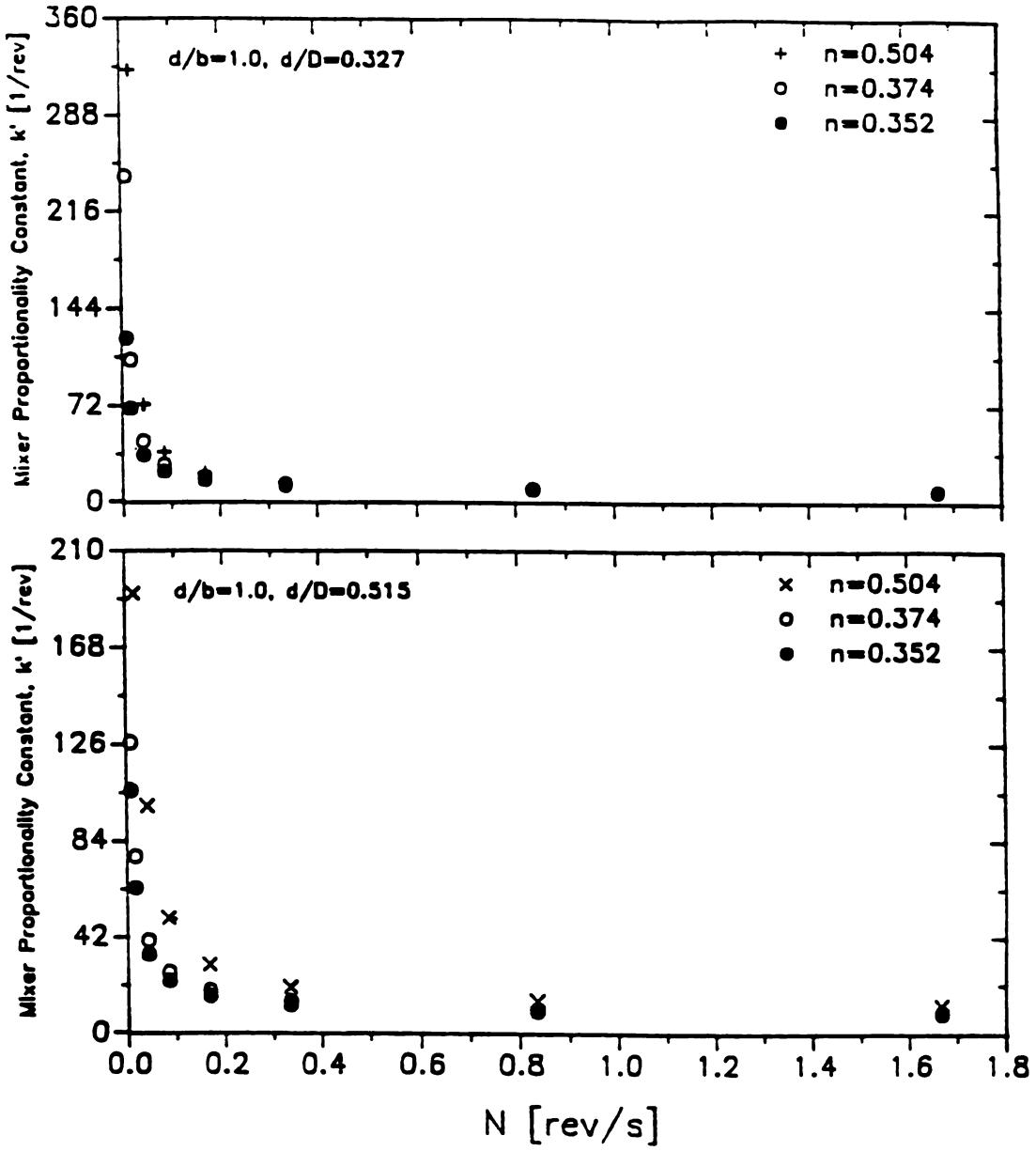

Figure 6.19: Plot of Mixer Proportionality Constant, k', Versus Rotational Speed, N, for Non-Newtonian Fluids (Paddle Impellers)

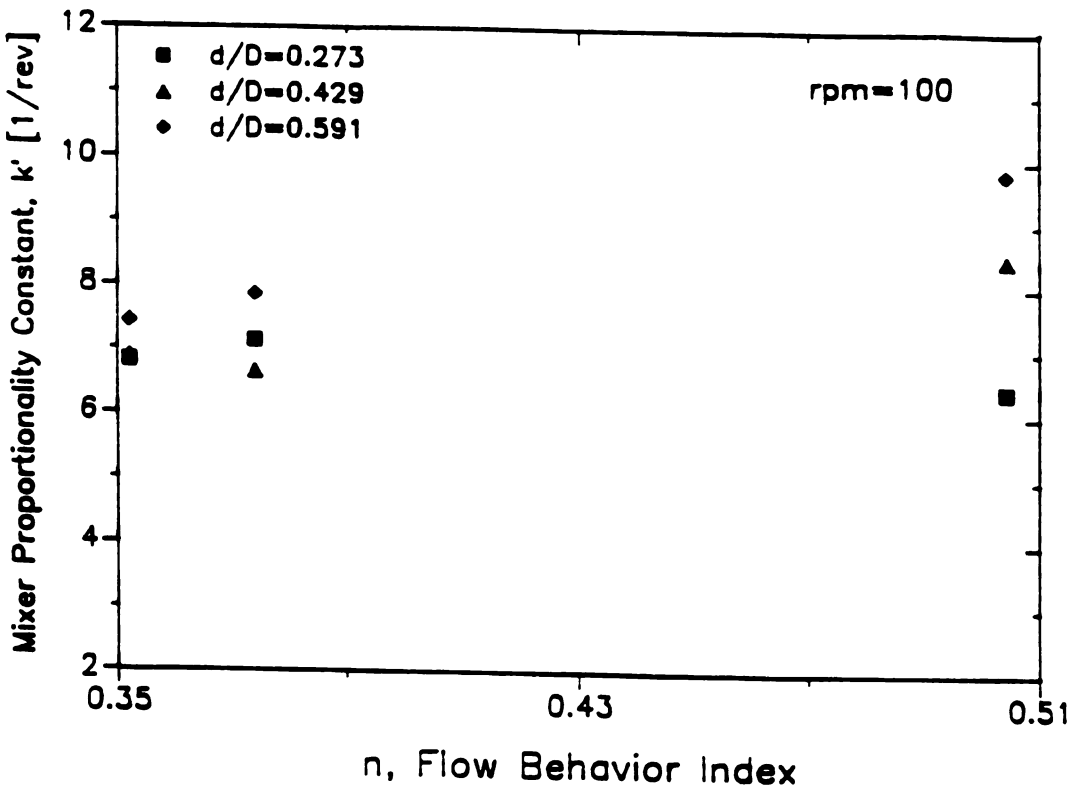

Figure 6.20: Plot of Mixer Proportionality Constant, k', as a Function of Flow Behavior Index, n (Flag Impeller)

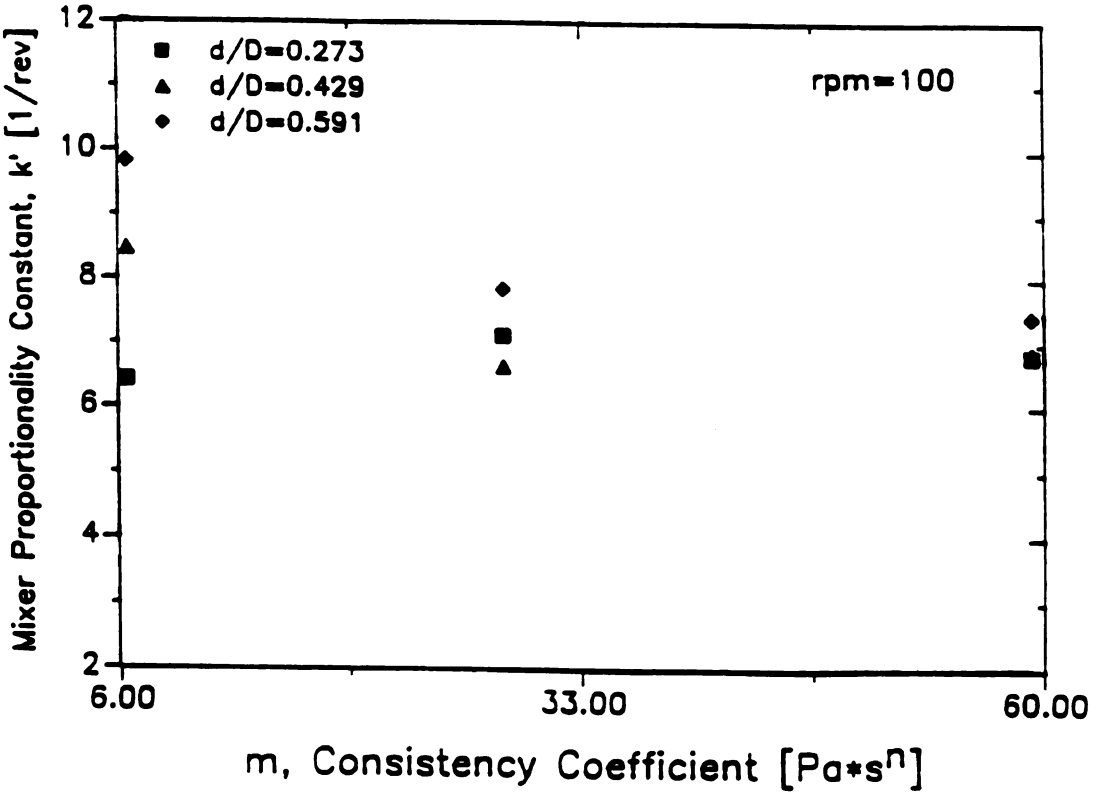

Figure 6.21: Plot of Mixer Proportionality Constant, k', as a Function of Fluid Consistency Coefficient, m (Flag Impeller)

the flow behavior index. The lower the n, the lower the value of k'. However, no conclusions can be made by analyzing only the effect of the flow behavior index. Figure 6.21 shows that the more viscous fluid (m= 59.275 Pa s^n) yields the lower values of k' (consequently, average shear rates). Figures 6.22 and 6.23 show similar plots for a paddle impeller (d/b=1.8) at 20 and 100 rpm (0.333 and 1.6667 rev/s). The effect of the agitated fluid on the values of k' was the same as for the flag impeller. No final conclusions can be drawn up to this point since variations occur when the impellers operate in different geometric systems and this needs further investigation. The effect of system geometry will be discussed in the following section.

6.1.1.2.1.3) Cup Diameter

Results indicate that the value of the proportionality constant, k', for the paddle impellers, is a function of the size of the cup (Figures 6.22 and 6.23). The bigger cup (i.e., big impeller-to-cup-diameter ratio, d/D=0.327) generates lower values of k' than the produced in the smaller cups when rotating at high speeds. At lower speeds (20 rpm) differences in the values of k' are only significant when agitating a low viscosity fluid (CMC 1%) (Figure 6.22). Figure 6.24b presents the changes in k' for a paddle impeller (d/b=1.0) rotating in three different cups at 2.5, 10 and 100 rpm. It may be seen that the diameter of the fluid container is an important parameter to consider for the design of a mixing system for mixer viscometry techniques when working at low rotational speeds. At higher speeds, the influence of cup diameter becomes almost negligible when agitating highly viscous fluids (n=0.352, m=59.275 Pa s^n).

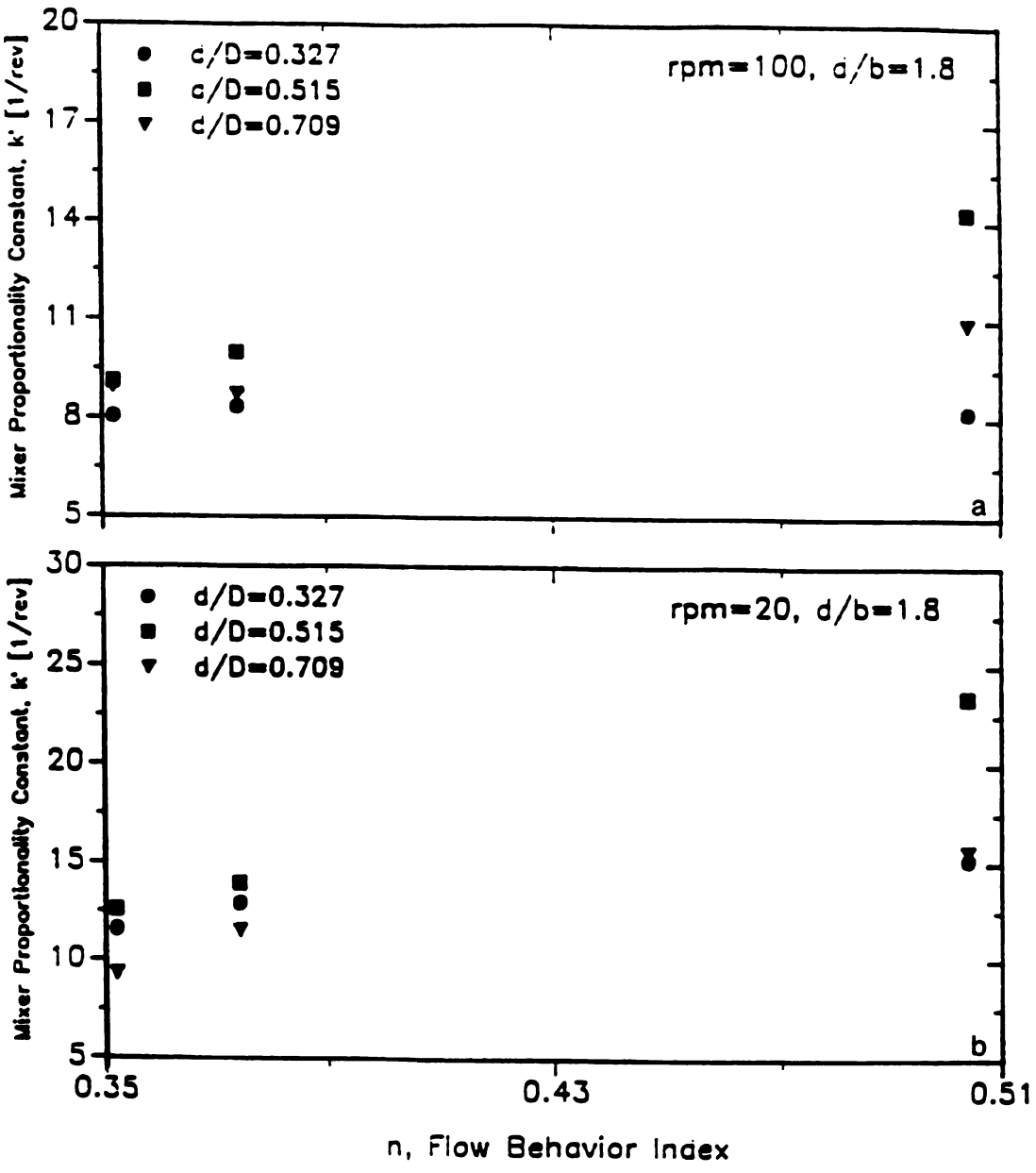

Figure 6.22: Plot of Mixer Proportionality Constant, k', as a Function of Flow Behavior Index, n (Paddle Impeller); a) 100 rpm; b) 20 rpm

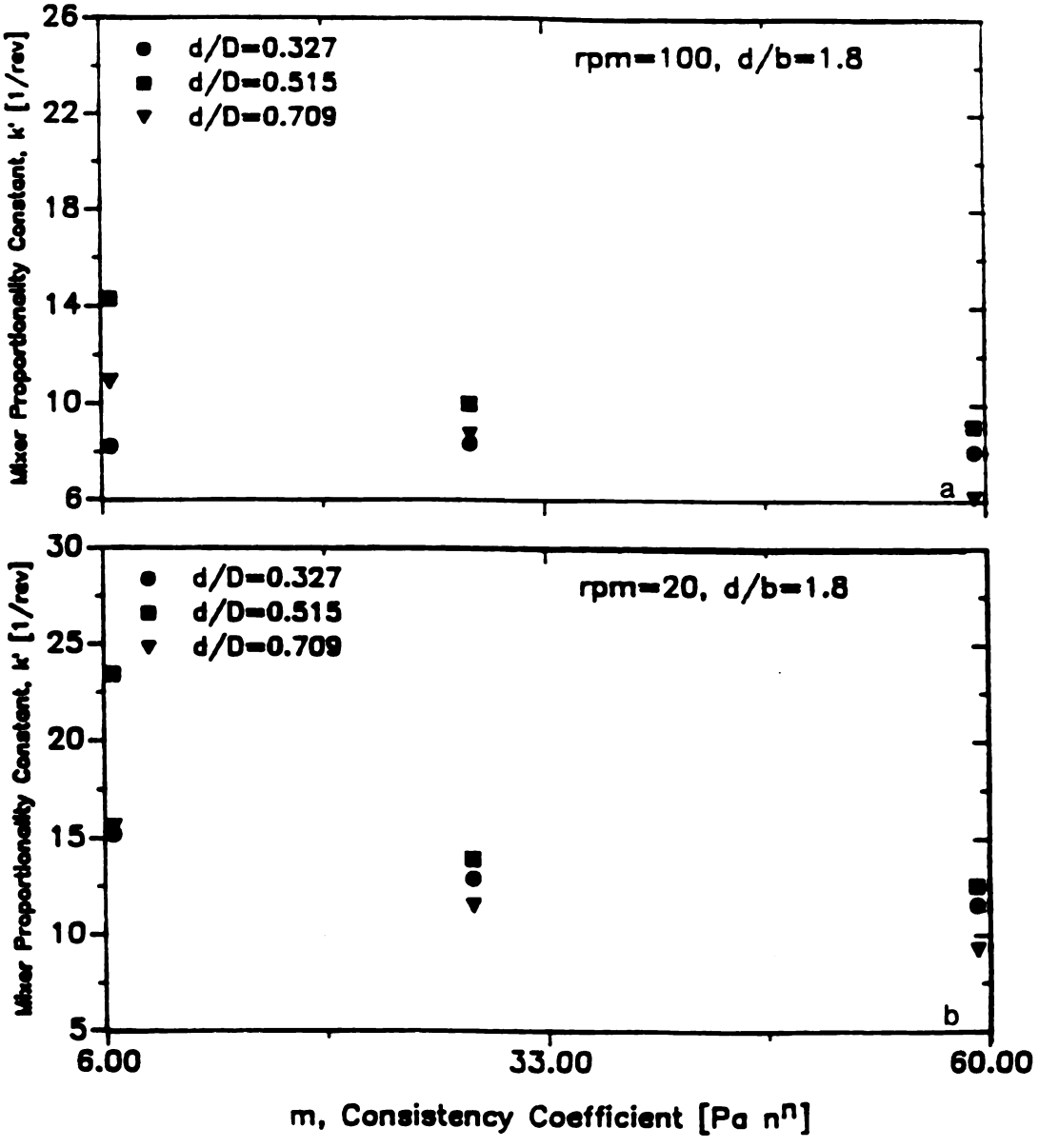

Figure 6.23: Plot of Mixer Proportionality Constant, k', as a Function of Fluid Consistency Coefficient, m (Paddle Impeller); a) 100 rpm; b) 20 rpm

Results presented in Figures 6.20 and 6.21 indicate that cup diameter becomes important only when agitating a low viscosity fluid, with changes in the values of k' ranging from 9 to 6.5 (1/rev), as compared to the values of k' of 7 to 7.5 (1/rev) for a high viscosity fluid. It is interesting to find that the value of k' is higher for the more shear-thinning fluid (n=0.352) when the flag impeller rotates in a bigger cup (d/D=0.273) than the value of the less shear-thinning fluid (n=0.504) (Figure 6.20). The trend is reversed for smaller impeller to cup diameter ratios. These results confitm the need for a better understanding of the influence of fluid properties on k'.

6.1.1.2.1.4) Impeller Size (Blade Height)

Figure 6.24a shows the changes of the values of k' as a function of impeller size (d/b). It is clear that k' is significantly affected by the height of the impeller's blade at low impeller speeds (2.5 rpm), especially when agitating the low viscosity fluid (n=0.504). As N increases, the effect of (d/b) becomes less important. The values of k' for the different paddle impellers rotating in a big cup are shown in Figure 6.25. Results agree with the previous observation that k' is not significantly dependent on impeller size when rotating at high speeds, independently of the rheology of the agitated fluid. At a rotational speed of 20 rpm, k' values varied from 15.2 to 10.2 (1/rev) when agitating a low viscosity fluid as compared to k' values from 11.5 to 8.7 (1/rev) for a higher viscosity fluid when using big and small paddles.

It may also be noted that the bigger impeller generated the lower k' values (i.e., shear rates). The same behavior was observed when using

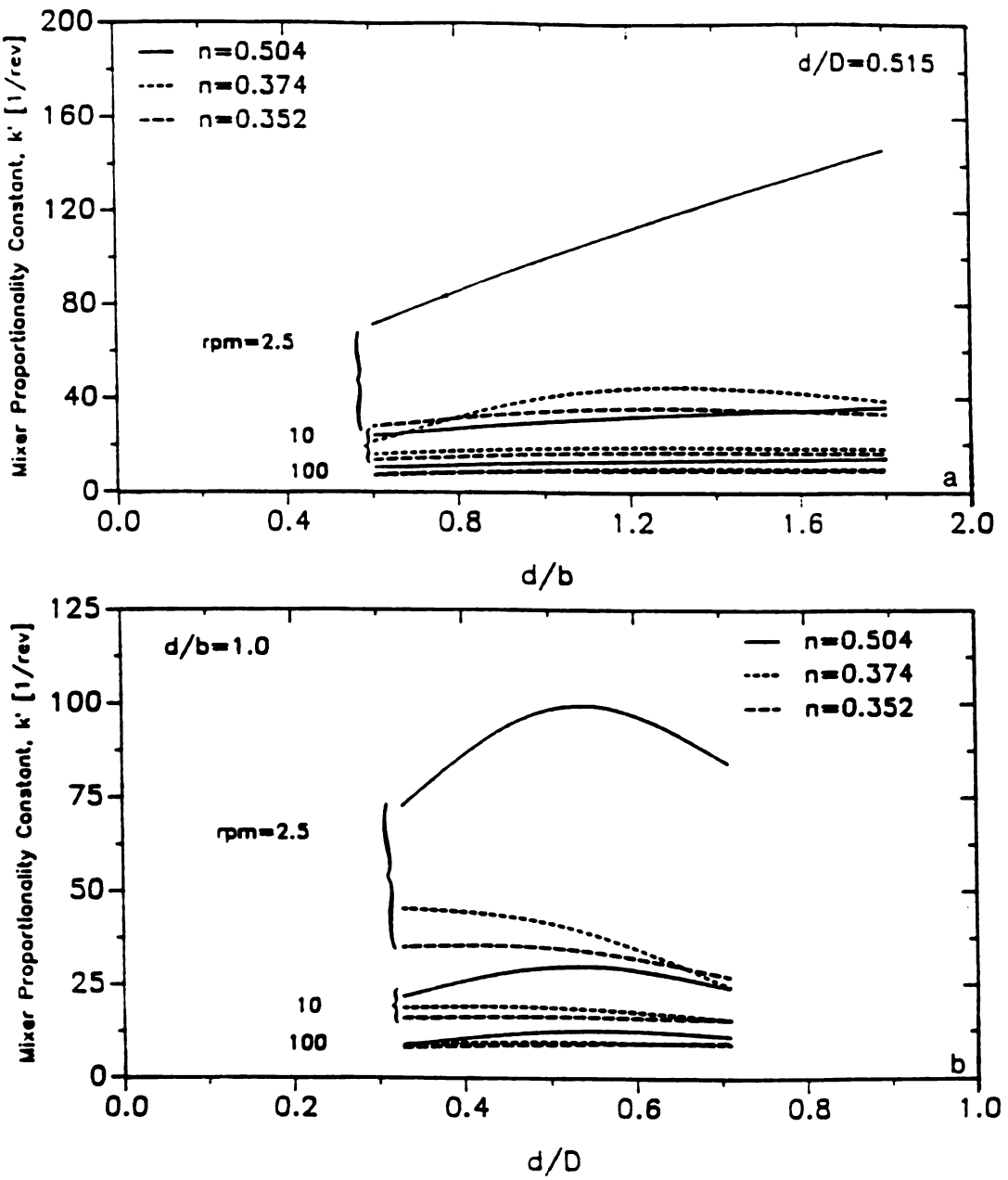

Figure 6.24: Plot of Mixer Proportionality Constant, k', as a Function of System Geometry. a) Impeller Size (d/b); b) Cup Size (d/D)

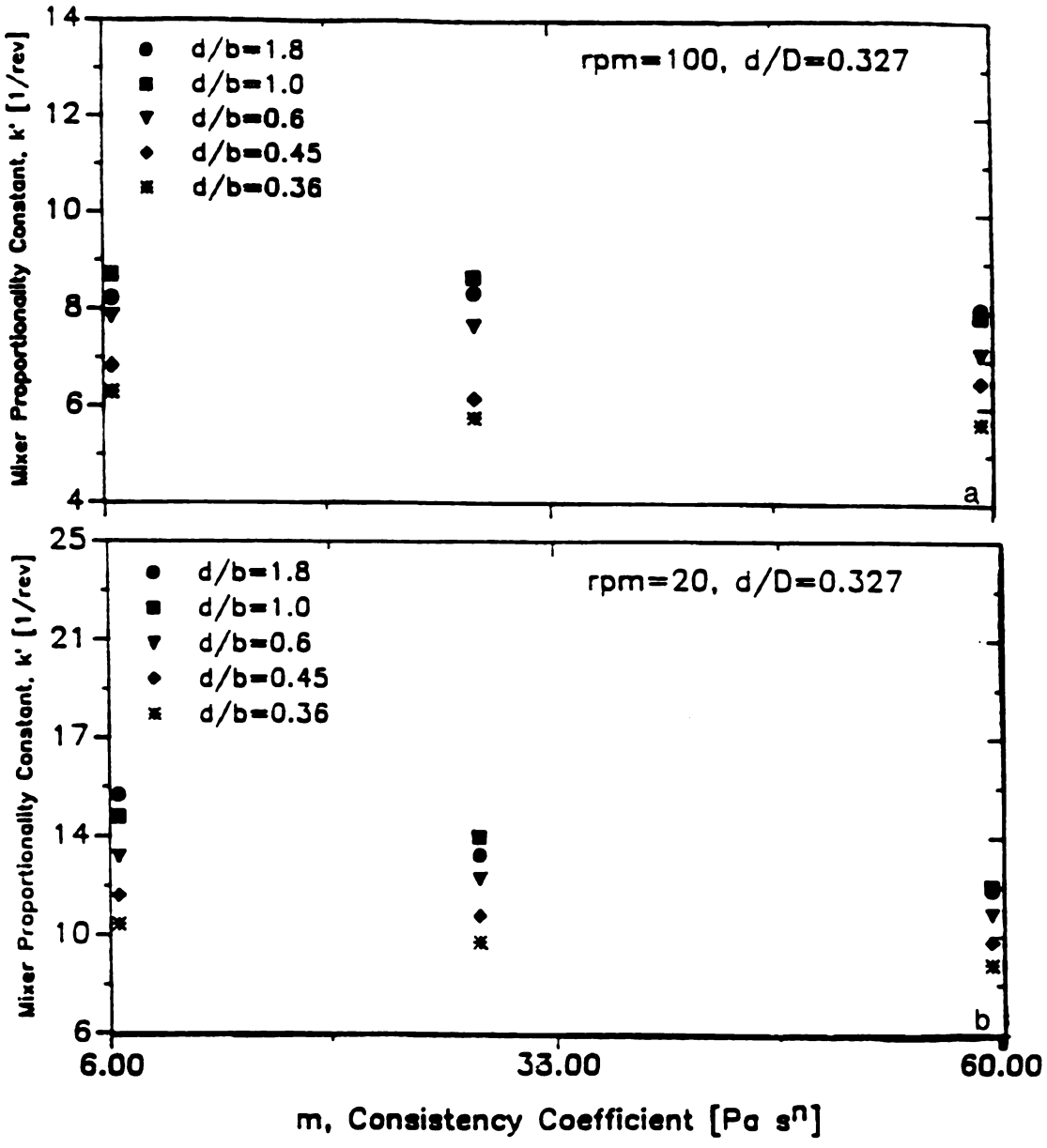

Figure 6.25: Plot of Mixer Proportionality Constant, k', as a Function of Fluid Consistency Coefficient, m (Pa s^n) for Different Paddle Impellers. a) 100 rpm; b) 20 rpm.

the Power Curves Method.

6.1.1.2.2) Estimation of Average Shear Rates

Using the values of the mixer proportionality constant k' determined from Eqn. (6.12), the mixing average shear rates were calculated from Eqn. (3.8). Shear rates were also calculated using a constant value of k' at selected rotational speeds of 10 and 50 rpm in order to determine the significance of using a constant value of k' when using mixer viscometry techniques. Results are presented in Figures 6.26 and 6.27 for the paddle impellers (Figure B6 presents other results). It is clear that the choice of a constant value of the proportionality constant at 10 rpm generates considerably higher average shear rates than when using the values of k' at 50 rpm and Eqn. (6.12). For the less viscous fluid, the larger impeller-to-cup diameter ratio (d/D=0.327) (Figure 6.26b) produces higher shear rates than the smaller gap (Figure 6.26a). Also, Eqn. (6.12) seems to produce unstable results at low values of rotational speeds.

Similar behavior was observed when agitating a high viscosity fluid (Figure 6.27b). However, interesting results are observed in the small gap situation (Figure 6.27a). In this case, the value of k' does not significantly lead to considerable differences in the determined shear rates. In all cases, Eqn. (6.12) presents unstability at low rotational speeds.

For the flag impeller, the significant differences in shear rates when using Eqn. (6.12) and a constant value of k' (at 10 rpm) are shown in Figures 6.28 and 6.29. Variations are bigger when agitating a less viscous fluid (Figure 6.28) than for the high viscosity fluid (Figure

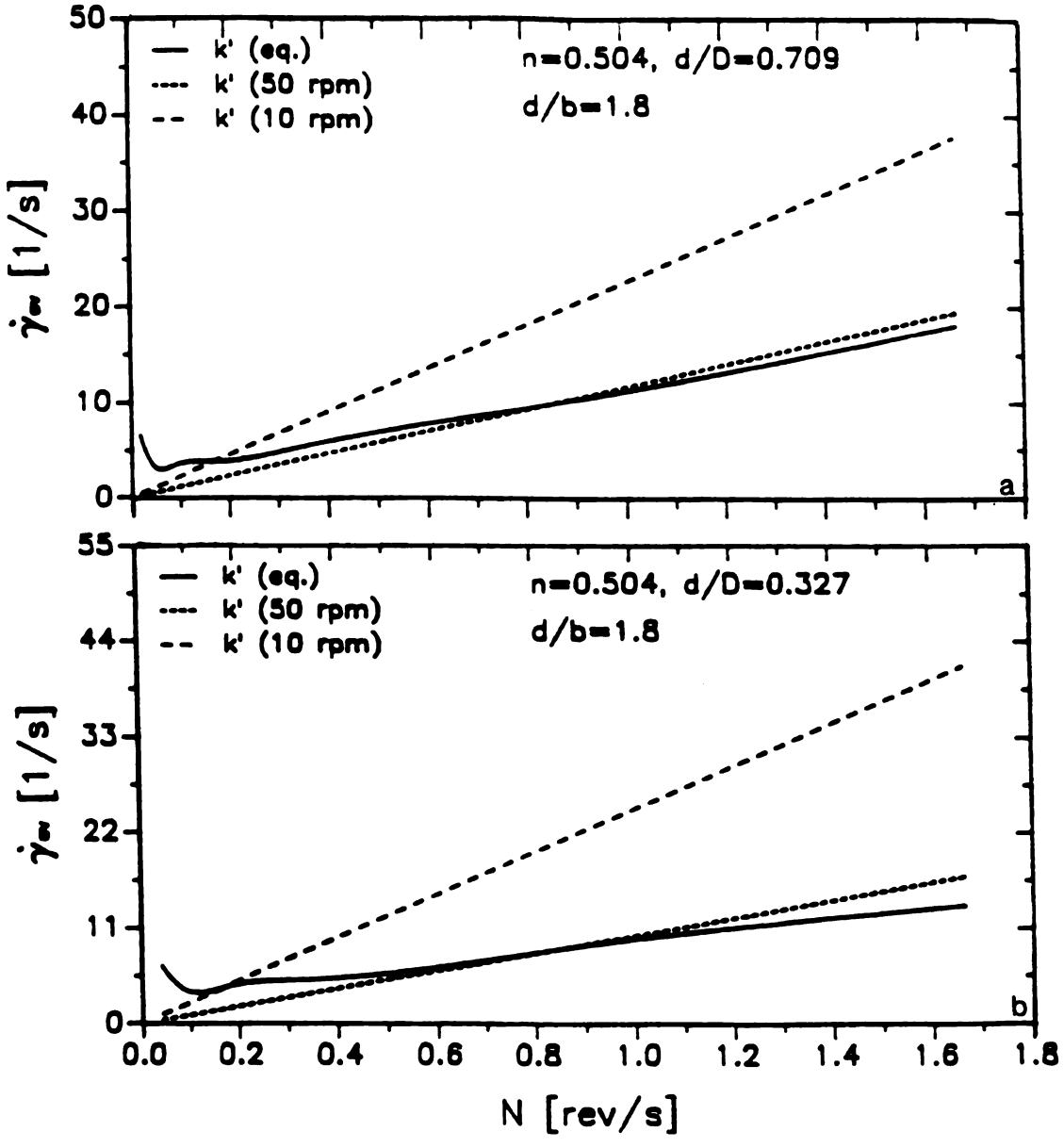

Figure 6.26: Average Shear Rate as a Function of Impeller Rotational Speed for a Paddle Impeller (CMC 1%); a) Small Gap; b) Large Gap

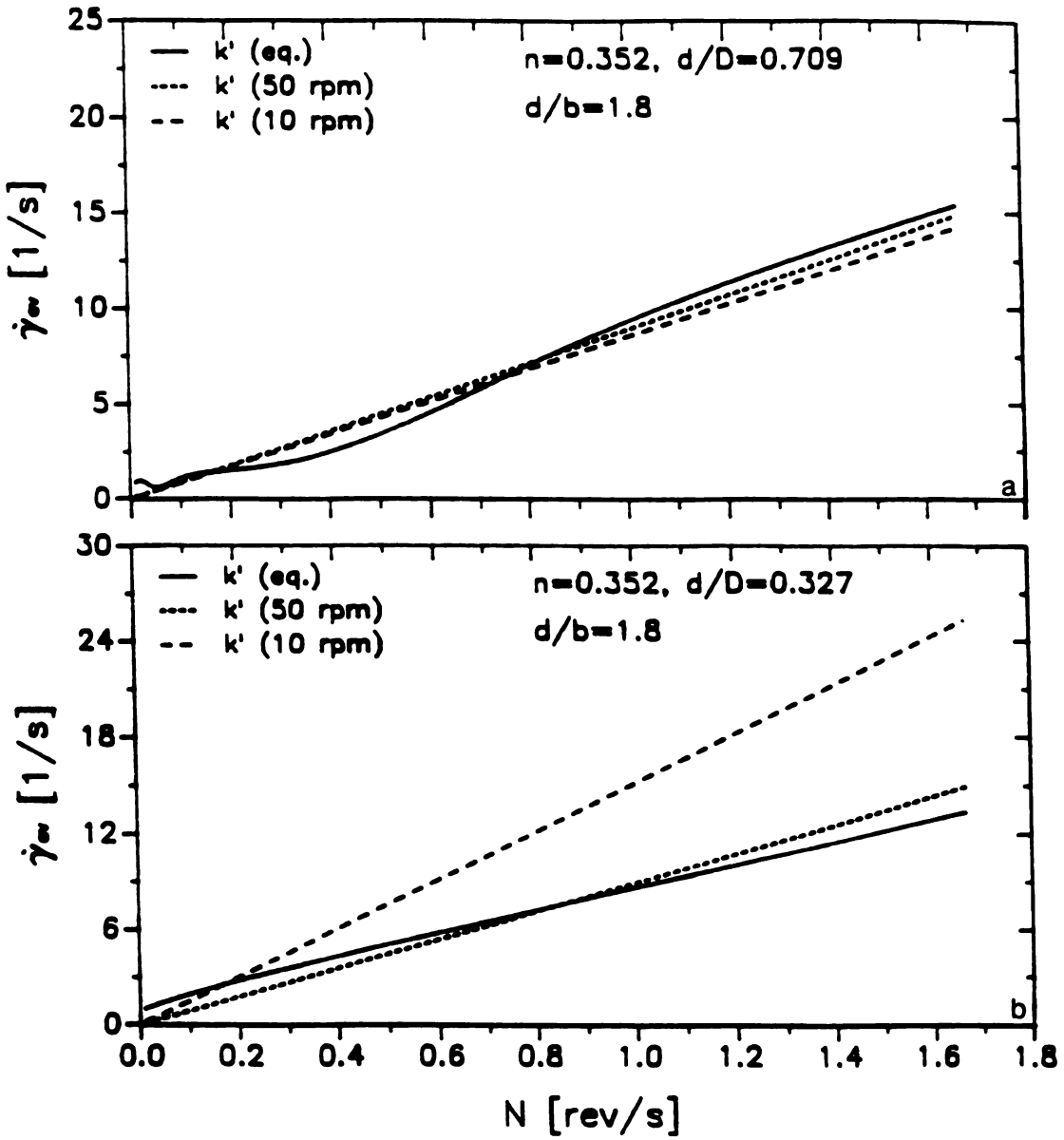

Figure 6.27: Average Shear Rate as a Function of Impeller Rotational for a Paddle Impeller (CMC 2%); a) Small Gap; b) Large Gap

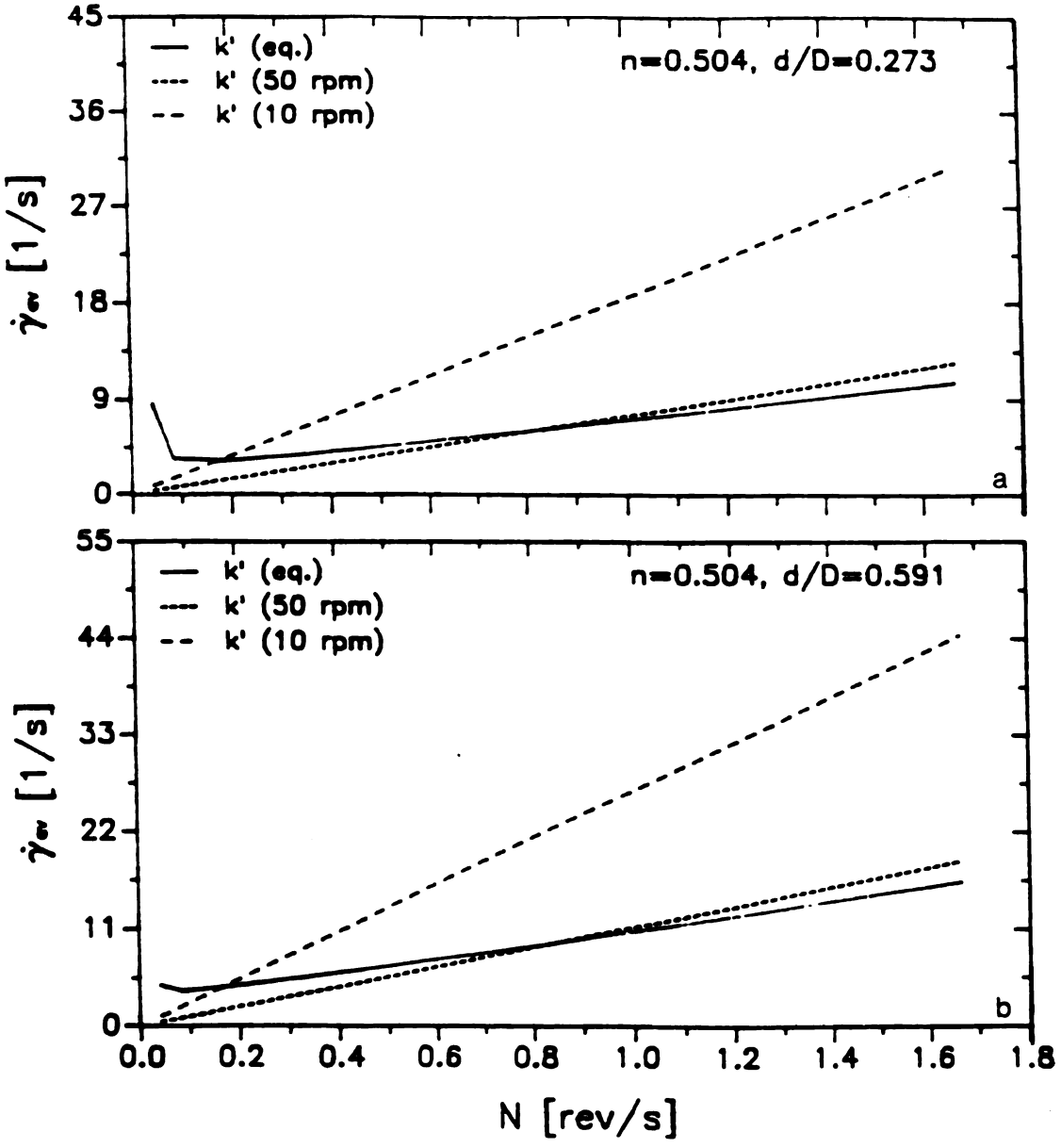

Figure 6.28: Average Shear Rate as a Function of Impeller Rotational Speed for a Flag Impeller (CMC 1%); a) Large Gap; b) Small Gap

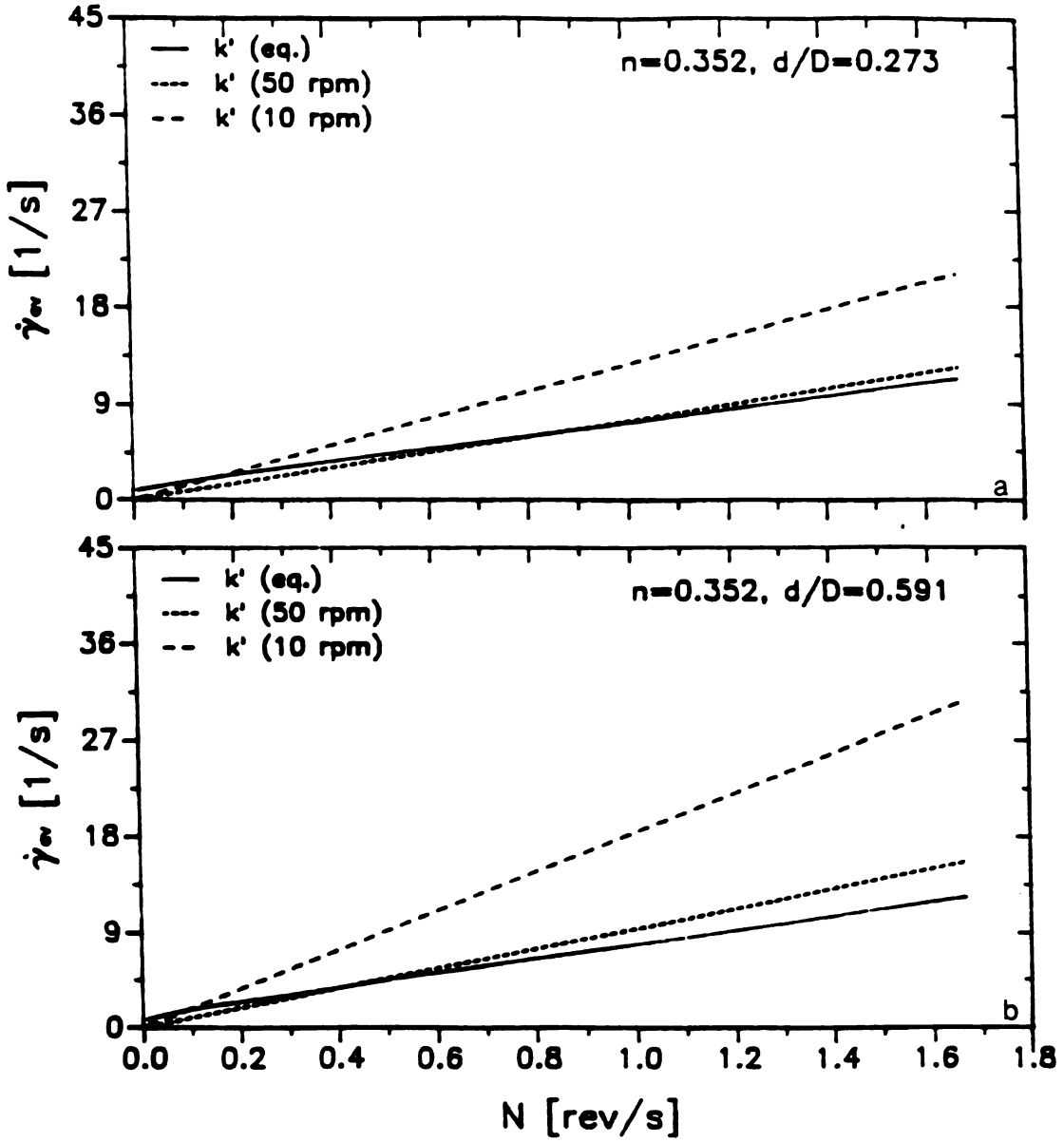

Figure 6.29: Average Shear Rate as a Function of Impeller Rotational Speed for a Flag Impeller (CMC 2%); a) Large Gap; b) Small Gap

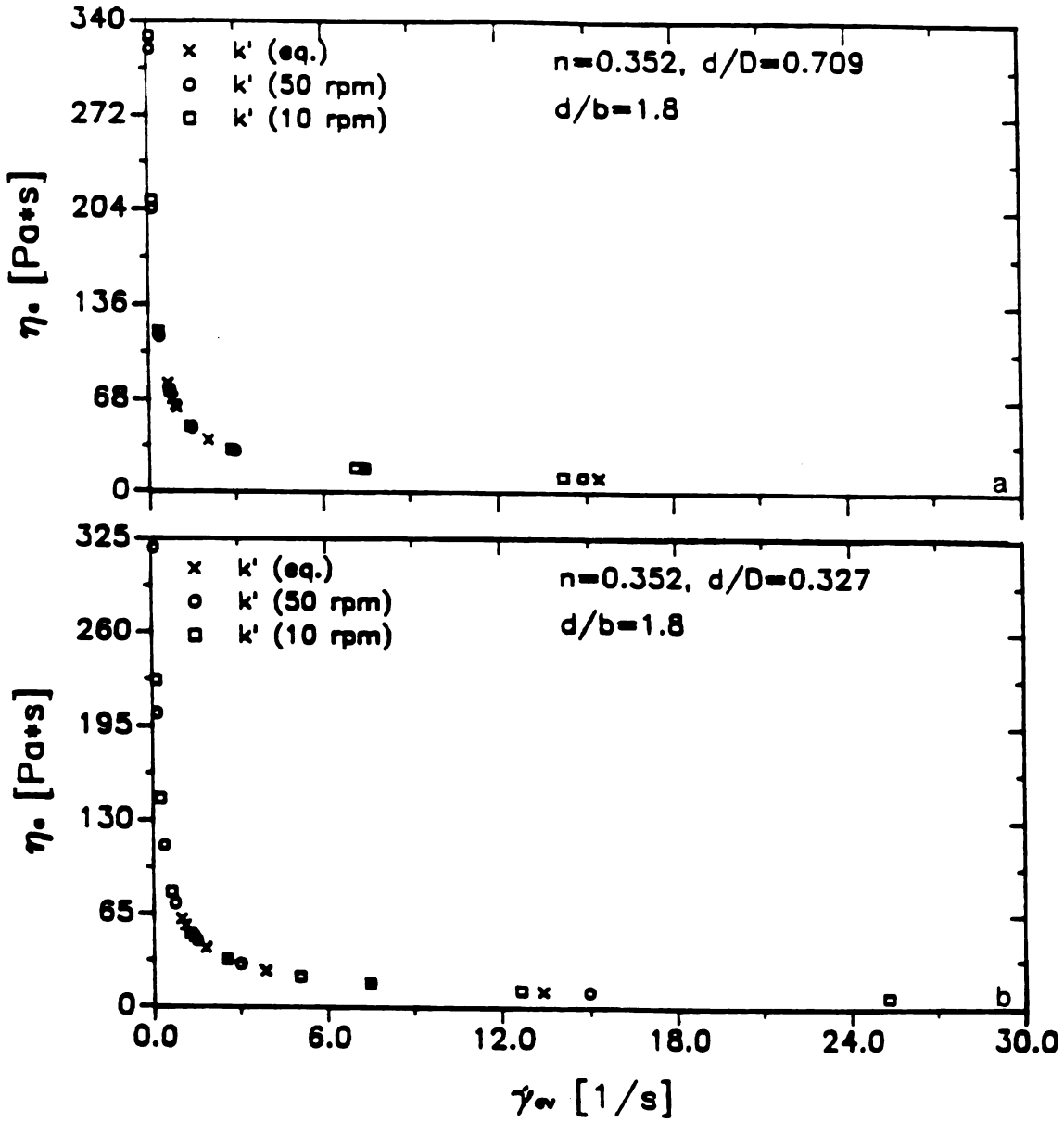

Figure 6.30: Apparent Viscosity as a Function of Average Shear Rate for A Paddle Impeller (CMC 2%); a) Small Gap; b) Large Gap

6.29).

Figure 6.30 shows the apparent viscosity-shear rate relationships when agitating the high viscosity fluid. The use of a constant k' value overestimates the values of η_a while the use of Eqn. (6.12) predicts lower values of η_a for the shear-thinning fluid. Figure 6.31 shows the results for a flag impeller (Other results are shown in Figures B7 and B8).

In summary, results indicate that the proportionality constant k' evaluated by the Mixer Torque Curves Method is significantly affected by impeller rotational speed, fluid properties and mixing system. The conventional mixer viscometry method of using a constant value of k' , depending only on impeller geometry, may lead to significant errors when measuring properties of shear-thinning fluids at low values of N.

6.1.2) Slope Method

The Slope Method consists of the construction of plots of log $[P/(md^3N^{n+1})]$ versus (1-n) [Eqn. (3.47)]. The value of the impeller proportionality constant, k', is obtained from the slope of the straight line ($k' = 10^{slope}$). Figure 6.32 shows a typical plot of log $[P/(md^3N^{n+1})]$ versus (1-n) for the paddle impellers. Figure 6.32a is the plot for a paddle impeller with blades 3 cm high. Figure 6.32b is the plot for a paddle impeller with blade heigth equal to 1 cm. Also shown in Figure 6.32 is the line obtained by linear regression analysis (R^2 = 0.980 and 0.983, respectively) of the experimental data. Similar results were obtained with the flag impeller (Figure 6.33) rotating in a cup of diameter (D) equal to 3.5 cm (d/D=0.591) (Results for the other impeller/cup combinations are presented in Figures B9 through B13).

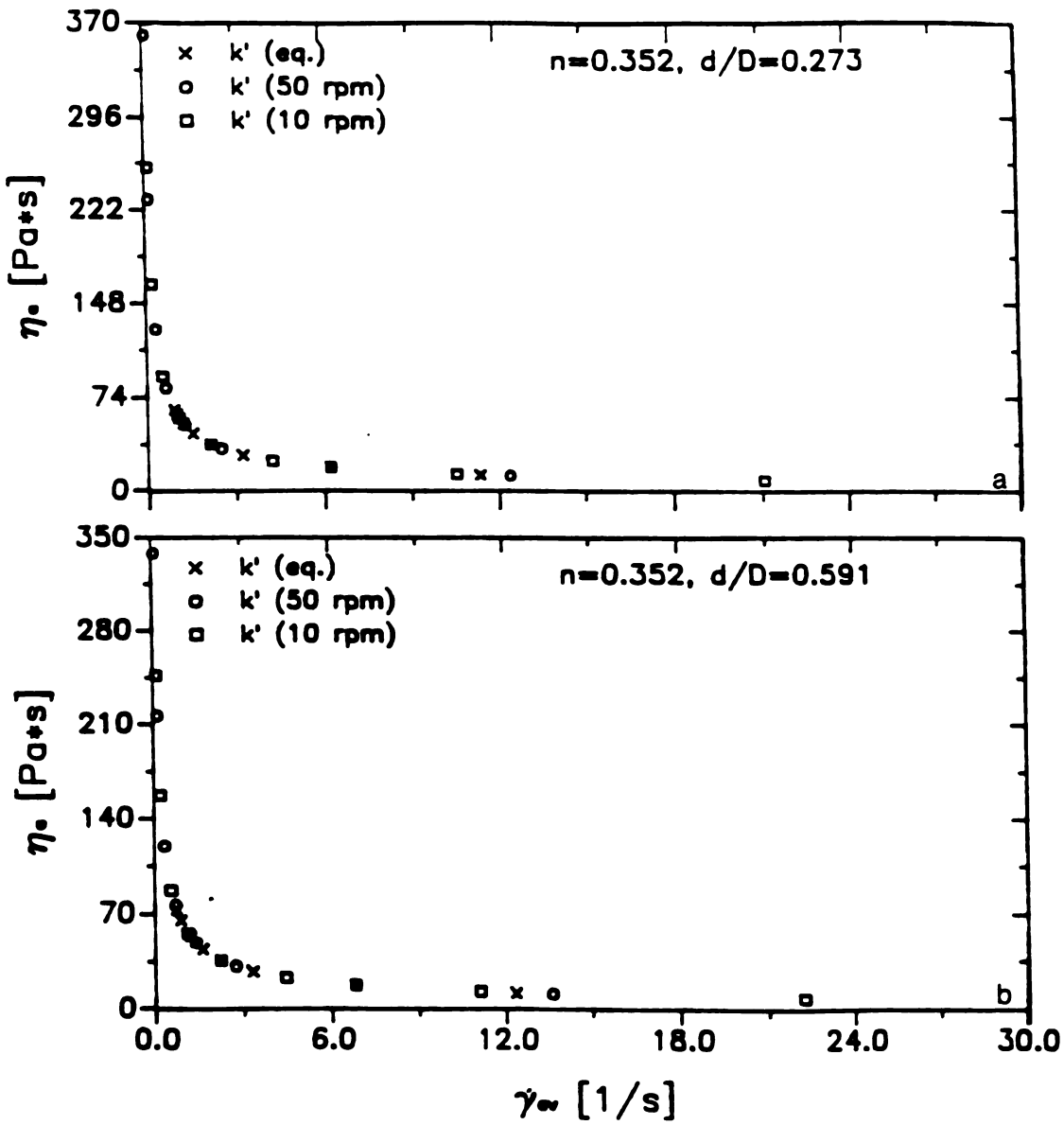

Figure 6.31: Apparent Viscosity Versus Average Shear Rate for a Flag Impeller (CMC 2%); a) Large Gap; b) Small Gap

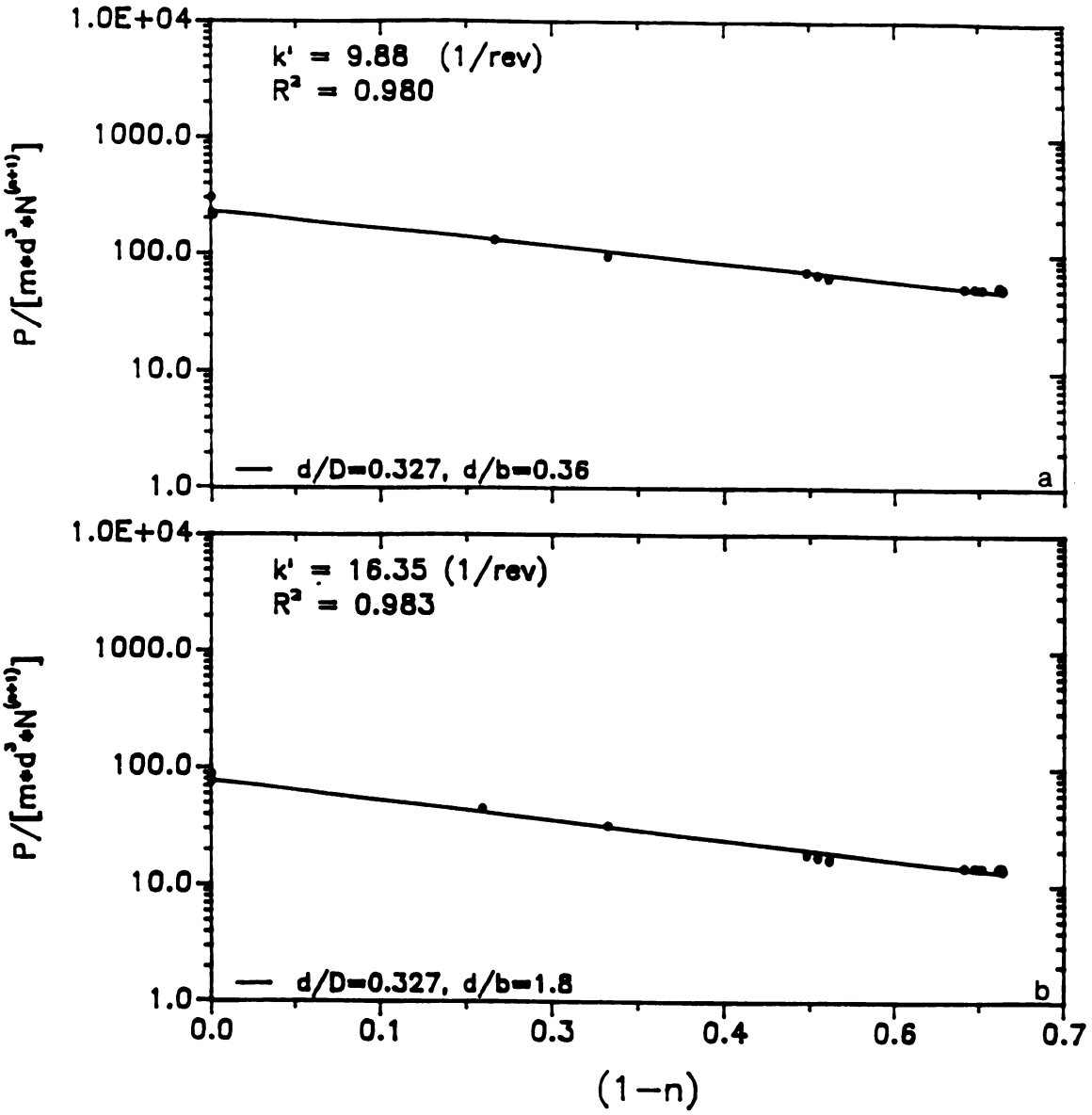

Figure 6.32: Plots of Dimensionless Functions $[P/(md^3N^{n+1})]$ Versus (1-n) For The Paddle Impellers; a) Impeller 5 (b=5 cm); b) Impeller 1 (b=1 cm)

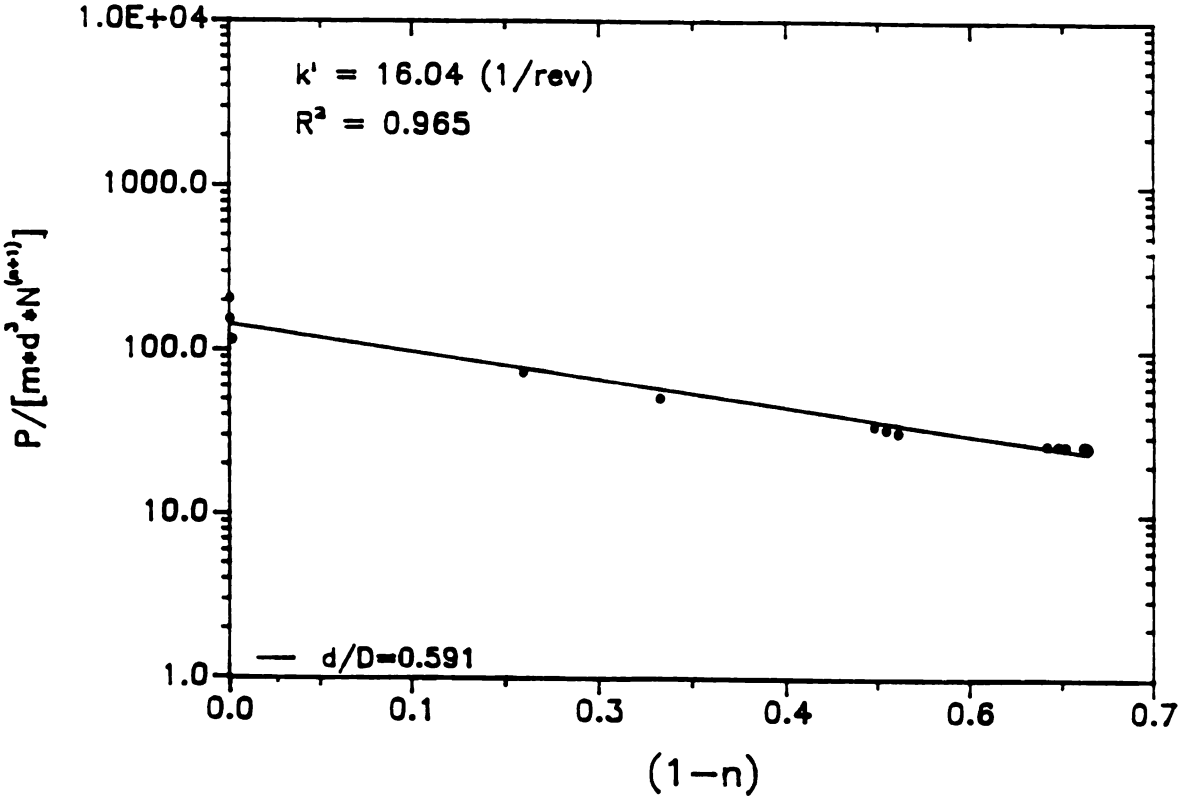

Figure 6.33: Plots of Dimensionless Functions $[P/(md^3N^{n+1})]$ Versus (1-n) For The Flag Impeller (Small Gap)

The scatter in the values of the function $[P/(md^3N^{n+1})]$ observed in Figures 6.32 and 6.33 is not uncommon, and it can be found for impellers studied by others researchers (Rieger and Novak, 1973; Rao and Cooley, 1984). Table 6.8 presents the values of the proportionality constant k' (evaluated using the Slope method) for the different geometries when agitating the fluids with the paddles and flag impeller. Considerable differences in the values of k' are observed for paddle impellers of different size (Systems 1 to 5). The effect of the geometric variables will be discussed in the following section.

6.1.2.1) Factors Affecting k'

6.1.2.1.1) System Geometry

The geometry of the system is an important factor in the evaluation of the proportionality constant (Table 6.8). As in the matching method (Power Curves Method), the bigger impeller produces the lower values of k' , and an increase in the values of k' is observed in the smaller cups (small gap). For the flag impeller, the smaller gap produced smaller values of k'. Thus, impeller shape seems to be a factor since different results are obtained for the two impeller types. Deviations from linearity in the plots of Eqn. (3.47) (Figures 6.32 and 6.33) were not observed for the impellers investigated in this study. This suggests that the value of the impeller proportionality constant is not a function of the properties of the fluid when using this mixer viscometry method.

It was suspected that the slope method may mask the effect of the impeller rotational speed on the value of k'. Since some researchers have sometimes used a single value of the impeller rotational speed for

Table 6.8: Values of k' (evaluated using the Slope Method)

Paddle Impellers

SYSTEM			k'	R^2
	d/D	d/b		
1	0.327	1.80	16.354	0.983
2	0.327	1.00	12.576	0.985
3	0.327	0.60	10.407	0.981
4	0.327	0.45	10.000	0.960
5	0.327	0.36	9.880	0.980
6	0.515	1.80	16.89	0.960
7	0.515	1.00	15.99	0.960
8	0.515	0.60	10.306	0.904
9	0.709	1.80	17.730	0.972
10	0.709	1.00	9.827	0.920

Flag Impeller

SYSTEM		k'	R^2
1	0.273	20.070	0.980
2	0.429	15.090	0.970
3	0.591	16.04	0.965

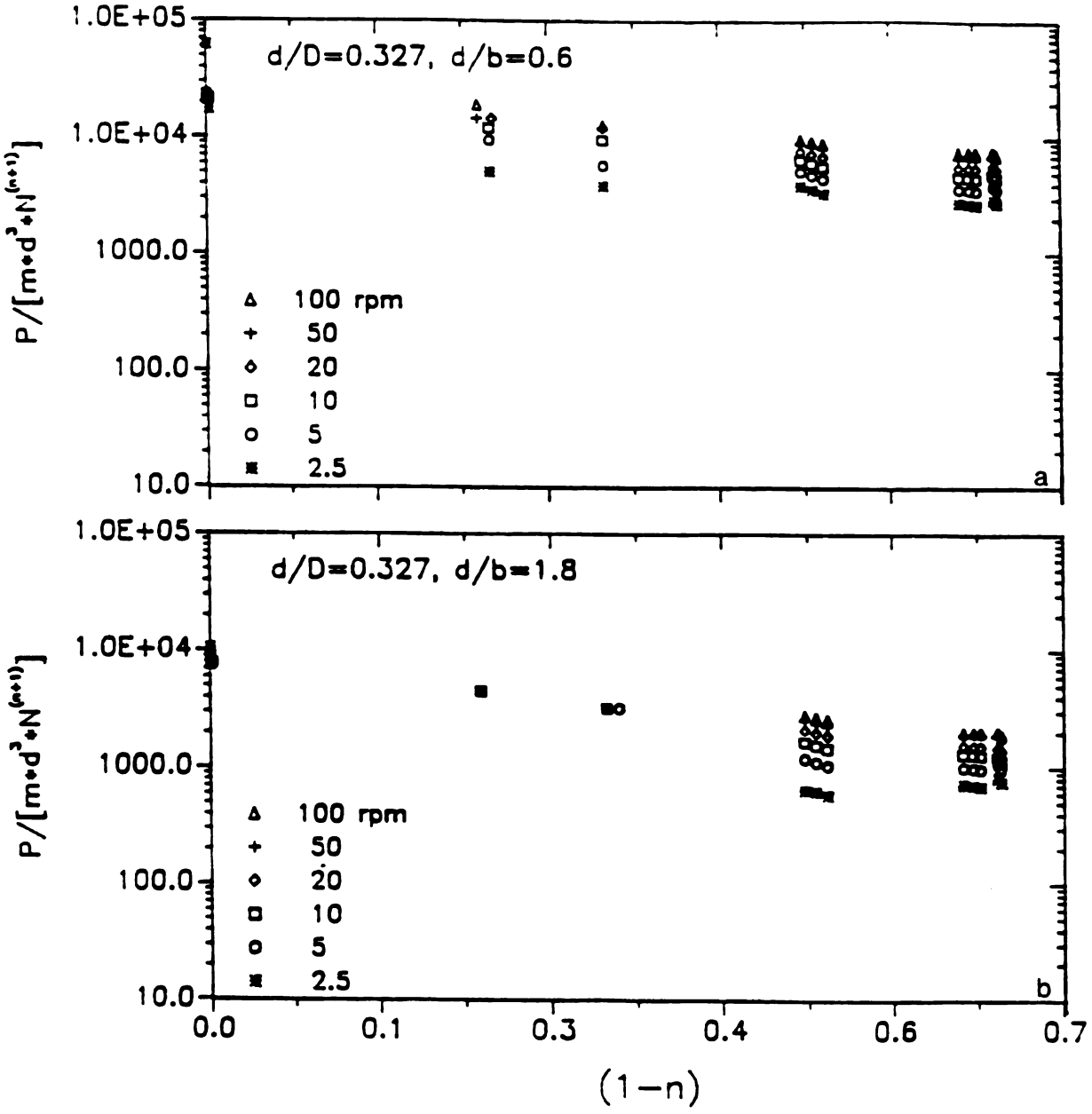

Figure 6.34: Plots of Dimensionless Functions $[P/(md^3N^{n+1})]$ Versus (1-n) For The Paddle Impellers at Different Values of N; a) Impeller 3 (b= 3cm); b) Impeller 1 (b=1 cm)

the development of plots such as Figure 6.32, this effect was investigated in this study. Figure 6.34 shows the changes in the slope of the lines when selecting different values of N for the paddle impellers. Similar results were obtained with the flag impeller (Figure 6.35). Table 6.9 presents the values of the proportionality constant k' (evaluated by using the slope method) for the different system geometries when agitating the fluids with the paddles and flag impeller obtained at three different values of N (5, 20 and 100 rpm). It is clear that if only a particular value of the impeller rotational speed is used for the evaluation of k', the selection of N becomes a critical step in the method since significant differences in the value of k' are observed at the different values of N: the lower the value of N, the higher the value of k'. Also, as N increases (100 rpm), k' becomes less dependent on system geometry.

Regression analysis was conducted for the data for the paddle impellers and results indicated that the diameter ratio (d/D) was not statistically significant (Table 6.10). The following model was proposed:

$$k' = \beta_0 \, (d/b)^{\beta_1} \, N^{\beta_2} \qquad (6.13)$$

Thus,

$$k' = 9.365 \, (d/b)^{0.41} \, N^{0.347} \qquad (6.14)$$

Comparing the magnitude of k' (Table 6.8) for the flag impeller with the one obtained for the paddle impeller with same blade height (Impeller # 3: b = 3 cm; b/d = 0.6), the magnitude of k' is higher for the flag impeller. Results in Table 6.9 also indicate that higher values

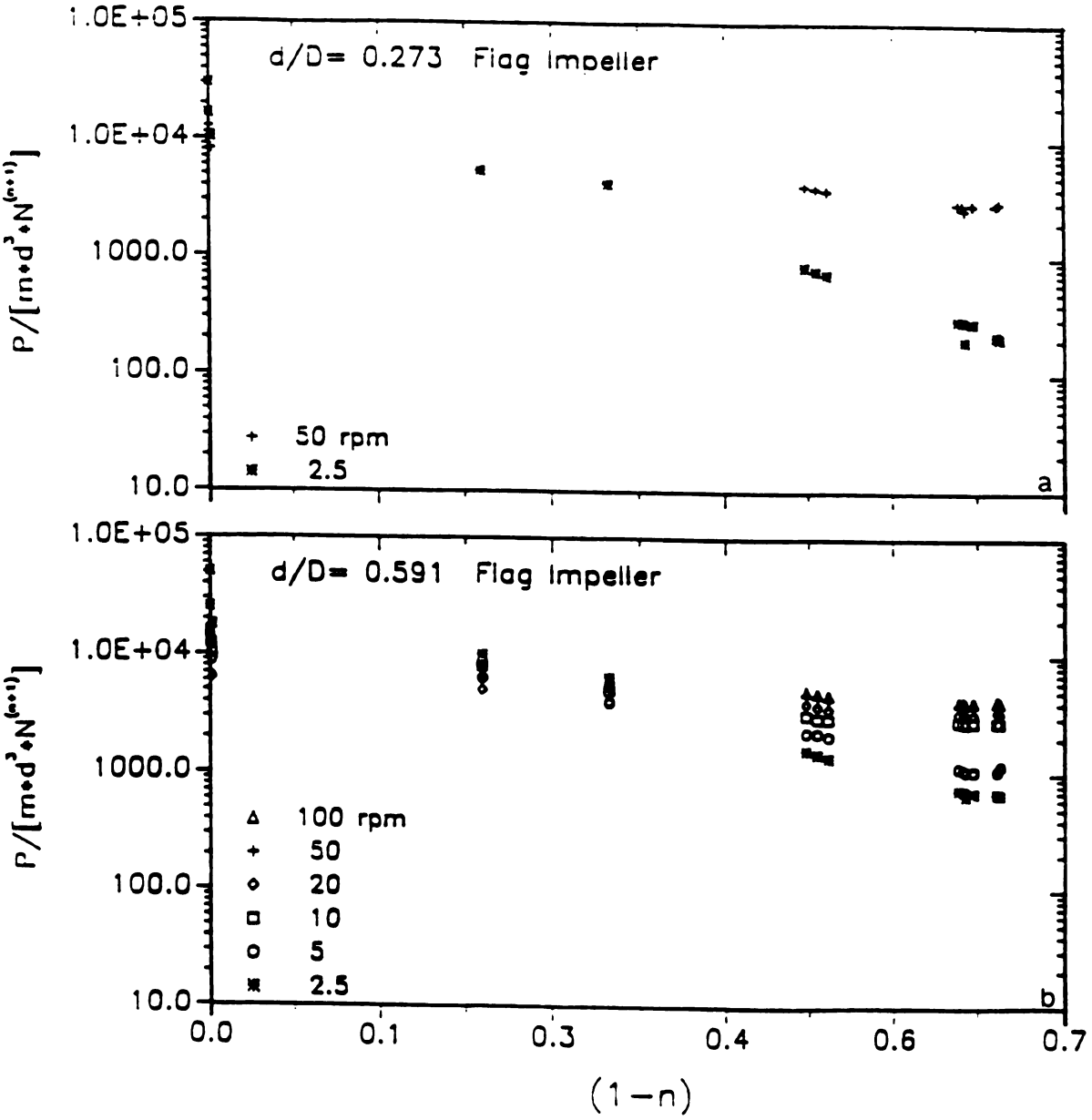

Figure 6.35: Plots of Dimensionless Functions $[P/(md^3N^{n+1})]$ Versus (1-n) For The Flag Impeller at Different Values of N; a) Large Gap; b) Small Gap

Table 6.9: Values of k' (evaluated using the Slope Method) as a Function of Impeller Rotational Speed

Paddle Impellers

SYSTEM			k'		
	d/D	d/b	5 rpm	20 rpm	100 rpm
1	0.327	1.80	30.196	13.542	8.685
2	0.327	1.00	20.705	11.719	8.154
3	0.327	0.60	19.217	9.895	7.020
4	0.327	0.45	14.348	9.732	6.469
5	0.327	0.36	14.290	9.375	6.038
6	0.515	1.80	56.959	13.651	8.526
7	0.515	1.00	34.825	13.343	7.839
8	0.515	0.60	19.405	9.932	6.807
9	0.709	1.80	28.859	16.528	12.365
10	0.709	1.00	17.312	11.151	8.405

Flag Impeller

SYSTEM		k'		
		5 rpm	20 rpm	100 rpm
1	0.273	134.986	14.544	7.592
2	0.429	52.150	12.478	7.577
3	0.591	40.885	9.760	6.883

Table 6.10: Regression Results of Eqn. (6.13) (Paddle Impellers)

Linear Multiple Regression Analysis

Regression Coefficient	Estimated Regression Coefficient	Estimated Standard Error	t^*
$\log \beta_0$	9.365	--	--
β_1	0.410	0.073	5.96
β_2	0.347	0.073	-11.39

Analysis of Variance

	Sum of Squares	Degrees of Freedom	Error Mean Squares	F^*
Regression	1.366	2	0.683	--
Residual	0.226	27	0.008	81.6
Total	1.592	30		

$R^2 = 0.900$

* $\alpha = 0.05$

of k' are encountered for the flag impeller, especially when using low rotational speeds. However, at higher values of N, the differences in the magnitude of k' become negligible and the average value of k' for the paddle impellers (k' = 8.03 ± 1.78 1/rev) is higher than the value for the flag impeller (k' = 7.35 ± 0.40 1/rev). This may be due to the larger surface area of the paddle impellers.

There is no published data on the value of k' for paddle impellers using this mixer viscometry method. Steffe and Ford (1985) reported k' values of 4.64 (at 60 rpm) for a pitched flag impeller. This magnitude is in reasonably good agreement with the average value of k' = 7.35 ± 0.40 1/rev (at 100 rpm) (Table 6.9) determined in this investigation. When using different values of N, the average value is k' = 17.067 ± 2.64 1/rev as compared to the value of 13.8 obtained by Rao and Cooley (1984) (d/D=0.8, d/b=1.5). Differences in the magnitudes of k' are due to differences in geometry.

6.1.2.2) Estimation of Average Shear Rates and Apparent Viscosity

Average shear rates were determined using Eqn. (3.8). Figures 6.36 and 6.37 present the average shear rates for the paddles and the flag impeller, respectively. The effect of impeller and cup size on average shear rates are presented in Figures 6.36a and 6.36b for the paddle impellers. As it was expected, no significant effect of cup diameter is observed.

Average apparent viscosities were calculated with Eqn. (3.13). Figure 6.38 presents the values of η_a for two non-Newtonian fluids as a function of $\dot{\gamma}_{av}$ for the different paddle impellers. It may be seen that the choice of impeller will produce different values of η_a. Figure 6.39

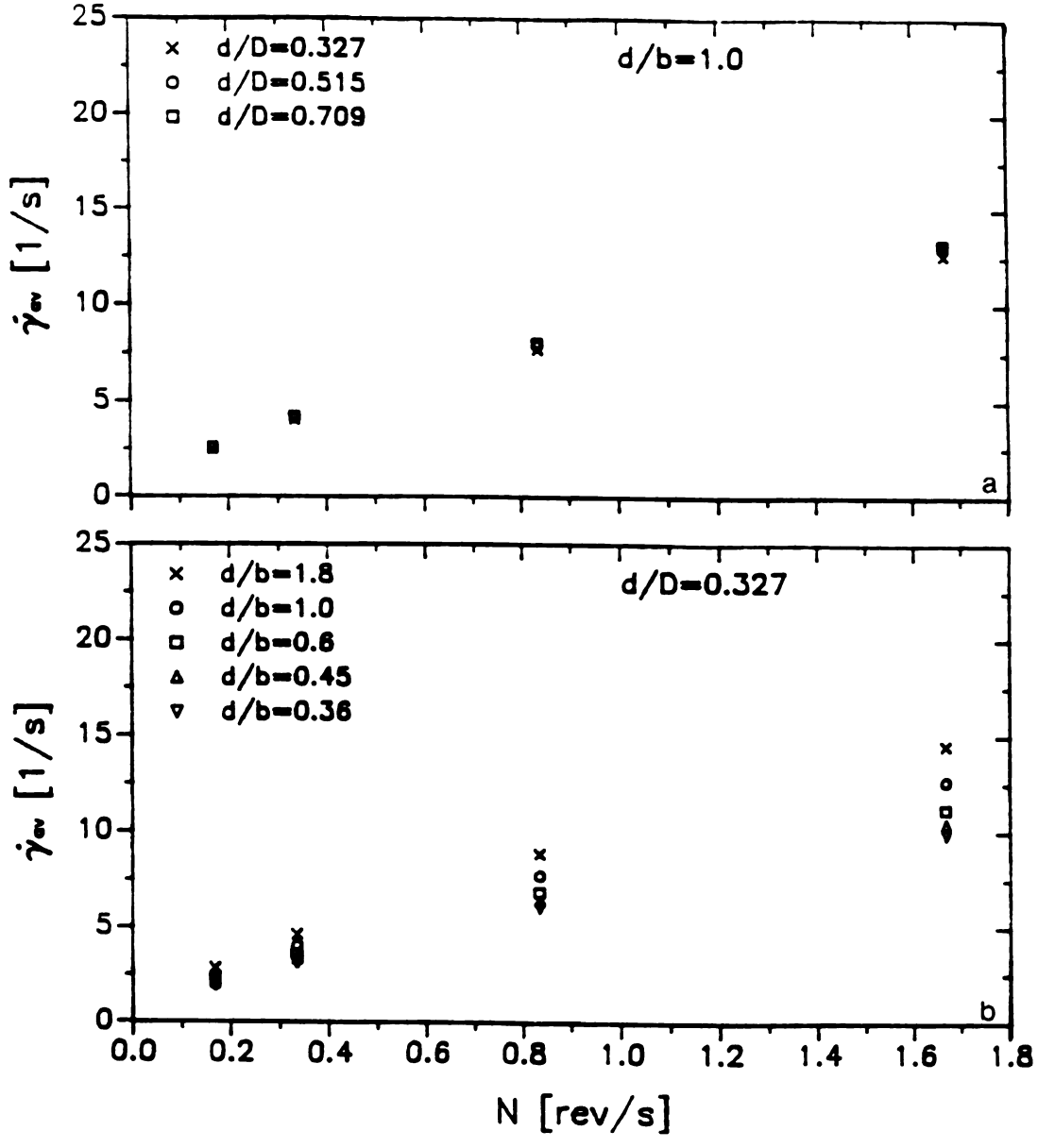

Figure 6.36: Average Mixing Shear Rate as a Function of Rotational Speed. a) Different Cups; b) Different Paddles

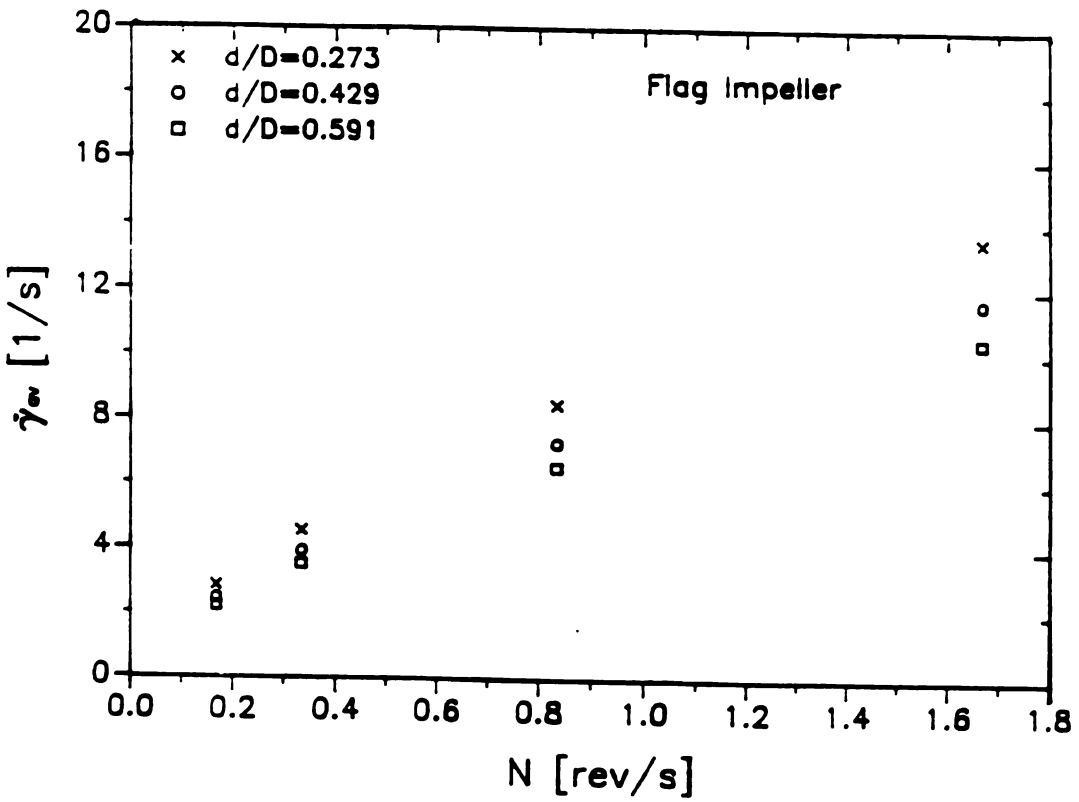

Figure 6.37: Average Mixing Shear Rate as a Function of Rotational Speed for the Flag Impeller

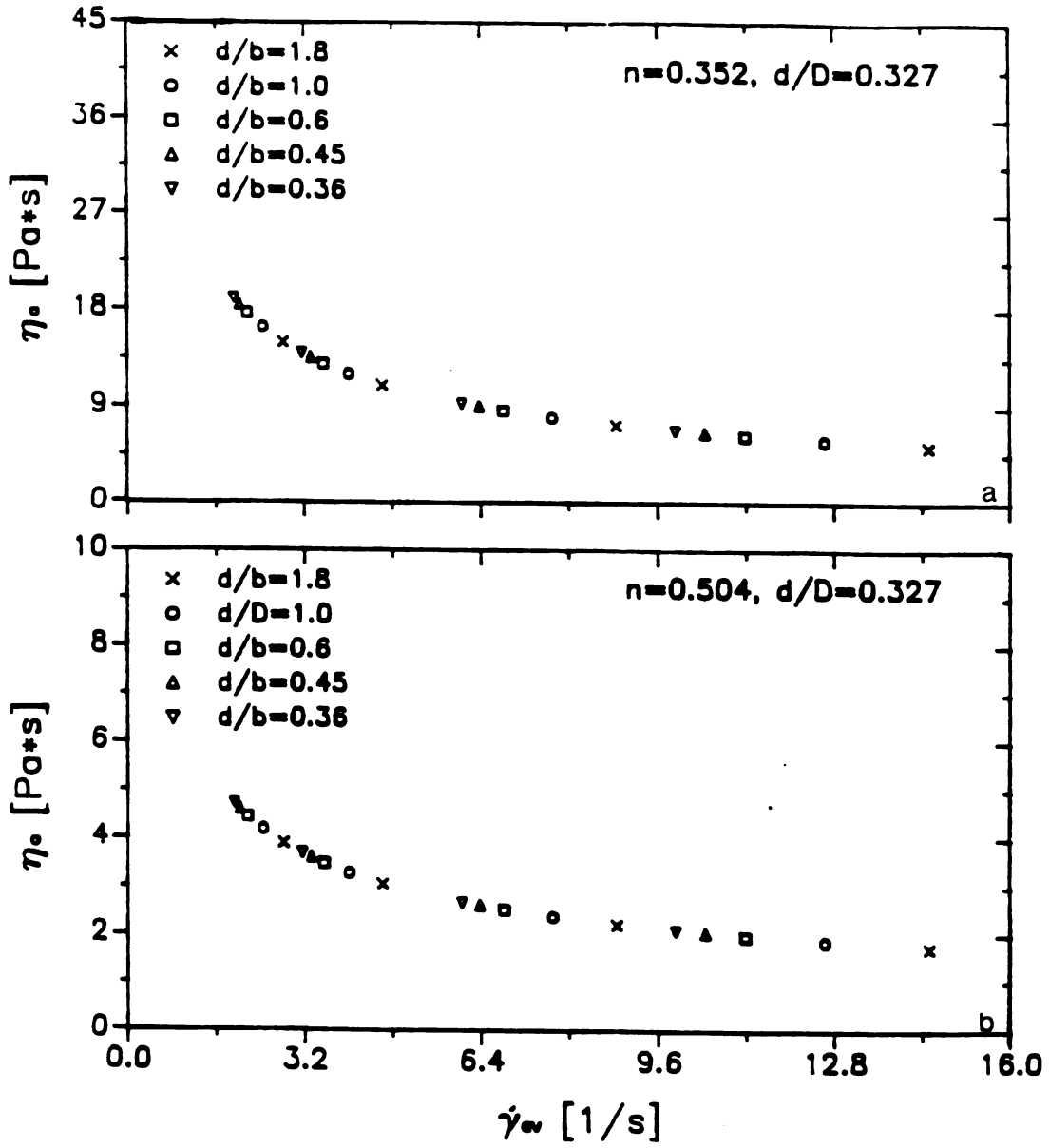

Figure 6.38: Apparent Viscosity as a Function of Average Shear Rate Using The Paddle Impellers. a) CMC 2%; b) CMC 1%

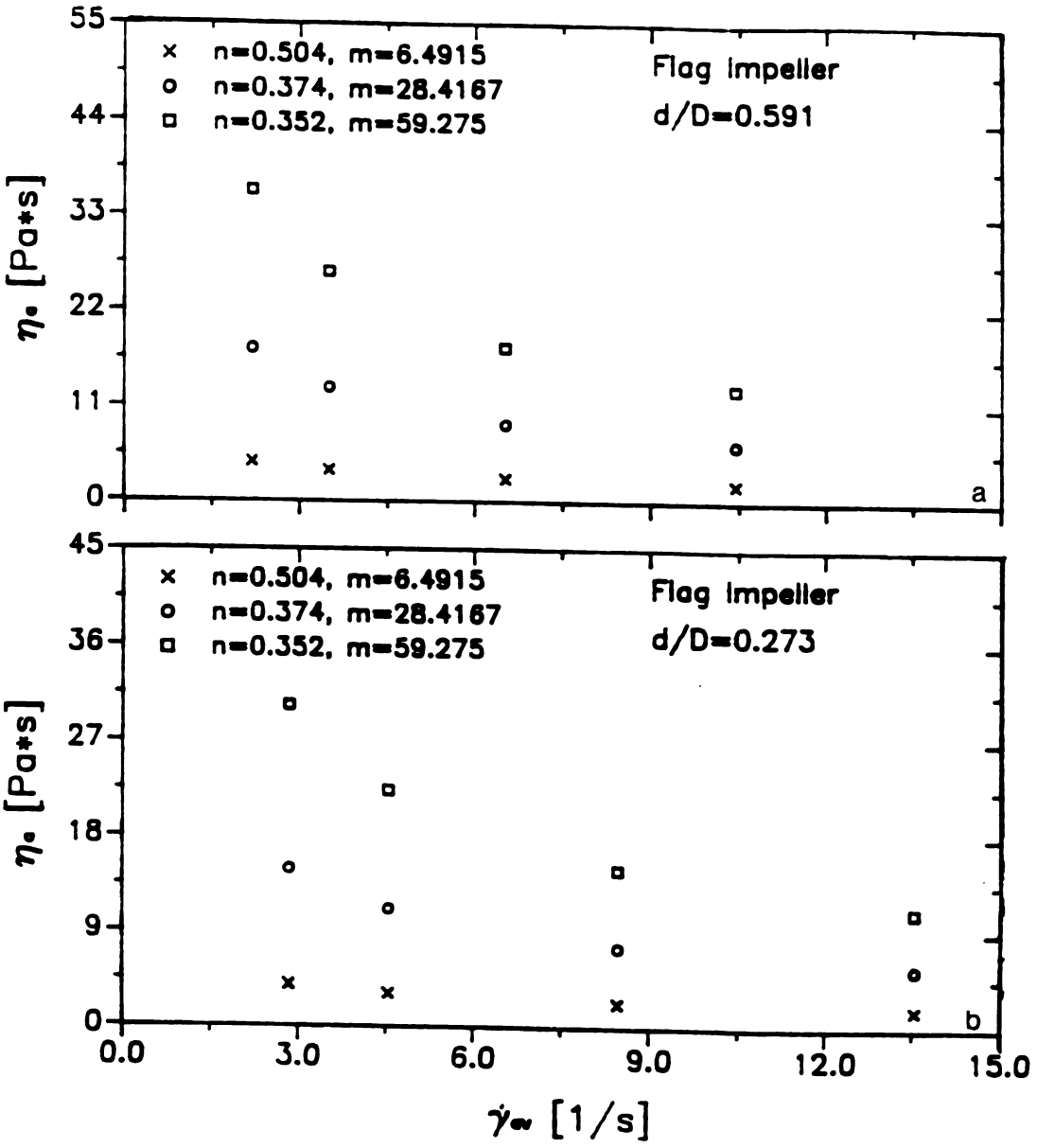

Figure 6.39: Apparent Viscosity as a Function of Average Shear Rate Using The Flag Impeller; a) Small Gap; b) Large Gap

shows results for the flag impeller. The size of the sample container also results in different values of η_a, and the bigger the cup, the smaller the values of η_a.

6.1.3) Summary of Discussion

Three mixer viscometry methods were reviewed and evaluated. The values of the mixer proportionality constant k' for determination of the mixing average shear rate $\dot{\gamma}_{av}$ evaluated using the three mixer viscometry methods have been presented in Tables 6.3 through 6.9 in the previous sections. The assumption $\dot{\gamma}_{av} = k'N$ [Eqn. (3.8)] is the basis for the three procedures. However, the original assumption of the work of Metzner and Otto (1957) of a constant value of k' is not always valid for variations in operating conditions (impeller rotational speed, N), fluid rheological properties and system geometry.

It is important to note that the three methods predict variations in k' with the geometry of the mixing system for the ranges investigated in this study. However, the Power Curves Method shows little variation with geometry for the flag impeller (Table 6.4). When working at high mixing speeds [N equal to 100 rpm (0.167 rps)], the values of k' obtained with the Torque Curves Method and the Slope Method show excellent agreement. Under this operating condition, the effect of the other parameters (fluid rheology and system geometry) become less significant. Thus, the assumption of a constant k' value is valid under these terms.

All the three mixer viscometry techniques require the determination of parameters using computer analytical techniques, i.e., small changes in experimental data result in big changes in results of regression analysis. The Power Curves Method can be very tedious and deviation from the basic assumption for the average shear rate ($\dot{\gamma}_{av} = k'N$) may

occur when using different impellers. The Mixer Torque Curves and the Slope methods are simpler since they require less data handling.

Results indicate that the basic assumption of traditional mixer viscometry methods of a direct proportionality between average shear rate in the agitated fluid and the rotational speed of the impeller [Eqn. (3.8)], with k' depending only on the geometry of the impeller, may be incorrect when working at low rotational speeds. Variation in fluid rheological properties has also proven to be an important factor for determination of the average shear rate in the mixing system.

6.2) DETERMINATION OF RHEOLOGICAL PROPERTIES OF POWER-LAW FLUIDS USING THE ALTERNATIVE MIXER VISCOMETRY METHOD

This section presents the experimental verification of the proposed procedure for determination of rheological properties of power-law fluids using a measuring system which consists of an impeller (paddle or flag) rotating in a cylindrical container.

6.2.1) Determination of the Flow Behavior Index, n

The measured torque on the impeller shaft is presented as a function of the rotational speed of the impeller for each non-Newtonian fluid, with the geometry of the impeller as a parameter. Figure 6.40 shows the results for the CMC 2% solution for the different paddle/cup combinations. Figure 6.41 shows results for the flag impeller. It follows from these plots that for every geometry of the impeller system the experimental points may be approximated by a straight line. All

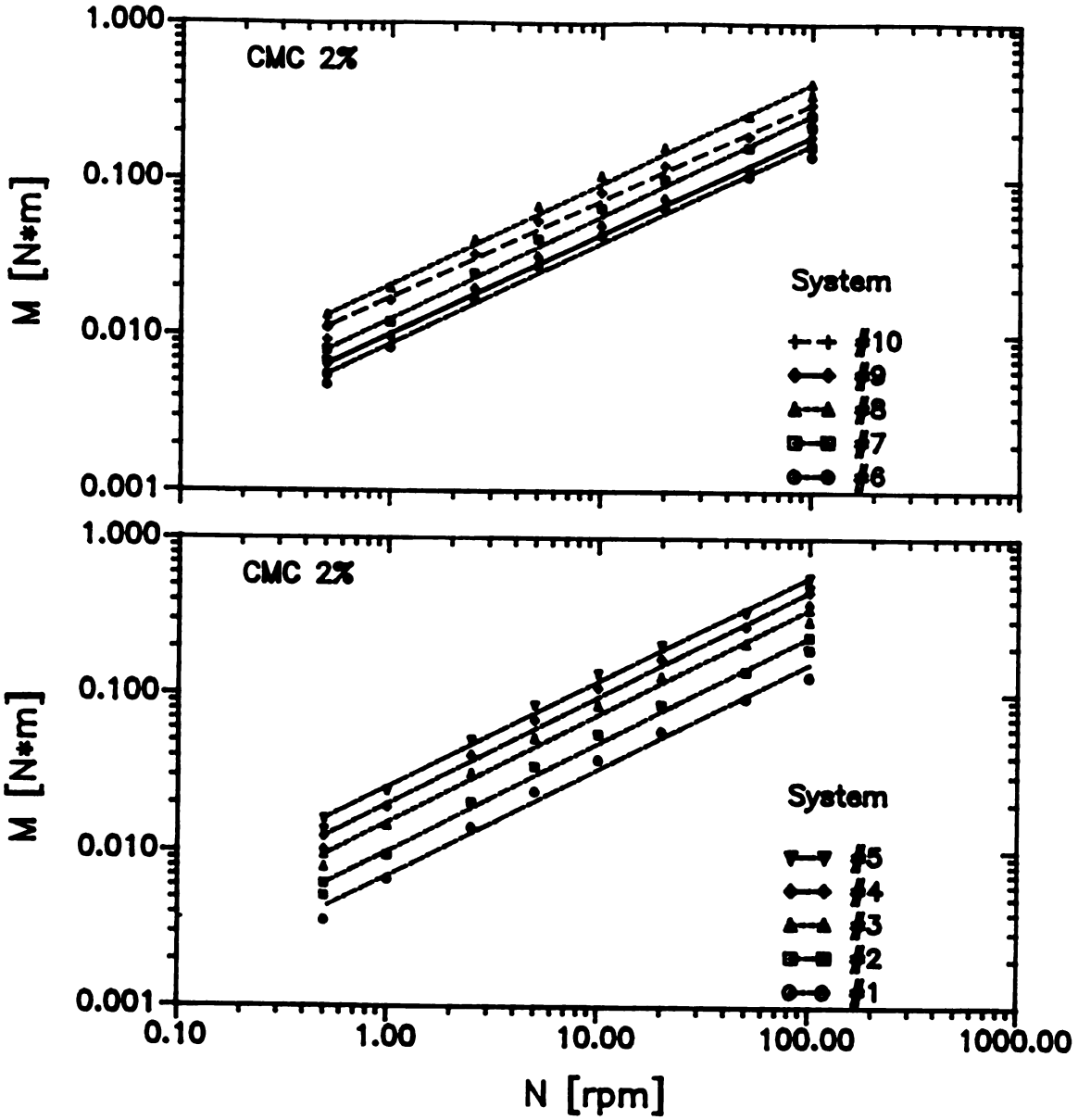

Figure 6.40: Plot of the torque on the impeller shaft M versus rotational speed of the impeller N for 2% wt% aqueous solution of CMC (Paddle Impellers) (See Table 6.9 for definition of systems)

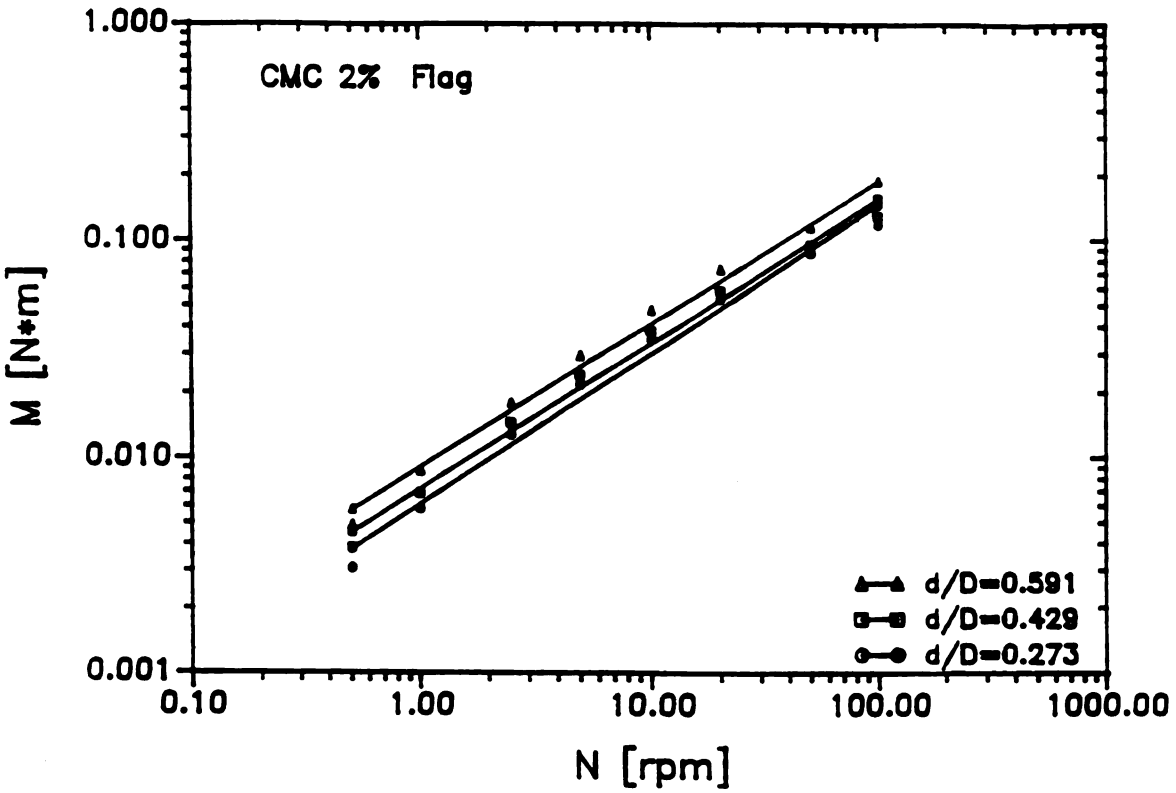

Figure 6.41: Plot of the torque on the impeller shaft M versus rotational speed of the impeller N for 2% wt% aqueous solution of CMC (Flag Impeller)

lines have similar slope, and this slope is equal to the value of the flow behavior index, n. Tables 6.11 and 6.12 present the values of the rheological parameter for all the systems. It is seen that the magnitudes of the flow behavior index n obtained with the impeller system for the standard fluids are in good agreement with those using the concentric cylinders viscometer when operating at the same range of shear rates (0-40 1/s).

6.2.2) Determination of Shear Stress-Shear Rate Relationships

6.2.2.1) Average Shear Rate In The Mixing System

To verify the applicability of Eqns. (4.4), (4.6) and (4.9) to approximate the values of the mixing average shear rates, the values of k' determined using the three investigated mixer viscometry techniques [Section (6.1)] were used (as average values) for comparison with the theoretical expressions. Initial values of the parameters of the equations (β_1, α_1, α_2 and α_3) were assigned following the concentric cylinders analogy to find the values of the constant β_1 and the parameters α_1 , α_2 and α_3 that showed best agreement with the experimental values of k'. These are the following:

$\beta_1 = 4\pi$

$\alpha_1 = \alpha_2 = 2/n$ and,

$\alpha_3 = n/2$, with n = power-law index.

Thus, Eqn. (4.5) can be written as follows,

$$k' = 4\pi \left[\frac{(D/d)^{2/n}}{(D/d)^{2/n} - 1} \right] (d/b)^{n/2} \qquad (6.13)$$

Table 6.11: Values of the Flow Behavior Index of Standard Power-Law Fluids Using the Mixer System (Paddles) and a Concentric Cylinders Viscometer (Haake Rotovisko)

		Flow Behavior Index, n	
FLUID	SYSTEM	Mixer[1]	Concentric Cylinders[2]
CMC 1%	1	0.902 ± 0.003	0.829 ± 0.005
	2	0.834 ± 0.004	
	3	0.896 ± 0.003	
	4	0.887 ± 0.002	
	5	0.842 ± 0.002	
	6	0.808 ± 0.003	
	7	0.807 ± 0.005	
	8	0.857 ± 0.004	
	9	0.869 ± 0.006	
	10	0.857 ± 0.005	
	n_{avg}	0.856 ± 0.030	
CMC 1.5%	1	0.599 ± 0.008	0.718 ± 0.005
	2	0.759 ± 0.004	
	3	0.726 ± 0.004	
	4	0.735 ± 0.003	
	5	0.718 ± 0.002	
	6	0.599 ± 0.007	
	7	0.687 ± 0.005	
	8	0.584 ± 0.006	
	9	0.660 ± 0.005	
	10	0.640 ± 0.005	
	n_{avg}	0.670 ± 0.060	
CMC 2%	1	0.679 ± 0.004	0.528 ± 0.003
	2	0.688 ± 0.003	
	3	0.648 ± 0.004	
	4	0.684 ± 0.002	
	5	0.676 ± 0.003	
	6	0.646 ± 0.001	
	7	0.662 ± 0.002	
	8	0.653 ± 0.003	
	9	0.641 ± 0.001	
	10	0.628 ± 0.001	
	n_{avg}	0.660 ± 0.020	

[1] Brookfield Mixer. Shear rate range: 0-30 1/s [Eqns. (6.18) and (6.19)]

[2] Haake MV-III (d/D=0.73). Shear rate range: 0-40 1/s

Table 6.12: Values of the Flow Behavior Index of Standard Power-Law Fluids Using the Mixer System (Flag) and a Concentric Cylinders Viscometer (Haake Rotovisko)

		Flow Behavior Index, n	
FLUID	SYSTEM	Mixer[1]	Concentric Cylinders[2]
CMC 1%	1	0.933 ± 0.005	
	2	0.805 ± 0.002	0.829 ± 0.005
	3	0.967 ± 0.007	
n_{avg}		0.901 ± 0.085	
CMC 1.5%	1	0.811 ± 0.004	
	2	0.711 ± 0.003	0.718 ± 0.005
	3	0.708 ± 0.001	
n_{avg}		0.743 ± 0.058	
CMC 2%	1	0.690 ± 0.003	
	2	0.667 ± 0.002	0.528 ± 0.003
	3	0.658 ± 0.002	
n_{avg}		0.672 ± 0.016	

[1] Brookfield Mixer. Shear rate range: 0-30 1/s [Eqn. (6.23)]

[2] Haake MV-III (d/D=0.73). Shear rate range: 0-40 1/s

Equation (6.13) differs from the original equation for the shear rate at the cylindrical bob,

$$\dot{\gamma}_b = \frac{2\Omega}{n}\left[\frac{(D/d)^{2/n}}{(D/d)^{2/n} - 1}\right] \qquad (4.3)$$

or

$$\dot{\gamma}_b = \frac{4\pi N}{n}\left[\frac{(D/d)^{2/n}}{(D/d)^{2/n} - 1}\right] \qquad (6.14)$$

with $\beta_1 = \frac{4\pi N}{n}$, $\alpha_1 = \alpha_2 = 2/n$, in the value of parameter β_1 , since the division by n is not present in the equation for the paddle impellers. As stated before, the effect of the power-law parameters on the value of k' is not clearly understood. For an impeller, the dependence on the value of n seems to be less significant than in the case of the concentric cylinders. The values of α_1 and α_2 are identical to the concentric cylinders analogy.

Values of k' obtained with Eqn. (6.13) are shown in Figure 6.42a. It is interesting to note that the above expression gives reasonably good results, except for the small gap case ($d/D \geq 0.709$). (These data are represented by the crosses (+) in Figure 6.42a). It is clear that Eqn. (6.13) predicts considerably higher values of k' when the impeller-to-cup diameter ratio is small [$(d/D) \geq 0.709$]. Thus, Eqn. (6.13) is a good approximation of the data when the diameter ratio follows within the range of $0.327 \leq d/D \leq 0.515$. An equation to approximate the values of k' when (d/D) was ≥ 0.709 was obtained (based on the concentric

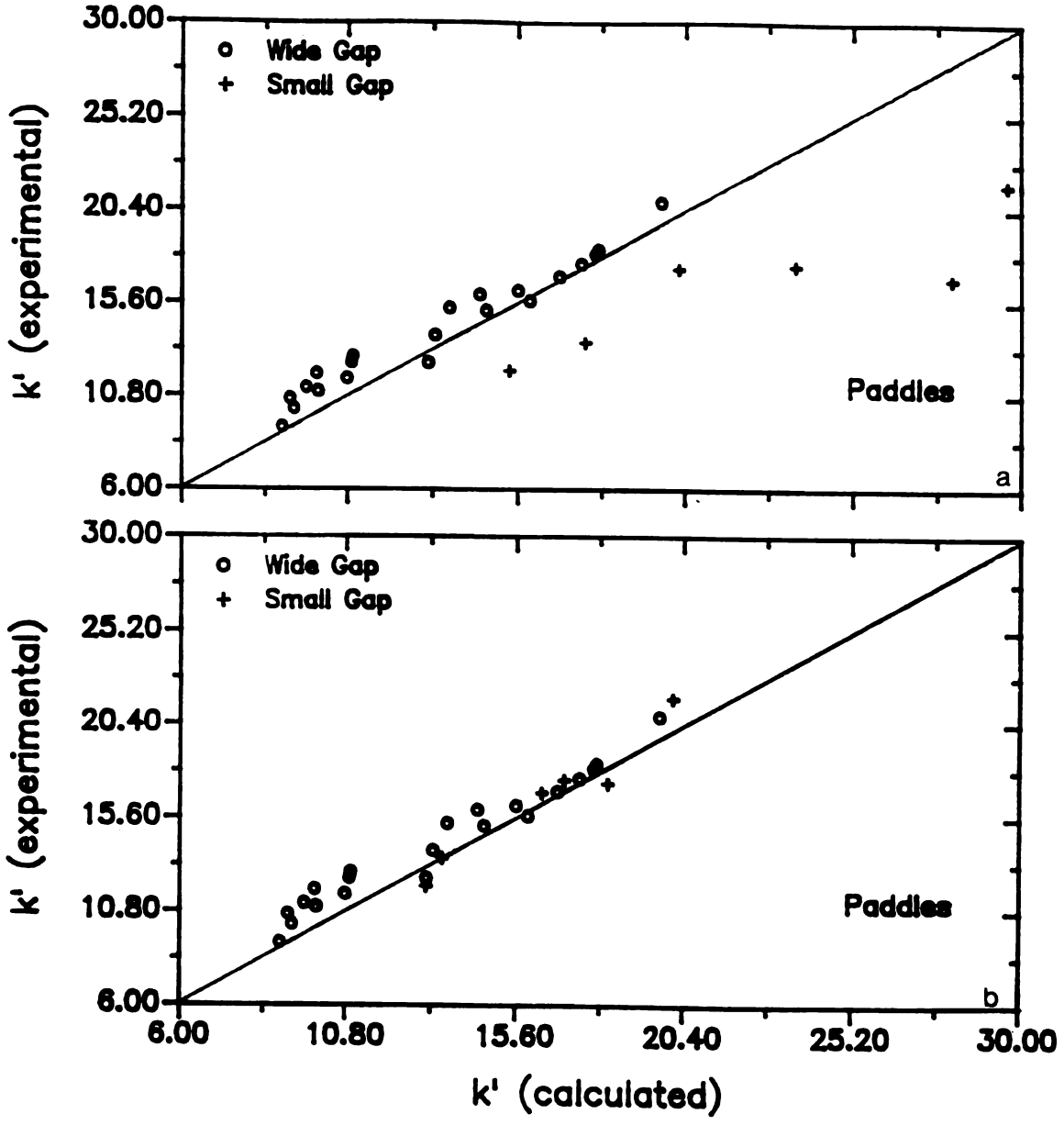

Figure 6.42: Experimental Versus Calculated Values of k'; a) k' defined by Eqn. (4.5); b) k' defined by Eqns. (4.5) and (6.13) for small gap (+) (Paddle Impellers)

cylinders analogy) by expressing the experimental values of k' by:

$$k' = 4\pi \left[\frac{(D/d)^{\frac{2-n}{n}}}{(D/d)^{2/n} - 1} \right] (d/b)^{n/2} \qquad (6.15)$$

Due to the empirical nature of Eqn. (6.15) it is difficult to physically explain the difference in the value of $\alpha_1 = (2-n)/n$. However, this result indicates that the gap between the impeller and the fluid container (cup) is a factor to be carefully taken into account when considering the use of mixer viscometry methods.

Figure 6.42b presents results for the values of k' calculated using Eqn. (6.13) for $0.327 \leq d/D \leq 0.515$ and Eqn. (6.15) for $(d/D) \pm 0.709$. The results are satisfactory for all the impellers and power-law fluids investigated. The agreement between experiment (mixer viscometry techniques) and theory [Eqn. (6.15)] was usually better than 10%.

Simplified equations were attempted by using the same procedure of data fitting. The final equations obtained were as follows:

$$k' = 4\pi \left[\frac{(D/d)^{n/2}}{(b/d)^{n/2}} \right] \qquad (6.16)$$

Simplifying, Eqn. (6.16) becomes

$$k' = 4\pi \, (D/b)^{n/2} \qquad (6.17)$$

Figure 6.43 shows the values of k' calculated from Eqn. (6.17) versus that determined from experimental data. Results show a reasonable agreement between predicted and average values. Even though not as good

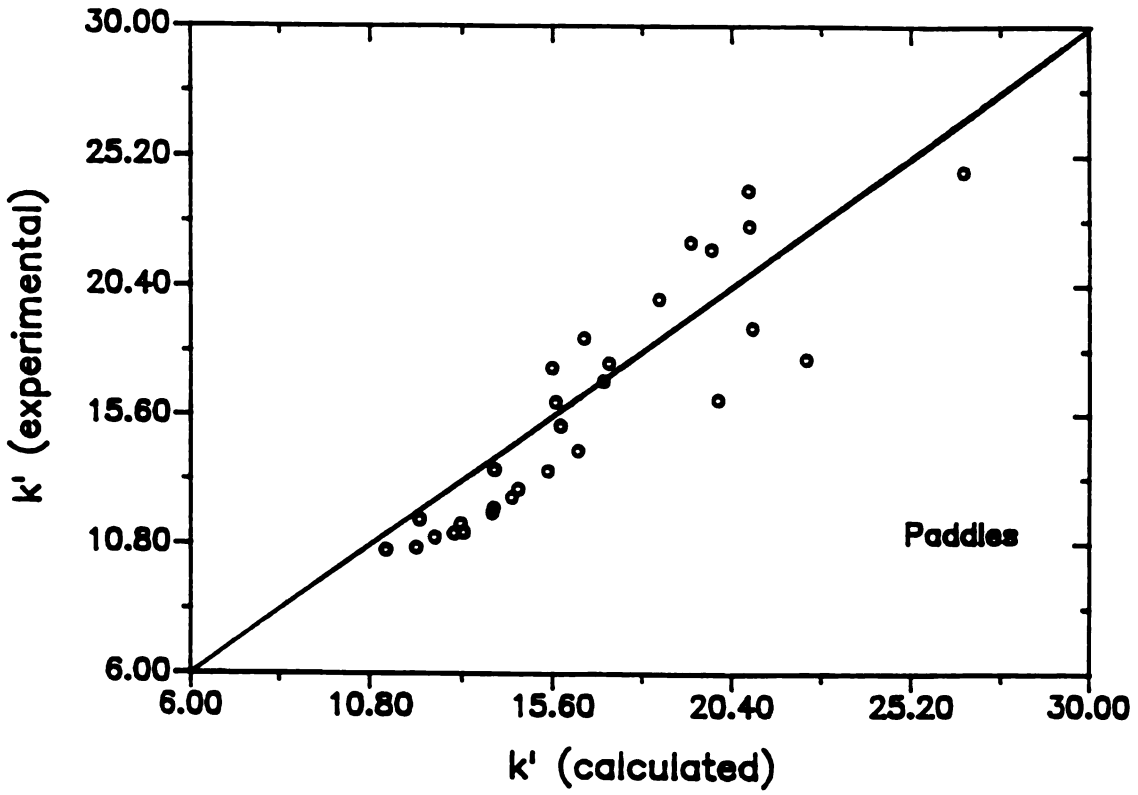

Figure 6.43: Experimental Versus Calculated Values of k'; a) k' defined by Eqn. (4.7) (Paddle Impellers)

as Eqn. (6.13), results fall within the range of k' values obtained using mixer viscometry techniques. The maximum error was less than 20%. It would seem that for the purposes of engineering design the use of Eqn. (6.17) is reasonable.

Thus, results indicate that it is possible to approximate the value of the impeller proportionality constant, k', for a particular impeller (paddle) by using Eqn. (6.13) for large to medium gaps, and by Eqn. (6.15) for small gap ($d/D \geq 0.709$). Only the geometry of the system and the value of the flow behavior index, n, for the investigated fluid are needed. Equations (6.13) and (6.15) [as well as Eqn. (6.17)] avoid the dangerous assumption of k' being a constant independent of the fluid properties. Also, it can be said that k' remains constant at each value of rotational speed. In terms of the average shear rate, these equations become,

$$\dot{\gamma}_{av} = \left\{ 4\pi \left[\frac{(D/d)^{2/n}}{(D/d)^{2/n} - 1} \right] (d/b)^{n/2} \right\} N \qquad (6.18.1)$$

or

$$\dot{\gamma}_{av} = 2\Omega \left[\frac{(D/d)^{2/n}}{(D/d)^{2/n} - 1} \right] (d/b)^{n/2} \qquad (6.18.2)$$

for a paddle impeller and $0.327 \leq d/D \leq 0.515$, and

$$\dot{\gamma}_{av} = \left\{ 4\pi \left[\frac{(D/d)^{\frac{2-n}{n}}}{(D/d)^{2/n} - 1} \right] (d/b)^{n/2} \right\} N \qquad (6.19.1)$$

or

$$\dot{\gamma}_{av} = 2\Omega \left[\frac{(D/d)^{\frac{2-n}{n}}}{(D/d)^{2/n} - 1} \right] (d/b)^{n/2} \qquad (6.19.2)$$

for $d/D \geq 0.709$ (with $1 \geq b \geq 5$ cm and $0.5 \geq n \geq 0.9$). Also, a simplified approximation is given by

$$\dot{\gamma}_{av} = [4\pi\ (D/b)^{n/2}]\ N \qquad (6.20.1)$$

or

$$\dot{\gamma}_{av} = [2\pi\Omega(D/b)^{n/2}] \qquad (6.20.2)$$

for the geometric range investigated ($0.327 \leq d/D \leq 0.709$).

In the case of a flag impeller (b/d=0.5), Eqn. (4.9) gave good results for the values of k', with $\beta_1 = 4\pi$ and $\alpha_1 = n/2$. An expression such as Eqn. (4.9) was preferred for the flag impeller because Eqn. (6.13) did not yield very good results for this type of impeller. Thus, Eqn. (4.9) becomes,

$$k' = 4\pi\ [\ (D/d)^{n/2}\ ] \qquad (6.21)$$

Equation (6.21) predicts the value of the proportionality constant, k', for a flag impeller rotating in a power-law fluid. Figure 6.44a shows the results obtained from Eqn. (6.21) when d= 1.5cm. Figure 6.44b shows the case for Model 3 ($d = d_e$). It seems that the assumption

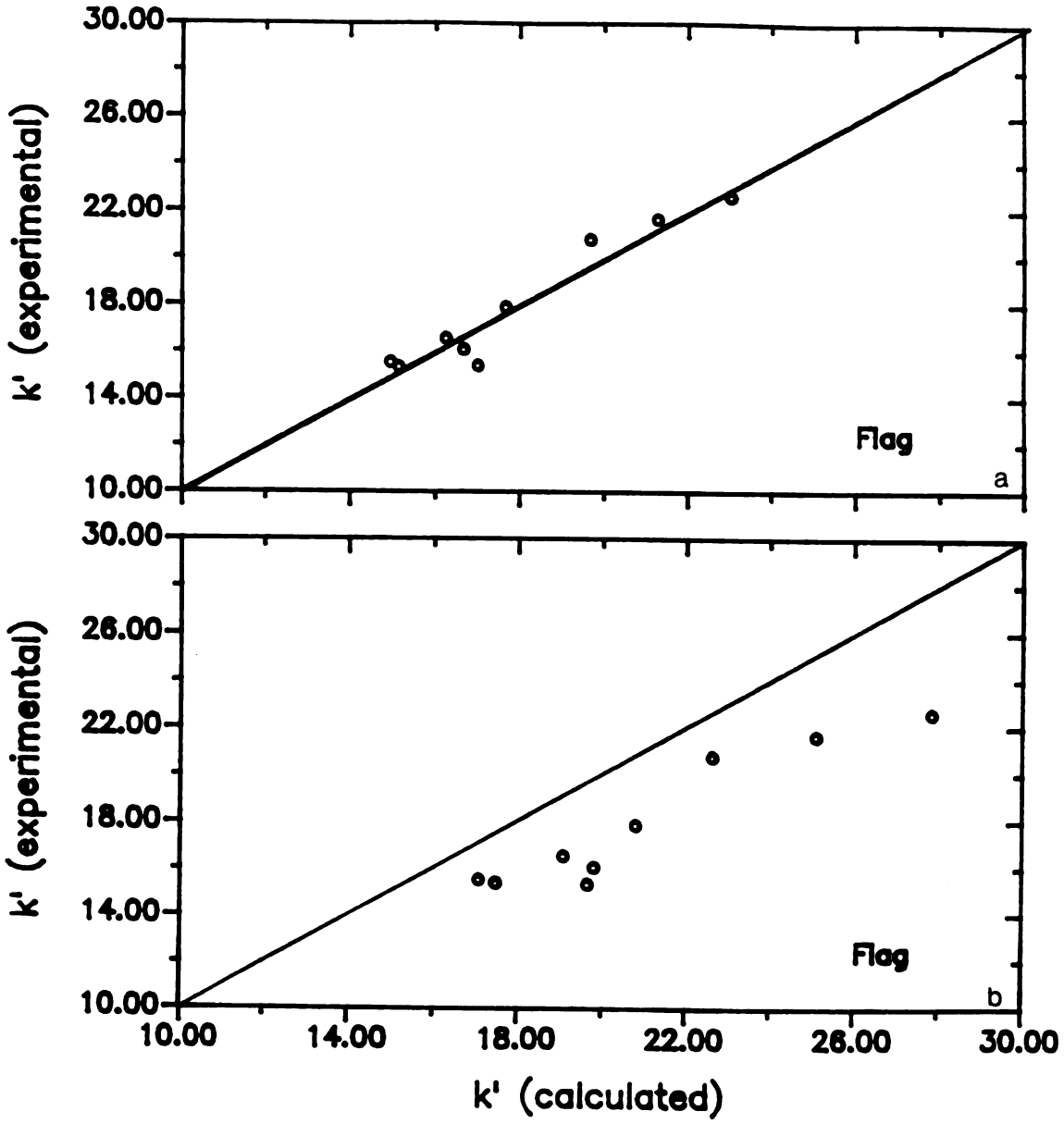

Figure 6.44: Experimental Versus Calculated k'; a) k' defined by Eqn. (4.7); b) k' defined by Eqn. (4.7) ($d=d_e$)

of a cylinder of equivalent diameter, d_e , as responsible for the shearing of the fluid when using a flag impeller tends to overestimate the values of k'. However, the values of k' fall within the range of k' determined from the traditional mixer viscometry methods with a maximum error of 15%. Again, the assumption of a constant k' value, only a function of impeller geometry, is avoided and proved not to be true for the cases investigated in this study.

Thus, the average shear rate in a mixing system (flag impeller) can be approximated by the following equation,

$$\dot{\gamma}_{av} = \left\{4\pi \left[(D/d)^{n/2} \right]\right\} N \qquad (6.22.1)$$

or

$$\dot{\gamma}_{av} = 2\Omega \left[(D/d)^{n/2} \right] \qquad (6.22.2)$$

6.2.2.2) Average Shear Stress in The Mixing System

6.2.2.2.1) Torque Approximations

To check the applicability of the shear stress equations, the experimentally measured values of torque for every mixing system were compared to those calculated using the following equations:

Model 1 (concentric cylinders analogy with negligible end effects):

$$M = 2\pi b (d/2)^2 \sigma_{av} \qquad (4.14)$$

Model 2 (concentric cylinders analogy with end effects):

$$M = \frac{\pi d^3}{2}\left[\frac{b}{d} + \frac{1}{3}\right]\sigma_{av} \qquad (4.21)$$

Model 3 (Flag impeller; d= d_e):

$$M = 2\pi b\,(d_e/2)^2\,\sigma_{av} \qquad (6.23.1)$$

and

$$M = \frac{\pi d_e^3}{2}\left[\frac{b}{d_e} + \frac{1}{3}\right]\sigma_{av} \qquad (6.23.2)$$

where

$\sigma_{av} = m\,(\dot{\gamma}_{av})^n$, with n from mixing system or a conventional concentric cylinders viscometer, and m from concentric cylinders viscometer. The value of the average shear rate can be evaluated using the appropriate equations [Eqns. (6.13) and (6.15) for the paddles and (6.21) for the flag for the ranges investigated in this study]. The average shear rate could also be determined by traditional mixer viscometry methods.

Figure 6.45 presents the values of torque for two fluids (1% and 1.5% CMC solutions) in a system consisting of a small paddle impeller (d/b=1.8) rotating in a large cylindrical cup (d/D=0.327). It can be seen that the Model 1 (concentric cylinders analogy with negligible end effects) [Eqn. (4.14)] gives better prediction of the torque values than the Model 2 (concentric cylinders analogy with end effects) [Eqn. (4.21)]. For a more viscous fluid (2% CMC), the Model 2 gives better results for the torque values (Figure 6.46). These results indicate that

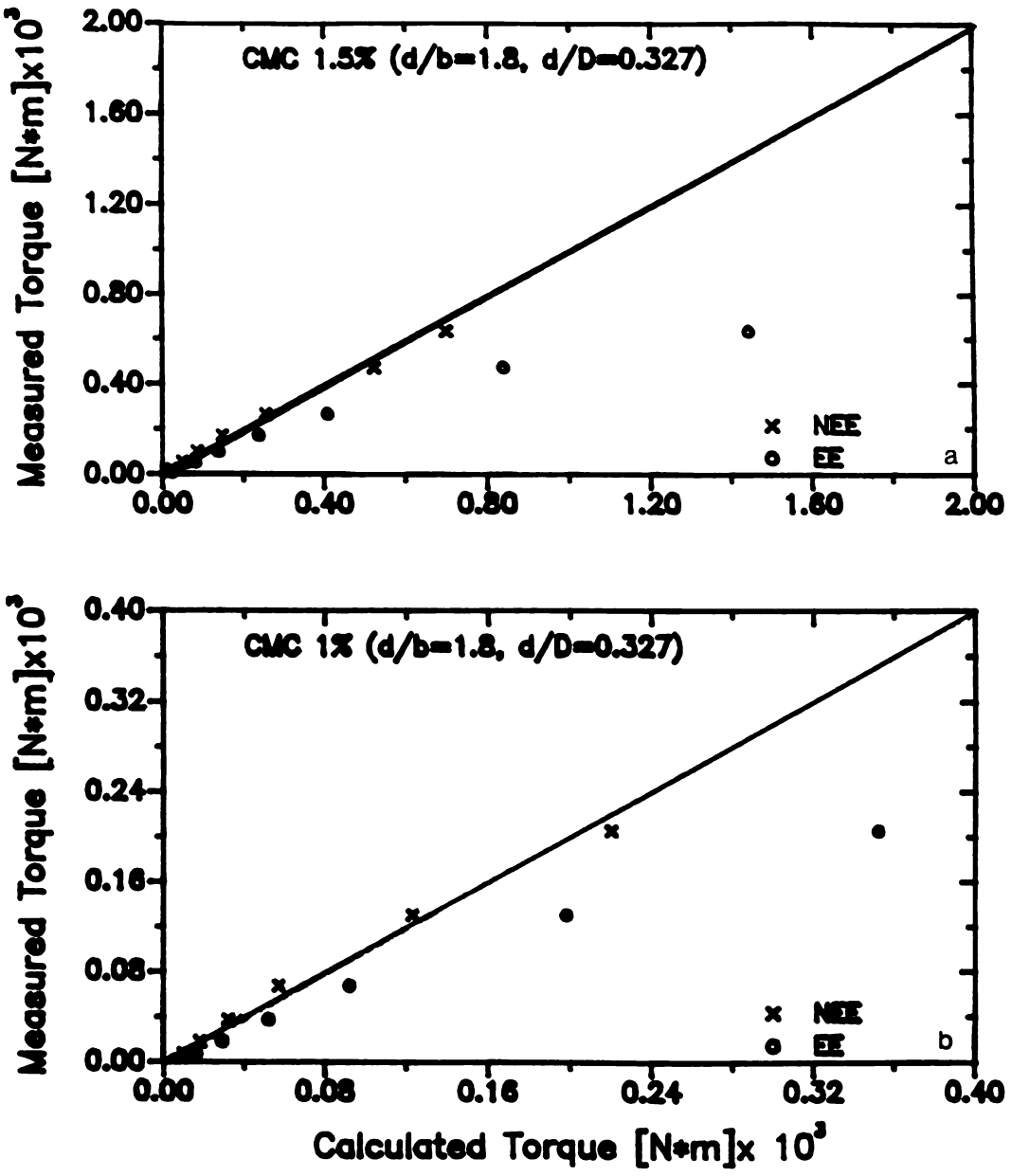

Figure 6.45: Measured Versus Predicted Values of Torque on the Impeller Shaft Using Eqn. (4.14) (o) and Eqn. (4.21) (x); a) CMC 1.5%; b) CMC 1% (Paddle Impeller # 1, (d/b) = 1.8) [EE = Model 2 (end effects); NEE = Model 1 (no end effects)]

the type of fluid being agitated is a significant factor for consideration when using mixer viscometry methods.

When using a larger paddle impeller (d/b=0.36) in the same cup [(d/D = 0.327] (Figure 6.47), the differences between the torque values predicted by the two models becomes smaller, with the assumption of negligible end effects (Model 1) showing better agreement between experiment and theory than the assumption of the presence of end effects (Model 2). Thus, when working in a large cup, the end effects can be assumed negligible.

For the other mixing systems, Model 2 (presence of end effects) (Figure 6.48) predicts values in close agreement with the experimentally measured torque values. This is due to the presence of a smaller gap between the impeller and the wall of the cup and the use of Eqn. (4.21) seems to account for any effect of the solid boundaries. Figure 6.48a indicates that Eqn. (4.14) predicts lower values of torque. Figure 6.48b indicates the applicability of Eqn. (4.21) to represent the torque on the shaft resulting from the rotation of the paddle impeller (approximated by a cylinder).

Based on the results presented in Figures 6.45 through 6.48, it can be concluded that when using a mixer viscometer with a small paddle in a large cup [(d/D) $\leq$ 0.327], assumption (iv) is valid, and the average shear stress can be approximated by Eqn. (4.15),

$$\sigma_{av} = \frac{2\,M}{\pi b d^2} \qquad (4.15)$$

for standard power-law fluids of low to medium viscosity. For a highly viscous standard fluid (CMC 2%), the effect of the solid boundaries

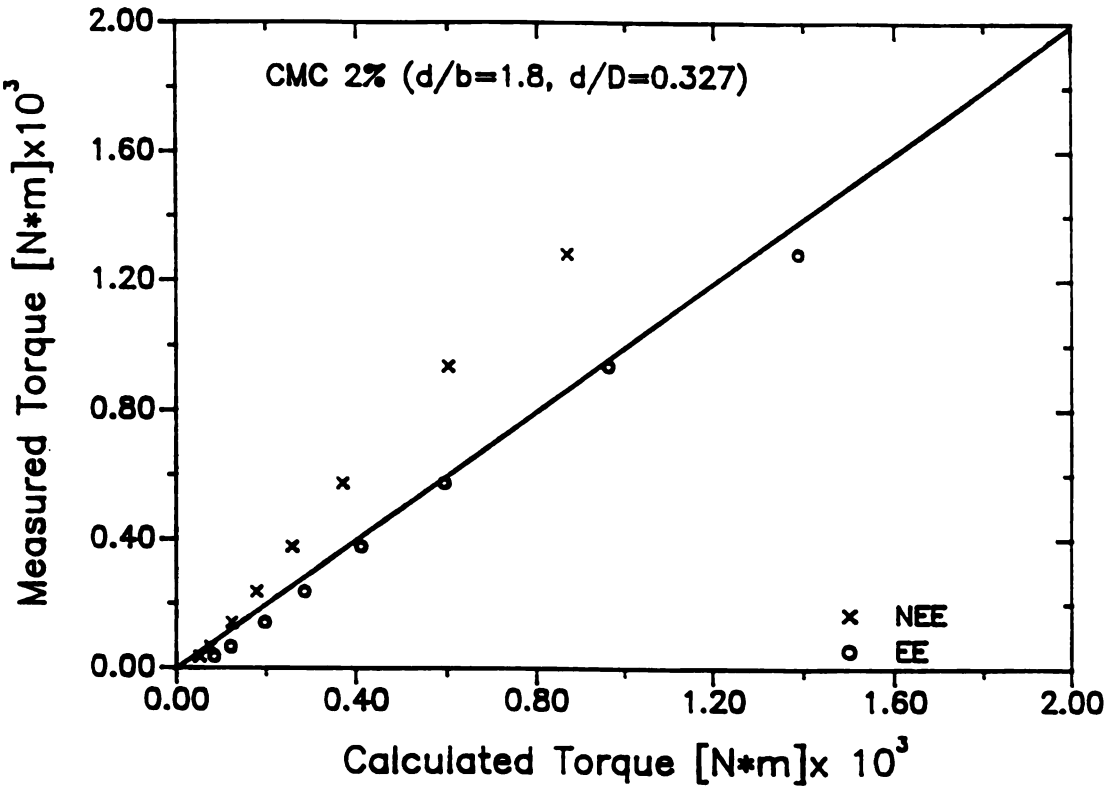

Figure 6.46: Measured Versus Predicted Values of Torque on the Impeller Shaft Using Eqn. (4.14) (o) and Eqn. (4.21) (x) CMC 2% [EE - Model 2 (end effects); NEE - Model 1 (no end effects)]

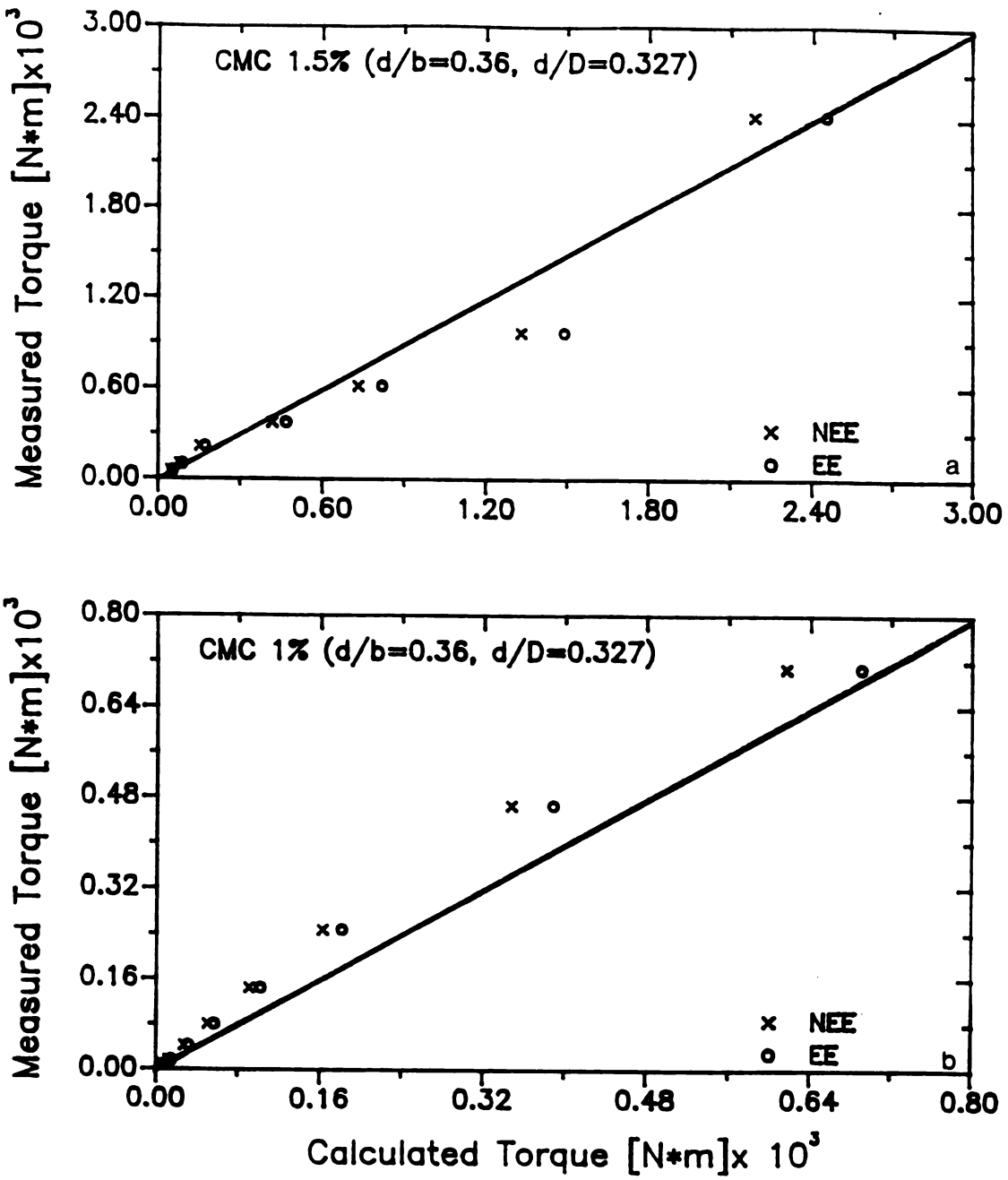

Figure 6.47: Measured Versus Predicted Values of Torque on the Impeller Shaft Using Eqn. (4.14) (o) and Eqn. (4.21) (x); a) CMC 1.5%; b) CMC 1% (Paddle Impeller # 5, (d/b) = 0.36) [EE = Model 2 (end effects); NEE = Model 1 (no end effects)]

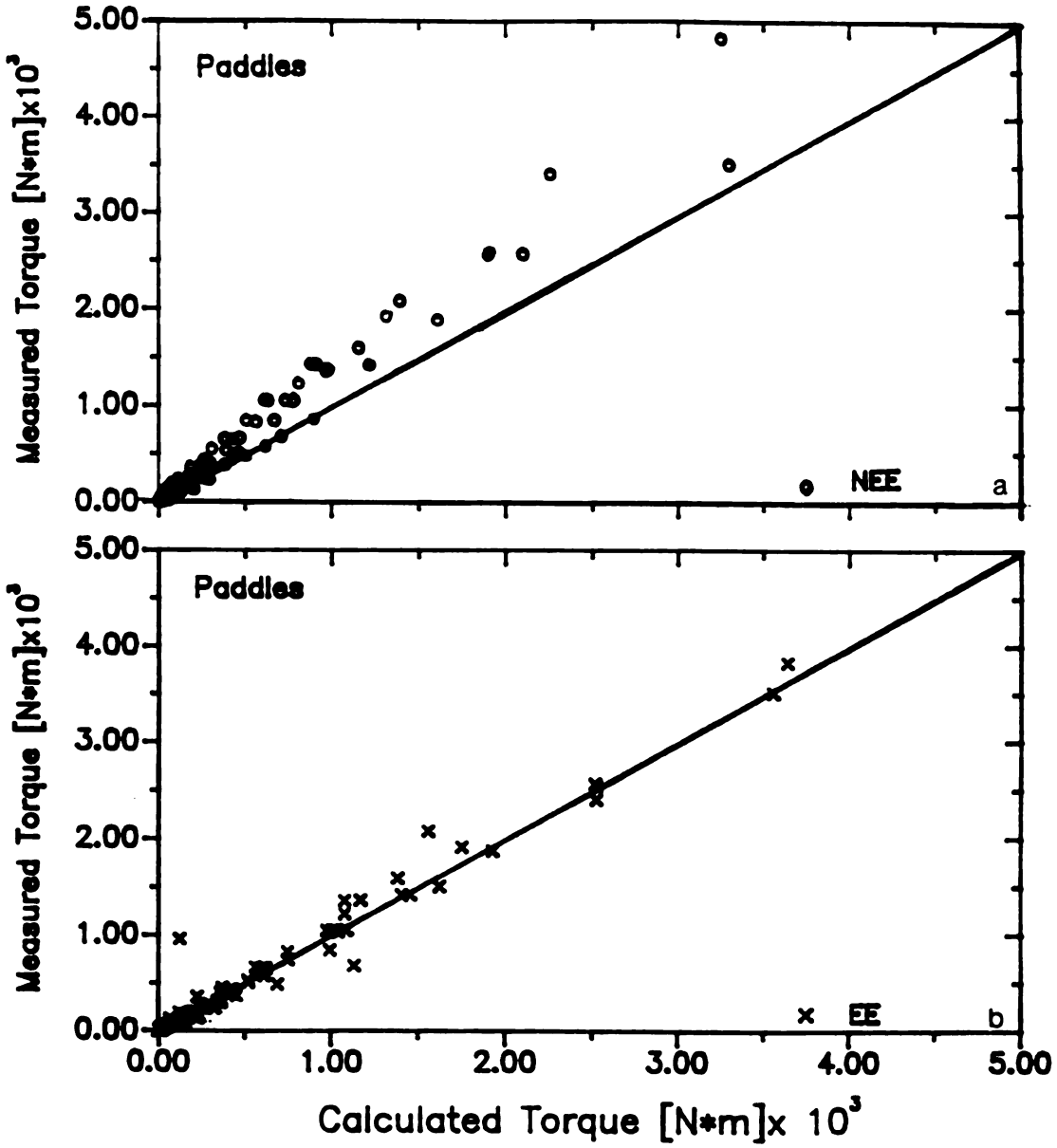

Figure 6.48: Measured Versus Predicted Values of Torque on the Impeller Shaft For All Systems And Fluids (Paddle Impellers); a) Eqn. (4.14) (Model 1 = NEE); b) Eqn. (4.21) (Model 2 = EE)

becomes significant and assumption (iv) is questionable. Thus, the average shear stress can be approximated by

$$\sigma_{av} = \left[\frac{\pi d^3}{2} \left[\frac{b}{d} + \frac{1}{3} \right] \right]^{-1} M \qquad (6.24)$$

Equation (6.24) also applies to the other impeller/cup combinations for the range of viscosities of the standard fluids.

The torque values calculated by equations (4.14), (4.21) and (6.23.1) were compared to those measured experimentally with the flag impeller. Figure 6.49 presents the measured torque values versus those calculated using Eqn. (4.14) (Model 1):

$$M = 2\pi b \, (d/2)^2 \, \sigma_{av} \qquad (4.14)$$

It is evident that this model yields values of torque considerably higher than the experimental values. Figure 6.50a presents the results using Eqn. (4.21) (Model 2):

$$M = \frac{\pi d^3}{2} \left[\frac{b}{d} + \frac{1}{3} \right] \sigma_{av} \qquad (4.21)$$

and it yields considerably lower values of torque. Equation (6.23.1) (Model 3),

$$M = 2\pi b \, (d_e/2)^2 \, \sigma_{av} \qquad (6.23.1)$$

seems to be the one that better represents the torque in the impeller

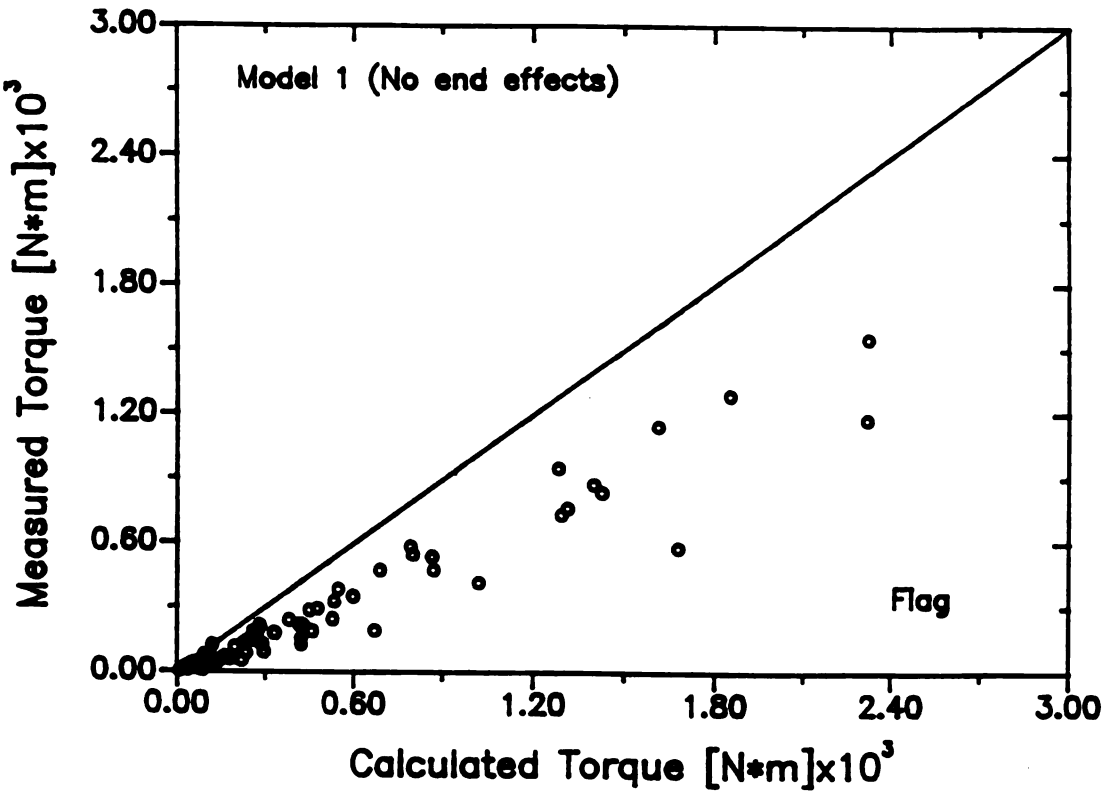

Figure 6.49: Measured Versus Predicted Values of Torque on the Impeller Shaft For All Systems And Fluids (Flag Impellers) Using Eqn. (4.14) (Model 1) (Negligible end effects)

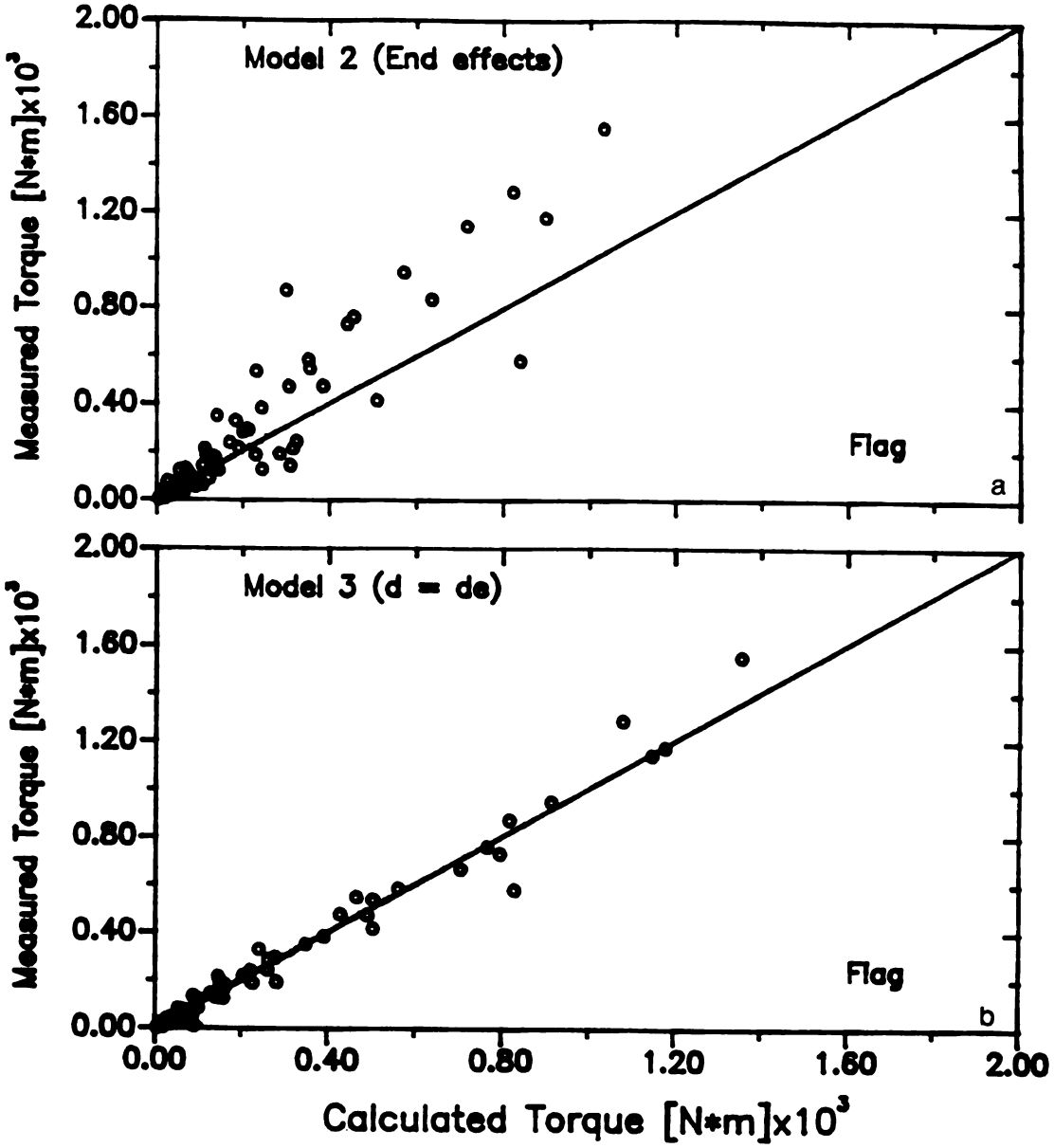

Figure 6.50: Measured Versus Predicted Values of Torque on the Impeller Shaft For All Systems And Fluids (Flag Impeller); a) Eqn. (4.21) (Model 2); b) Eqn. (6.23.1) (Model 3)

shaft (Figure 6.50b).

Thus, the average shear stress for the flag impeller may be expressed by

$$\sigma_{av} = \left[\frac{\pi d_e^3}{2} \left[\frac{b}{d_e} + \frac{1}{3} \right] \right]^{-1} M \qquad (6.25)$$

Equation (6.25) implies that the effect of the end boundaries (top and bottom) is important when using a mixing system with a flag impeller.

6.2.2.3) Flow Curves

6.2.2.3.1) Ideal Fluids

Average shear stress-average shear rate curves were obtained for the standard power-law fluids using Eqns. (6.18) and (6.19) for evaluation of the average shear rate of paddle impellers and Eqn. (6.21) for the flag impeller. The average shear stress was determined using Eqn. (4.21) for the paddles and Eqn. (6.23.1) for the flag impeller. Figure 6.51 presents a typical shear stress-shear rate plot for the CMC 2% solution obtained using the mixer viscometer with a paddle impeller. Similar results were obtained with the other fluids and geometries (Figures B14 and B15).

As indicated before, the values of the flow behavior index were calculated as the slope of the log-log plot of torque, M, versus the rotational speed of the impeller, N. The values of the consistency coefficient, m, were obtained by linear regression of the power model, $\sigma_{av} = m (\gamma'_{av})^n$. The values are shown in Tables 6.13 through 6.17 for every system geometry and Models analized in this investigation.

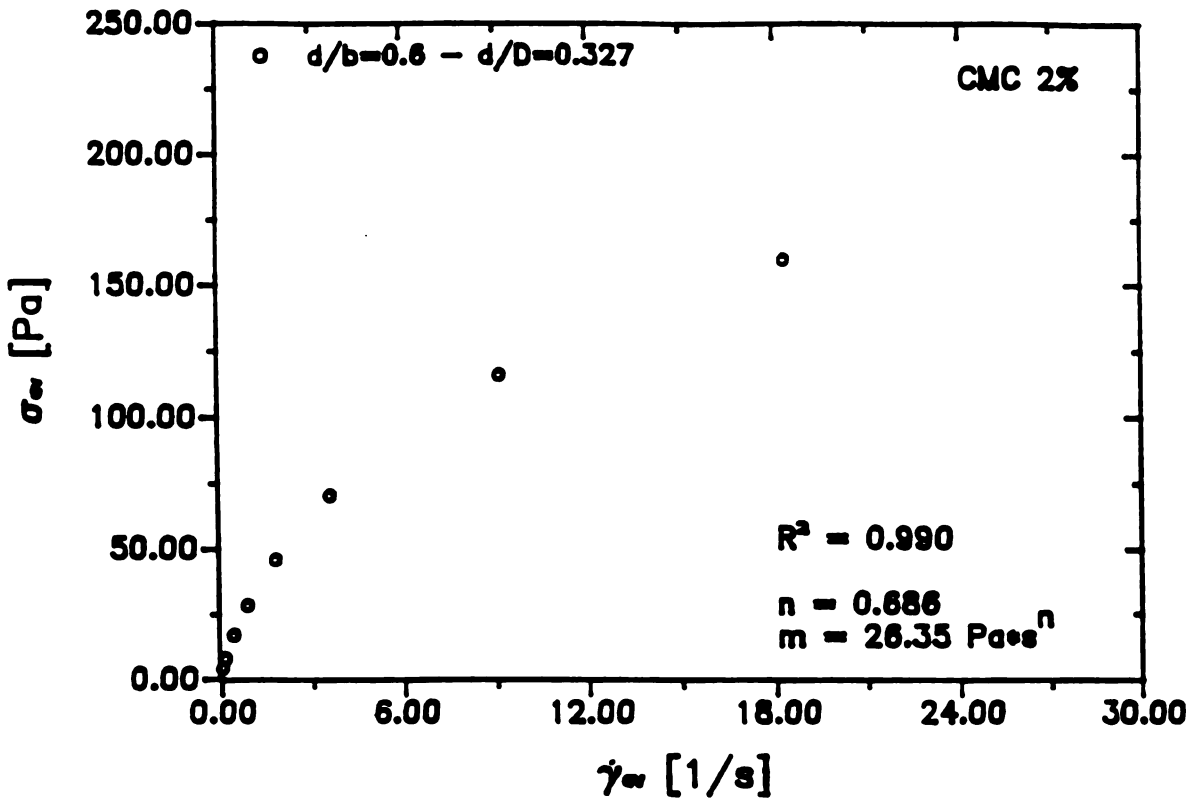

Figure 6.51: Flow Curve For 2% wt% Aqueous Solution of CMC Determined Using the Mixer Viscometer with a Paddle Impeller

Table 6.13: Values of the Fluid Consistency Coefficient of Standard Power-Law Fluids Using the Mixer System (Paddles) [Model 1: negligible end effects; Eqn. (4.14)] and a Concentric Cylinders Viscometer (Haake Rotovisko)

		Consistency Coefficient, m (Pa s^n)	
FLUID	SYSTEM	Mixer[1]	Concentric Cylinders[2]
CMC 1%	1	2.139 ± 0.003	2.619 ± 0.003
	2	2.664 ± 0.004	
	3	2.835 ± 0.003	
	4	3.173 ± 0.005	
	5	3.557 ± 0.002	
	6	2.492 ± 0.003	
	7	2.737 ± 0.004	
	8	2.823 ± 0.002	
	9	2.937 ± 0.001	
	10	2.906 ± 0.003	
	m_{avg}	2.826 ± 0.378	
CMC 1.5%	1	18.892 ± 0.004	15.620 ± 0.004
	2	12.261 ± 0.007	
	3	13.781 ± 0.005	
	4	14.702 ± 0.004	
	5	15.687 ± 0.003	
	6	18.892 ± 0.002	
	7	15.299 ± 0.002	
	8	22.967 ± 0.003	
	9	21.619 ± 0.004	
	10	24.742 ± 0.003	
	m_{avg}	17.877 ± 4.200	
CMC 2%	1	33.209 ± 0.002	33.170 ± 0.005
	2	30.656 ± 0.004	
	3	33.379 ± 0.002	
	4	32.980 ± 0.001	
	5	35.142 ± 0.003	
	6	37.737 ± 0.002	
	7	34.793 ± 0.004	
	8	38.149 ± 0.001	
	9	45.239 ± 0.002	
	10	47.738 ± 0.005	
	m_{avg}	36.900 ± 5.540	

[1] Brookfield Mixer. Shear rate range: 0-30 1/s [Eqns. (6.18), (6.19)]

[2] Haake MV-III (d/D=0.73). Shear rate range: 0-40 1/s

Table 6.14: **Values of the Fluid Consistency Coefficient of Standard Power-Law Fluids Using the Mixer System (Flag) [Model 1: negligible end effects; Eqn. (4.14)] and a Concentric Cylinders Viscometer (Haake Rotovisko)**

		Consistency Coefficient, m (Pa s^n)	
FLUID	SYSTEM	Mixer[1]	Concentric Cylinders[2]
CMC 1%	1	0.750 ± 0.007	
	2	1.288 ± 0.005	2.619 ± 0.003
	3	1.155 ± 0.004	
m_{avg}		1.064 ± 0.280	
CMC 1.5%	1	4.152 ± 0.003	
	2	7.100 ± 0.003	15.620 ± 0.004
	3	8.961 ± 0.002	
m_{avg}		6.738 ± 2.421	
CMC 2%	1	12.400 ± 0.004	
	2	15.926 ± 0.002	33.170 ± 0.003
	3	21.318 ± 0.003	
m_{avg}		16.548 ± 4.491	

[1] Brookfield Mixer. Shear rate range: 0-30 1/s [Eqn. (6.21)]

[2] Haake MV-III (d/D=0.73). Shear rate range: 0-40 1/s

Table 6.15: Values of the Fluid Consistency Coefficient of Standard Power-Law Fluids Using the Mixer System (Paddles) [Model 2: concentric cylinders with end effects; Eqn. (4.21)]) and a Concentric Cylinders Viscometer (Haake Rotovisko)

		Consistency Coefficient, m (Pa s^n)	
FLUID	SYSTEM	Mixer[1]	Concentric Cylinders[2]
CMC 1%	1	1.526 ± 0.003	2.619 ± 0.003
	2	2.046 ± 0.003	
	3	2.643 ± 0.002	
	4	2.759 ± 0.005	
	5	3.161 ± 0.002	
	6	1.562 ± 0.003	
	7	1.056 ± 0.004	
	8	2.353 ± 0.001	
	9	1.836 ± 0.002	
	10	2.219 ± 0.004	
	m_{avg}	2.116 ± 0.642	
CMC 1.5%	1	7.699 ± 0.004	15.620 ± 0.004
	2	9.362 ± 0.007	
	3	11.484 ± 0.005	
	4	12.784 ± 0.004	
	5	14.006 ± 0.003	
	6	11.808 ± 0.002	
	7	11.473 ± 0.002	
	8	19.139 ± 0.003	
	9	13.523 ± 0.004	
	10	18.556 ± 0.002	
	m_{avg}	13.001 ± 3.644	
CMC 2%	1	22.115 ± 0.002	33.170 ± 0.005
	2	24.334 ± 0.004	
	3	26.354 ± 0.001	
	4	28.348 ± 0.001	
	5	31.378 ± 0.003	
	6	23.595 ± 0.003	
	7	27.543 ± 0.004	
	8	31.794 ± 0.002	
	9	26.356 ± 0.003	
	10	36.085 ± 0.004	
	m_{avg}	27.790 ± 4.268	

[1] Brookfield Mixer. Shear rate range: 0-30 1/s

[2] Haake MV-III (d/D=0.73). Shear rate range: 0-40 1/s

Table 6.16: Values of the Fluid Consistency Coefficient of Standard Power-Law Fluids Using the Mixer System (Flag) [Model 2: concentric cylinders with end effects; Eqn. (4.21)] and a Concentric Cylinders Viscometer (Haake Rotovisko)

		Consistency Coefficient, m (Pa s^n)	
FLUID	SYSTEM	Mixer[1]	Concentric Cylinders[2]
CMC 1%	1	0.640 ± 0.007	
	2	1.104 ± 0.005	2.619 ± 0.003
	3	1.120 ± 0.004	
	m_{avg}	0.954 ± 2.720	
CMC 1.5%	1	4.001 ± 0.003	
	2	6.350 ± 0.003	15.620 ± 0.004
	3	7.574 ± 0.002	
	m_{avg}	5.975 ± 1.816	
CMC 2%	1	12.210 ± 0.004	
	2	13.782 ± 0.002	33.170 ± 0.003
	3	18.324 ± 0.003	
	m_{avg}	14.772 ± 3.175	

[1] Brookfield Mixer. Shear rate range: 0-30 1/s

[2] Haake MV-III (d/D=0.73). Shear rate range: 0-40 1/s

Table 6.17: Values of the Fluid Consistency Coefficient of Standard Power-Law Fluids Using the Mixer System (Flag) [Model 3: $d = d_e$; Eqn. (6.23.1)] and a Concentric Cylinders Viscometer (Haake Rotovisko)

		Consistency Coefficient, m (Pa s^n)	
FLUID	SYSTEM	Mixer[1]	Concentric Cylinders[2]
CMC 1%	1	1.522 ± 0.006	
	2	2.648 ± 0.004	2.619 ± 0.003
	3	2.328 ± 0.004	
m_{avg}		2.166 ± 0.580	
CMC 1.5%	1	8.408 ± 0.003	
	2	14.379 ± 0.003	15.620 ± 0.004
	3	18.417 ± 0.003	
m_{avg}		13.735 ± 5.035	
CMC 2%	1	25.120 ± 0.004	
	2	32.250 ± 0.002	33.170 ± 0.003
	3	43.280 ± 0.002	
m_{avg}		33.550 ± 9.149	

[1] Brookfield Mixer. Shear rate range: 0-30 1/s [Eqn. (6.23.1)]

[2] Haake MV-III (d/D=0.73). Shear rate range: 0-40 1/s

Tables 6.13 and 6.14 present the values of the fluid consistency coefficient, m, obtained by replacing the mixing system with the Model 1 [negligible end effects, Eqn. (4.14)], for the paddles and flag impeller, respectively. Comparison with the values obtained using the concentric cylinders viscometer show that the results with the paddle impellers are satisfactory. However, the flag impeller gives considerably lower values of the rheological parameter, m, when using Model 1 (Table 6.14). Also, the effect of the gap seems to be more important for this impeller, since the value of the consistency coefficient obtained with the small gap case (System 3, d/D = 0.591) is twice as high as the value of the consistency coefficient in the large gap case (System 1, d/D = 0.273) (See Table 6.14). A small gap also gives higher values of the rheological parameter when using a paddle impeller (Systems 9 and 10, d/D = 0.327), especially for the fluid of higher viscosity (CMC 2%) (Table 6.13).

Tables 6.15 and 6.16 present the values of the consistency coefficient, m, calculated by replacing the mixing system with the Model 2 [presence of end effects, Eqn. (4.21)], for the paddles and flag impeller, respectively. No big differences with the values from Tables 6.13 and 6.14 are observed, with results from Model 2 [Eqn. (4.14)] lower than those obtained with Model 1 [Eqn. (4.21)]. The same behavior was observed in results for the flag impeller (Table 6.16).

Table 6.17 presents the results obtained by replacing the flag impeller with a cylinder of dimensions as in Model 3 [$d = d_e$, Eqn. (6.23.1)]. It can be seen that this model gives considerably higher values of the fluid consistency coefficient than the previous models. In

comparison to the values obtained using a concentric cylinders viscometer, results also show better agreement.

Rheograms (shear stress-shear rate curves) were developed for all fluids and systems. Figure 6.52 shows the flow curves for the 1% CMC (Figure 6.52a) and the 2% CMC (Figure 6.52b) solutions using the mixer viscometer with the paddle impellers in a large cup [(d/D) = 0.327]. The model selected for approximation of the average shear stress was Model 2 (concentric cylinders analogy with end effect) since it gave more consistent values of torque (Figure 6.48b). Results were compared with those obtained with the concentric cylinders viscometer (Haake Rotovisko with the MV-III sensor which provided a range of shear rates similar to that obtained with the Brookfield viscometer and the mixer impellers) and proved to be satisfactory. Figures 6.53a and 6.53b present results for a small gap [(d/D) = 0.709]. Results indicate that the method works better when the agitated fluid is highly viscous (CMC 2%) than when agitating a low viscosity fluid (CMC 1%) when a small gap is present.

Figure 6.54 presents the flow curves obtained for the flag impeller using the Model 3 ($d = d_e$). Results show excellent agreement with those obtained using the concentric cylinder viscometer, with better results for the more viscous fluid (CMC 2%). For comparison, Figures 6.55 and 6.56 present the flow curves obtained using Model 1 [Eqn. (4.14)] and Model 2 [Eqn. (4.21)], respectively. It is clear that the Model 3 [Eqn. (6.23.1)] is still the best approximation for the mixing system when agitating standard power-law fluids.

6.2.2.3.2) Food Product

Flow curves for an actual food product (Rancher's Choice Creamy

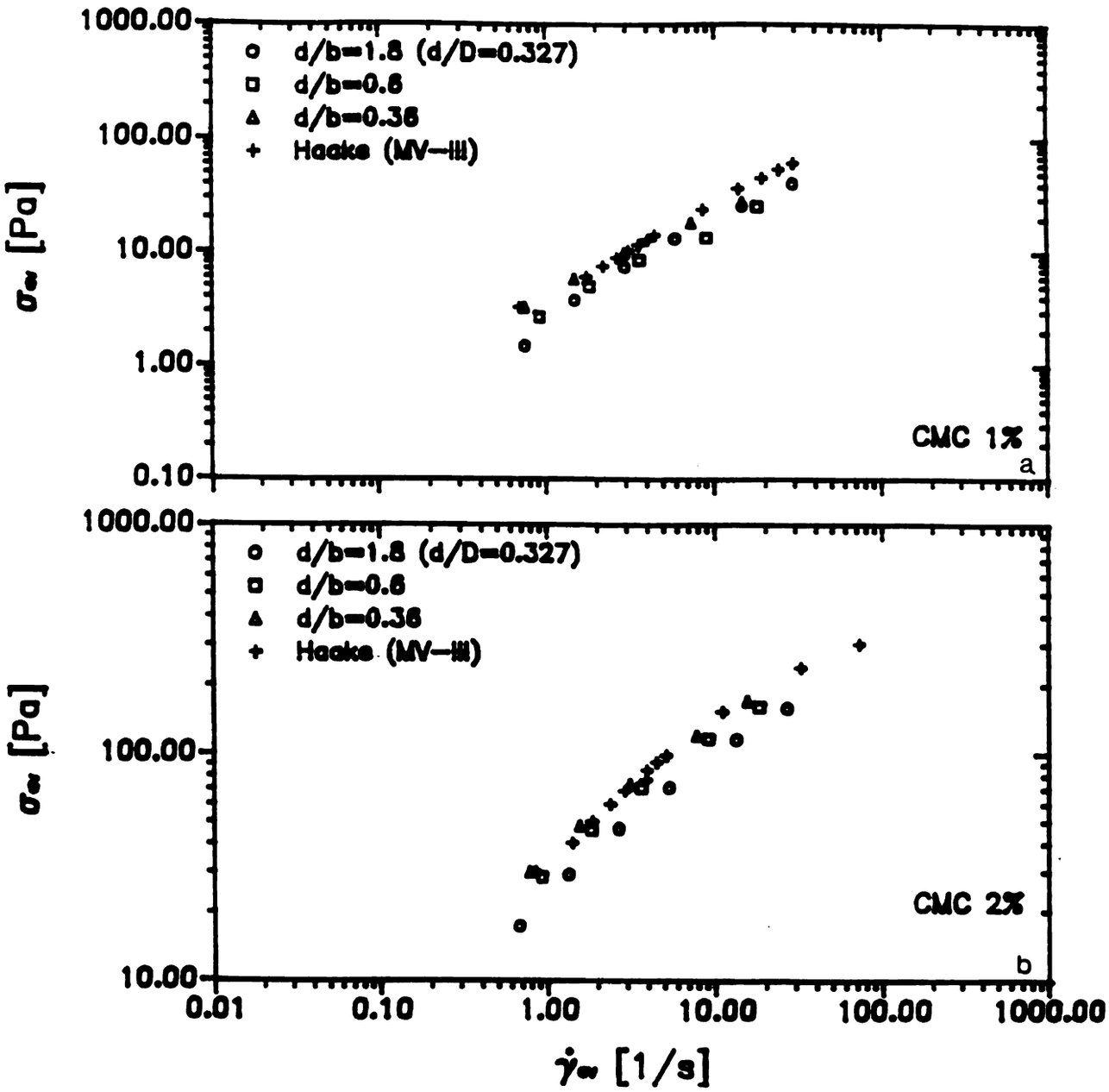

Figure 6.52: Comparison of the Flow Curve for a Standard Fluid Determined Using the Concentric Cylinders Viscometer with the Data Obtained Using the Mixer Viscometer with the Paddle Impellers in a Large Cup [Model 2, Eqn. (4.21)]; a) CMC 1%; b) CMC 2%

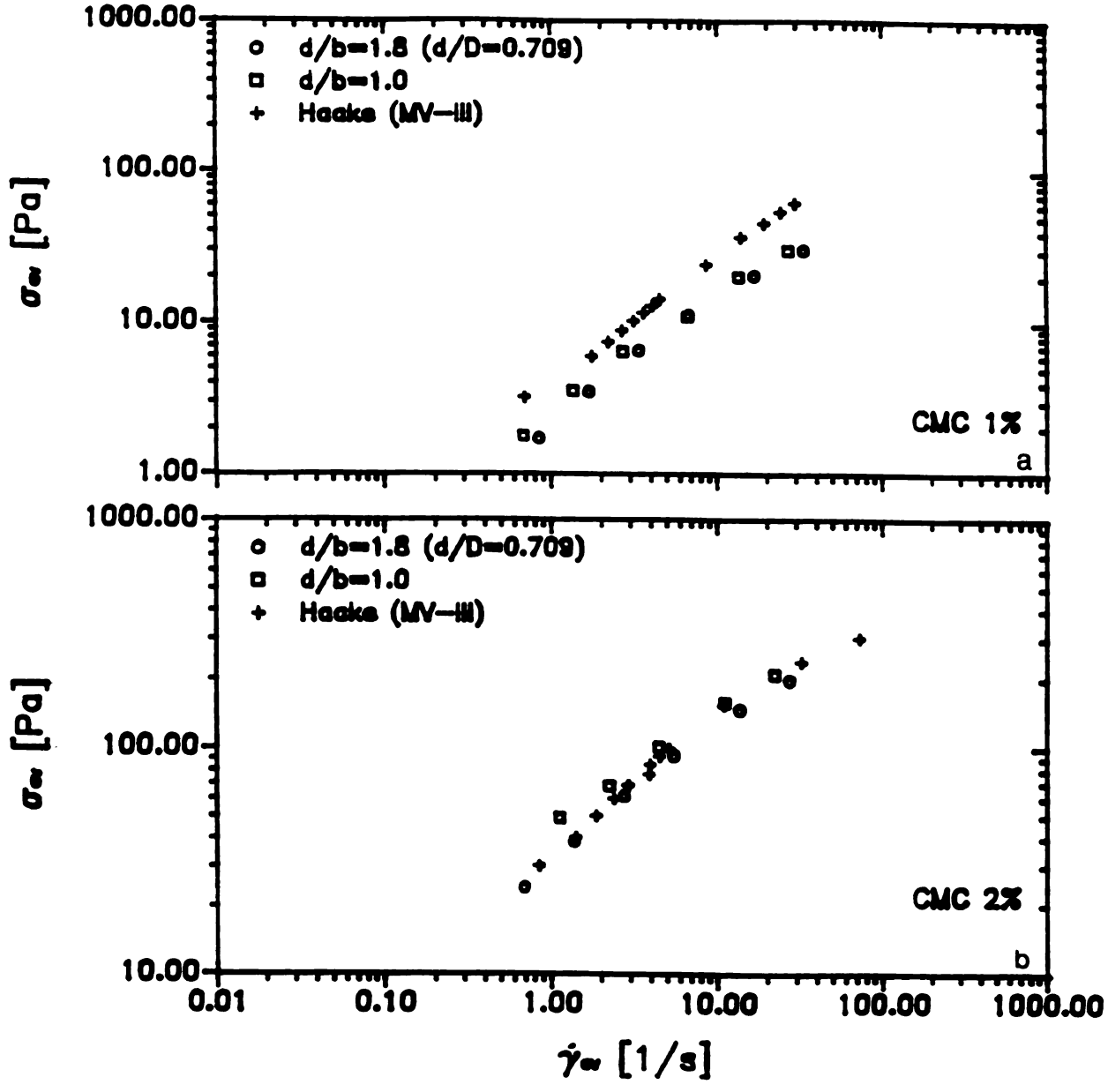

Figure 6.53: Comparison of the Flow Curve for a Standard Fluid Determined Using the Concentric Cylinders Viscometer with the Data Obtained Using the Mixer Viscometer with the Paddle Impellers in a Small Cup [Model 2, Eqn. (4.21)]; a) CMC 1%; b) CMC 2%

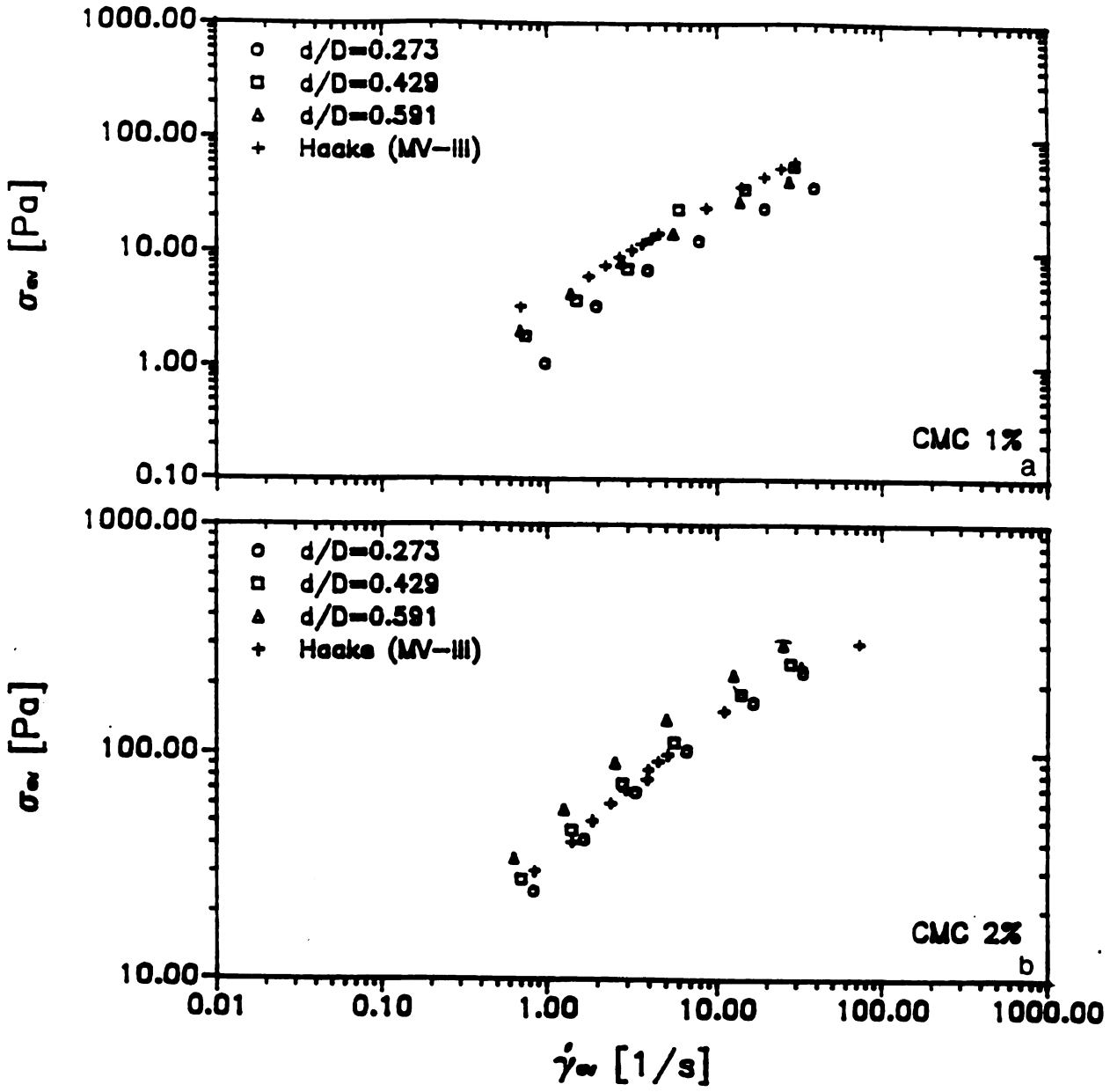

Figure 6.54: Comparison of the Flow Curve for a Standard Fluid Determined Using the Concentric Cylinders Viscometer with the Data Obtained Using the Mixer Viscometer with a Flag Impeller [Model 3, Eqn. (6.23.1)]; a) CMC 1%; b) CMC 2%

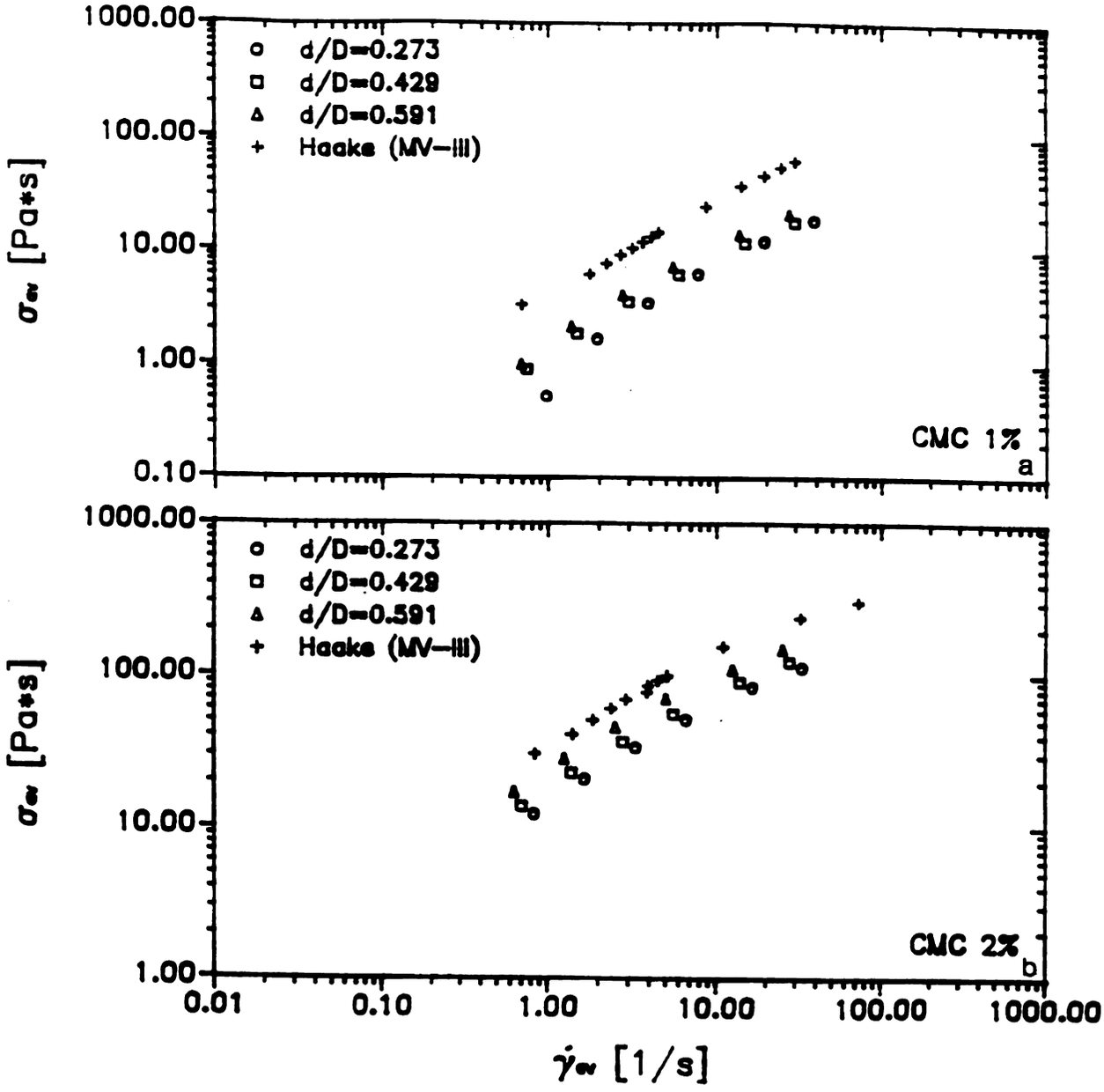

Figure 6.55: Comparison of the Flow Curve for a Standard Fluid Determined Using the Concentric Cylinders Viscometer with the Data Obtained Using the Mixer Viscometer with a Flag Impeller [Model 1, Eqn. (4.14)]; a) CMC 1%; b) CMC 2%

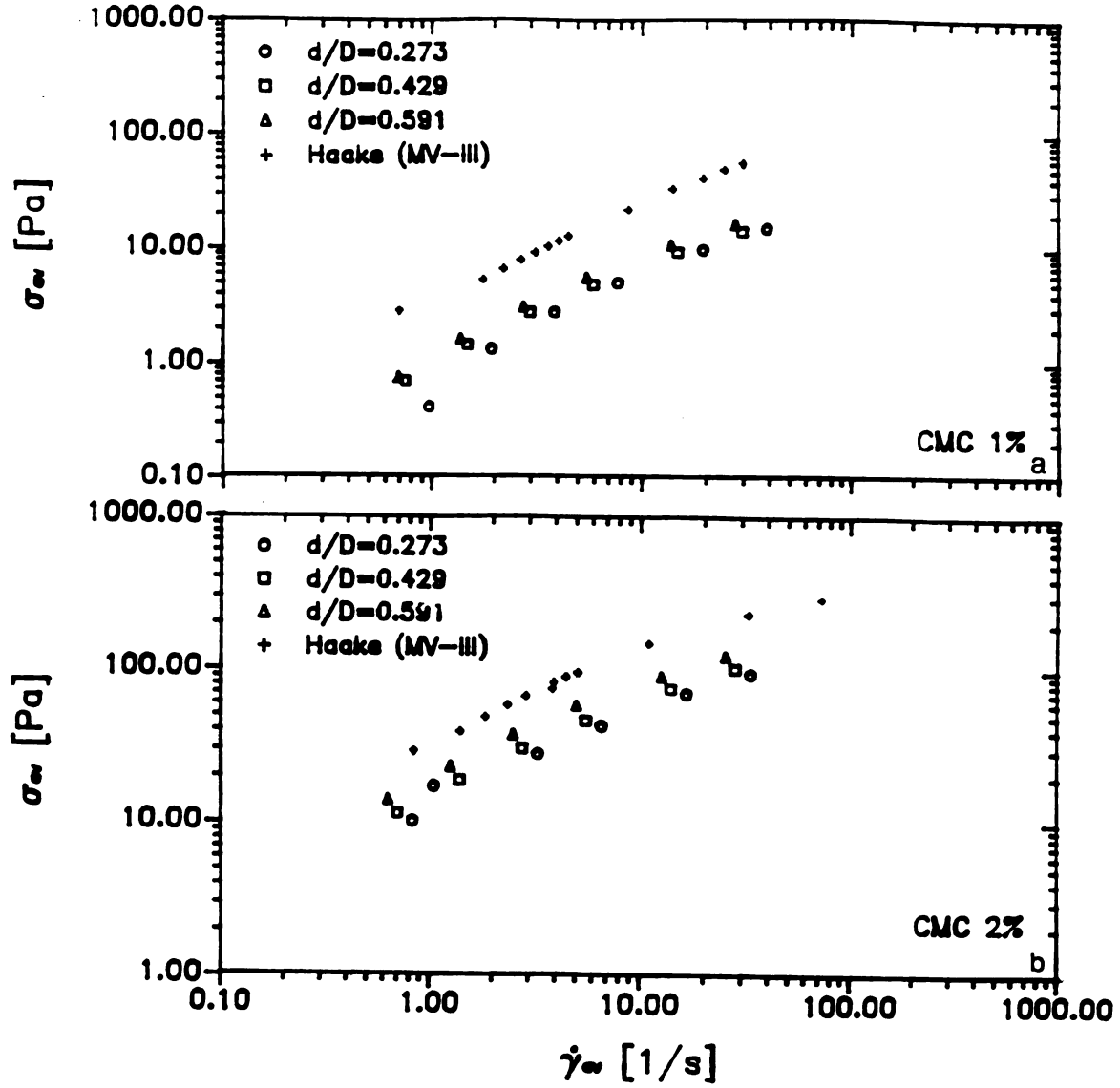

Figure 6.56: Comparison of the Flow Curve for a Standard Fluid Determined Using the Concentric Cylinders Viscometer with the Data Obtained Using the Mixer Viscometer with a Flag Impeller [Model 2, Eqn. (4.21)]; a) CMC 1%; b) CMC 2%

Dressing; Kraft, INC., Glenview, Illinois) were estimated to check the applicability of the proposed procedure. Figure 6.57 presents the results using the paddle impellers [Model 2, Eqn. (4.21)] in comparison with the ones obtained with the concentric cylinders viscometer. The agreement of the data is evident for different impeller and cup sizes. Tables 6.18 and 6.19 present the values of the rheological parameters (n and m) for the salad dressing, evaluated using Model 1 [Eqn. (4.14)] and Model 2 [Eqn. (4.21)] for approximation of the average shear stress with the paddle impellers, respectively. The proposed procedure seems to be able to approximate the rheological behavior of a food product when using the mixer viscometer with the paddle impellers. The approach takes into account the variations in impeller and cup geometry.

It is interesting to note that the differences due to variation in impeller are less than the observed in the developed curve flows for the standard fluids (See Figures 6.53 and 6.57, for instance). The same trend was observed with the flag impeller (Figures 6.56 and 6.58).

For the flag impeller, peculiar results were obtained. Table 6.20 shows the values of the rheological parameters of the tested fluid with the three models investigated in this study. Figure 6.58 shows the flow curves obtained for the food product by approximating the flag impeller with a cylinder of diameter d_e (Model 3). Approximation of the shear stress-shear rate data with Model 3 gives higher values of the flow curve as compared with the concentric cylinders viscometer (Haake Rotovisko with MV-III). Figures 6.59 and 6.60 present results using Model 1 and 2, respectively. Results indicate that the two models show excellent agreement with the concentric cylinders data for the food product as compared with Model 3 (Figure 6.58). It might be said that

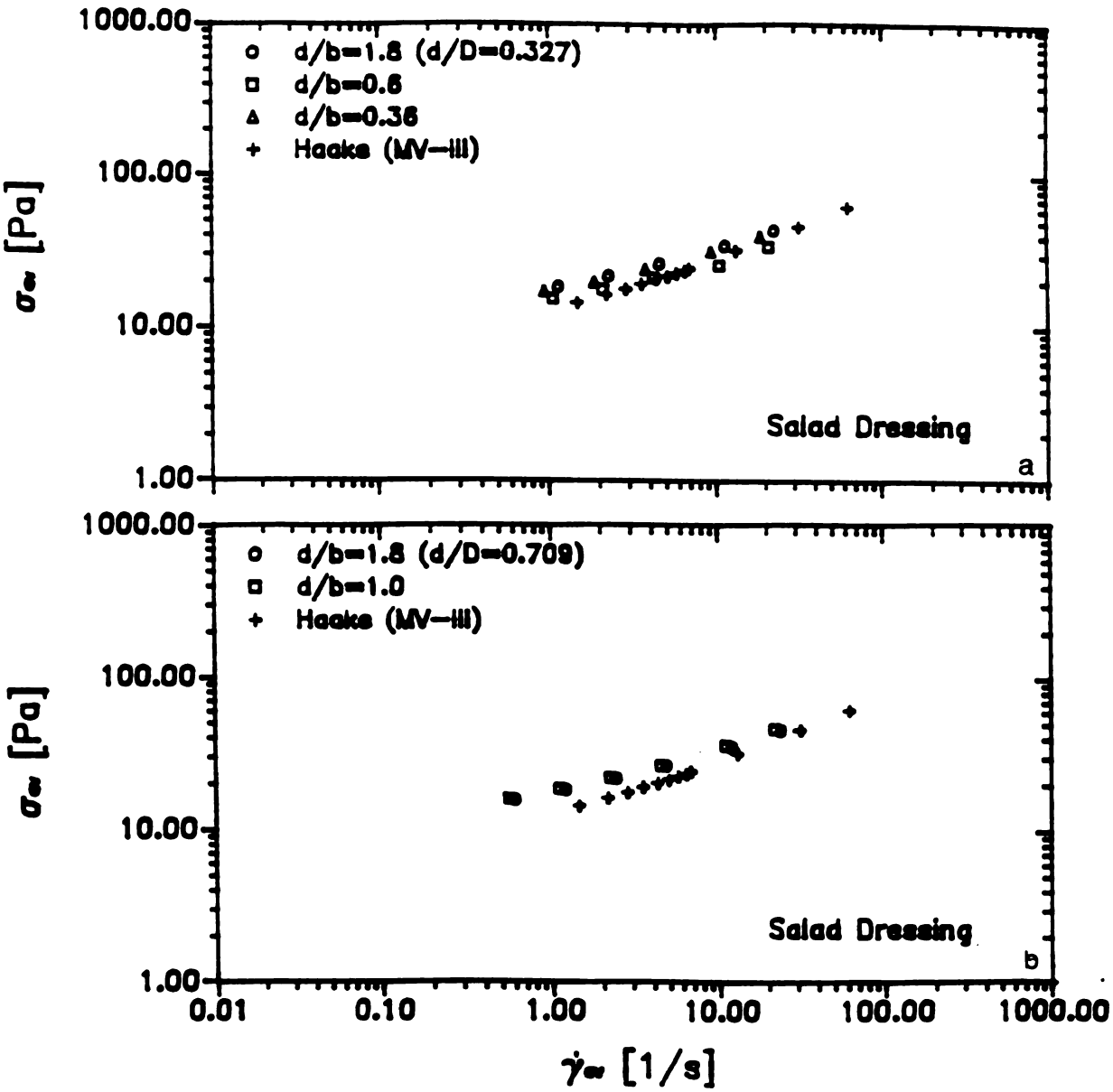

Figure 6.57: Comparison of the Flow Curve for Salad Dressing Determined Using the Concentric Cylinders Viscometer with the Data Obtained Using the Mixer Viscometer with the Paddle Impellers [Model 2, Eqn. (4.21)]; a) Large Cup; b) Small Cup

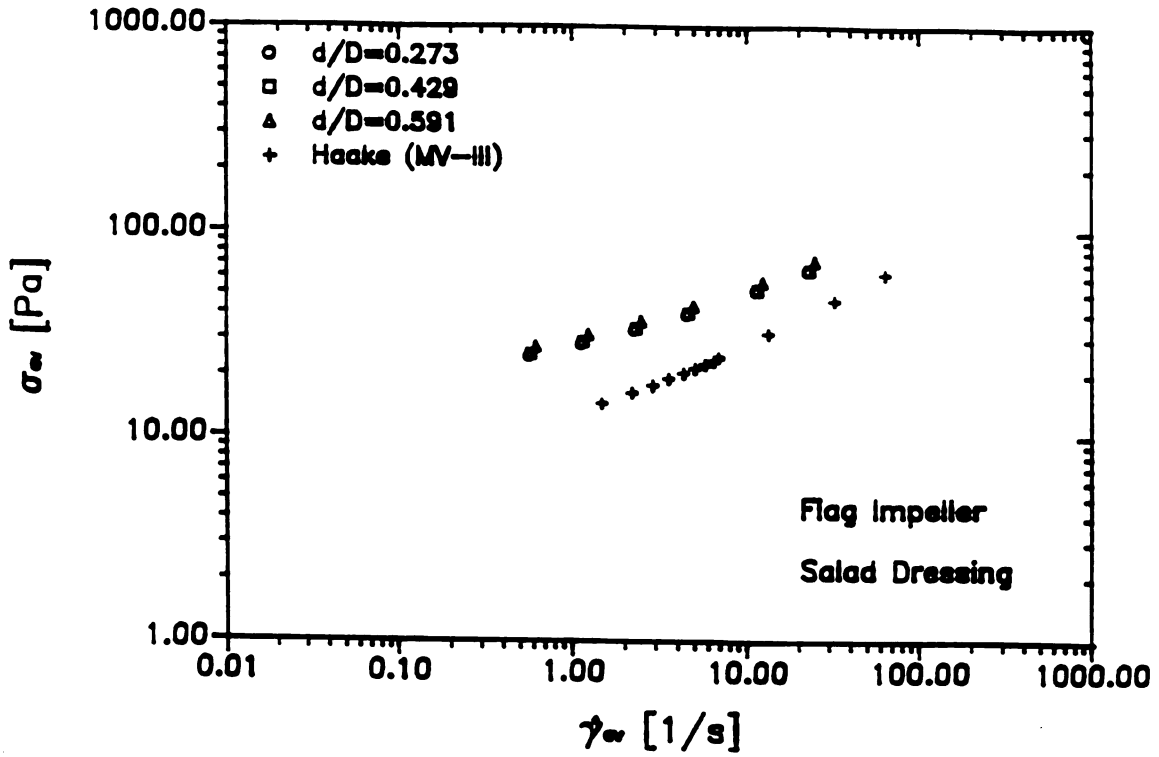

Figure 6.58: Comparison of the Flow Curve for Salad Dressing Determined Using the Concentric Cylinders Viscometer with the Data Obtained Using the Mixer Viscometer with a Flag Impeller [Model 3, Eqn. (6.23.1)]

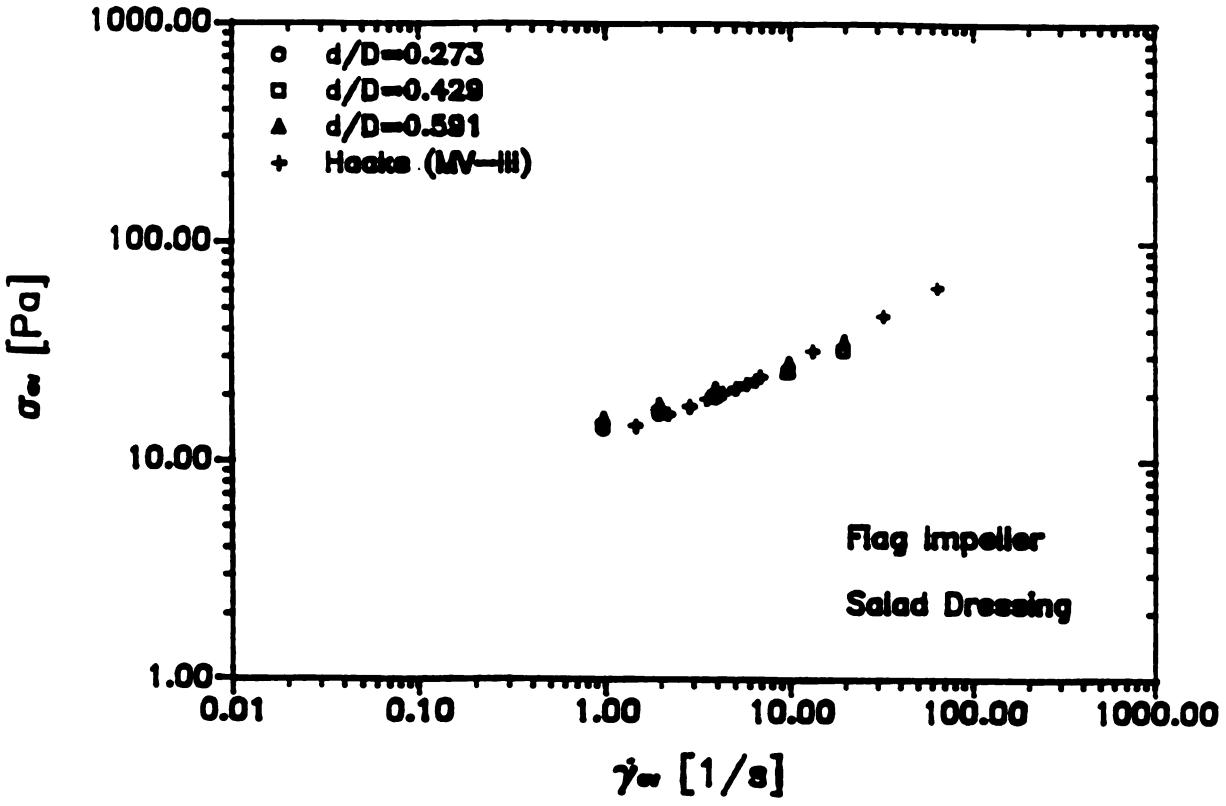

Figure 6.59: Comparison of the Flow Curve for Salad Dressing Determined Using the Concentric Cylinders Viscometer with the Data Obtained Using the Mixer Viscometer with a Flag Impeller [Model 1, Eqn. (4.14)]

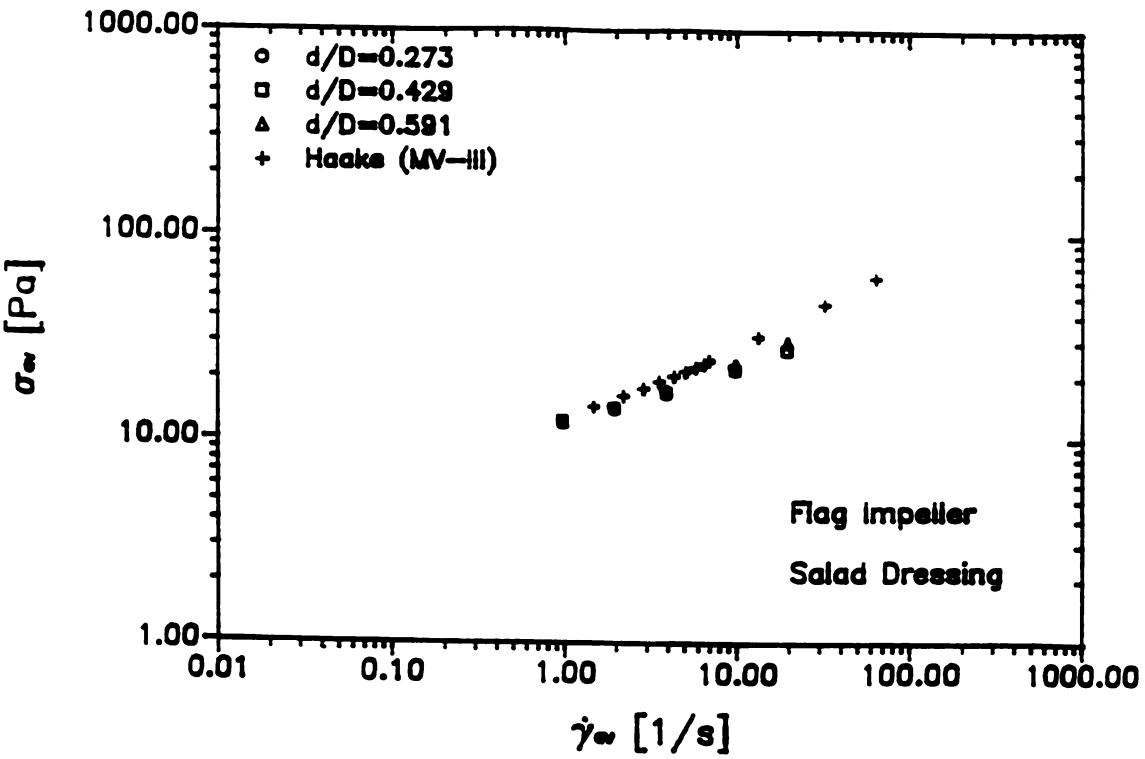

Figure 6.60: Comparison of the Flow Curve for Salad Dressing Determined Using the Concentric Cylinders Viscometer with the Data Obtained Using the Mixer Viscometer with a Flag Impeller [Model 2, Eqn. (4.21)]

Table 6.18: Values of the Flow Behavior Index (n) and the Fluid Consistency Coefficient of Salad Dressing Using the Mixer System (Paddles) [Model 1, Eqn. (4.14)] and a Concentric Cylinders Viscometer (Haake Rotovisko)

	n	Consistency Coefficient, m (Pa s^n)
SYSTEM	Mixer	Viscometer[1]
1	0.248 ± 0.003	29.811 ± 0.003
3	0.243 ± 0.001	20.186 ± 0.002
5	0.236 ± 0.001	30.057 ± 0.005
6	0.239 ± 0.002	25.475 ± 0.005
8	0.227 ± 0.003	19.039 ± 0.003
9	0.257 ± 0.002	32.007 ± 0.004
10	0.258 ± 0.002	27.701 ± 0.003
Average	0.244 ± 0.011	26.325 ± 5.029

Haake data[2]: n = 0.399 ± 0.005
m = 15.00 ± 0.003 Pa s^n

[1] Brookfield Mixer. Shear rate range: 0-30 1/s [Eqns. (6.18) and (6.19)]

[2] Haake MV-III (d/D=0.73). Shear rate range: 0-40 1/s

Table 6.19: Values of the Flow Behavior Index (n) and the Fluid Consistency Coefficient of Salad Dressing Using the Mixer System (Paddles) [Model 2, Eqn. (4.21)] and a Concentric Cylinders Viscometer (Haake Rotovisko)

	n	Consistency Coefficient, m (Pa s^n)	
SYSTEM	Mixer	Viscometer[1]	
1	0.248 ± 0.002	19.314 ± 0.003	
3	0.236 ± 0.003	15.484 ± 0.004	
5	0.243 ± 0.001	18.023 ± 0.002	
6	0.239 ± 0.002	18.793 ± 0.005	
8	0.227 ± 0.003	15.867 ± 0.002	
9	0.257 ± 0.002	18.313 ± 0.003	
10	0.258 ± 0.002	18.999 ± 0.004	
Average	0.244 ± 0.011	17.853 ± 1.554	

Haake data[2]: n = 0.399 ± 0.005
m = 15.00 ± 0.003 Pa s^n

[1] Brookfield Mixer. Shear rate range: 0-30 1/s [Eqns. (6.18) and (6.19)]

[2] Haake MV-III (d/D=0.73). Shear rate range: 0-40 1/s

Table 6.20: Values of the Flow Behavior Index (n) and the Fluid Consistency Coefficient of Salad Dressing Using the Mixer System (Flag) and a Concentric Cylinders Viscometer (Haake Rotovisko)

	n	Consistency Coefficient, m (Pa s^n)
SYSTEM	Mixer	Viscometer[1]
Model System 1		
1	0.257 ± 0.003	14.916 ± 0.004
2	0.230 ± 0.002	15.030 ± 0.004
3	0.235 ± 0.002	16.249 ± 0.003
Average	0.240 ± 0.014	15.398 ± 0.739
Model System 2		
1	0.257 ± 0.003	12.570 ± 0.005
2	0.230 ± 0.002	12.907 ± 0.003
3	0.235 ± 0.002	12.740 ± 0.003
Average	0.240 ± 0.014	12.739 ± 0.168
Model System 3		
1	0.257 ± 0.003	28.691 ± 0.003
2	0.230 ± 0.002	29.240 ± 0.002
3	0.235 ± 0.002	30.690 ± 0.004
Average	0.240 ± 0.014	29.873 ± 0.742

Haake data[2]: n = 0.399 ± 0.005
m = 15.00 ± 0.003 Pa s^n

[1] Brookfield Mixer. Shear rate range: 0-30 1/s [Eqn. (6.21)]

[2] Haake MV-III (d/D=0.73). Shear rate range: 0-40 1/s

the area of the flag impeller of diameter d and blade height b contributes to the torque values when agitating the food product. In the case of a standard power-law fluid such as the CMC solutions, this is not the case, since the assumption of the total area of the flag impeller yielded higher values of torque as compared with the geometry given by Model 3 ($d = d_e$). These results indicate that the fluid to be investigated using mixer viscometry is of great importance when selecting the appropriate equations to approximate the flow curves since the food product (salad dressing) shows more shear-thinning behavior ($n = 0.244 \pm 0.011$) than the standard CMC solutions ($0.5 \leq n \leq 0.9$).

In terms of comparison, plots of the apparent viscosity, η_a, versus the average shear rate, $\dot{\gamma}_{av}$, were developed for the different Models using the flag impeller and the results obtained with the concentric cylinders viscometer. Figures 6.61 to 6.63 present the results for the three models analyzed in this investigation. The agreement of results is clear and excellent. It may be seen that the differences obtained with the Model 3 ($d = d_e$) is not so drastic (Figure 6.63). Figure 6.64 presents the results for two different gaps. Figure 6.64a shows the results when agitating the food product with a flag impeller and a small gap is present (d/D=0.591). Figure 6.64b shows the results for the wide gap case (d/D=0.273). It may be noted that the effect of the mixing system (in this case, the impeller-to-cup diameter ratio, d/D) is not significant.

In summary, analytical systems were developed for the mixing systems based on the original development for a power-law fluid agitated in a concentric cylinders viscometer. These systems (or models) take into account differences in impeller shape (paddle or flag) and

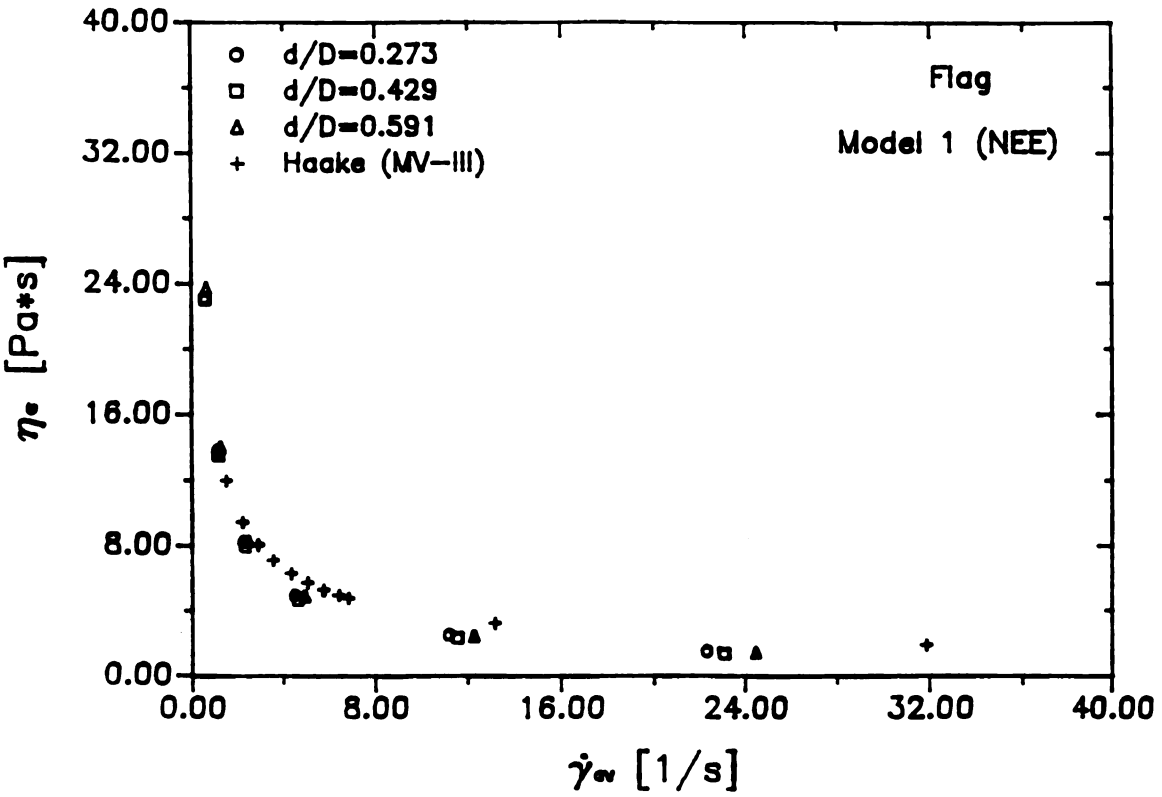

Figure 6.61: Apparent Viscosity as a Function of Average Shear Rate For Salad Dressing. Flag Impeller (Model 1: concentric cylinders with no end effects [NEE]).

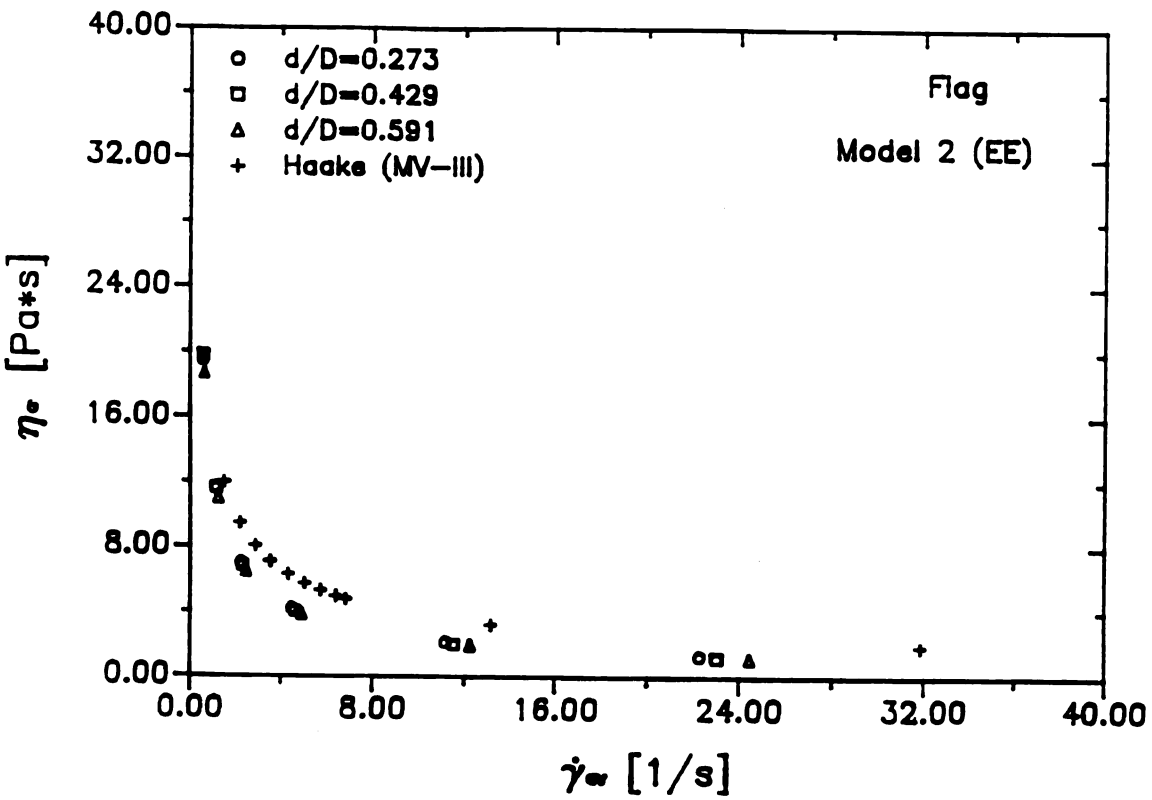

Figure 6.62: Apparent Viscosity as a Function of Average Shear Rate For Salad Dressing. Flag Impeller (Model 2: concentric cylinders with end effects [EE]).

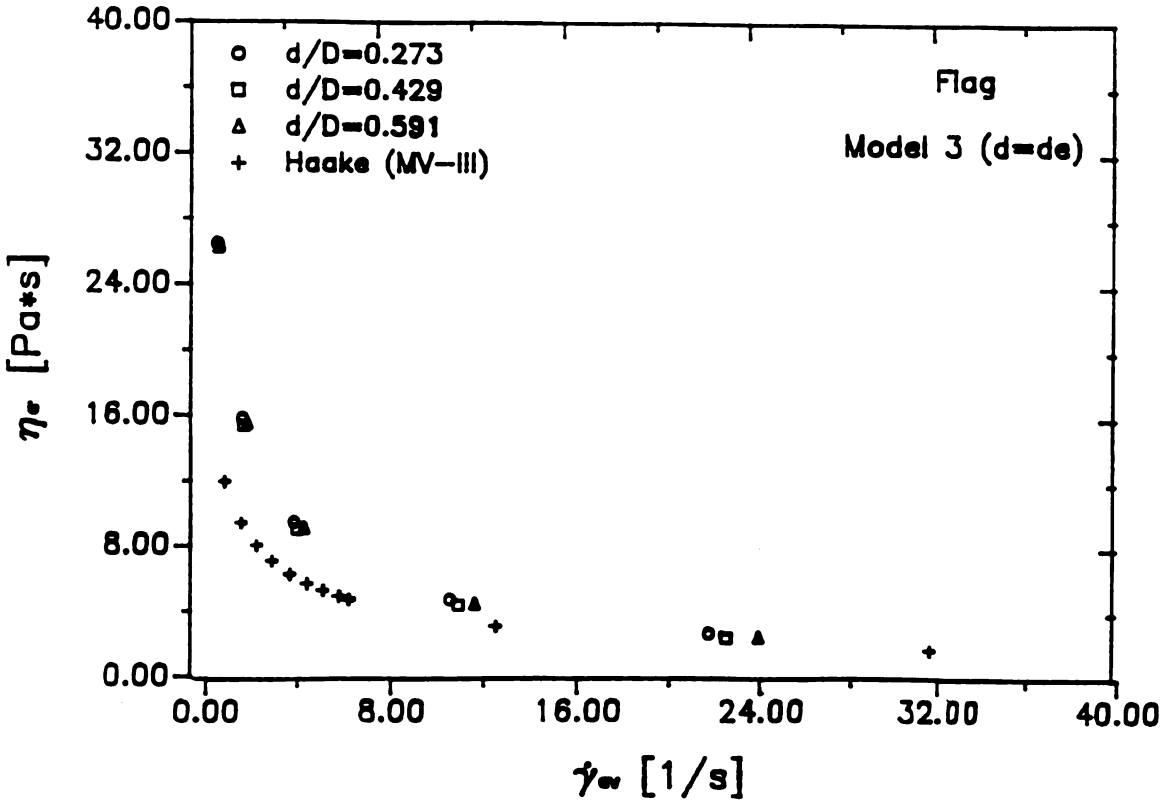

Figure 6.63: Apparent Viscosity as a Function of Average Shear Rate For Salad Dressing. Flag Impeller (Model 3: concentric cylinders with end effects; d = d_e).

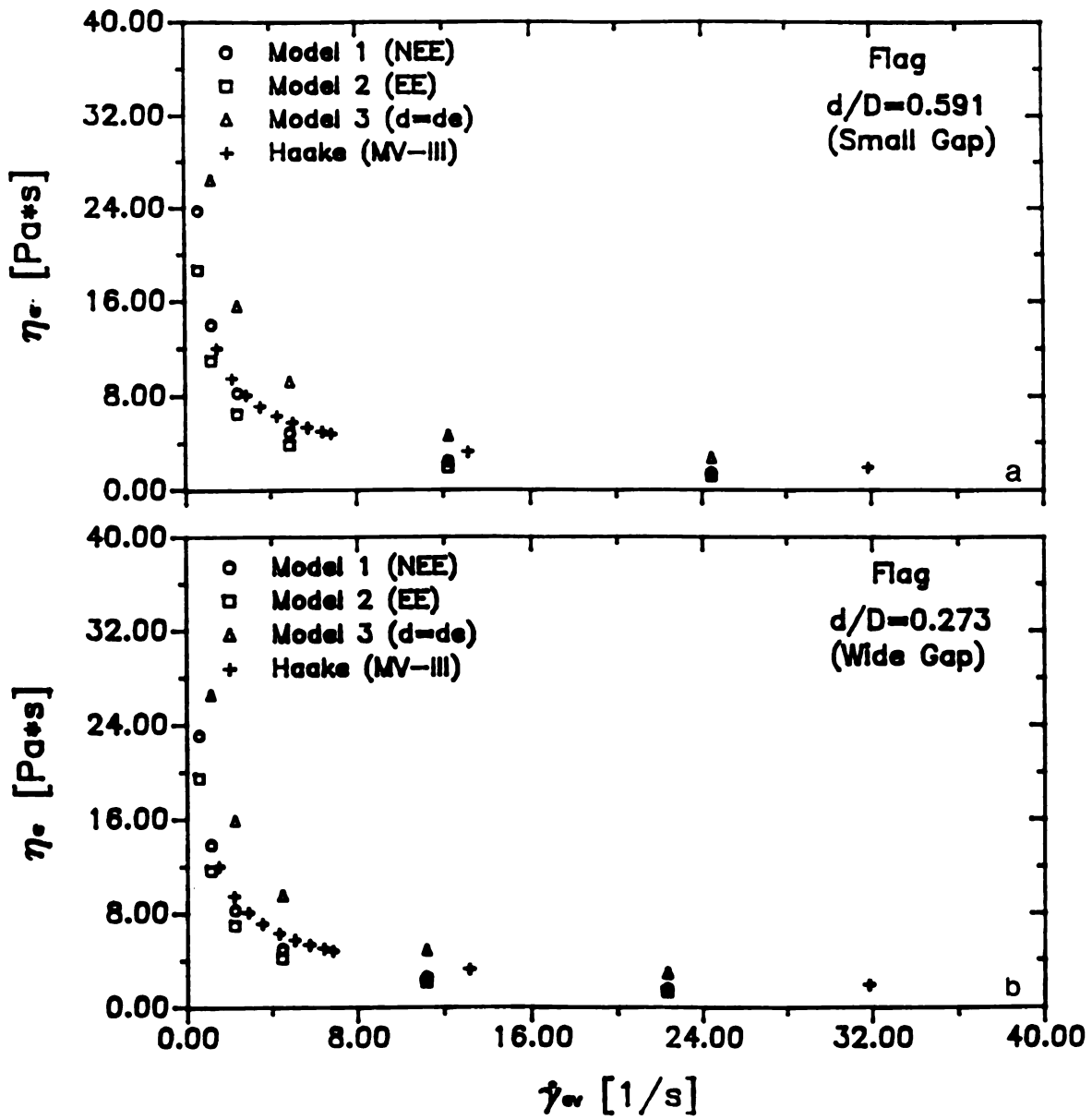

Figure 6.64: Apparent Viscosity as a Function of Average Shear Rate For Salad Dressing. Flag Impeller. a) Small Gap; b) Wide Gap.

differences in system geometry (impeller-to-cup diameter ration, d/D, and impeller blade height, b). Thus, flow curves can be directly determined by only measuring the torque needed to rotate the impeller as a function of the rotational speed of the impeller. The selection of the model can be checked with data from a conventional viscometer when available.

6.3 GENERAL RECOMMENDATIONS FOR THE APPLICATION OF MIXER VISCOMETRY

This section presents the recommendations for a general procedure (mixing system and unknown power-law fluid). Figure 6.65 shows the flow diagram of the procedure. The procedure has been developed for use with a simple and easy to handle data collection system. However, it can be applied to different combinations of viscometers and mixing systems.

6.3.1 Mixer System Used in This Study

The procedure is as follows:

1. Maintain a constant temperature of the fluid.
2. Impeller and cup dimensions (d/D and d/b) must be known.
3. Other geometric parameters should remain constant for a set of experiments (fluid height, distance from bottom of impeller to bottom of container).
4. Check for time-dependent effects (there should be none for power law fluids). Agitate fluid for a period of 10 minutes to reach an equilibrium value of torque.
5. Select range of rotational speeds. The criterium to follow is

$R_e \leq 10$. Also, check for presence of surface waves or turbulence. The maximum allowable value of rotational speed, N, will be that which does not produce formation of surface waves on agitated fluid. Operating values of the rotational speed (rev/s) greater than 20 rpm are recommended.

6. Measure the torque in the shaft required to agitate the fluid, M, as a function of impeller rotational speed, N.
7. From log-log plot of M vs. N, evaluate the value of the flow behavior index, n, of the fluid.
8. To determine the flow curve of the fluid, a model is required. Therefore, expressions for an average mixing shear rate, $\dot{\gamma}_{av}$, and an average shear stress, σ_{av} , were developed. Different models were evaluated to determine the best model for flow curve determination.
9. If working with a paddle impeller [$0.36 \leq (d/b) \leq 1.8$], use Eqn. (6.19.1) or (6.19.2) if $d/D \geq 0.709$ (small gap) and Eqn. (6.18.1) or (6.18.2) if [$0.327 \leq (d/D) \leq 0.515$] (wide to medium gap). For a flag impeller [$(d/b)=0.3$], use Eqn. (6.21). Thus,

$$\dot{\gamma}_{av} = \left\{ 4\pi \left[\frac{(D/d)^{2/n}}{(D/d)^{2/n} - 1} \right] (d/b)^{n/2} \right\} N \qquad (6.18.1)$$

or

$$\dot{\gamma}_{av} = 2\Omega \left[\frac{(D/d)^{2/n}}{(D/d)^{2/n} - 1} \right] (d/b)^{n/2} \qquad (6.18.2)$$

for a paddle impeller and $0.327 \leq d/D \leq 0.515$, and

$$\dot{\gamma}_{av} = \left\{ 4\pi \left[\frac{(D/d)^{\frac{2-n}{n}}}{(D/d)^{2/n} - 1} \right] (d/b)^{n/2} \right\} N \qquad (6.19.1)$$

or

$$\dot{\gamma}_{av} = 2\Omega \left[\frac{(D/d)^{\frac{2-n}{n}}}{(D/d)^{2/n} - 1} \right] (d/b)^{n/2} \qquad (6.19.2)$$

for $d/D \geq 0.709$ (with $1 \geq b \geq 5$ cm and $0.5 \geq n \geq 0.9$).

Flag impeller (b/d=0.5),

$$k' = 4\pi \left[(D/d)^{n/2} \right] \qquad (6.21)$$

10. Determine the best model to approximate the average shear stress. A way to check the applicability of the shear stress equations [Model 1 (Eqn. (4.14); Model 2 (Eqn. (4.21) and Model 3 (Eqn. (6.23.1) and (6.23.2)] is to compare the values of torque calculated using these equations with the experimentally measured values of torque. The best equation will be the one that shows better agreement with the experimental data. Thus,

Model 1 (concentric cylinders analogy with negligible end effects):

$$M = 2\pi b (d/2)^2 \sigma_{av} \qquad (4.14)$$

Model 2 (concentric cylinders analogy with end effects):

$$M = \frac{\pi d^3}{2}\left[\frac{b}{d} + \frac{1}{3}\right]\sigma_{av} \qquad (4.21)$$

Model 3 (Flag impeller; d= d_e):

$$M = 2\pi b\,(d_e/2)^2\,\sigma_{av} \qquad (6.23.1)$$

and

$$M = \frac{\pi d_e^3}{2}\left[\frac{b}{d_e} + \frac{1}{3}\right]\sigma_{av} \qquad (6.23.2)$$

11. Develop plots of average shear stress versus average shear rate for the fluid (flow curves). The value of the consistency coefficient, m, can be evaluated by linear regression of the plots.
12. Evaluate the apparent viscosity of the fluid from $\eta_a = m\,(\dot{\gamma}_{av})^{n-1}$.
13. If available, compare results with data obtained with a traditional concentric cylinders viscometer. Make sure the range of shear rates are comparable.

6.3.2 <u>New Mixer Viscometer System</u>

If an impeller other than a flag or a paddle impeller considered in this study is used, the following procedure is recommended:

1. Follow previous steps (1-7).
2. Evaluate k' of the particular impeller using the <u>Slope method</u>. The main reason for selection of this mixer viscometry method is its

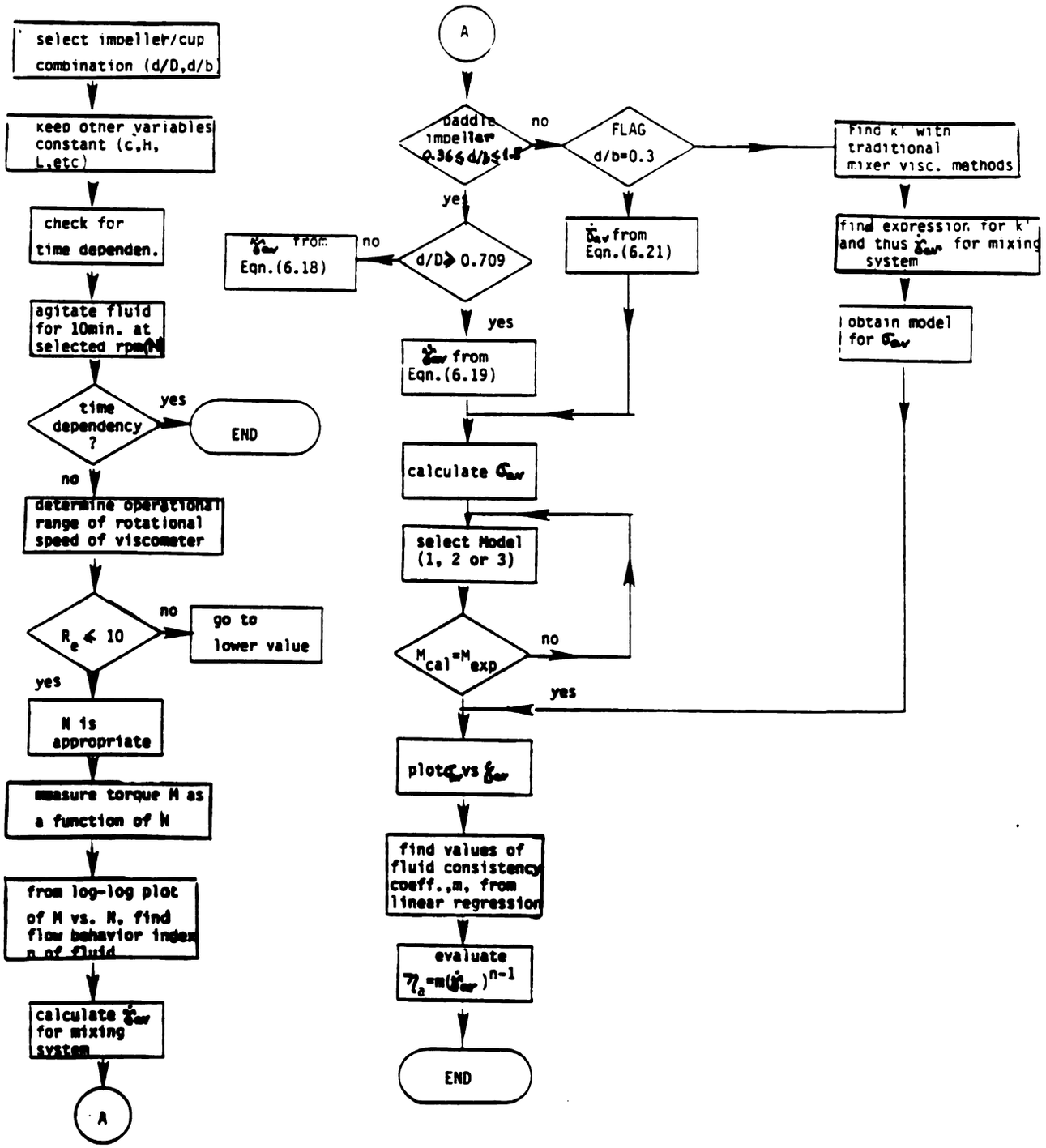

Figure 6.65: Flow Diagram of General Procedure For Mixer Viscometry

simplicity. If differences in fluid properties are considered, the Viscosity matching method should be used.

3. Seek a range of variable where k' is constant (i.e., (d/D), (d/b) and N).
4. With the values of k' obtained in (2) find an expression for k' as a function of system geometry and fluid properties. As a start, use the concentric cylinders analogy approach developed in this study [Equations (6.18.1), (6.18.2), (6.19.1), (6.19.2), or (6.21)]. Different expressions may be obtained when different (d/D) ranges are considered.
5. From (3), find expressions for $\dot{\gamma}_{av}$.
6. Follow previous step (10) to find approximations of the σ_{av} of the fluid under study for the new mixing system.
7. Follow steps (11-13) to develop the flow curves (shear stress-shear rate relationship).
8. Repeat procedure for different impeller/cup combination.

CHAPTER 7

SUMMARY AND CONCLUSIONS

1. A procedure for determination of the rheological behavior of power-law fluids using a mixer viscometer was developed.

2. Based on the concentric cylinders system analogy, an expression for the average shear rate in the mixing system can be determined. Average shear rates are a direct function of impeller to cup diameter ratios, impeller rotational speed and the value of the flow behavior index, n.

3. The size of the gap has a significant effect on the determination of expressions for the average shear rate in the mixing system. Hence, two different expressions were obtained for different d/D ranges: Eqn. (6.18) for $0.327 \leq d/D \leq 0.515$ and Eqn. (6.19) for $d/D \geq 0.709$ when using paddle impellers.

$$\dot{\gamma}_{av} = \left\{ 4\pi \left[\frac{(D/d)^{2/n}}{(D/d)^{2/n} - 1} \right] (d/b)^{n/2} \right\} N \qquad (6.18)$$

$$\dot{\gamma}_{av} = \left\{ 4\pi \left[\frac{(D/d)^{\frac{2-n}{n}}}{(D/d)^{2/n} - 1} \right] (d/b)^{n/2} \right\} N \qquad (6.19)$$

4. Impeller shape plays an important role in the development of equations for development of average shear stress-average shear rate

relationships for power-law fluids. Thus, the expression for the average shear rate for a flag impeller is different from the ones obtained for the paddle impellers [Eqns. (6.18) and (6.19)], and is given by Eqn. (6.21).

$$\dot{\gamma}_{av} = k'N = 4\pi \left[(D/d)^{n/2} \right] N \qquad (6.21)$$

5. The analogy made with the concentric cylinders with the addition of end effects is the best model [Eqn. (4.21)] for approximation of the average shear stress of power-law fluids when agitated with a paddle impeller rotating in a cylindrical cup. Results apply for all the different impeller/cup combinations and power-law fluids tested in this study ($0.327 \leq d/D \leq 0.709$; $0.36 \leq d/b \leq 1.8$; $0.5 \leq n \leq 0.9$).

$$M = \frac{\pi d^3}{2} \left[\frac{b}{d} + \frac{1}{3} \right] \sigma_{av} \qquad (4.21)$$

6. The best model for approximating the average shear stress when agitating a standard power-law fluid with a flag impeller rotating in a cylindrical cup is given by the assumption of the flag as a cylindrical surface with two blades attached, with a total diameter equal to d_e , with negligible end effects [From Eqn. (6.23.1)],

$$\sigma_{av} = \frac{\pi d_e^2}{2} M$$

7. Flow curves (average shear stress versus average shear rate) were

determined for power-law fluids without the need for calibration with Newtonian fluids.

8. The applicability of the concentric cylinders analogy procedure was experimentally verified with both ideal (standard) and actual (food product) power-law fluids.

9. Comparison of results obtained with the concentric cylinders analogy procedure with those obtained using a conventional concentric cylinders viscometer show excellent agreement for the range of impeller and cup sizes investigated in this study.

10. The concentric cylinders analogy procedure is capable of estimating the rheological behavior of a food product when using the mixer viscometer with the paddle impellers.

11. The concentric cylinders analogy procedure is simple and requires little data collection (torque measurements at selected values of impeller rotational speed) in comparison to the more tedious approach of established mixer viscometry methods.

12. The developed concentric cylinder procedure has proven to yield excellent approximation of the rheological behavior of power-law fluids using a low-cost viscometer.

13. Established mixer viscometry methods have been reviewed and evaluated for power-law (shear-thinning) fluids.

14. System geometry (impeller and cup), fluid properties and operating conditions (impeller rotational speed) were varied to investigate the effect of these parameters on the value of the mixer proportionality constant, k', using traditional mixer viscometry methods.

15. Traditional mixer viscometry methods (viscosity matching and slope) predict variations in the mixer proportionality constant, k', with geometry of the mixing system. The power curve method is very tedious and deviation from the basic assumption ($\dot{\gamma}_{av} = k'N$) may occur. The mixer torque Curve and the slope methods are simpler with the slope method requiring less data handling.

16. The common assumption of $\dot{\gamma}_{av} = k'N$, with k' a constant depending on the geometry of the impeller only, may lead to significant errors in the values of the average shear rate when measuring properties of shear-thinning fluids at low rotational speeds. The determined critical rpm range was found to be $N \leq 20$ rpm.

17. The effect of system geometry and fluid rheological behavior becomes almost negligible at higher rotational speeds. Thus, the assumption of a constant k' is valid under these conditions ($N > 20$ rpm).

18. There is a relation between the average shear rate and the type of fluid being agitated. However, the influence of the power-law rheological parameters, m and n, on mixer viscometry methods is not clearly understood. It seems that the more shear-thinning the fluid

(lower value of n), the lower the average shear rate. However, it must be noticed that the fluid with lower n values in this study was also the more viscous fluid (larger value of m). Thus, further investigation is necessary to identify the effect of the power-law parameters in mixer viscometry methods.

19. The shape of the impeller has an important influence on average shear rates as determined by established mixer viscometry methods since different values of k' are obtained for the two impeller shapes investigated in this study, especially at low values of rotational speed, N.

CHAPTER 8

SUGGESTIONS FOR FUTURE STUDY

1. To study the influence of the power-law parameters (n and m) on the value of the impeller proportionality constant, k'; one possibility is to vary the values of the rheological parameters and identify separate relationships for each parameter.

2. To test the developed procedure (concentric cylinders analogy) with different types of fluids and impeller shapes.

3. To test the developed procedure (concentric cylinders analogy) for a wider range of shear rates using different viscometers.

4. To review and evaluate the mixer viscometry methods when agitating fluids that do not obey the power-law model. The presence of a yield stress and time dependent characteristics should also be evaluated.

5. To extend the results from this investigation to scale-up of mixing tanks.

6. To evaluate shear fields in mixing systems.

APPENDICES

APPENDIX A

APPENDIX A

DIMENSIONLESS ANALYSIS FOR MIXING VESSELS (NEWTONIAN FLUIDS)

When using dimensional analysis to design an experiment, the first step is to define the pertinent quantities as shown in Table A.1. The number of required pi terms (dimensionless quantities) is defined from Buckingham's theorem as the number of pertinent quantities minus the number of dimensions. Therefore the number of pi terms required to design the experiment is 10 minus 3, which equals 7.

By describing the motion of a fluid in a mixing vessel only in terms of length [L], time [T] and mass [M], the following set of dimensionless products is obtained (Rushton et al., 1950):

$\pi_1 (D) = d^{\beta_1} N^{\beta_2} \rho^{\beta_3} D^{-1}$. Thus,

$$\pi_1 = L^0 T^0 M^0 = L^{\beta_1} T^{-\beta_2} (M/L^3)^{\beta_3} D^{-1}$$

L: $\beta_1 - 3\beta_3 - 1 = 0$ $\qquad \beta_1 = 1$

T: $-\beta_2 = 0$

M: $\beta_3 = 0$ $\qquad \pi_1 = d/D = D/d$

By inspection, $\pi_2 = H/d$

$\pi_3 = b/d$

$\pi_4 = L/d$

$$\pi_5 = c/d$$

With $\nu = \eta/\rho$, $\pi_6 (\nu) = d^{\beta_1} N^{\beta_2} \rho^{\beta_3} \nu^{-1}$ then,

$$L^0 T^0 M^0 = L^{\beta_1} T^{-\beta_2} (M/L^3)^{\beta_3} (L^2/T)^{-1}$$

L: $\beta_1 - 3\beta_3 - 2 = 0$ $\quad \beta_1 = 2$

T: $-\beta_2 + 1 = 0$ $\quad \beta_2 = 1$

M: $\beta_3 = 0$

$$\pi_6 = \frac{d^2 N}{\nu} = \frac{d N \rho}{\eta} = \text{mixing Reynolds Number, } R_e$$

$\pi_7 (g) = d^{\beta_1} N^{\beta_2} \rho^{\beta_3} g^{-1}$. Thus,

$$L^0 T^0 M^0 = L^{\beta_1} T^{-\beta_2} (M/L^3)^{\beta_3} (1/T^2)^{-1}$$

L: $\beta_1 - 3\beta_3 - 1 = 0$ $\quad \beta_1 = 1$

T: $-B_2 + 2 = 0$ $\quad \beta_2 = 2$

M: $\beta_3 = 0$

$$\pi_7 = \frac{d N^2}{g} = \text{Froude Number, } F_r$$

$\pi_8 (P) = d^{\beta_1} N^{\beta_2} \rho^{\beta_3} P^{-1}$. Thus,

$$L^0 T^0 M^0 = L^{\beta_1} T^{-\beta_2} (M/L^3)^{\beta_3} (ML^2/T^3)^{-1}$$

L: $\beta_1 - 3\beta_3 - 2 = 0$ $\qquad \beta_1 = 5$

T: $-\beta_2 + 3 = 0$ $\qquad \beta_2 = 3$

M: $\beta_3 - 1 = 0$ $\qquad \beta_3 = 1$

$$\pi_8 = \frac{d^5 N^3 \rho}{P} = \frac{P}{d^5 N^3 \rho} = \text{Power Number, } P_o$$

According to the Buckingham's theorem (Langhaar, 1981), the power consumption of mixer impellers is given by an equation of the form:

$$P_o = f\left[(R_e)^{\beta_1} (F_r)^{\beta_2} (D/d)^{\beta_3} (H/d)^{\beta_4} (L/d)^{\beta_5} (b/d)^{\beta_6} (c/d)^{\beta_7} \right]$$

or [Eqn. (3.91)]

$$\frac{P}{\rho N^3 d^5} = A \left[\frac{d^2 N \rho}{\eta}\right]^{\beta_1} \left[\frac{d N^2}{g}\right]^{\beta_2} \left[\frac{D}{d}\right]^{\beta_3} \left[\frac{H}{d}\right]^{\beta_4} \left[\frac{L}{d}\right]^{\beta_5} \left[\frac{b}{d}\right]^{\beta_6} \left[\frac{c}{d}\right]^{\beta_7}$$

In the current investigation, (H/d), (L/d) and (c/d) remained constant. Therefore, Eqn. (3.91) becomes

$$\frac{P}{\rho N^3 d^5} = A \left[\frac{d^2 N \rho}{\eta}\right]^{\beta_1} \left[\frac{d N^2}{g}\right]^{\beta_2} \left[\frac{D}{d}\right]^{\beta_3} \left[\frac{b}{d}\right]^{\beta_4}$$

Table A.1: Pertinent Quantities Involved In Fluid Agitation Processes (Newtonian Fluids)

Pertinent Quantities				
Number	Symbol	Description	Units	Dimensions
Independent Variables				
1	d	Impeller diameter	m	L
2	D	Tank diameter	m	L
3	b	Impeller blade height	m	L
4	H	Fluid depth	m	L
5	L	Tank length	m	L
6	N	Impeller Speed	rev/s	T^{-1}
7	ρ	Fluid Density	kg/m^3	ML^{-3}
8	η	Fluid Viscosity	kg/ms	$ML^{-1}T^{-1}$
9	g	Gravitational Acceleration	m/s^2	LT^{-2}
Dependent Variable				
10	P	Power	kgm^2/s^3	ML^2T^{-3}

The fundamental factors affecting the mixing process are the configuration of the system, the behavior of the fluid and the process control variables (rotational speed). The most significant variables that can be manipulated to affect power consumption are rotational speed, N; impeller and tank geometry, (d, D, b); and fluid properties, ρ and η (Temperature dependency is built in ρ and η. Therefore, temperature was not included as one of the pertinent quantities for the analysis).

A.1 Development of Dimensionless Functions for Power-Law Fluids (Used in Slope method)

When agitating non-Newtonian (power-law fluids), the viscosity η is replaced by the flow behavior index, n, and the fluid consistency coefficient, m (kg s^{n-2}/m). Thus, the power requirement is a function of

$$P = f(d, N, \rho, m, n)$$

$$0 = C\, P^{\beta_1}\, d^{\beta_2}\, N^{\beta_3}\, \rho^{\beta_4}\, m^{\beta_5} \quad \text{(n is dimensionless and enters in m)}$$

$$0 = (ML^2/T^3)^{\beta_1}\, L^{\beta_2}\, T^{-\beta_3}\, (M/L^3)^{\beta_4}\, (MT^{n-2}/L)^{\beta_5}$$

$$\text{L:} \quad 2\beta_1 + \beta_2 - 3\beta_4 - \beta_5 = 0$$

$$\text{T:} \quad -3\beta_1 - \beta_3 + (n-2)\beta_5 = 0$$

$$\text{M:} \quad \beta_1 + \beta_4 + \beta_5 = 0$$

Let $\beta_1 = \beta_4 = 0$. Then, $\beta_5 = -1$

$$\beta_2 = -3$$

$$\beta_3 = -n-1$$

$$\pi_1 = \frac{P}{m\, d^3\, N^{n+1}}$$

Let $\beta_1 = 0$ and $\beta_4 = 1$. Then, $\beta_5 = -1$

$$\beta_3 = -n-2$$

$$\beta_2 = 2$$

$$\pi_2 = \frac{\rho\, d^2 N^{2-n}}{m}$$

And $\pi_3 = n$; $\pi_4 = d/D$; $\pi_5 = d/b$, etc...

APPENDIX B

EXPERIMENTAL RESULTS

APPENDIX B

EXPERIMENTAL RESULTS

Table B.1: Regression Results of $P_o = \alpha_0 (R_e)^{\alpha_1} (Fr)^{\alpha_2}$ (Paddle Impellers)

Linear Multiple Regression Analysis

Regression Coefficient	Estimated Regression Coefficient	Estimated Standard Error	t^*
$\log \alpha_0$	88.299	--	--
α_1	-0.976	0.023	-43.53
α_2	-0.023	0.023	-1.08

Analysis of Variance

	Sum of Squares	Degrees of Freedom	Error Mean Squares	F^*
Regression	48.346	2	24.173	--
Residual	0.585	312	0.022	1115.37
Total	48.931	314		

$$R^2 = 0.988$$

Test of hypothesis for α_2 : C_1: $\alpha_2 = 0$
C_2: $\alpha_2 \neq 0$

For a level of significance of 0.05, $t(0.975,\infty) = 1.960$

Since $t^* = 1.08 < t(0.975,\infty)$, we accept C_1 and conclude that $\alpha_2 = 0$

Table B.2: Regression Results of $P_o = \beta_0 (R_e)^{\beta_1} (Fr)^{\beta_2}$ (Flag Impeller)

Linear Multiple Regression Analysis

Regression Coefficient	Estimated Regression Coefficient	Estimated Standard Error	t^*
$\log \beta_0$	12.567	--	--
β_1	-0.983	0.045	-20.07
β_2	-0.056	0.045	-1.87

Analysis of Variance

	Sum of Squares	Degrees of Freedom	Error Mean Squares	F^*
Regression	61.373	2	30.669	--
Residual	2.015	87	0.032	958.66
Total	63.388	90		

$$R^2 = 0.968$$

Test of hypothesis for β_2 : C_1: $\beta_2 = 0$
C_2: $\beta_2 \neq 0$

For a level of significance of 0.05, $t(0.975,87) = 1.990$

Since $t^* = 1.87 < t(0.975,87)$, we accept C_1 and conclude that $\beta_2 = 0$

Table B.3: Values of β_1, β_2 and β_3 from $k' = \beta_1 (d/b)^{\beta_2} + \beta_3$ (Matching Method of Power Curves) For Power-Law Fluids

FLUID	β_1	β_2	β_3	R^2
1	5.029	2.618	10.159	0.985
2	5.898	1.764	7.734	1.000
3	4.137	1.459	7.179	0.971

Fluid 1: Hydroxypropyl Methylcellulose 1% (n=0.504, m=6.49 Pa s^n)

Fluid 2: Hydroxypropyl Methylcellulose 1.5% (n=0.374, m=28.42 Pa s^n)

Fluid 3: Hydroxypropyl Methylcellulose 2% (n=0.352, m=59.27 Pa s^n)

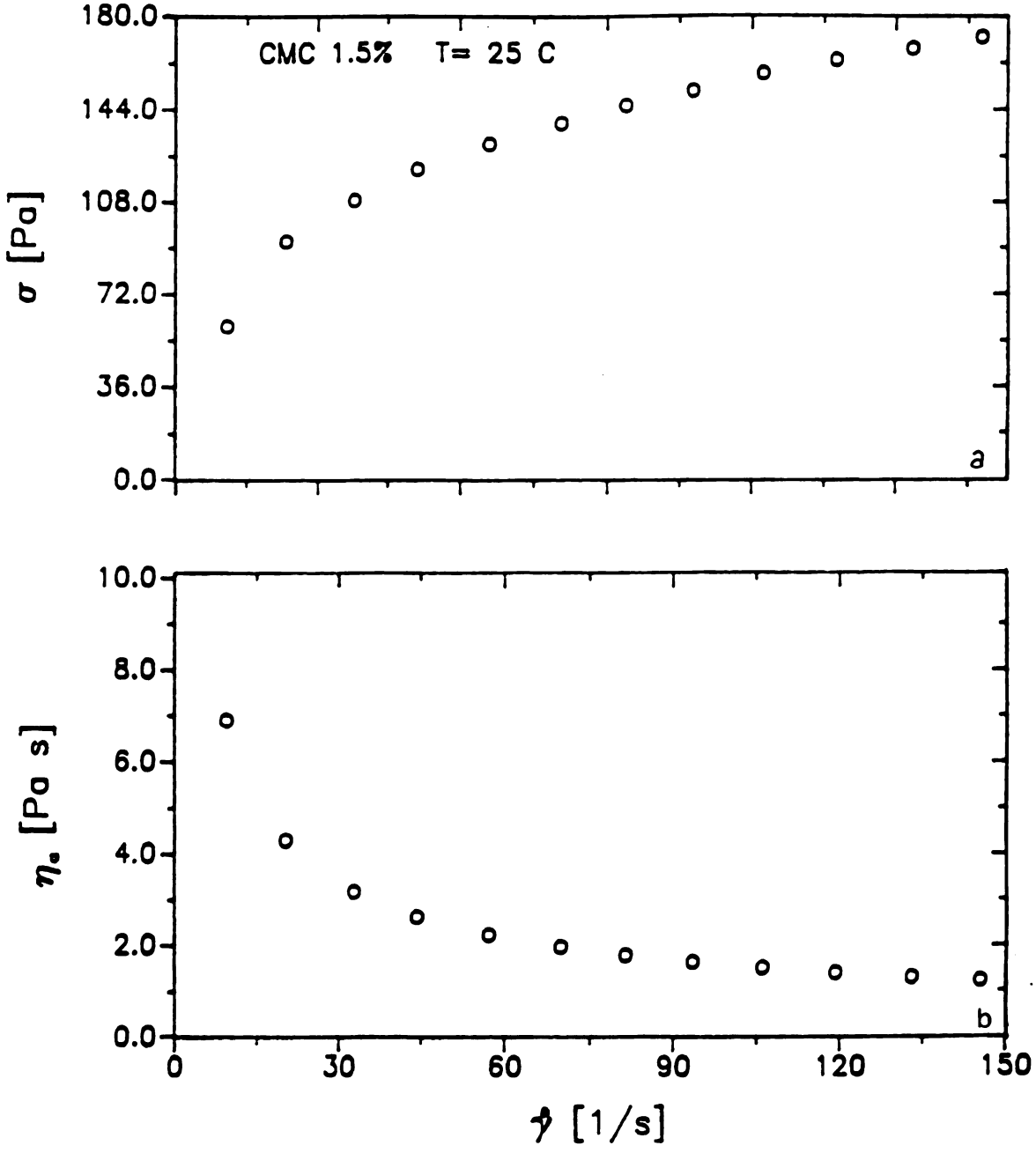

Figure B.1: a) Shear Stress Versus Shear Rate; b) Apparent Viscosity Versus Shear Rate (Hydroxypropyl Methylcellulose 1.5%)

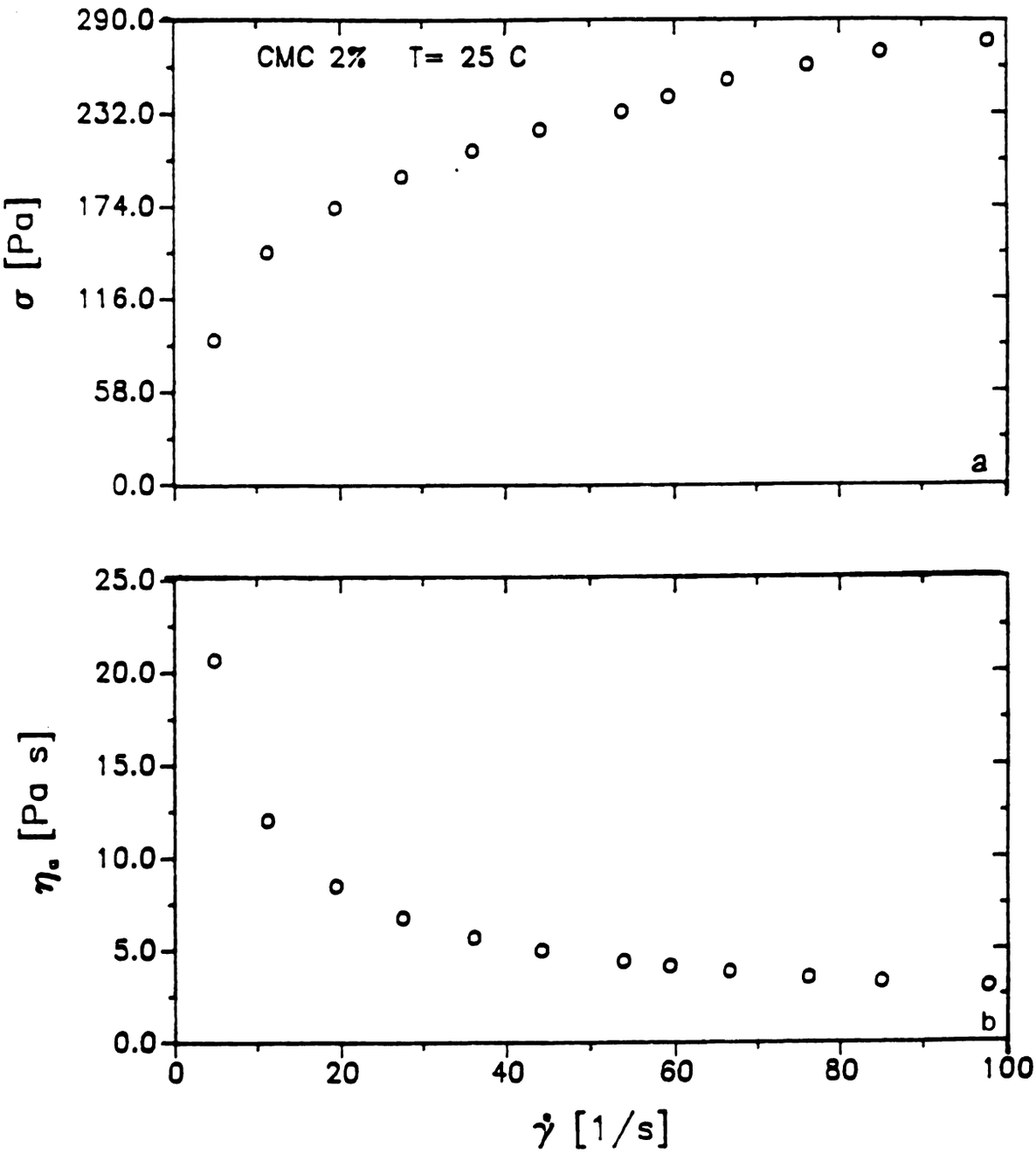

Figure B.2: a) Shear Stress Versus Shear Rate; b) Apparent Viscosity Versus Shear Rate (Hydroxypropyl Methylcellulose 2%)

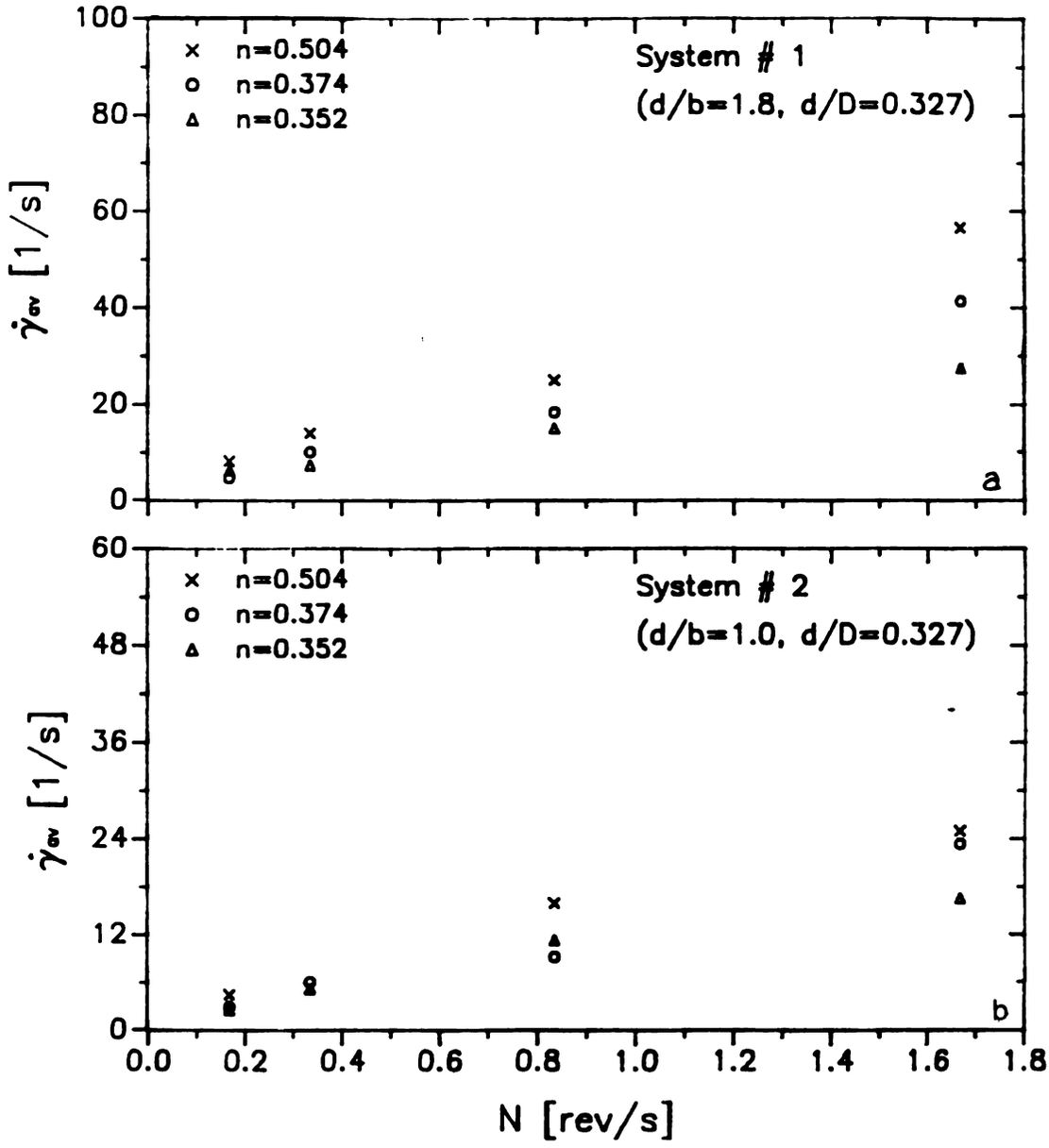

Figure B.3: Average Mixing Shear Rate as a Function of Rotational Speed of the Paddle Impellers. a) System 1; b) System 2 (Torque Curves - Matching Method)

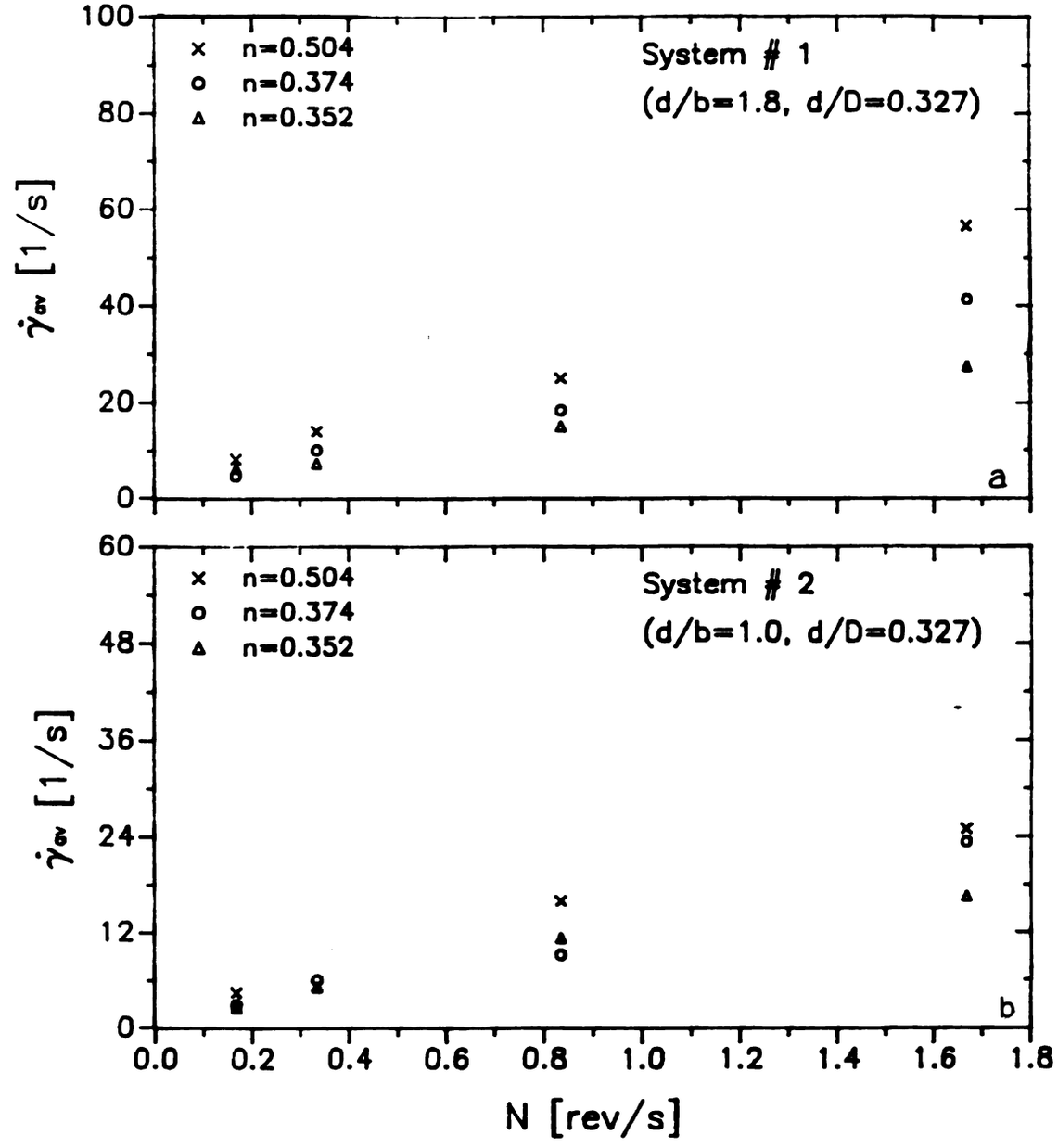

Figure B.3: Average Mixing Shear Rate as a Function of Rotational Speed of the Paddle Impellers. a) System 1; b) System 2 (Torque Curves - Matching Method)

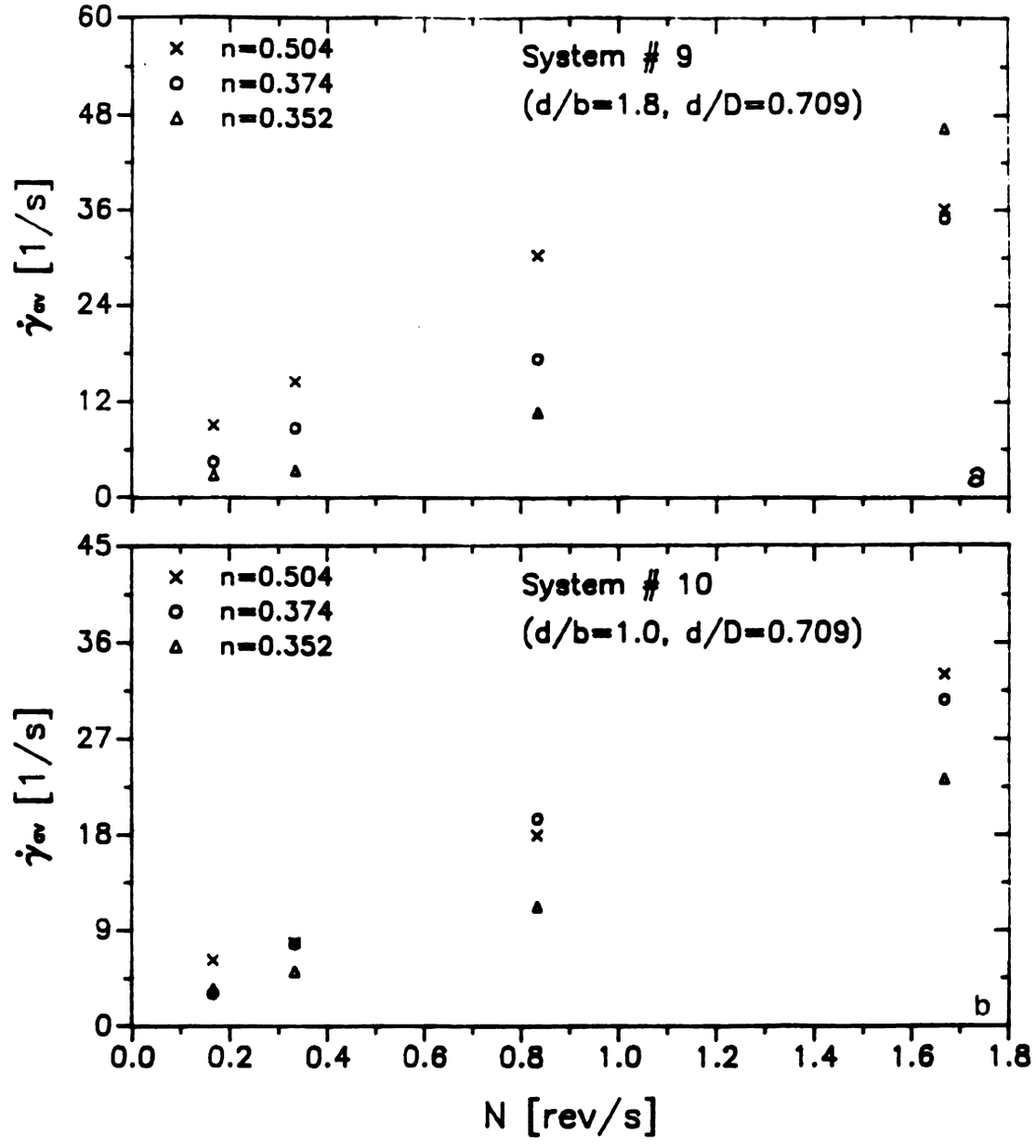

Figure B.4: Average Mixing Shear Rate as a Function of Rotational Speed of the Paddle Impellers. a) System 9; b) System 10 (Torque Curves - Matching Method)

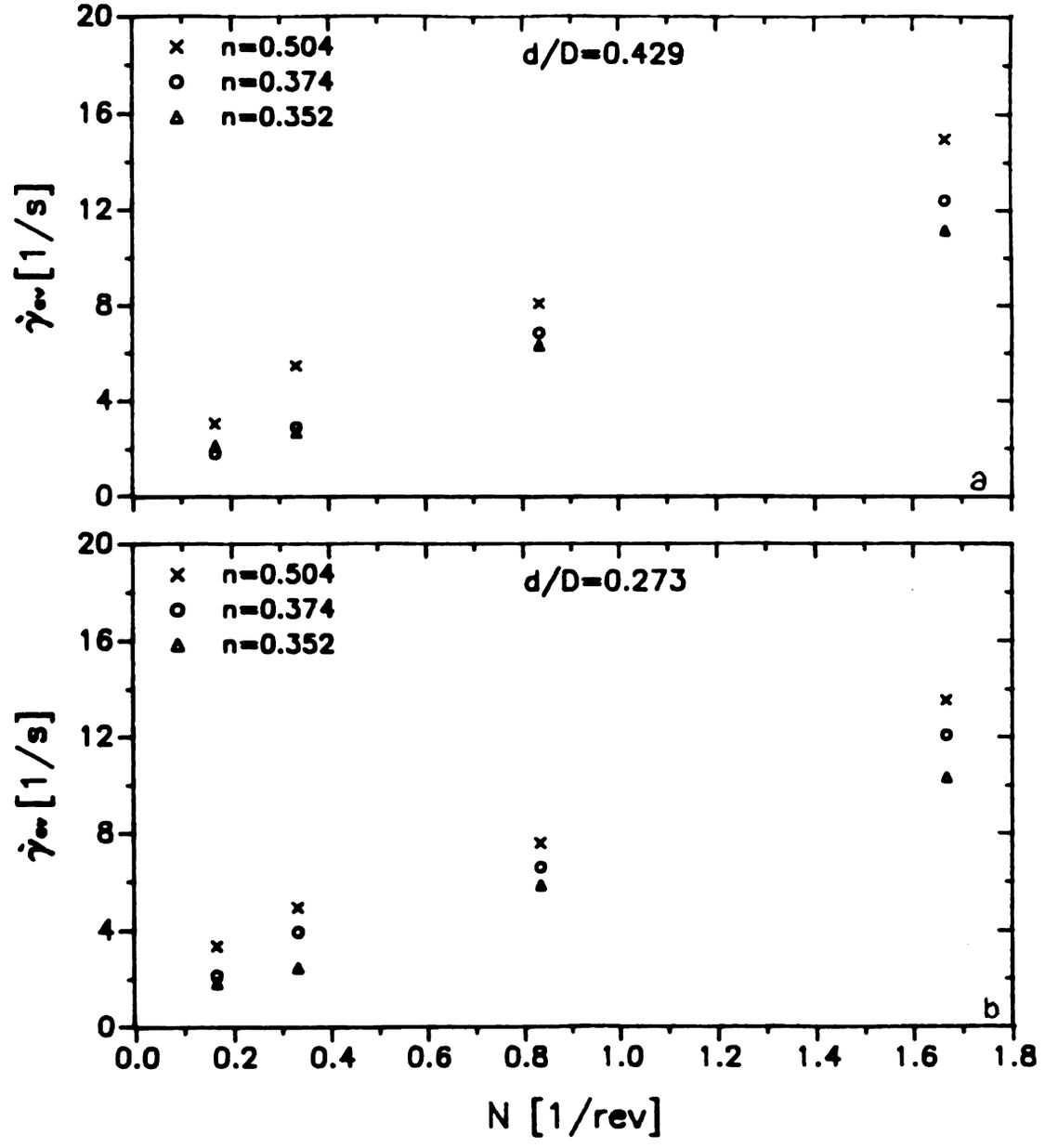

Figure B.5: Average Mixing Shear Rate as a Function of Rotational Speed of the Flag Impeller. a) System 2; b) System 1 (Torque Curves - Matching Method)

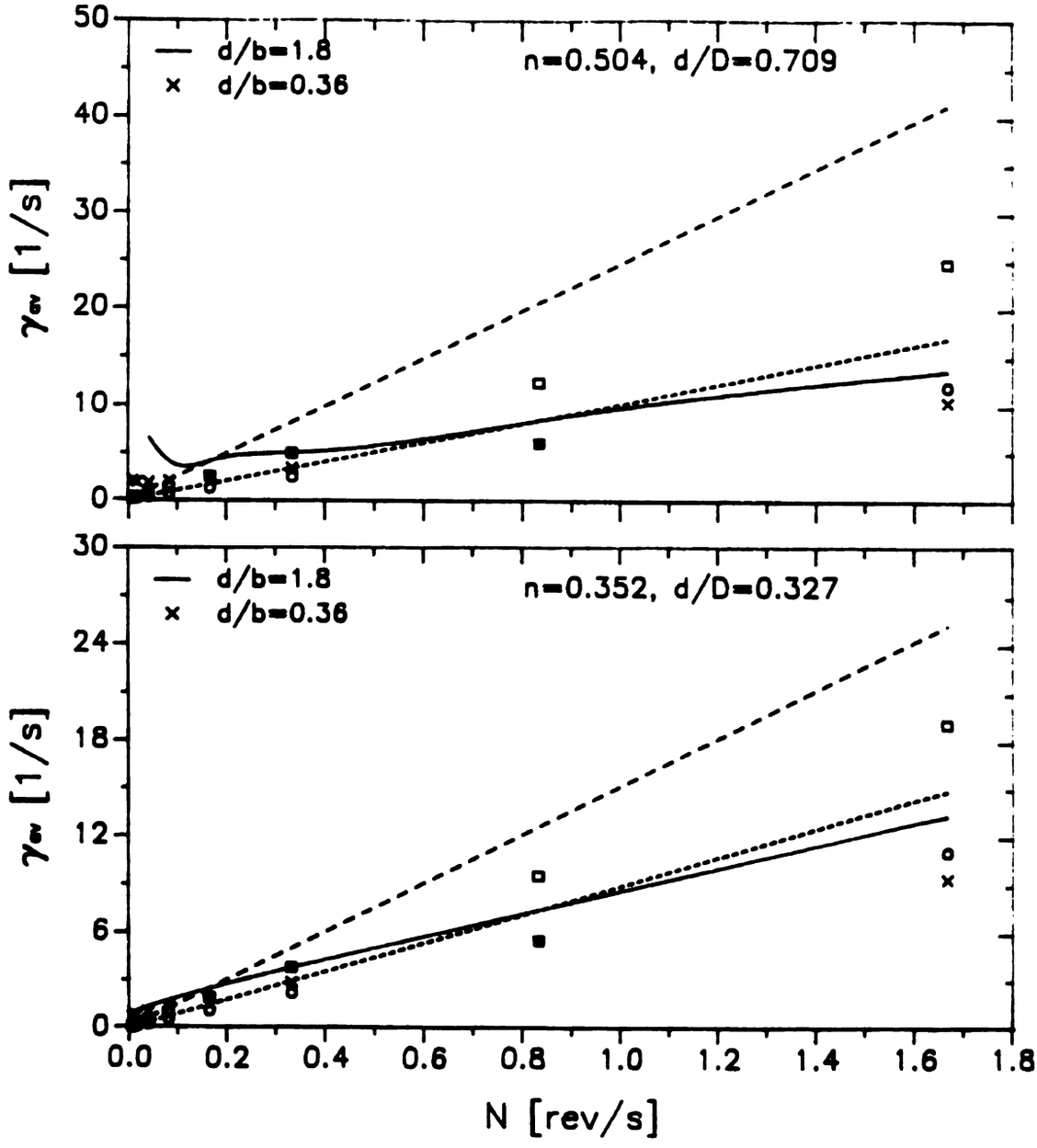

Figure B.6: Average Shear Rate as a Function of Impeller Rotational Speed for Two Paddle Impellers (Torque Curves - Matching Method)

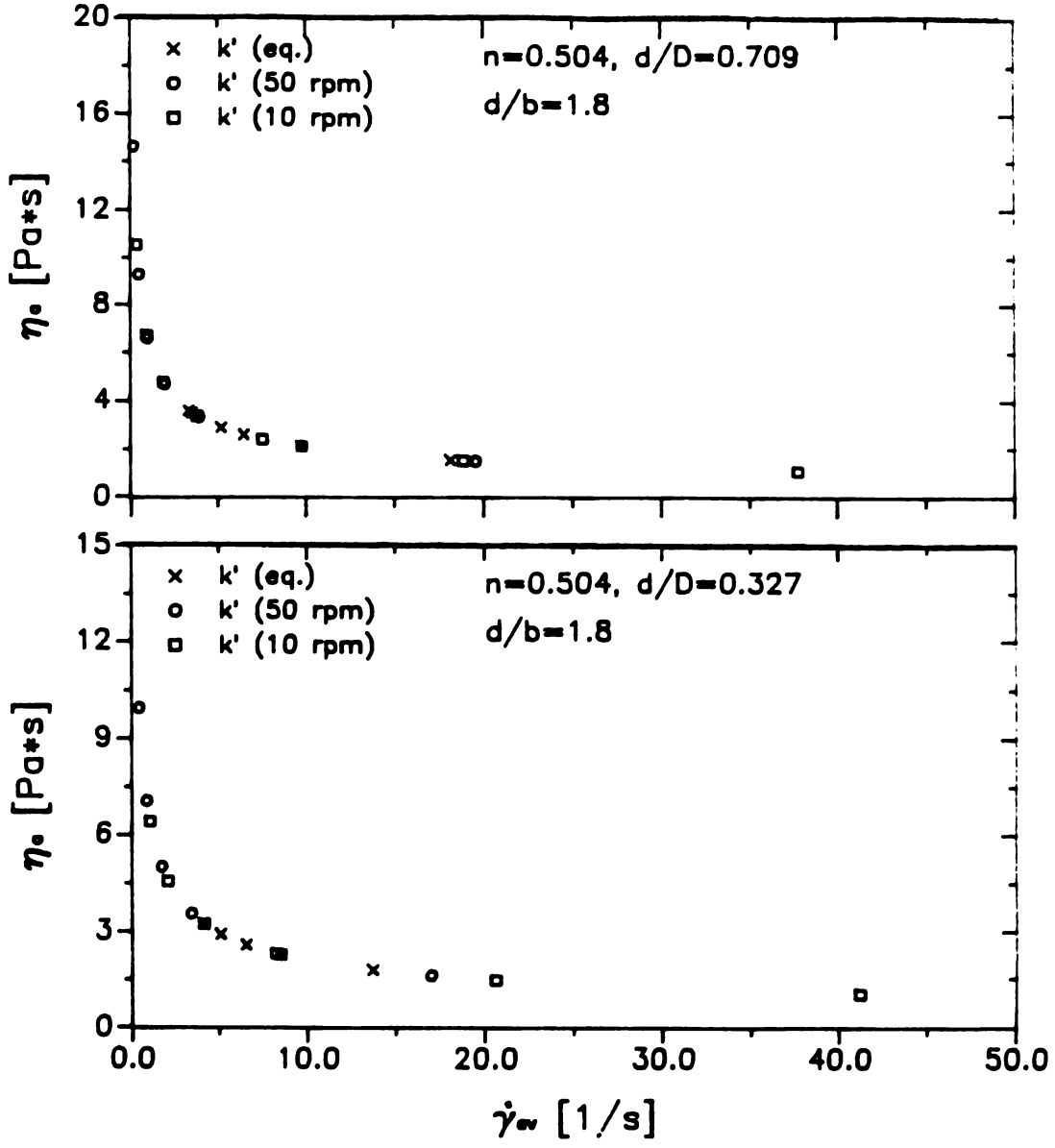

Figure B.7: Apparent Viscosity as a Function of Average Shear Rate for a Paddle Impeller (CMC 1%) (Torque Curves - Matching Method)

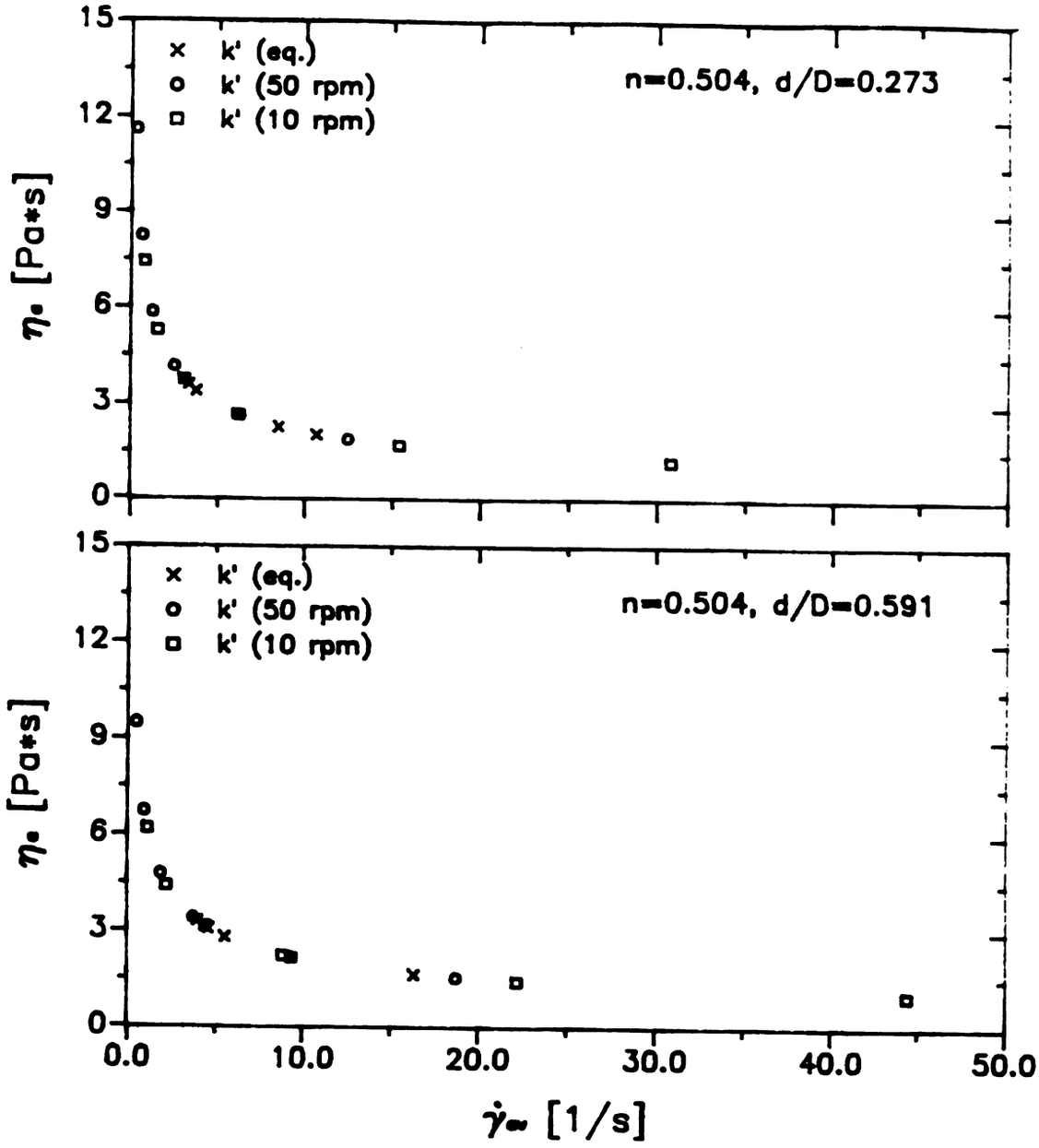

Figure B.8: Apparent Viscosity as a Function of Average Shear Rate For a Flag Impeller (CMC 1%) (Torque Curves - Matching Method)

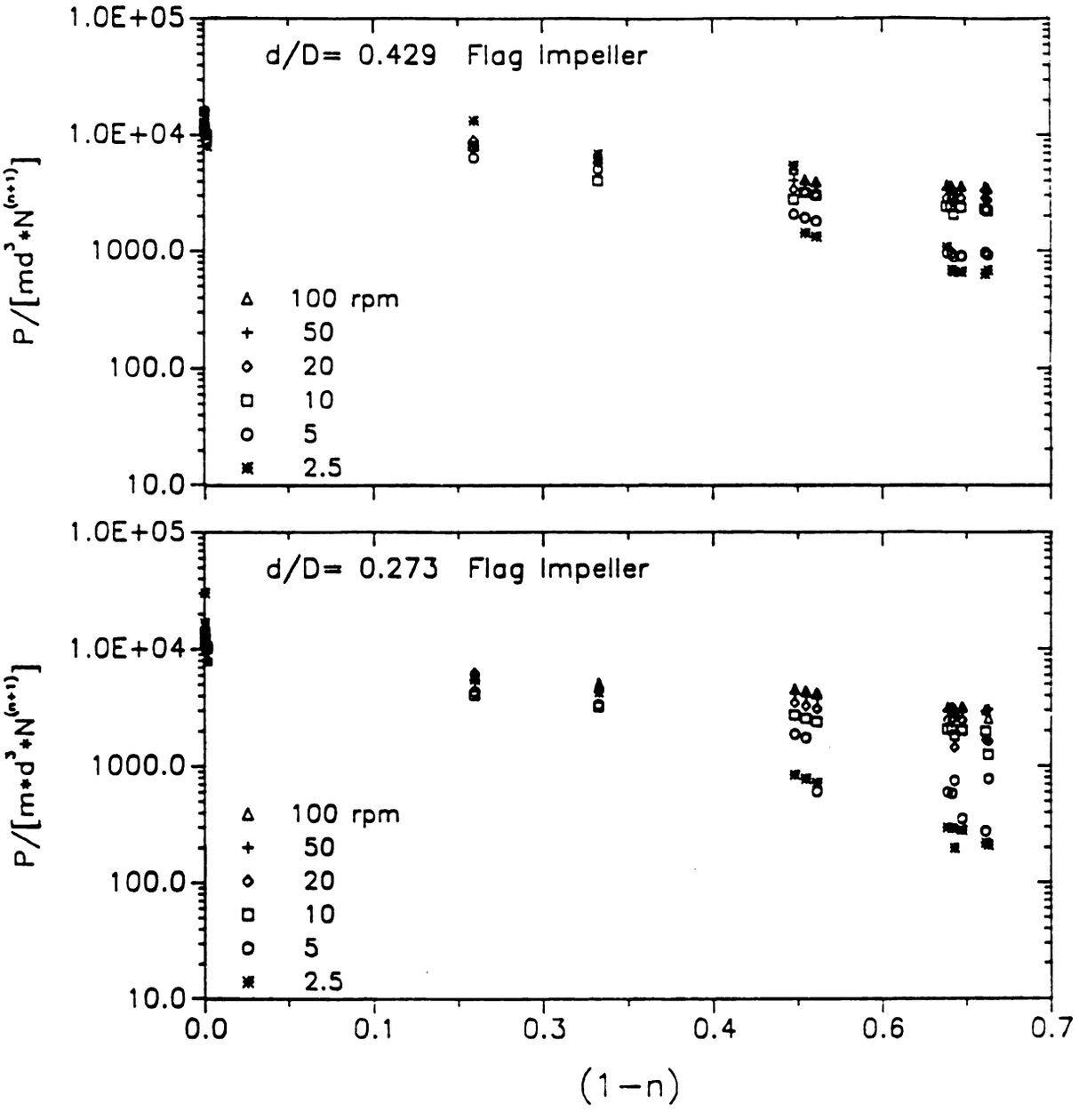

Figure B.9: Plots of Dimensionless Functions $[P/(md^3N^{n+1})]$ Versus (1-n) For The Flag Impeller (Slope Method)

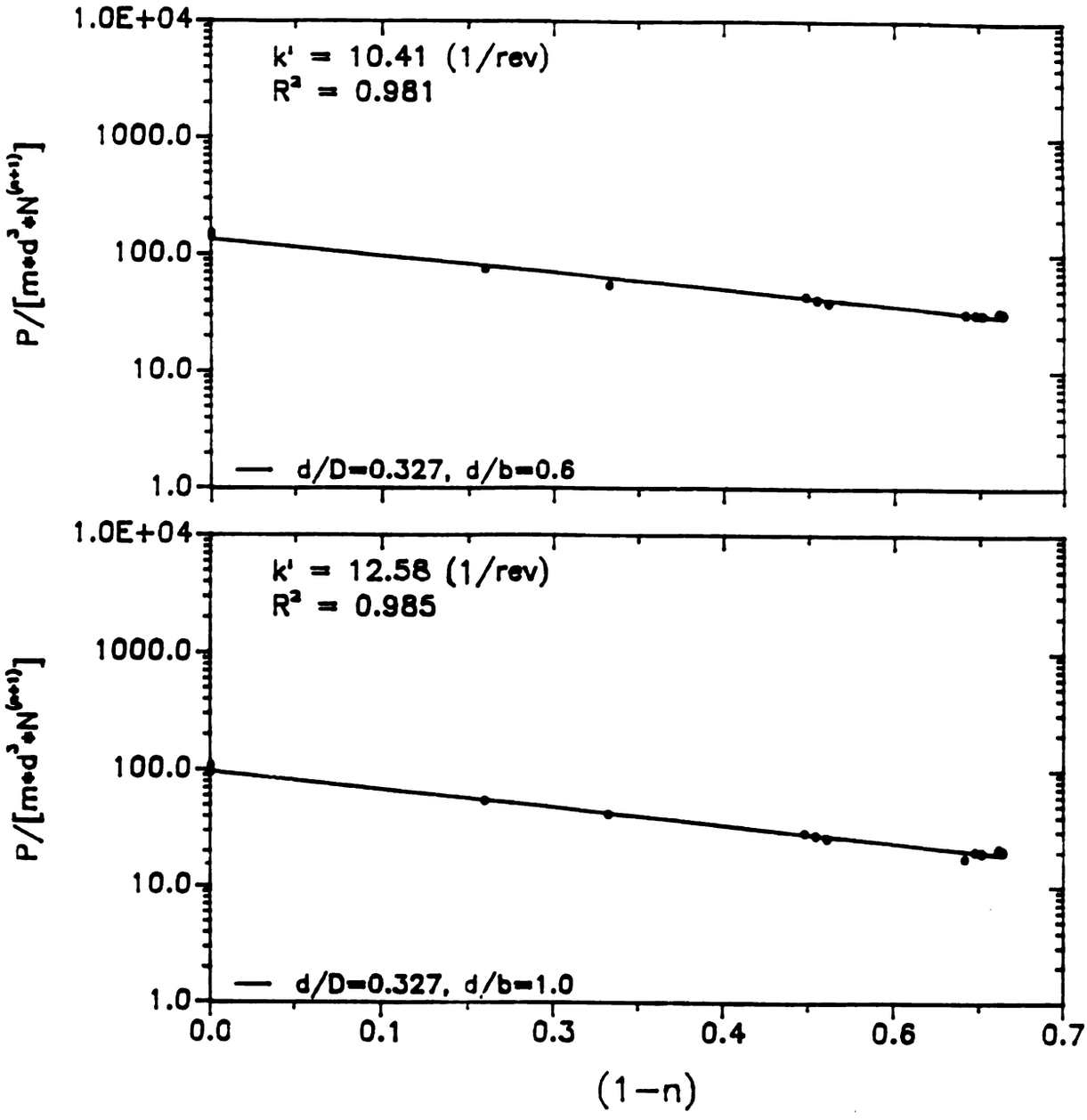

Figure B.10: Plots of Dimensionless Functions $[P/(md^3N^{n+1})]$ Versus (1-n) For The Paddle Impellers (Slope Method)

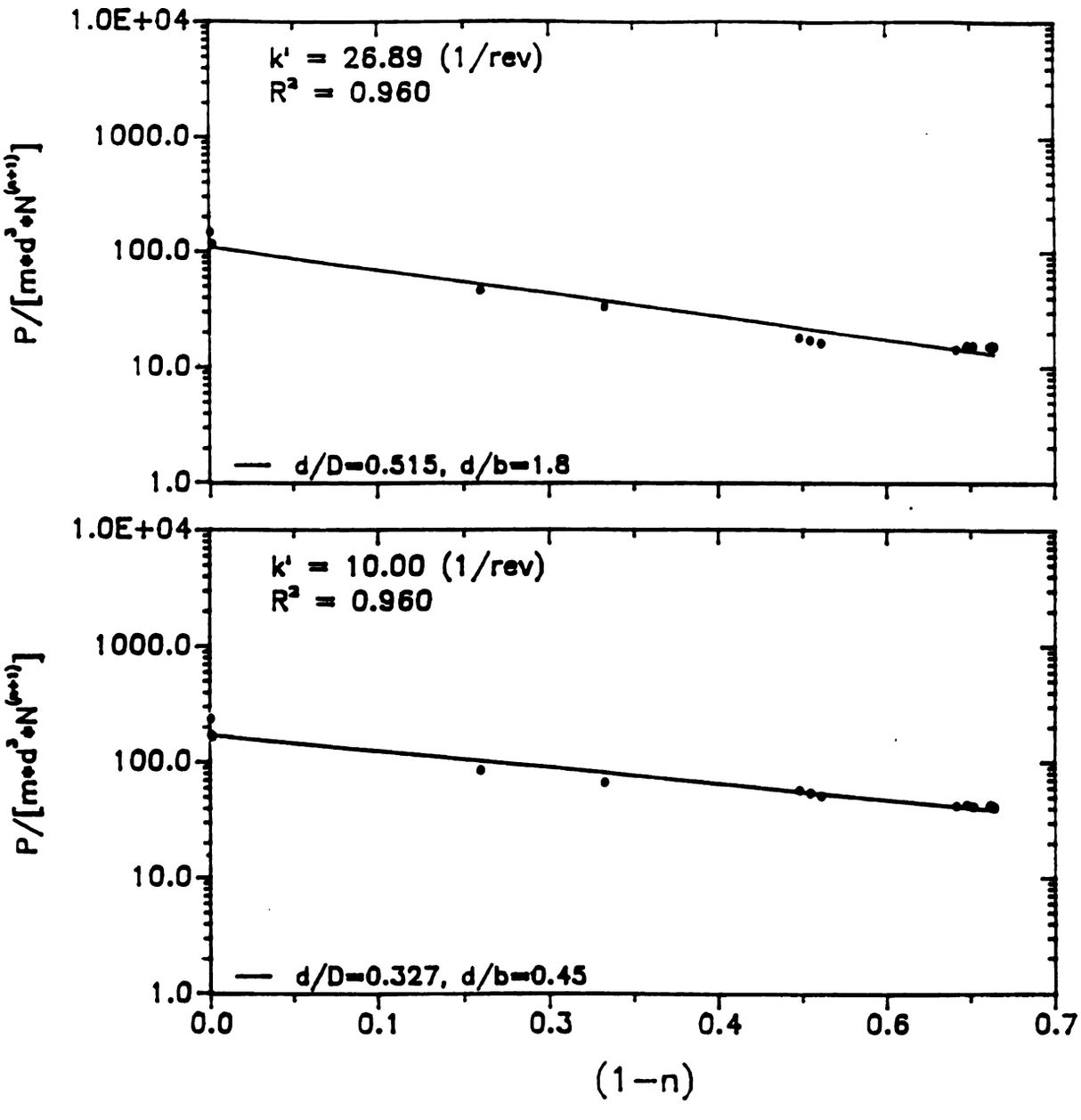

Figure B.11: Plots of Dimensionless Functions $[P/(md^3N^{n+1})]$ Versus (1-n) For The Paddle Impellers (Slope Method)

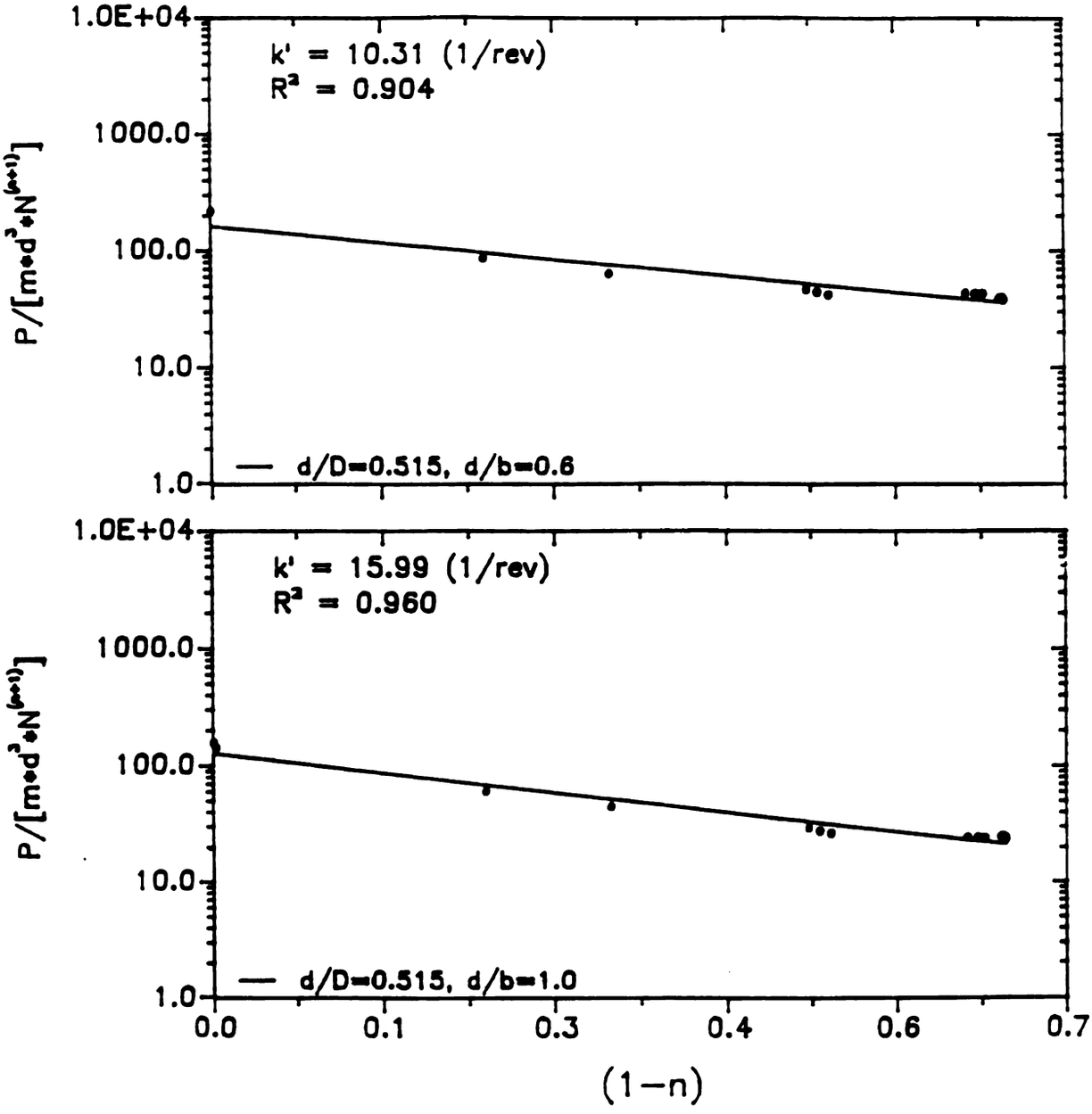

Figure B.12: Plots of Dimensionless Functions $[P/(md^3N^{n+1})]$ Versus (1-n) For The Paddle Impellers (Slope Method)

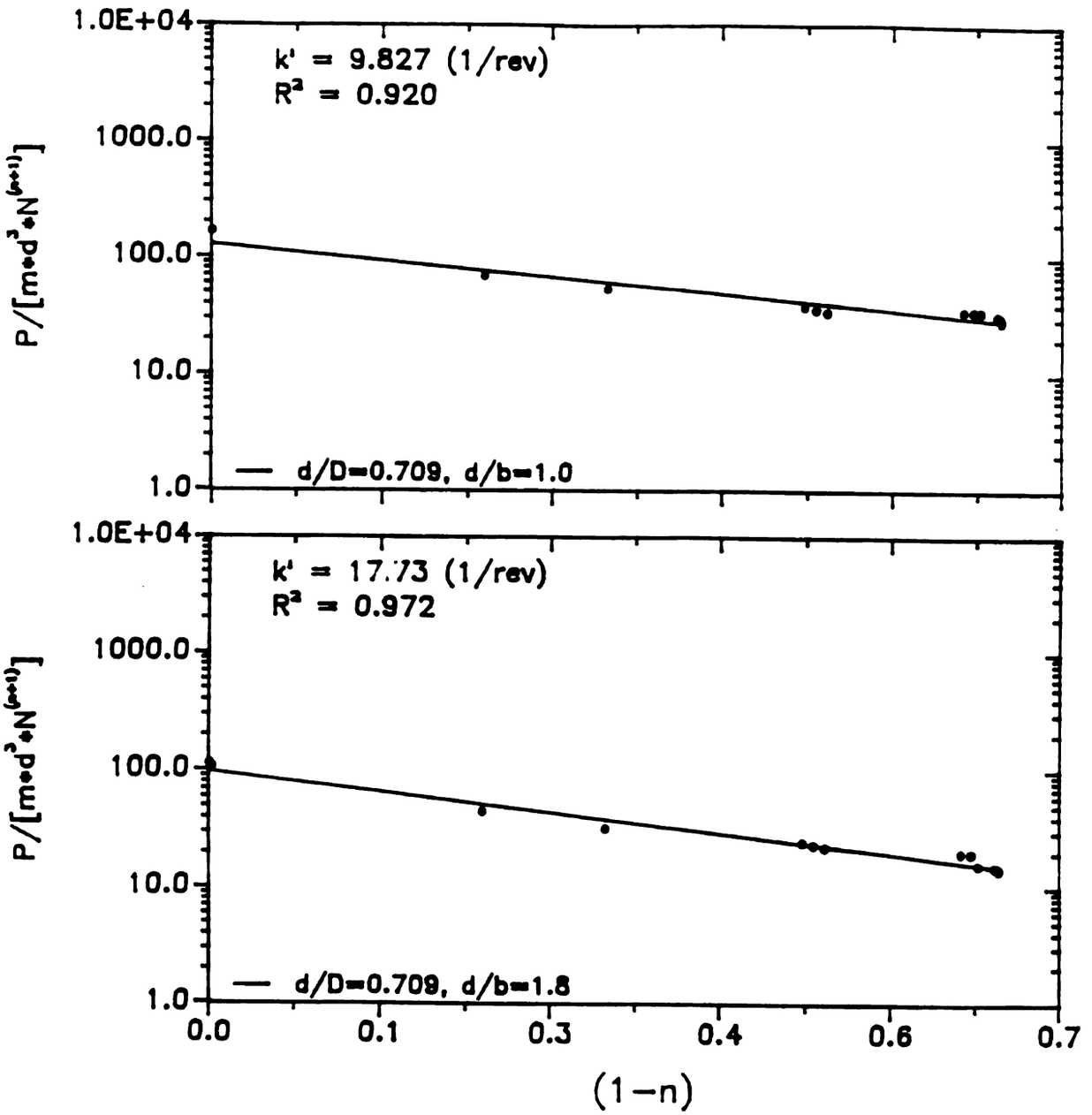

Figure B.13: Plots of Dimensionless Functions $[P/(md^3N^{n+1})]$ Versus (1-n) For The Paddle Impellers (Slope Method)

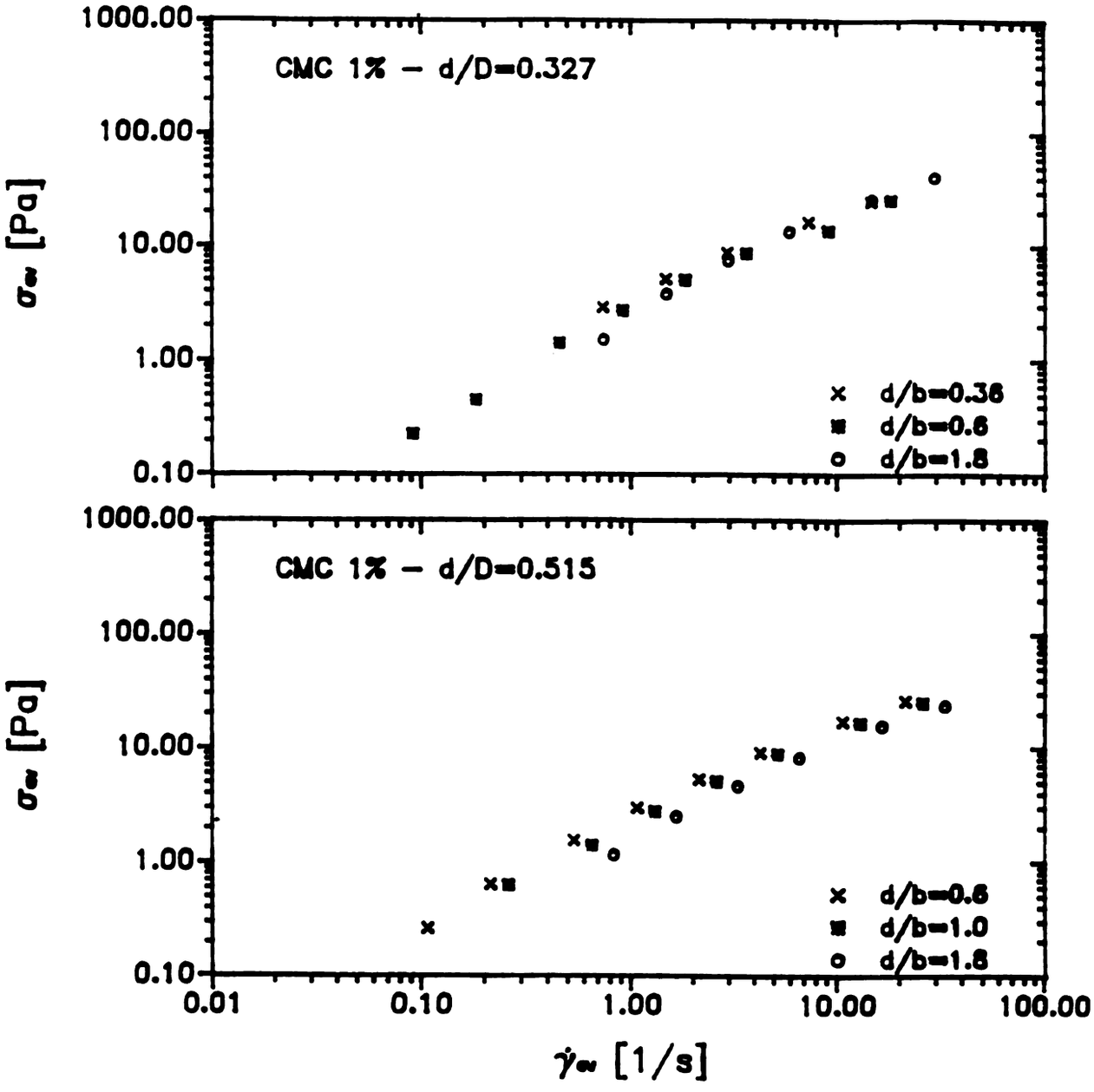

Figure B.14: Flow Curve For 1% wt% Aqueous Solution of CMC Determined Using the Mixer Viscometer with the Paddle Impellers

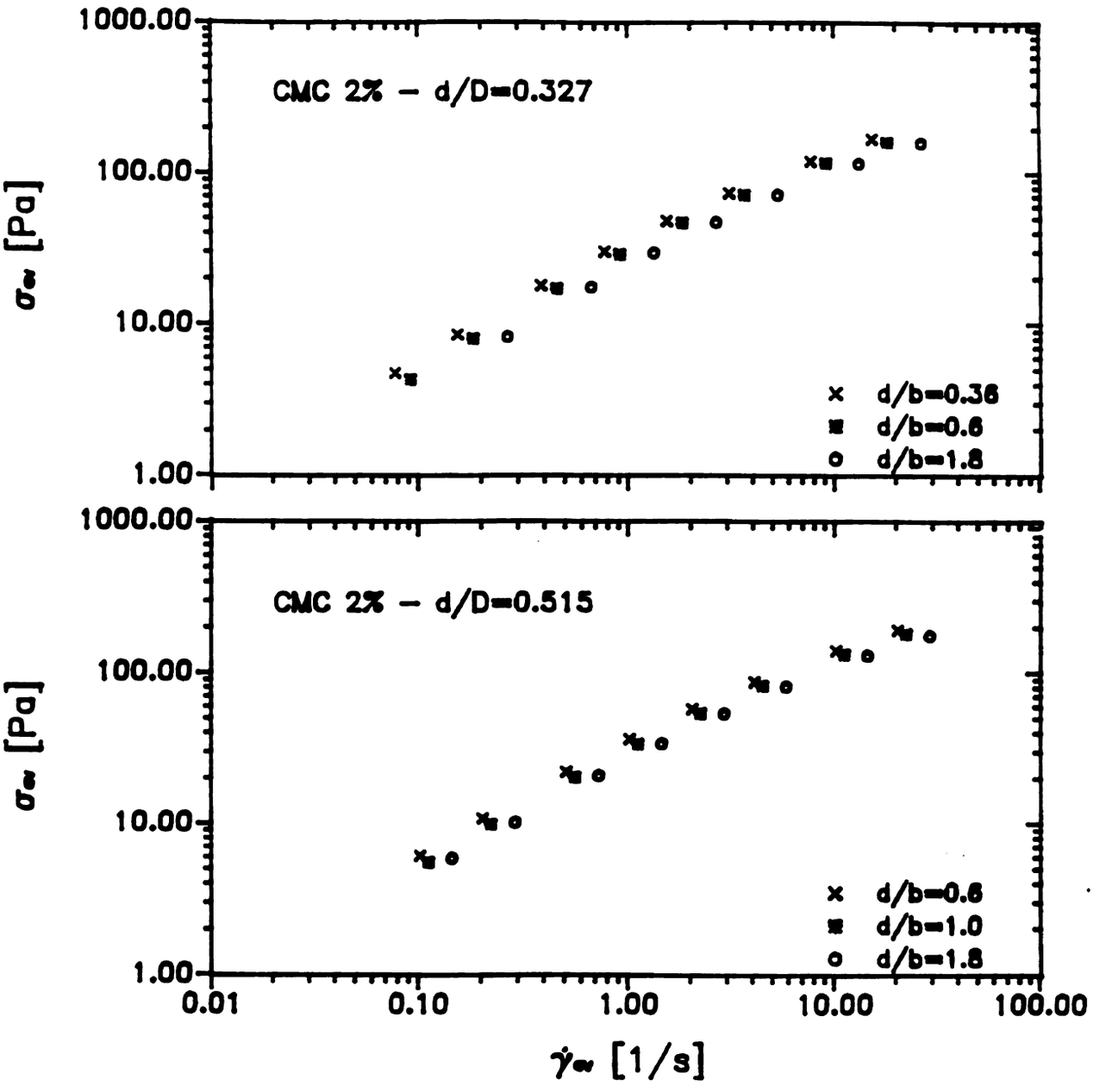

Figure B.15: Flow Curve For 2% wt% Aqueous Solution of CMC Determined Using the Mixer Viscometer with the Paddle Impellers

APPENDIX C

APPENDIX C

PROCEDURE FOR USE OF THE MIXER BROOKFIELD VISCOMETER FOR NEWTONIAN FLUIDS

This section provides the user of Brookfield Viscometers with the information required to obtain viscosity readings with the "mixer impellers" (flag and paddle type). This information consists of the impeller "factors" and viscosity ranges for use of the impeller/cup combinations with a Brookfield Viscometer. These factors are equivalent to the Factor Finder supplied with the Viscometer for other spindle geometries.

C.1) Determination of Impeller Factors

Brookfield Viscometers use a Factor for every spindle/speed combination the user selects. It is simply multiplied by the Viscometer reading to evaluate viscosity (in centipoise).

Table C.1 presents the values of the Factors for the flag and paddle impellers for evaluation of the viscosity of Newtonian fluids. The recommended range of viscosity for the Viscometer model is also shown to assure proper use of the equipment.

The procedure for data collection and analysis was:

1. The torque required to rotate the impeller, at each value of rotational speed for several Newtonian fluids of known viscosity at constant temperature, was measured.

Table C.1: Factors for Use of the Mixer Impellers with the Brookfield Viscometer

Paddle Impellers

SYSTEM	FACTOR VISCOMETER MODEL HBTD	FACTOR VISCOMETER MODEL RVTD	VISCOSITY RANGE (Pa s) Min - Max HBTD	VISCOSITY RANGE (Pa s) Min - Max RVTD
1	45.1/N	5.7/N	4.51 - 451	0.57 - 57
2	33.8/N	4.2/N	3.38 - 338	0.42 - 42
3	22.7/N	2.8/N	2.70 - 227	0.28 - 28
4	19.0/N	2.3/N	1.90 - 190	0.23 - 23
5	15.5/N	2.0/N	1.50 - 150	0.20 - 20
6	45.0/N	5.0/N	4.50 - 450	0.50 - 50
7	29.0/N	3.3/N	2.90 - 290	0.33 - 33
8	21.0/N	2.3/N	2.10 - 210	0.23 - 23
9	34.0/N	4.1/N	3.40 - 340	0.41 - 41
10	22.5/N	2.8/N	2.25 - 225	0.28 - 28

Flag Impeller

1	55.0/N	6.5/N	5.50 - 550	0.65 - 65
2	55.0/N	6.6/N	5.50 - 550	0.66 - 66
3	42.5/N	5.3/N	42.5 - 425	0.53 - 53

N in rpm
Recommended RPM = 10 - 100

1 Pa s = 10^3 cp

Viscosity ranges (in Pa s):
Maximum: Factor x 100
Minimum: Factor x 10

2. Plots of Newtonian viscosity, η, versus torque, M, for each value of rotational speed, N and each system geometry (impeller/cup combination) were made. Figure C.1b is a typical plot for a selected impeller/cup combination. 3. A relationship between Newtonian viscosity, η, and torque reading, was found to be of the form:

$$\eta = C_1 M \qquad (C.1)$$

where:

C_1 = constant, s/m^3

M = torque reading, N m

4. The proportionality constant, C_1, was plotted as a function of N for each system geometry as in Figure C.1a.
5. From Eqn. (C.1) and the plot of (4), the following expression for the Newtonian viscosity was obtained for the different systems (Table C.2):

$$\eta = B_1 (N/60)^{B_2} M \qquad (C.2)$$

with N = impeller rotational speed, rpm

B_1 = constant, $1/m^3$

B_2 = constant, -n

Thus, the Newtonian viscosity, η, can be calculated from the following equation:

$$\eta = \text{FACTOR} * \text{Torque} \qquad (C.3)$$

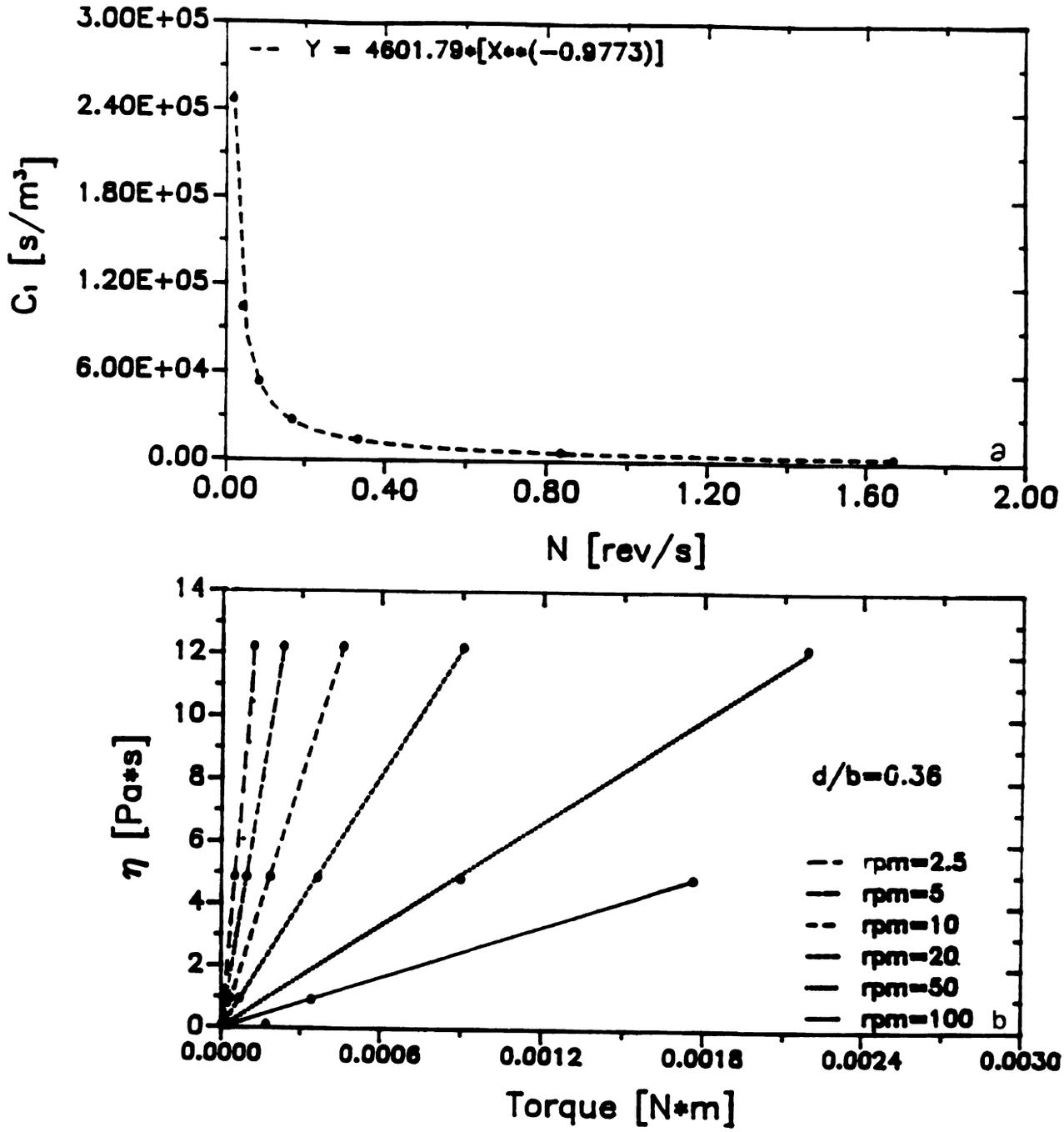

Figure C.1: a) Plot of C_1 Versus Impeller Rotational Speed; b) Plot of η Versus Torque Reading (Paddle Impeller, d/b=0.45)

Table C.2: Table for the fit of Eqn. (C.2)

Paddle Impellers

SYSTEM	B_1	B_2	R^2
1	131.6462	-0.9541	0.999
2	97.2958	-0.9827	1.000
3	65.1144	-0.9753	1.000
4	54.3087	-0.9750	1.000
5	46.0179	-0.9773	1.000
6	139.0464	-0.8527	0.990
7	92.6439	-0.9134	0.989
8	61.7416	-0.9388	0.995
9	99.0534	-0.9771	1.000
10	65.6778	-0.9905	1.000

Flag Impeller

1	162.9035	-0.9816	1.000
2	158.2457	-0.9755	1.000
3	124.8972	-0.9973	1.000

with FACTOR = $B_1(N/60)^{B_2}$

Factors were converted to constants for use with the Brookfield display readings as follows:

$$[\text{FACTOR} \times \text{spring constant (Nm)} \times 10^{-9}] \times N = \text{FACTOR}_2 \quad (C.3)$$

$$\text{with FACTOR} = \frac{\text{FACTOR}_2}{N} \quad (C.4)$$

Table C.2 shows average values for every system (at all values of N).

The mixer impeller Factors for every impeller/cup combination presented in Table C.2 allow the user for direct determination of viscosity readings. Torque readings were converted to Viscometer display readings to facilitate the procedure.

Table C.3 shows the values of viscosity obtained with the different impeller/cup combinations at two selected values of N (10 and 50 rpm). It may be seen that the maximum error obtained is about 10% which indicates that the prediction factors provide accurate estimation of the Newtonian viscosity.

C.2) Procedure For Determination Of Newtonian Viscosity

The following procedure is a useful tool for analysis of viscosity data of food products of unknown behavior. It is also a starting point from which more advanced techniques can be explored.

The procedure for determination of Newtonian viscosity with the Mixer Brookfield Viscometer is as follows:

Table C.3: Values of Viscosity of a Newtonian Fluid (η = 4.84 Pa s) Obtained with The Impeller Factors

Paddle Impellers

SYSTEM	N (rpm)	η (Pa s) HBTD	RVTD	% Error	
1	10	4.71	4.76	-2.7	-1.7
	50	4.50	4.55	-7.0	-6.0
2	10	5.00	4.98	3.3	2.9
	50	4.75	4.72	-1.9	-2.5
3	10	4.68	4.62	-3.3	-4.5
	50	4.66	4.60	-3.7	-4.9
4	10	4.99	4.84	3.0	0.0
	50	4.93	-- *	1.9	--
5	10	4.95	5.11	2.3	5.6
	50	4.84	--	0.0	--
6	10	5.25	4.67	8.5	-3.5
	50	4.66	4.79	-3.7	-1.0
7	10	4.79	4.95	-1.0	2.3
	50	4.53	4.66	-6.4	-3.7
8	10	5.29	4.99	9.3	3.1
	50	4.96	--	2.5	--
9	10	4.85	4.67	0.2	-3.5
	50	4.70	4.55	-2.3	-5.9
10	10	4.95	4.93	2.3	1.9
	50	4.91	4.89	1.4	1.0

Flag Impeller

1	10	4.60	4.55	-4.9	-5.9
	50	4.56	4.49	-5.7	-7.2
2	10	5.11	5.21	5.6	7.6
	50	4.85	5.04	0.2	4.1
3	10	4.61	4.62	-4.7	-4.5
	50	4.51	4.51	-6.8	-6.8

* Reading out of range of viscometer

1. Determine if the fluid is Newtonian. To do so, record display reading with impeller rotating at different values of rotational speed. A plot of the reading values as a function of N should give a straight line with slope equal to 1.
2. Select impeller/cup combination and value of rotational speed according to standard Brookfield procedure. Generally, a reading display of 10 or higher assures that proper selection of equipment has been made.
2. Read digital display from Viscometer.
3. Find FACTOR for selected system and N in Table C.1.
4. To obtain viscosity readings (Pa s), multiply Brookfield reading by the Factor at specified value of rotational speed (in rpm) from step (2).

REFERENCES

REFERENCES

Beavers, G.S., Yoo, J.Y. and Joseph, D.D. 1980. The free surface on a liquid between cylinders rotating at different speeds. Part III. Rheol. Acta 19, 19-31.

Beckner, J.L. and Smith, J.M. 1966. Anchor-agitated systems: power input with Newtonian and pseudoplastic fluids. Trans. Instn. Chem. Engrs. 44, T224-T235.

Begachev, V.I., Gurvich, A.R. and Braginski, L.N. 1980. A generalized method of power calculation in mixing highly viscous Newtonian and non-Newtonian media. Theor. Found. Chem. Engng. 14(1), 98-104.

Bertrand, J. and Courdec, J.P. 1988. Numerical and experimental study of flow induced by an anchor in viscous, Newtonian and pseudoplastic fluids. Int. Chem. Engng. 28(2), 257-270.

Bird, R.B., Stewart, W.E. and Lightfoot, E.D. 1960. Transport Phenomena. John Wiley & Sons Inc.

Blasinski, H. and Rzyski, E. 1976. Mixing of non-Newtonian fluids with turbine, propeller and paddle agitator. Int. Chem. Engng. 16(4), 751-754.

Blasinski, H., Kochanski, B. and Rzyski, E. 1970. The Froude number in the mixing process. Int. Chem. Engng. 10(2), 176-179.

Boger, D.V. 1977/1978. A highly elastic constant-viscosity fluid. J. Non-Newt. Fluid Mech. 3, 87-91.

Bohme, G., Vo , R. and Warnecke, W. 1985. Die freie oberflache einer flussigkeit uber einer rotierenden scheibe. Rheol. Acta 24, 22-33.

Bongenaar, J.J.T.M., Kossen, N.W.F., Metz, B. and Meijboom, F.W. 1973. A method for characterizing the rheological properties of viscous fermentation broths. Biotech. Bioengng. 15, 201-206.

Bourne, J.R. 1965. Brit. J. Appl. Phys. 16, 1411.

Bourne, J.R. and Butler, H. 1969. Power consumption of helical ribbon impellers in viscous liquids. Trans. Instn. Chem. Engrs. 47, T263-T270.

Bourne, J.R., Buerli, M. and Renegass, W. 1981. Power and heat transfer to agitated suspensions: Use of heat flow calorimetry. Chem. Engng. Sci. 36, 782-784.

Calderbank, P.H. and Moo-Young, M.B. 1959. The prediction of power consumption in the agitation of non-Newtonian fluids. Trans. Instn. Chem. Engrs. 37, 26-33.

Calderbank, P.H. 1958. Part I: The interfacial area in gas-liquid contacting with mechanical agitation. Trans. Instn. Chem. Engrs. 36, 443-463.

Calderbank, P.H. and Moo-Young, M.B. 1961. The power characteristics of agitators for the mixing of Newtonian and non-Newtonian fluids. Trans. Instn. Chem. Engrs. 39, 338-347.

Castell-Perez, M.E. and Steffe, J.F. 1989. Using Mixing to evaluate rheological properties. Chapter 14 in Viscoelastic Properties of Solid, Fluid and Semi-solid Foods. (Rao, M.A., ed.) Elsevier Applied Science Publishers Ltd., Barking, England.

Castell-Perez, M.E., Steffe, J.F. and Morgan, R.G. 1987. Adaptation of a Brookfield (HBTD) viscometer for mixer viscometry studies. J. Texture Stud. 18, 359-365.

Charles, M. 1978. Technical aspects of the rheological properties of microbial cultures. Adv. Biochem. Engng. 8, 1-61.

Chavan, V.V. and Ulbrecth, J. 1973. Power correlation for off-centred helecal screw impellers in highly viscous Newtonian and non-Newtonian liquids. Trans. Instn. Chem. Engrs. 51, 349-354.

Chavan, V.V. and Ulbrecht, J. 1972. Power correlation for helical ribbon impellers in inelastic non-Newtonian fluids. Chem. Engng. J. 3, 308-311.

Chavan, V.V. and Mashelkar, R.A. 1980. Mixing of viscous Newtonian and non-Newtonian fluids. In Advances in Transport Processes, New Delhi, 210-246.

Chavan, V.V., Arumugam, M. and Ulbrecht, J. 1975. On the influence of liquid elasticity on mixing in a vessel agitated by a combined ribbon-screw impeller. AIChE J. 21(3), 613-615.

Chavan, V.V., Jhaveri, A.S. and Ulbrecht, J. 1972. Power consumption for mixing of inelastic non-Newtonian fluids by helical screw agitators. Trans. Instn. Chem. Engrs. 50, 147-155.

Choplin, L. 1987. Mixing of highly viscoelastic fermentation broths. Presented at the 11th Conference on Mixing, August 1987, Henniken, NH. In Nauman, E.B., Etchells, A.W.III and Tatterson, G.B. 1988. Mixing: The state-of-the-art. Chem. Engng. Prog. 84, 58-69.

Collias, D.J. and Prud'homme, R.K. 1985. The effect of fluid elasticity on power consumption and mixing times in stirred tanks. Chem. Engng. Sci. 40(8), 1495-1505.

Conti, R., Sicardi, S. and Specchia, V. 1981. Effect of the stirrer clearance on particle suspension in agitated vessels. The Chem. Engng. J. 22, 247-249.

Crochet, M.J. and Walters, K. 1983. Numerical methods in non-Newtonian fluid mechanics. Ann. Rev. Fluid Mech. 15, 241-260.

Deak, A., Havas, G. and Sawinsky, J. 1985. The power requirements for anchor, ribbon and helical screw agitators. Int. Chem. Engng. 25(3), 558-565.

Dealy, J.M. and Vu, T.K.P. 1977/1978. The Weissenberg effect in molten polymers. J. Non-New. Fluid Mech. 3, 127-140.

Ducla, J.M., Desplanches, H. and Chevalier, J.L. 1983. Effective viscosity of non-Newtonian fluids in a mechanically stirred tank. Chem. Engng. Comm. 21, 29-36.

Edwards, M.F., Godfrey, J.C. and Kashani, M.M. 1976. Power requirement for the mixing of thixotropic liquids. J. Non-New. Fluid Mech. 1, 309-322.

Eitelberg, G. 1983. Weissenberg effect and its dependence upon the experimental geometry. Rheol. Acta 22, 131-136.

Ford, E.W. 1984. Rheological analysis of starch-thickened apricots using mixer viscometry techniques. M.S. Thesis, Department of Agricultural Engineering, Michigan State University, East Lansing, Michigan.

Ford, E.W. and Steffe, J.F. 1986. Quantifying thixotropy in starch-thickened, strained apricots using mixer viscometry techniques. J. Texture Stud. 17, 71-85.

Foresti, R. Jr. and Liu, T. 1959. How to measure power requirements for agitation of non-Newtonian liquids in the laminar region. Ind. and Eng. Chem. 51(7), 860-864.

Godleski, S. and Smith, J.C. 1962. Power requirements and blend times in the agitation of pseudoplastic fluids. AIChE J. 8(5), 617-620.

Green, S.J. 1953. Agitation in process design. Trans. Instn. Chem. Engrs. 31, 327-347.

Griffith, D.L. and Rao, V.N.M. 1978. Flow characteristics of non-Newtonian foods utilizing a low-cost rotational viscometer. J. Food Science 43, 1876-1877.

Haimoni, A. and Hannant, D.J. 1988. Developments in the shear vane test to measure the gel strength of oilwell cement slurry. Adv. Cement Res. 1(4), 221-229.

Hall, K.R. and Godfrey, J.C. 1970. Power consumption by helical ribbon impellers. Trans. Instn. Chem. Engrs. 48, T201-T208.

Hiraoka, S., Yamada, I. and Mizoguchi, K. 1979. Two dimensional model analysis of flow behavior of highly viscous non-Newtonian fluid in agitated vessel with paddle impeller. J. Chem. Engng. Japan 12(1), 56-62.

Hirsekon, F.S. and Miller, S.A. 1953. Agitation of viscous solid-liquid suspensions. Chem. Engng. Prog. 49(9), 459-466.

Hoffman, A.H. and Gottenberg, W.G. 1973. Determination of the material functions for a simple fluid from a study of the climbing effect. Trans. Soc. Rheol. 17(3), 465-486.

Holland, F.A. and Chapman, F.S. 1966. Liquid Mixing and Processing in Stirred Tanks. Chapman and Hall, Ltd. London

Hyman, D. 1962. Mixing and agitation. Adv. Chem. Engng. 3 (Drew, Hoopes and Vermeilen, eds.)

Joseph, D.D., Beavers, G.S., Cers, A., Dewald, C., Hoger, A. and Than, P.T. 1984. Climbing constants for various liquids. J. Rheol. 28(4), 325-345.

Kale, D.D., Mashelkar, R.A. and Ulbrecht, J. 1973. Drag reduction in rotational viscoelastic boundary layer flows. Nature Phys. Sci. 242, 29-30.

Keentok, Mo., Milthorpe, J.F. and O'Donovan, E. 1985. On the shearing zone around rotating vanes in plastic liquids: theory and experiment. J. Non-New. Fluid Mech. 17, 23-25.

Kemblowski, Z. and Kristiansen, B. 1986. Rheometry of fermentation liquids. Biotech. Bioeng. 28, 1474-1483.

Kemblowski, Z., Sek, J. and Budzynski, P. 1988. The concept of a rotational rheometer with helical screw impeller. Rheol. Acta 21, 82-91.

Kraynik, A.M., Aubert, J.H., Chapman, R.N. and Gyure, D.C. 1984. The helical screw rheometer: A new concept in rotational rheometry. In Proceedings of the Annual Technical Conference of the Society of Plastics Engineers, 14 Fairfield Drive, P.O. Box 0403, Brookfield Center, Connecticut 06804.

Krieger, I.M. and Maron, S.H. 1954. Direct determination of the flow curves of non-Newtonian fluids. III. Standardized treatment of viscometric data. J. Appl. Phys. 25(1), 72-75.

Langhaar, H.L. 1980. Dimensional Analysis and Theory of Models. Robert E. Krieger Publishing Company Inc., Huntington, New York.

Leong, Y.K., Creasy, D.E., Boger, D.V. and Nguyen, Q.D. 1987. Rheology of brown coal-water suspensions. Rheol. Acta 26, 291-300.

Mackey, K.L., Morgan, R.G. and Steffe, J.F. 1987. Effects of shear-thinning behavior on mixer viscometry techniques. J. Texture Stud. 18, 231-240.

Magelli, F., Fajner, D. and Pasquali, G. 1986. Backmixing in multistage mixer columns - III. Slightly viscoelastic liquids. Chem. Engng. Sci. 41(9), 2431-2433.

Magnusson, K. 1952. Effektbehouets beroende au den effektiva viskositeten vid omroring av strukturviskosa vatskor. IVA 23(2), 86-91.

Mashelkar, R.A., Kale, D.D. and Ulbrecht, J. 1975a. Rotational flows of non-Newtonian fluids. Part I. Turbulent flow of inelastic fluids around discs. Trans. Instn. Chem. Engrs. 53, 143-149.

Mashelkar, R.A., Kale, D.D. and Ulbrecht, J. 1975b. Rotational flow of non-Newtonian fluids. Part II. Torque suppression with agitators. Trans. Instn. Chem. Engrs. 53, 150-153.

Metzner, A.B. 1956. Non-Newtonian technology: Fluid mechanics, mixing and heat transfer. Adv. Chem. Engng. 1, 77.

Metzner, A.B. and Otto, R.E. 1957. Agitation of non-Newtonian fluids. AIChE J. 3(1), 3-10.

Metzner, A.B. and Taylor, J.S. 1960. Flow patterns in agitated vessels. AIChE J. 6(1), 109-114.

Metzner, A.B., Feehs, R.H., Lopez Ramos, H., Otto, R.E. and Tuthill, J.D. 1961. Agitation of viscous Newtonian and non-Newtonian fluids. AIChE J. 7(1), 3-9.

Mitsuishi, N. and Hirai, N. 1969. Power requirements in the agitation of non-Newtonian fluids. J. Chem. Engng. Japan 2(2), 217-224.

Mizushina, T., Ito, R. and Hiraoka, S. 1966. In Heat and Mass Transfer (in Russian), Vol 4. Nauka i Tekhnika, Minsk, 287.

Nagata, S. 1975. Mixing Principles and Applications. John Wiley & Sons, New York.

Nagata, S., Nishikawa, M., Tada, H. and Gotoh, S. 1971. Power consumption of mixing impellers in pseudoplastic liquids. J. Chem. Engng. Japan 4(1), 72-76.

Nagata, S., Yamamoto, K., Hashimoto, K. and Naruse, Y. 1960. Studies on the flow patterns of liquids in a cylindrical mixing vessel, over a wide range of Reynolds number. Mem. Fac. Engng. Kyoto Univ. 22(1), 68-85.

Nagata, S., Yokogama, T. and Yaragimoto, M. 1957. A study on the mixing of high-viscosity liquid. Chem. Engng. Japan 21, 278-286.

Nguyen, Q.D. and Boger, D.V. 1983. Yield stress measurement for concentrated suspensions. J. Rheol. 27(4), 321-349.

Nguyen, Q.D. and Boger, D.V. 1985a. Direct yield stress measurement with the vane method. J. Rheol. 29(3), 335-347.

Nguyen, Q.D. and Boger, D.V. 1985b. Thixotropic behavior of concentrated bauxite residue suspensions. Rheol. Acta 24, 227-237.

Nguyen, Q.D. and Boger, D.V. 1987. Characterization of yield stress of fluids with concentric cylinder viscometers. Rheol. Acta 26, 508-515.

Nienow, A.W. and Elson, T.P. 1988. Aspects of mixing in rheologically complex fluids. Chem. Engng. Res. Des. 66, 5-15.

Nienow, A.W., Wisdom, D.J., Solomon, J., Machon, V. and Vlcek, J. 1983. The effect of rheological complexities on power consumption in an aerated, agitated vessel. Chem. Engng. Comm. 19, 273-293.

Oldshue, J.Y. 1983. Fluid Mixing Technology. McGraw-Hill Co., New York.

Oliver, D.R., Nienow, A.W., Mitson, R.J. and Terry, K. 1984. Power consumption in the mixing of boger fluids. Chem. Engng. Res. Des. 62, 123-127.

Pavlushenko, I.S. and Gluz, M.D. 1968. Shear rate gradient in a vessel with stirrer. Theor. Found. Chem. Engng. 2(1), 105-109.

Pollard, J. and Kantyka, T.A. 1969. Heat transfer to agitated non-Newtonian fluids. Trans. Instn. Chem. Engrs. 47, T21-T27.

Prokopec, L. 1972. Agitated polymerization reactor for highly viscous media. Instn. Chem. Engng. 12(4), 712-719.

Prud'homme, R.K. and Shaqfeh, E. 1984. Effect of elasticity on mixing torque requirements for Rushton turbine impellers. AIChE J. 30(3), 485-486.

Qiu, C.G. and Rao, M.A. 1988. Role of pulp content and particle size in yield stress of apple sauce. J. Food Sci. 53, 1165-1170.

Ranade, V.R. and Ulbrecht, J. 1977. Gas dispersion in agitated viscous inelastic and viscoelastic liquids. Proc. 2nd. European Conference on Mixing, Cambridge, F683-F100.

Rao, M.A. 1975. Measurement of flow properties of food suspensions with a mixer. J. Texture Stud. 6, 533-539.

Rao, M.A. 1977. Rheology of liquid foods - A review. J. Texture Stud. 8, 135-168.

Rao, M.A. and Cooley, H.J. 1984. Determination of effective shear rates in rotational viscometers with complex geometries. J. Texture Stud. 15, 327-335.

Reher, E. and Bohm, R. 1970. Chem. Tech. 22, 134. Cited by Rieger, F., Novak, Z. and Havelkova,). 1988. The influence of the geometrical shape on the power requirement of ribbon impellers. Int. Chem. Engng. 28(2), 376-383.

Rieger, F. and Novak, V. 1973. Power consumption of agitators in highly viscous non-Newtonian liquids. Trans. Instn. Chem. Engrs. 51, 105-111.

Rieger, F. and Novak, V. 1974. Power consumption scale-up in agitating non-Newtonian fluids. Chem. Engng. Sci. 29, 2229-2234.

Roels, J.A., Van den Berg, J. and Voncken, R.M. 1974. The rheology of mycelial broths. Biotech. Bioengng. 16, 181-208.

Rushton, J.H. and Oldshue, J.Y. 1953. Mixing - Present theory and practice. Part I and II. Chem. Engng. Prog. 49(4/5), 161-168, 267-275.

Rushton, J.H., Costich, E.W. and Everett, H.J. 1950. Power characteristics of mixing impellers. Chem. Engng. Prog. 46(8), 395-404.

Sadowska, M., Naczk, M., Sikorski, Z.E. and Ziminska, H. 1982. Effect of fish protein preparations on rheological properties of meat sausages. J. Texture Stud. 13, 371-379.

Saravacos, G.D. and Moyer, J.C. 1967. Heating rates of fruit products in an agitated kettle. Food Technol. 21(3), 372-376.

Sawinsky, J., Havas, G. and Deak, A. 1976. Power requirement of anchor and helical ribbon impellers for the case of agitating Newtonian and pseudoplastic liquids. Chem. Engng. Sci. 31, 507-509.

Schilo, D. 1969. Power requirement of tangential mixers in the mixing of non-Newtonian liquids. Chem.-Ing. tech. 5, 253.

Sestak, J., Houska, M. and Zitny, R. 1982. Mixing of thixotropic fluids. J. Rheol. 26(5), 459-475.

Sestak, J., Zitny, R. and Houska, M. 1986. Anchor-agitated systems: power input correlation for pseudoplastic and thixotropic fluids in equilibrium. AIChE J. 32(1), 155-158.

Shamlou, P.A. and Edwards, M.F. 1985. Power consumption of helical ribbon mixers in viscous Newtonian and non-Newtonian fluids. Chem. Engng. Sci. 40(9), 1773-1781.

Sinevic, V., Kuboi, R. and Nienow, A.W. 1986. Power numbers, Taylor numbers and Taylor vortices in viscous Newtonian and non-Newtonian fluids. Chem. Engng. Sci. 41(11), 2915-2923.

Solomon, J., Elson, T.P. and Nienow, A.W. 1981. Cavern sizes in agitated fluids with a yield stress. Chem. Engng. Comm. 11, 143-164.

Solomons, G.L. 1971. Fermentation equipment. Adv. Appl. Micro. 14, 231-247.

Steffe, J.F. and Ford, E.W. 1985. Rheological techniques to evaluate the shelf-stability of starch-thickened, strained apricots. J. Texture Stud. 16, 179-192.

Steffe, J.F., Castell-Perez, M.E., Rose, K. and Zabik, M.E. 1989. Rapid testing method for characterizing the rheological behavior of gelatinizing corn starch slurries. Cereal Chemistry 66(1), 65-68.

Takahashi, K., Yokota, T. and Konno, H. 1984. Power consumption of helical ribbon agitators in highly viscous pseudoplastic liquids. J. Chem. Engng. Japan 17(6), 657-659.

Tamura, M.S., Shoemaker, C.F. and Henderson, J.M. 1988. Helical screw rheometer for on-line viscosity measurements. Paper # 519, presented at IFT Meeting, New Orleans, LA.

Thomas, R.H. and Walters, K. 1964. The motion of an elastico-viscuos liquid due to a sphere rotating about its diameter. Quart. J. Mech. and Appl. Math. 17, 39-42.

Tiu, C. and Boger, D.V. 1974. Complete rheological characterization of time-dependent food products. J. Texture Stud. 5, 329-338.

Treybal, R.E. 1956. Mechanically aided liquid extraction. Adv. Chem. Engng. 1, 229-329.

Ulbrecht, J. 1974. Mixing of viscoelastic fluids by mechanical agitation. The Chem. Engr. June, 347-367.

Ulbrecht, J.J. andeau, P. 1985. Mixing of viscous non-Newtonian fluids. Chapter 4 in Mixing of Liquids by Mechanical Agitation. Vol 1. (Ulbrecht, J.J. and Patterson, G.K., eds.). Gordon and Breach Science Publishers, New York.

Vocadlo, J.J. and Charles, M.E. 1971. Measurement of yield stress of fluid-like viscoplastic substances. The Can. J. Chem. Engng. 49(10), 576-582.

Voisey, P.W., Paton, D. and Timbers, G.E. 1977. The Ottawa starch viscometer- A new instrument for research and quality control applications. Cereal Chem. 54(3), 534-557.

Walker, C.E., Ross, A.S., Wrigley, C.W. and McMaster, G.J. 1988. Accelerated starch-paste characterization with the Rapid Visco-Analyzer. Cereal Foods World 33(6), 491-494.

Whalen, P.J., Anantheswaran, R.C. and Shahani, K.M. 1987. Power consumption of a whey-corn mash as compared to a full corn mash during liquefaction. Biotec. Letters 9(7), 523-528.

White, A.M. and Brenner, E. 1934. Studies in agitation. V. The correlation of power data. AIChE J. 30, 585-597.

White, A.M., Brenner, E., Phillips, G.A. and Morrison, M.S. 1934a. Studies in agitation. IV: Power measurements. AIChE J. 30, 570-584.

White, J.L., Chankraiphon,S. and Ide, Y. 1977. Rheological behavior and flow patterns around agitators in polymer solutions. Trans. Soc. Rheol. 21(1), 1-18.

Wichterle, K. and Wein, O. 1981. Threshold of mixing of non-Newtonian liquids. Int. Chem. Engng. 21(1), 116-120.

Wichterle, K., Kadlec, M., Zak, L. and Mitschka, P. 1984. Shear rates on turbine impeller blades. Chem. Engng. Commun. 26, 25-32.

Williams, R.W. 1979. Determination of viscometric data from the Brookfield R.V.T. viscometer. Rheol. Acta 18(3), 345-359.

Wood, F.W. and Goff, T.C. 1973. The determination of the effective shear rate in the Brabender Viscograph and in other systems of complex geometry. Die Starke 25, 89-91.

Yagi, H. and Yoshida, F. 1975. Gas absorption by Newtonian and non-Newtonian fluids in sparged agitated vessels. Ind. Engng. Chem. Process Des. Dev. 14(4), 488-493.

Yap, C.Y., Patterson, W.I. and Carreau, P.J. 1979. Part III. Non-Newtonian fluids. AIChE J. 25(3), 516-521.

Yoshimura, A.S., Prud'homme, R.K., Princen, H.M. and Kiss, A.D. 1987. A comparison of techniques for measuring yield stresses. J. Rheol. 31(8), 699-710.